MSEL

Materials Science and Engineering Laboratory

NIST CENTER FOR NEUTRON RESEARCH

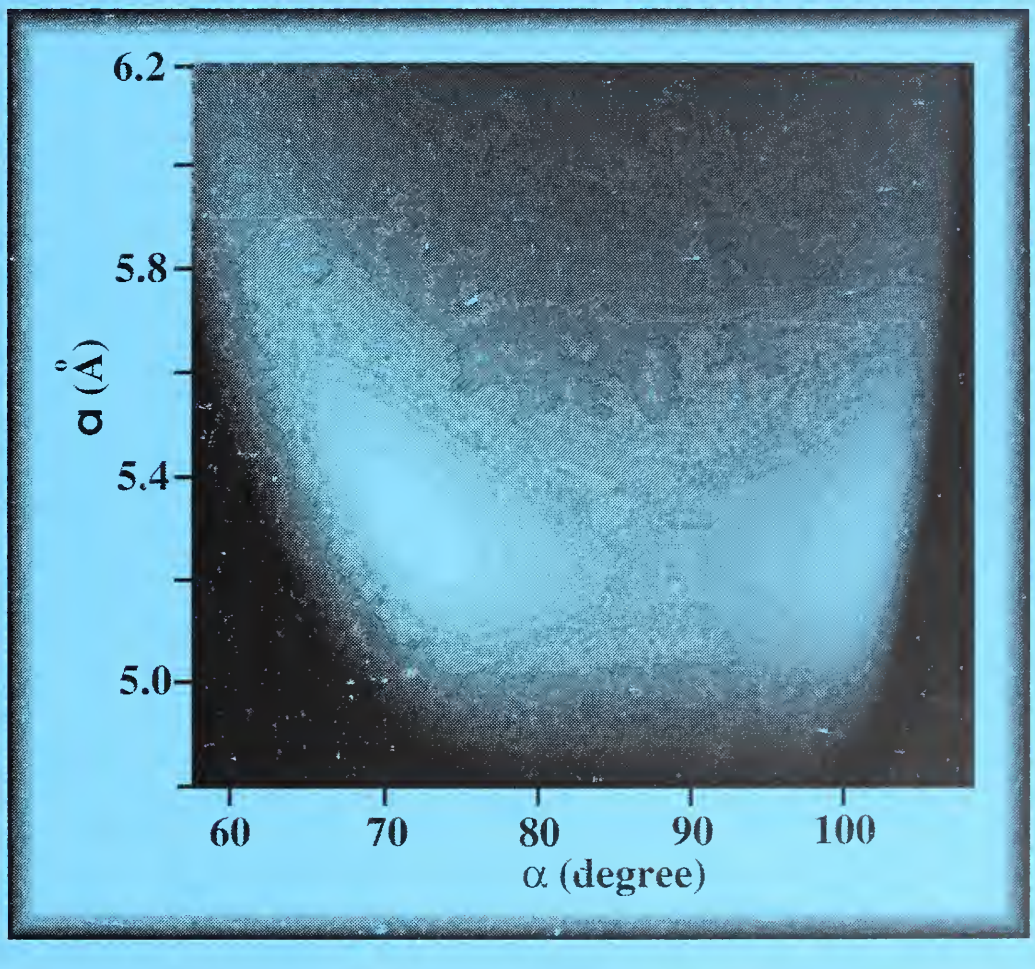

NISTIR 6067
U.S. Department of Commerce
Technology Administration
National Institute of Standards
and Technology

Technical Activities 1997

NIST Center for Neutron Research (NCNR)

Contour plot of the intermolecular potential energy calculated for solid cubane in the α – *alpha* (the rhombohedral lattice parameters) plane. The two white regions are minima that correspond to the experimentally observed structures in the orientationally ordered and disordered phases. The variation in grayscale covers a range in potential energy from –0.36 eV (black) to –0.67 eV (white). This represents the most complete understanding achieved to date of this fascinating molecule.

MSEL

Materials Science and Engineering Laboratory

NIST CENTER FOR NEUTRON RESEARCH

J.M. Rowe, Director
T.M. Raby, Deputy

NISTIR 6067
U.S. Department of Commerce
Technology Administration
National Institute of Standards
and Technology

Technical Activities 1997

U.S. DEPARTMENT OF COMMERCE
William M. Daley, Secretary
TECHNOLOGY ADMINISTRATION
Gary Bachula, Acting Under Secretary for Technology
NATIONAL INSTITUTE OF STANDARDS
AND TECHNOLOGY
Robert E. Hebner, Acting Director

Abstract

This report summarizes research results for the programs that use the facilities at the NIST Center for Neutron Research (NCNR) for the period from October 1996 through September 1997. The programs range from the use of thermal and cold neutron beams for studies of the structure and dynamics of materials to nuclear physics and neutron standards to sample irradiations for activation analysis. The NCNR is a national user facility, which served more than 1300 participants during the year, including scientists and engineers from 57 companies, 92 universities, and 38 other Government agencies in the U.S.A.

KEY WORDS: activation analysis; cold neutrons; crystal structure; diffraction; molecular dynamics; national user facility; neutron scattering; nondestructive evaluation; nuclear reactor.

DISCLAIMER

In order to adequately specify the experimental procedure, certain trade names and company products are identified. In no case, does such identification imply recommendation or endorsement by the National Institute of Standards and Technology, nor does it imply that the products are necessarily the best for the purpose.

Foreword

The past fiscal year, which was the second since the long shutdown for installation of the new liquid hydrogen cold neutron source, has met all of our expectations. In spite of two extra shutdowns for special maintenance on the reactor and the neutron guides, we operated for 248 20 MW days, only one less than last year. The overall reliability of reactor and cold source was better than 95 % (defined as percent of days operated on the day scheduled), while availability (percent of days operated to days scheduled) was better than 98 %. The number of users continues to increase (by approximately 8 % this past year), and the breadth of the community served continues to increase. In response to this continued growth, we have re-organized the facilities at the reactor into the NIST Center for Neutron Research (NCNR), which comprises three groups – Reactor Operations and Engineering, Neutron Condensed Matter Science, and Research Facility Operations. This new organization should help us to better serve the scientific and engineering community that uses these measurement capabilities.

The final three instruments in the cold neutron guide hall (Back Scattering, Spin Echo Spectrometer, and Disk Chopper Time of Flight Spectrometer) are all in the final stages of installation, and should be available for general use during the coming year, in the order given. The upgrade to the thermal neutron instruments in the reactor confinement building is proceeding, with construction of new monochromator shielding drums well underway. A second generation hydrogen cold source has been designed for installation at the next long shutdown (in fiscal year 2000) which should provide twice the cold neutron intensity with ¼ the fast neutron background at the reactor face.. Additional instrumentation developments are now being planned for installation over the next 5 – 10 years.

The scientific output of the NCNR has grown commensurately with the capabilities and performance of the facility. Not only does the number of users continue to grow, but also the number of non-traditional neutron scatterers grows both in absolute numbers and as a percentage. This in turn imposes a heavier responsibility on the staff, who are now dealing with more inexperienced users, which represents a heavier burden since staff numbers are not growing. On the average, 20 % of NCNR users each year are here for the first time, a statistic with which we are quite happy as it represents success in developing the idea of neutron techniques as a tool for problem solving. The output from these users is being published in the high impact journals, and is receiving citation rates substantially above average for the journals in question.

Finally, we continue to work on the relicensing project to allow the reactor to continue operation past the expiration of the present license in 2004. We are also developing a new generation of thermal neutron instrumentation for the facility, with the intent of operating until 2024. In these endeavors, we have the strong support of the NIST management as we move to improve all aspects of our operation.

Contents

Abstract iv

Foreword v

Introduction 1

Chemical Physics of Materials 5
Structure and Dynamics of Cubane 5
Hydrogen in Metals Studies 8
Inelastic Neutron Scattering of Hydrogen in Vycor 11
The Formation of Calcium Hydroxide During Cement Curing 12
Neutron Scattering Studies of Alkali-Doped Polyacetylene 14
Research Topics 16
Affiliations 19

Magnetism and Superconductivity 21
Exchange Biasing 21
Magnetoresistive Materials 22
Magnetic Resonance Gap 23
Magnetic Theory for R_2CuO_4 24
Spin Ladders 26
Research Topics 27
Affiliations 29

Crystallography 31
Instrumentation 31
Crystal Structures 31
NIST Crystallographic Data Center 34
Research Topics 35
Affiliations 37

Surface and Interfacial Studies 39
Studies of Wetting of D-Pentane on Water 39
Effects of Copolymer Additives on the Phase Behavior of Polymer Blend Films 40
Order vs. Microphase Separation I Thin Diblock Copolymer Films 42
Polymer Interdiffusion Near the Polymer/Solid Interface 44
Interfacial Width Determination I Immiscible Homopolymer/Random Copolymer Bilayers 46
Field History of the Magnetic Structure in GMR Co/Cu Multilayers 47
Antiferromagnetic Phase Transition and Interlayer Spin Coherence in Short-period EuTe/PbTe Superlattices 49
Neutron Reflectivity, X-ray Reflectivity and Spectroscopic Ellipsometry Characterization of SiO_2 on Si (100) 51
Neutron and X-ray Reflectometry Studies of Rough Interfaces in a Langmuir-Blodgett Film 53
Direct Inversion of Specular Reflectometry 54
Research Topics 56
Affiliations 57

Macromolecular and Microstructure Studies 59
Polymerization of Rod-Like Surfactant micelles 59
Diblock Copolymer Mixtures under Shear 60
Shear-Induced Micellar Crystal Structures in Triblock Copolymer Solutions 61
Scaling Laws for Polymers in Marginal Solvents 62
Research Topics 63
Affiliations 65

Neutron Beam Applications **67**
Neutron Diffraction Measurement of Residual Stress 67
Texture Studies 73
Research Topics 73
Affiliations 74

Instrumentation Development **75**
The Disk Chopper Spectrometer 75
The High Flux Backscattering Spectrometer 77
The Neutron Spin Echo Spectrometer 78
Thermal Neutron Modernization Program 79
The Filter Analyzer Neutron Spectrometer (FANS) 80
Monochromator Development 81
Perfect Crystal SANS Diffractometer 82
Research Topics 84
Affiliations 84

Reactor Operations and Engineering **85**

Polymers Division Programs **87**
Blends 87
Filled Polymers 88
Interfaces and Thin Films 88
Investigation of the Regimes in Dendrimer Solution 90
Effect of Solvent Quality on Starburst Dendrimers 90
Domain Structure in Polylectrolyte Solutions 90
SANS Study of a Labeled PAMAM Dendrimer 91
Research Topics 93
Affiliations 93

Other MSEL Programs with NCNR Participation **95**
Ceramic Coatings 95
Evaluated Materials Data 95
High Temperature Superconductivity 96

Exxon Research at the NCNR **99**
Effect of Pressure on the Thermodynamics of Polyolefin Blends 100
Micelles and Microemulsions of Polyelectrolytes Copolymers 100
Polymer Aggregates with Crystalline Cores: The System Polyethylene-Poly (ethyleneprophylene) 100
Melt Chain Dimension s of Poly (ethylene-1-butene) Copolymers 100
Characterization of Soot in Diesel Engine Oils 100
Neutron Imaging for In-Situ Measurements of Water Transport Gradients in Polymer Electrolyte Fuel Cells 101
Research Topics 101
Affiliations 101

University of Minnesota Programs **103**
Research Projects 103
Research Topics 104
Affiliations 104

Neutron Interactions and Dosimetry **105**
Fundamental Neutron Physics 105
Research Topics 107
Affiliations 108

Analytical Chemistry **109**
Nuclear Methods Group 109
Food and Drug Administration 114
Smithsonian Institution 115
University of Maryland 115
Research Topics 117
Affiliations 118

NCNR Guest Researchers and Collaborations: 1997 ..... **121**

Organizational Charts **123**
NCNR/NIST Resident Staff and Visiting Scientists 127
Research and Engineering Staff 129

Technical and Professional Committee Participation and Leadership **135**

Publications **139**

INTRODUCTION

The NIST Center for Neutron Research (NCNR) was formed in 1996 from the Reactor Radiation Division with the mission of assuring the availability of neutron measurement methods for U.S. science and technology. The core of the Center is the 20 MW research reactor located at the Gaithersburg Maryland site, which provides neutron beams and irradiation facilities for a wide variety of measurements and uses. The NCNR is operated as a national facility, with several different modes of access for users, including a formal peer reviewed (written) proposal mode, a Participating Research Team mode in which partners build and operate specific instruments, a collaborative research mode, and a proprietary research mode (for which full cost recovery is required). During Fiscal Year 1997, 1360 research participants representing 57 companies, 92 universities, 38 government organizations and over 100 non-U.S. organizations were served by the NCNR. The organization of the Center is directed towards responsibility for three aspects of the mission - Reactor Operations and Engineering, Neutron Condensed Matter Science, and Research Facility Operations. However, in practice, there are strong overlaps between all three groups, so that the organization of program results which follows should not be interpreted too literally as the product of any one group or subgroup.

The NBSR was designed as a multipurpose facility, with a broad range of experimental capabilities incorporated from the beginning, a design that provides a great deal of flexibility. There are many irradiation facilities of different characteristics, as shown in the table below. These facilities support a number of different programs, primarily in analytical chemistry, for NIST and other federal agencies (e.g. FDA, EPA) and for private sector organizations (e.g. Smithsonian, UMd). The reactor also contains a large graphite thermal column, which provides intense beams of well-thermalized neutrons (note data for RT-5 in table). This port is used by many diverse programs in the areas of neutron dosimetry, neutron radiography, neutron autoradiography (e.g. of paintings) and instrumentation tests (e.g. CCD based neutron detectors).

The reactor also has nine radial neutron beam ports (14 and 16.5 cm D), for which the thermal/fast neutron ratio is greatly improved by a split core design. In addition to these ports, there is a large (54 cm D) radial port that contains a liquid hydrogen cold source of novel design. This source serves seven neutron guides that take cold neutrons into a guide hall, and one port inside the reactor confinement building. These ports are used for various beam experiments, as described below. There are also two tangential through tubes which pass below the core (12 cm D), which are used primarily to produce filtered neutron beams for neutron dosimetry.

Irradiation Facilities in the Reactor

Facility[1]	Thermal Flux 10^{14} (n/cm^2/s)	Fast Neutron Flux [2] 10^{10} (n/cm^2/s)	Comments
RT-1	1.05	15.7	
RT-2	0.5	2.7	Rapid transfer system (0.5 s)
RT-3	1.03	~1.5	Not currently in service
RT-4	0.33	1.2	
RT-5	0.0032	< .001	Located in thermal column
G-4	3.7	~50	Heavy water cooled samples
			There are 6 additional 9 cm D and 4 unused 5 cm D thimbles which could be developed
V-n			There are 7 available thimbles in the reflector with lower thermal fluxes, but high thermal/fast ratios

[1]Facilities labeled by RT-n is pneumatic tube systems.
[2]Determined from ^{58}Ni(n,p)^{58}Co reactions, and includes all neutrons with energies greater than 2.9 MeV

Reactor Confinement Building Instruments

Triple axis spectrometers

At present, there are three triple axis spectrometers available, each with different characteristics. One features polarized beam analysis for studies of magnetic systems, and another has a filter analyzer option for neutron vibrational spectroscopy of solids. The spectrometers are used primarily for the study of excitations in single crystals.

High resolution powder diffractometer

This is a 32 detector diffractometer used for the measurement of powder diffraction patterns, which are subsequently fit by Rietveld analysis. There are several options for resolution, determined by the three available monochromators – Ge (311), Cu (311), and Si (531) at angles of 75, 90, and 120 degrees, and the two available Soller collimators before the monochromator. Diffraction peaks as narrow as 0.15 degrees FWHM are available.

Residual stress and single crystal diffractometer

This is a variable wavelength diffractometer optimized for the study of residual strain, with several options for sample translation and orientation. It can also be used for single crystal diffraction studies.

Cold neutron depth profiling and neutron optics

These two instruments view the hydrogen cold source through a short, segmented bent guide, providing clean cold neutron beams of high intensity. The depth profiling station is used to study near-surface impurities and dopants non-destructively, while the neutron optics station uses the transmitted beam to study neutron devices.

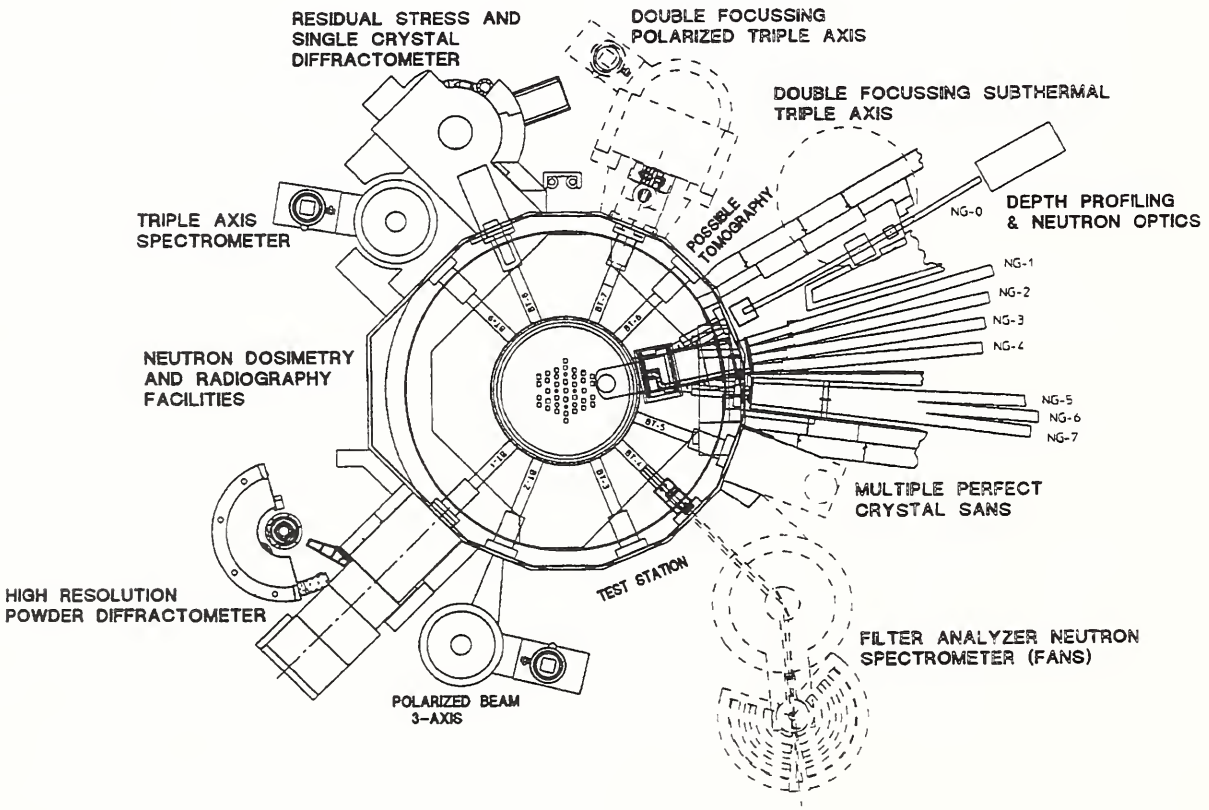

Plan view of the experimental floor inside the reactor confinement building. Instruments shown by dashed lines are presently under design or construction.

Cold Neutron Guide Hall Instruments

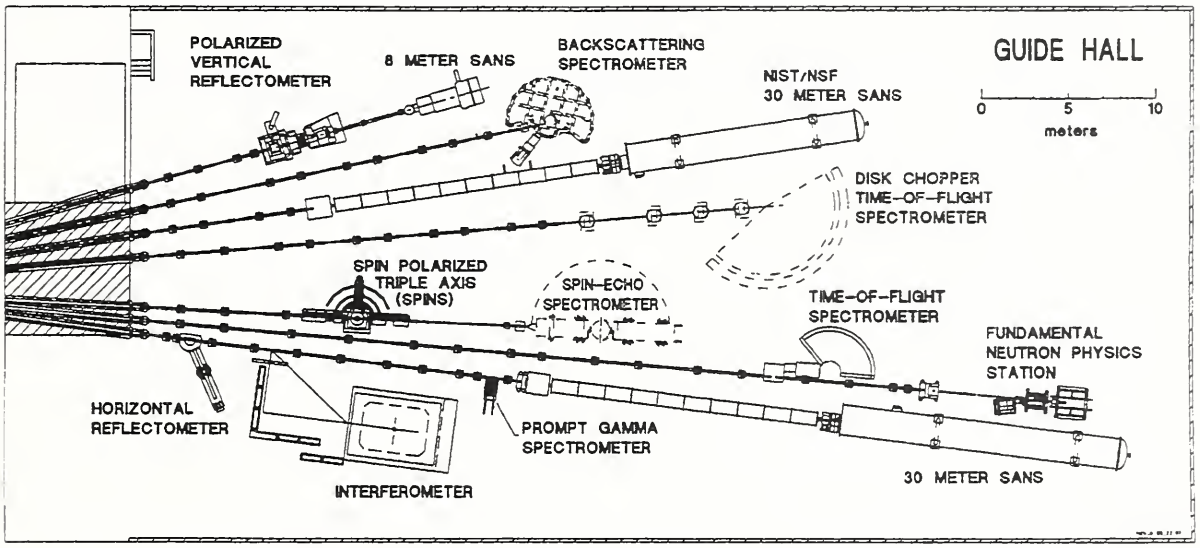

Plan view of cold neutron guide hall. Instruments shown by dashed lines are presently being installed.

Small angle neutron scattering (SANS) instruments

There are three SANS instruments available – two 30 m (high resolution) and one 8 m in overall length. The 8 m machine is operated by the Polymers Division, MSEL; one 30 m machine is operated by NIST, Exxon Research and Engineering Company and the University of Minnesota; and the other 30 machine is part of the Center for High Resolution Neutron Scattering funded by the National Science Foundation and NIST. The instruments are used for the study of microstructure in a wide range of materials, including polymers, biological samples, metals, and ceramics.

Neutron reflectometers

There are two reflectometers in the guide hall - one with horizontal scattering geometry and polarized beam capability and the other with vertical scattering geometry suitable for free liquid surface studies. The instruments are used for surface and interface studies of polymer, biological and magnetic systems.

Spin polarized triple axis spectrometer

This is a triple axis spectrometer optimized for cold neutron research. It provides neutron polarization analysis, and can be used with a horizontally focusing analyzer. It is used primarily for studies of low energy excitations in solids.

Neutron time of flight spectrometers

There are two TOF spectrometers in the guide hall – one with crystal monochromator and Fermi chopper for medium resolution studies, and the other with phased choppers allowing very good energy resolution. These instruments are primarily used for studies of excitations and diffusion (atomic or molecular) in polycrystalline or amorphous samples.

Very high resolution spectrometers

There is one back scattering and one spin echo spectrometer in the guide hall. These instruments provide the best resolution available for studies of dynamics in materials; each optimized for different types of study.

Instruments for neutron physics

There are two instruments used to study the physics of neutrons. One is a neutron interferometer mounted on a very stable platform (vibration acceleration 10^{-7} g), which is used for studies of the wave nature of the neutron. The other is a neutron beam at which different experiments can be installed for longer-term experiments (e.g. neutron lifetimes, parity violation in neutron decay).

Prompt gamma activation analysis

This instrument is designed to allow quantitative, non-destructive analysis of trace amounts of elements that do not become radioactive when they capture a neutron. The best example is hy-

drogen, which can be detected at levels near 1 μg in 1 g in favorable cases.

The remainder of this report is organized into section describing activities of the three NCNR groups, followed by similar sections for independent programs, and ending with organizational and statistical details.

The Neutron Condensed Matter Science Group is further subdivided into five groups consisting of Chemical Physics of Materials, Magnetism and Superconductivity, Crystallography, Surface and Interfacial studies, and Macromolecular and Microstructure Studies. Once again, there is substantial overlap between these teams, but the summaries presented below are provided within these headings for simplicity, along with a separate section on Neutron Beam Applications. These independent programs are motivated by other NIST organizations (Physics and Chemical Science and Technology Laboratories, Polymers Division of the Materials Science and Engineering Laboratory), and by members of Participating Research Teams (Exxon Research and Engineering and University of Minnesota).

Included within the report are lists of individual research topics, representing all of the research undertaken during the year. Further information on any topic can be obtained by directly contacting to the researchers listed, or by contacting Linda Clutter, who will then contact the appropriate scientists or engineers. We welcome any feedback that you might wish to give on any aspect of this report. Please send comments or suggestions to Linda Clutter, NIST Center for Neutron Research, Building 235, Gaithersburg, MD 20899 or email at linda.clutter@nist.gov.

Chemical Physics of Materials

Research in this category typically involves inelastic neutron scattering measurements of the dynamics of molecular solids, various inclusion compounds, and structurally disordered materials. These studies are often combined with structural studies and a variety of theoretical and modeling approaches yielding detailed information on the interatomic interactions in these systems.

Structure and Dynamics of Cubane

Cubane (C_8H_8) is a molecule whose shape is an atomic scale replica of a cube (Fig. 1). The unique geometry of the molecule imposes an angle of 90° on the C-C-C bond instead of the 109.5° normally found in regular sp^3--bonding. Cubane therefore possesses a tremendous amount of strain energy, roughly 150 kcal/mole, or 6.5 eV/molecule.

Before its synthesis in 1964 by Eaton and Cole at the University of Chicago [1], there was doubt that such a molecule could even hold together. Despite its exceptional structure, cubane remained an academic curiosity until the 1980's when it was recognized that its high heat of formation (+159 kcal/mole) and high density (1.29 gm/cm^{-3}), higher than almost all other hydrocarbons, made certain derivatives of cubane potential candidates for novel high energy density materials. These could be used as fuel additives, explosives, and propellants. It has been estimated that octanitrocubane (not yet synthesized), obtained by replacing the H atoms with NO_2 groups would have nearly twice the energy density of TNT. Remarkably, recent results have shown that certain complex cubane derivatives may also have biomedical applications.

In addition to the intriguing molecular properties of cubane, of great interest is the fact that these molecules crystallize into a solid, in which weak van der Waals forces are the dominant interaction between molecules. Raman, adiabatic and differential-scanning calorimetry, and NMR studies have shown that solid cubane undergoes a transition at T_p = 394 K from a low-temperature orientationally ordered phase to a (supposed) high temperature orientationally-disordered (or *plastic*) phase, before it melts at 405 K. Although these transitions have been the subject of numerous experimental and theoretical studies, no temperature dependent X-ray or neutron scattering measurements of cubane had been reported. Such studies are intrinsically difficult due to the high vapor pressure and rate of sublimation of cubane, and its strong tendency to recrystallize.

We recently surmounted these problems and presented the first structural characterization of the plastic crystal phase of solid cubane [2]. This work has revived an enormous interest in the cubane system within the physics community as evidenced by recent articles in *The New York Times* (July 15,1997), *Science News* 52, p. 34, 1997), and *Physics Today News Updates* (p. 9 August 1997), all of which have cited our work. We find that the high temperature phase of cubane is rhombohedral. This is a very unusual result because the disordered phases of most molecular solids, such as C_{60}, are face-centered cubic. Finally, the high symmetry of the cubane molecule, plus its extreme rigidity makes it readily amenable to theoretical modeling. Cubane is thus a rare example of a nearly ideal system that can be used to test our current understanding of orientational fluctuations, dynamics and phase transitions.

The 300 K X-ray profile of solid cubane can be indexed on a rhombohedral lattice with a = 5.32 Å and α = 72.69°, suggesting one molecule per unit cell and one of two possible space groups, either $R\bar{3}$ or $R\bar{3}m$. Rietveld refinements were performed to test these space groups. $R\bar{3}$ gave the best fit, in agreement with previous room temperature results. The unit cell can be viewed as a fcc lattice that has been squashed along one particular [111] axis (which remains a threefold axis) such that α increases from its fcc value of 60° to 72.69°. This space group does not, however, fix the orientation of the cubane molecule, as it allows rotation of the molecule through an arbitrary setting angle ϕ about the [111] axis. The best fit is obtained when the molecule is rotated by ϕ = 47.5°. This orientation brings the edges of the cubane skeleton (hydrogen atoms) into close proximity to the middle of the faces of the neighboring molecules (midpoint of the C-C bonds). This relative orientation of two nearest-neighbor cubane molecules is shown in Fig.1.

The most important result of our study [2] is the characterization of the plastic phase of solid cubane. The X-ray profile of this phase can not be indexed on a cubic lattice, but rather requires a rhombohedral cell with α = 103.3°. We simulated several different X-ray profiles for the plastic phase assuming a variety of different types of orientational disorder. The best fit is obtained

when the molecular orientational disorder is modeled by a constant distribution of setting angles ϕ between 50° and 70°. However, fits using a single value of ϕ in the same range are almost as good. Conversely, models assuming either spherical disorder or uniaxial disorder (about [111]) gave inferior fits. Thus, our X-ray data demonstrate that, contrary to previous expecta

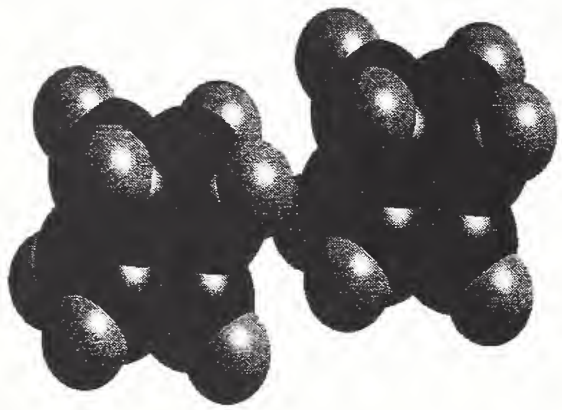

Fig. 1. Relative orientation of two nearest neighbor cubane molecules along one of the cell axes in the orientationally ordered phase. The darker spheres represent the carbon atoms and the lighter spheres represent the hydrogen atoms. The spheres have been arbitrarily expanded to a dameter corresponding to 0.7 times the Van der Waals radius for each atom.

tions, the plastic phase of solid cubane is rhombohedral. This is unexpected because the orientational disorder in the plastic phase should tend to average out the molecular symmetry, making it more spherical. In such a case one would expect a close-packed structure (fcc). However, our potential energy calculations show that in such a case the lattice constant would be too large for the solid to hold together. Therefore, the solid melts before the system adopts a fcc structure.

We also measured X-ray diffraction profiles for solid cubane from liquid N_2 temperature to well above the melting temperature. The results are summarized in Fig. 2. Note that α does not change within the experimental uncertainities until $T = T_p$. Similarly ϕ changes only weakly from 46.0° at 77 K to 47.5° at 300 K. In contrast, a varies by 5% from 77 K to T_p. The jump in the lattice constant at the orientational transition is about 0.05 Å, which corresponds to a 5.4% volume expansion, among the largest ever observed for a van der Waals solid. The large thermal expansion of cubane is mostly due to the cubic molecular shape which strongly couples orientational fluctuations to the lattice constant. When cubane is orientationally ordered, the molecules can move closer together, resulting in a smaller lattice constant. As the temperature increases, the amplitude of the rotational excitations increases, giving the molecules a larger effective radius. This causes the lattice to expand faster than in most other crystals.

The rhombohedral structure of both phases of solid cubane, as well as the strong first-order phase transition, can be understood using a model potential of the form

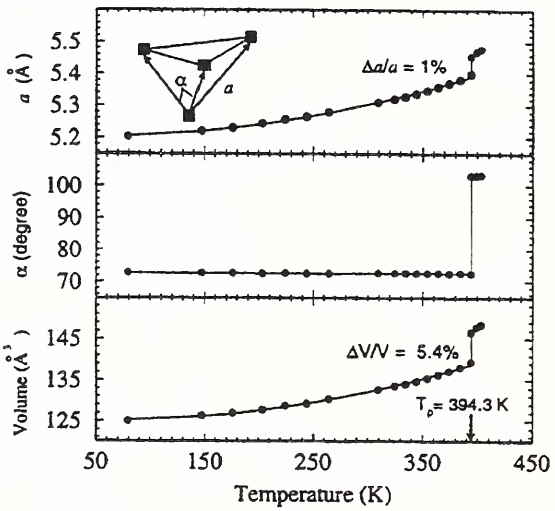

Fig. 2. Variation of lattice constant a, rhombohedral angle α, and unit cell volume as a function of temperature. The inset to the top panel defines the rhombohedral unit cell, a, and α; the solid squares represent individual cubane molecules

$$V_{ij}(r_{ij}) = - A_{ij}/r^6_{ij} + B_{ij}\, exp\,(- C_{ij}r_{ij}), \qquad (1)$$

where typical values of A_{ij}, B_{ij}, and C_{ij} for hydrocarbons were taken from a standard text book without modifications. Working in the rhombohedral basis, the ground state energy of solid cubane, E is a function of a, α, and ϕ. By varying these parameters, the energies of various possible structures can be calculated. To find minima in this three dimensional parameter space, we minimized the potential energy with respect to ϕ for each value of a and α. The resulting contour plot in the a-α plane is shown in the inset to Fig. 3. It is apparent that the potential predicts one global and one local minimum. Remarkably these minima correspond to the observed low and high-temperature phases. In order to demonstrate this better; we plot the potential energy curve in Fig. 3 (and on the cover) as a function of α with the lattice parameter a fixed at its room temperature value. From this curve it is clear that the cubic

structures (i. e. fcc for $\alpha = 60°$ and bcc for $\alpha = 109.47°$ have very high energies. The simple cubic (sc) structure ($\alpha = 90°$) is actually a local maximum. The global and local minima of the potential correspond to non-cubic structures with $\alpha \sim 72°$ and $\alpha \sim 102°$ respectively, very close to the experimentally determined values.

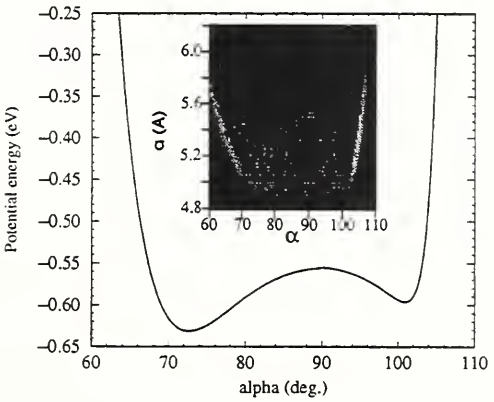

Fig. 3. Potential energy of solid cubane as a function of the rhombohedral cell angle α with *a* fixed at 5.32 Å. The inset shows the contour plot of potential energy in the *a*-α plane, clearly showing the local and global anima, as observed experimentally.

Perhaps the most interesting feature of our calculation is the finding that the potential energy as the molecules are rotated about the [111] axis in the disordered phase. It is nearly independent of ϕ between 30° and 90°. The plastic phase of cubane therefore represents a nearly perfect example of a system with *collective large-amplitude motions*, which suggests that the softening of the librational modes is the driving mechanism for the observed orientational phase transition. The increase in the ground state energy during the transformation from the ordered to disordered phase is therefore balanced by the collapse of the librations.

To further elucidate the rotational dynamics of cubane we have performed quasielastic scattering. Our experimental data and model calculations are summarized in Fig. 4. We have analyzed the observed broadening of the incoherent component of the neutron scattering in terms of models based on jump rotations about principle axes of the cubane molecule. In the ordered phase close to the orientational phase transition (at T= 385 K), the measured EISF corresponds to $2\pi/3$ and/or π jumps about the three--fold and/or four--fold axis of the cubane molecule respectively. Based on model calculations that predict a much smaller barrier for rotation about a four--fold axis than about a three-fold axis, we tentatively conclude that the major reorientational motion of cubane involves π jumps about four-fold axes.

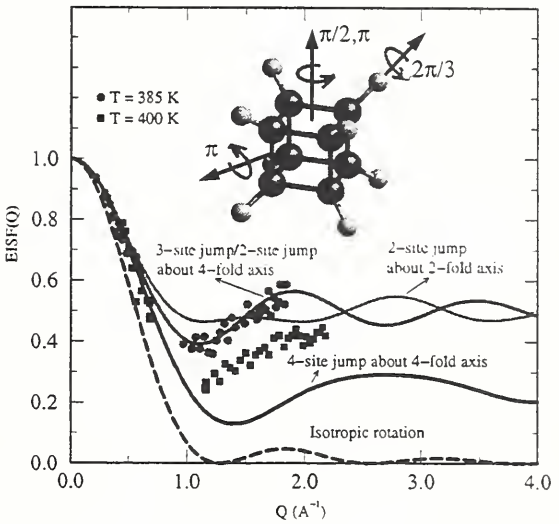

Fig. 4. Elastic Incoherent Structure Factor (EISF) of solid cubane obtained from various site jump models (solid lines) and the experimental data at T = 385 K (circles) and at T = 400 K (squares).

The measured EISF shown in Fig. 4 excludes the possibility of $\pi/2$ jumps about a four-fold axis. The reason that cubane jumps by π rather than $\pi/2$ is not clear yet, but this type of behavior is also seen in other molecular systems and must have something to do with the cooperative dynamics of the molecules. In the disordered phase (at T=400 K), unlike the plastic phases of most molecular solids, the EISF excludes isotropic and free uniaxial rotational motions of the molecule but suggest a more complex motion presumably due to the large-amplitude collective motions observed in the potential calculations. Currently we are performing molecular dynamics simulations in order to gain a better understanding the observed EISF, and thus the reorientational motion of cubane in the disordered phase.

Hydrogen in Metals Studies

- **Hydrogen Dynamics in Crystalline Pd_9Si_2**

Certain compounds between transition metals and non-metals are able to accommodate hydrogen in interstitial sites. Among them, the palladium-phosphorus and palladium-silicon systems are interesting because of their thermodynamic properties and the variety in their structural

compositions. However, investigations of the dynamics of absorbed hydrogen and deuterium have only been carried out for amorphous $Pd_{85}Si_{15}$ [3,4]. Little is known about the behavior of the dissolved hydrogen in the crystalline compounds.

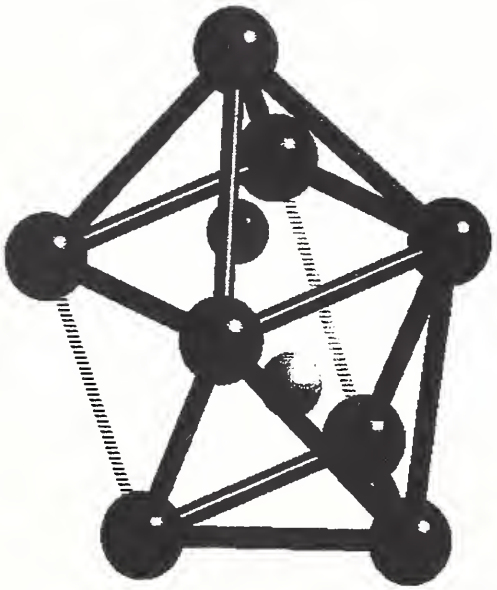

Fig. 5. The major interstitial pyramidal site for H (small black atom) in solution with Pd_9Si_2, defined entirely by Pd (large black atoms). The secondary pyramidal site is also shown (white atom).

Recently, we investigated the structure and dynamics of H and D dissolved in crystalline Pd_9Si_2 by means of neutron powder diffraction (NPD), neutron vibrational spectroscopy (NVS), and quasielastic neutron scattering (QENS). Crystalline Pd_9Si_2 forms peritectically at 1096 K with an orthorhombic structure (*Pnma*) characterized by augmented triangular prismatic coordination of the silicon atoms such as that which occurs in several metal-rich transition-metal silicides (*e.g.*, Co_2Si). NPD results for $Pd_9Si_2(D/H)_{0.25}$ show that D and H favor one type of interstice at low temperature, *i.e.*, a Pd-defined pyramidal site in a four-fold position situated on a quadrilateral face of an empty triangular prism (see Fig. 5). The dissolved D(H) atoms have five Pd neighbors at distances between 1.74(8) and 2.09(8) Å, and the nearest Si atom is at a distance of 3.02 Å. With increasing temperature, some of these D(H) atoms shift to a neighboring pyramidal site with two Si atoms at distances of 2.9 and 3.1 Å and involving one of the remaining two quadrilateral faces of the empty triangular prism in Fig. 5. For higher H concentrations, there are indications from NVS and NPD data for some additional H occupation of a third site, probably an octahedral interstice outside the triangular prism. It is clear that crystalline Pd_9Si_2 behaves differently than amorphous $Pd_{85}Si_{15}$, where only distorted Pd_6 octahedral sites along with a range of tetrahedral sites have been identified as H interstitial sites by NVS [3].

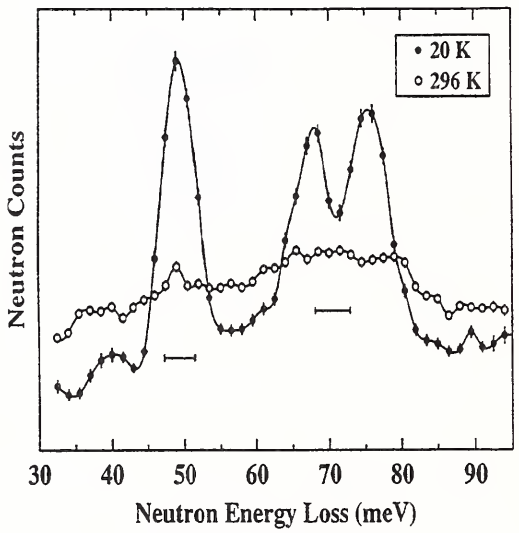

Fig. 6. DOS spectra of $Pd_9Si_2H_{0.25}$ at 20 and 296 K. The horizontal bars represent the instrumental resolution.

Figure 6 shows the vibrational density-of-states (DOS) spectra of H in crystalline $Pd_9Si_2H_{0.25}$. The low-temperature spectrum indicates three well-defined vibrational features located at 49.4, 67.2, and 75.5 meV. This is in contrast to the broad distribution of vibrational energies (maximized at ~ 60 meV) that was observed for H dissolved in amorphous $Pd_{85}Si_{15}$. A simple three-Gaussian fit of the crystalline $Pd_9Si_2H_{0.25}$ spectrum (ignoring the minor contributions of multiphonon scattering at energies above the main features) indicates three modes of roughly equal intensity, consistent with the majority occupation of the favored pyramidal site. More sophisticated fits of the vibrational spectra as a function of both temperature and H concentration clearly delineate the presence of the other minor H components. By symmetry considerations, the lowest-energy feature in Fig. 6 is assigned to the normal-mode vibration perpendicular to the pyramidal base and the two higher-energy features are assigned to the two orthogonal normal-mode vibrations parallel to this base. The nondegeneracy found for the higher-energy modes reflects the non-square nature of the pyramidal base. A similar low-temperature DOS spectrum of D in $Pd_9Si_2D_{0.25}$

yielded corresponding normal-mode energies at 31.4, 50.8, and 57.2 meV, which translates into H/D energy ratios of 1.57 for the soft mode and 1.32 for both higher-energy modes, reflecting an unusual potential for this pyramidal site. At 295 K, a substantial smearing of the vibrational features occurs, which would suggest the presence of significant H diffusional motion at this temperature.

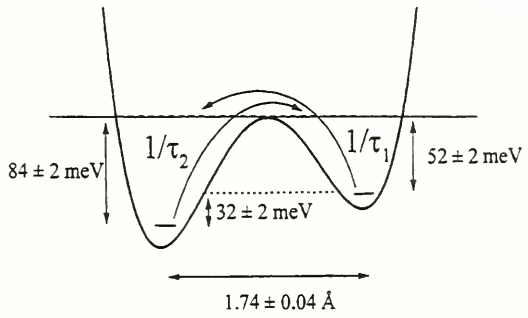

Fig. 7. Asymmetric double-well H potential between the two pyramidal sites in Pd_9Si_2 determined by analysis of the QENS data.

The presence of a localized H(D) motion was confirmed by QENS measurements of both hydrogenated and deuterated samples. The data are consistent with a jump diffusion model between the two pyramidal sites in Fig. 5. The temperature dependence of both the elastic incoherent structure factor (EISF) determined by QENS measurements and the site occupancies suggested by the NPD and NVS results pointed to an asymmetric double-well potential between the two pyramidal sites (see Fig. 7). For H, the Arrhenius law for the asymmetry parameter was found to be

$$\rho = \tau_1/\tau_2 = (0.8 \pm 0.1)\exp(32 \pm 2)\text{meV}/kT\}$$

where jump rates $1/\tau_1$ and $1/\tau_2$ obey the Arrhenius laws:

$$1/\tau_1 = (23\pm4)\ 10^{11}\exp\{-(52\pm4)\text{meV}/kT\}s^{-1}$$

and

$$1/\tau_2 = (19\pm2)\ 10^{11}\exp\{-(84\pm2)\text{meV}/kT\}s^{-1}.$$

The calculated jump distance of 1.74(3) Å was in fair agreement with the NPD-derived crystallographic distance of 1.59(8) Å between the two sites. Moreover, the jump trajectory along the double-well-potential surface is chiefly in the direction of the soft vibrational mode, which is also the mode with the somewhat larger H/D vibrational energy ratio, reflecting the anharmonicity of the potential-well.

- **Hydrogen Dynamics in Rare-Earth Trihydrides**

Recently, the physical properties of the rare-earth hydrides have attracted increased attention due to the discovery [5] that these materials become optically transparent for H/metal stoichiometric ratios approaching three. This unusual property has potential applications in the design of optical-switching devices. Various theories have been postulated for explaining the nature of these optical transitions, which remarkably occur for both the hcp (*e.g.*, YH_{3-x}) and fcc (*e.g.*, LaH_{3-x}) rare-earth trihydrides. Nonetheless, the precise physics behind these transitions has yet to be satisfactorily resolved. One impediment is the lack of reliable experimental data on the structural and physical properties of those rare-earth hydrides. In this light, we have continued to use neutron scattering methods over the past year in order to develop a better understanding of the true structures, phases, and dynamics associated with these materials. One aspect of these studies is the characterization of the hydrogen dynamics in both hcp YH_{3-x} and fcc LaH_{3-x} using QENS.

Figure 8 illustrates representative QENS spectra for YH_{3-x} and LaH_{3-x} at high temperature.

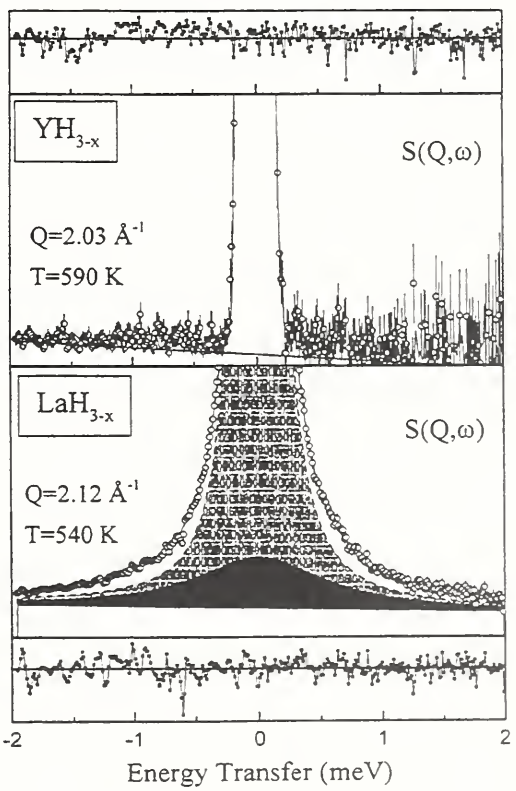

Fig. 8. QENS spectra for YH_{3-x} and LaH_{3-x} at high temperature using 4.8 A neutrons.

Our previous NPD results for YD_{3-x} [6] suggested the possibility of localized hydrogen motions. Yet for YH_{3-x}, no deviation from purely elastic scattering is evident in Fig. 8, indicating the lack of any observable local or long-range hydrogen motions within this particular neutron energy window. We are currently pursuing these investigations with solid-state NMR methods in search of hydrogen motions on a slower timescale. Unlike YH_{3-x}, LaH_{3-x} has an fcc La sublattice with H atoms occupying the two tetrahedral (*t*) interstices and 1-*x* of the one octahedral (*o*) interstice per La atom. There were suggestions that the *o*-site H atoms prefer to be displaced along the [111] directions closer to three metal atoms rather than be situated exactly in the center of the relatively large octahedral interstice. This led us to believe that these H atoms may undergo localized "rattling" motions within the *o* site, and be observable by QENS. Indeed, the LaH_{3-x} data clearly indicate two Lorentzian quasielastic components with distinctively different halfwidths at half maximum (HWHM). From the Q dependences of the two components, the geometries of the underlying motions were extracted. In particular, the narrower Lorentzian component was associated with long-range jump diffusion. As seen in Fig. 9, the corresponding HWHM was in excellent agreement with an orientationally-averaged Chudley-Elliott model:

$$\text{HWHM} \propto (1-\sin(Ql)/(Ql)).$$

The preliminary data analysis revealed a jump distance *l* close to the distance between the *o* and *t* sites (2.44 Å), strongly suggesting that the *x* *o*-site vacancies present in the substoichiometric trihydrides act as available sites for long-range hydrogen diffusion via *o*-*t* jumps. The temperature dependence of the narrow component yielded an activation energy of 150±10 meV for the long-range diffusion. The broad Lorentzian component could be modelled with a nearly constant HWHM for all Q values at a given temperature. This was a strong indication that this component represented a localized hydrogen motion. The geometry of this motion could be derived from the Q dependence of the elastic incoherent structure factor (EISF), *i.e.*, the ratio of the intensity of the narrow Lorentzian to the total quasielastic intensity, as exemplified in Fig. 10. The line corresponds to an isotropic rotational motion on a sphere of 0.23 Å radius for one-third of the hydrogen atoms (i.e., the *o*-site H atoms), although other related localized jump diffusion models such as jumps amongst the eight corners of a cube (which represents possible *o*-site H displacements away from the center position along the [111] directions) also fit the data. The small radius observed in the model fit is in line with the displacements expected for the postulated "rattling" motion of the *o*-site H atoms. The temperature dependence of the broad component yielded an activation energy of 73±12 meV for the localized motion. The derived activation energies for both the long-range and localized hydrogen motions are in agreement with energy barriers for hydrogen motions observed in solid-state NMR studies of LaH_{3-x} [7]. Future studies will focus on the effects of *o*-site vacancy concentration on the long-range and localized hydrogen dynamics in LaH_{3-x}.

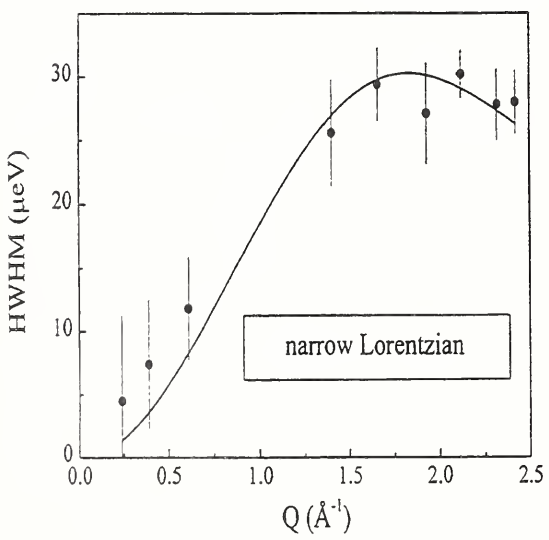

Fig. 9. The Q dependence of the HWHM for the LaH_{3-x} narrow Lorentzian component at 540 K fit to an orientationally-averaged Chudley-Elliott model.

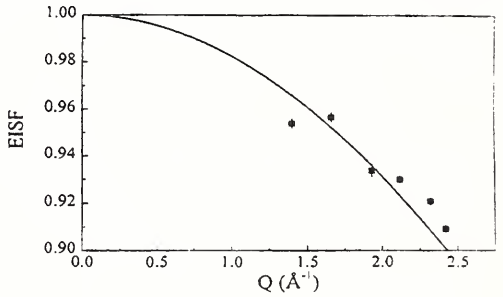

Fig. 10. The Q dependence of the EISF for a H_{3-x} at 540 K. The data are fit with a model for isotropic rotational motion on a sphere for one-third of the H atoms.

Inelastic Neutron Scattering of Hydrogen in Vycor

The behavior of adsorbed hydrogen and how it differs from that of the bulk has been studied for many host systems such as grafoil, CoNa A zeolite, intercalated graphite compounds, and recently porous vycor glass. Studies with vycor have mostly focused on the fact that confinement of a liquid in small pores suppresses the liquid-solid transition temperature. This introduces the exciting possibility of being able to keep the confined hydrogen in a liquid state down to a temperature at which it would become superfluid.

The properties of the confined system are modified as a result of the confining geometry and the interactions between the adsorbed system and the pore surface. Both of these effects alter dynamics of the individual molecules confined within the pores. In this report we examine these effects directly by looking at the rotational excitations of trapped hydrogen molecules. Hydrogen is an unusual system in that even in its solid form the molecules rotate quite freely. Effects due to interactions with a host medium modify this behavior. Hydrogen molecules attached to the surface of the vycor pores should experience a significant barrier to rotation which leads to a shifting and splitting of the rotational transitions. Those molecules trapped within the interior of the pore should be affected to a much smaller degree, but the effects of the confined geometry are still expected to modify the behavior relative to bulk.

The sample was prepared by placing cleaned vycor, with pore diameter of 70 Å in a tight fitting Al cell. The cell was cooled in an ILL cryostat and liquid hydrogen condensed on the vycor at a temperature of 18 K. The incoherent inelastic neutron scattering data were obtained using the Ferri chopper time-of-flight spectrometer operating at an incident wavelength of 4.8 Å.

Figure 11 shows the neutron gain part of the spectrum for a series of H_2 fill fractions ranging from 10 to 82%. It is essential to obtain the spectra immediately after loading since, over a period of several hours, the H_2 undergoes a conversion from its normal state of 25% para to a 100% para state. It can be seen that for fill fractions below roughly 30% the spectra consist of just one broad peak centered at 10 meV. For higher fill fractions a second narrower peak centered at 14 meV emerges. From these results it is clear that initially all the hydrogen loaded into the vycor forms a layer around the surface of the pores. The rotational motion of this surface is significantly constrained. It is only after the pores are roughly 1/3 filled than any measurable amount of hydrogen forms in the core. This core material behaves very much like bulk solid hydrogen which has a transition energy of 14.2 meV for a 75 % ortho mixture.

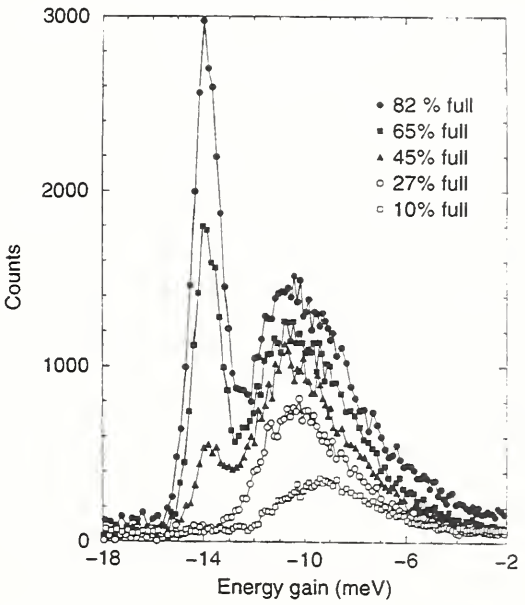

Fig. 11. Low temperature neutron gain spectrum for various fill fractions of H_2 in vycor.

Figure 12 shows the extracted parameters for the two modes. The intensity of the surface mode increases steadily for all fill volumes and it accounts for roughly 2/3 of the total signal at 100% filling. Both the energy and width of the surface mode increase sharply in the fill volume region from 20 to 27 %. These effects are consistent with the idea that the first monolayer of H_2 occupies the most deeply bound sites on the surface. These sites have the largest barrier to rotation and hence the largest shift from the free rotor position. Further H_2 molecules added to the system should experience a slightly smaller barrier and thus the mean shift in energy is less. Overall the results are consistent with a mean surface barrier to rotation on the order of 19 meV. Theoretical models predict that this surface interaction leads to a splitting in the first rotational excited state. However since the spectra were measured at low temperature in neutron energy gain we were only able to observe the transition from the lowest energy excited state.

The core mode which occurs for fill volumes above roughly 1/3 shows almost no change in width or center position. In all cases the results are very similar to those found for bulk solid hy-

drogen. The mode energy of 14.0 meV is reduced by 1.4 % from that of bulk and the FWHM, measured at 1.1 meV, is limited by the resolution of the spectrometer.

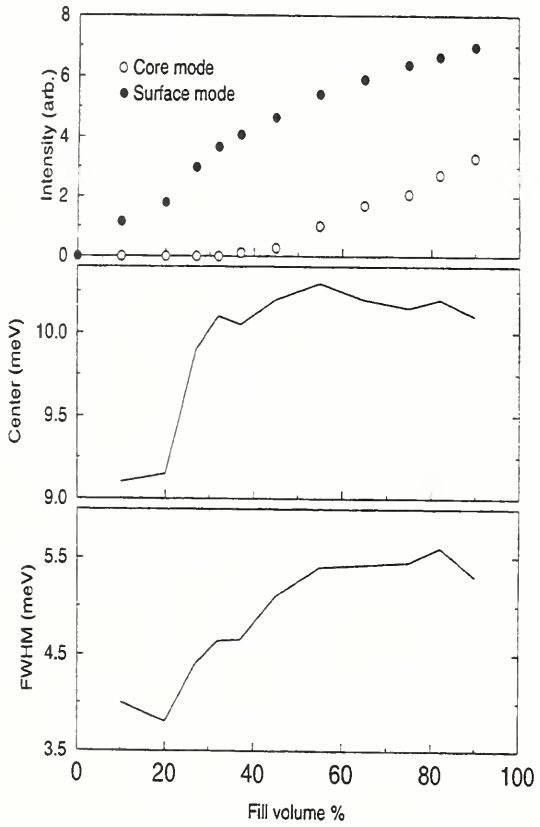

Fig. 12. Parameters of both the surface and core rotational modes of H_2 as a function of fill function.

In other work on this system we have looked at the ortho to para conversion of the trapped H_2. Surprisingly the conversion rate for the core material is much higher than that of the surface bound molecules. This indicates that the interactions between neighboring H_2 molecules are more effective at converting than those between H_2 and vycor. Future work will probe these effects in more detail by measuring the isotope effect when D_2 is introduced to the system.

The Formation of Calcium Hydroxide During Cement Curing

The reaction between tricalcium silicate (C3S) and water is the principal factor in the setting and hardening of Portland cement. Given its importance, this reaction has been studied by numerous investigators in order to obtain a detailed understanding of the development of strength in concrete. However the kinetics of the reaction and even the specific mechanisms are still not completely understood.

The overall hydration process which proceeds in several different reaction steps can be summarized as [8]

$$Ca_3SiO_5 + (3+y-x)H_2O \rightarrow (CaO)_x(SiO_2)(H_2O)_y + (3-x)Ca(OH)_2 \quad (1a)$$

which is written in cement notation as [9]

$$C3S + (3+y-x)H \rightarrow C_xSH_y + (3-x)CH, \quad (1b)$$

where x determines the Ca to Si ratio of the C-S-H and y is the sum of hydroxyl ions and bound water molecules incorporated into the C-S-H gel structure. Both x and y change over the course of the reaction and vary throughout the sample. C-S-H is an amorphous gel-like material which provides the cured paste's strength while CH occurs in a crystalline phase.

The overall hydration of C3S, summarized in Eq. 1, consists of three separate chemical reactions. After mixing, the C3S dissolves in an irreversible exothermic reaction.

$$Ca_3SiO_5(s) + 3H_2O \rightarrow 3Ca_2{+}(aq) + 4OH^-(aq) + H_2SiO_4^{2-}(aq). \quad (2)$$

Formation of the C-S-H gel occurs through a secondary reaction in which

$$H_2SiO_4^{2-}(aq) + xCa^{2+}(aq) + (2x-2)OH^-(aq) + (y-x)H_2O(l) \rightarrow (CaO)_x(SiO_2)(H_2O)_y. \quad (3)$$

Similarly CH starts to precipitate once the concentration of Ca^{2+} ions reaches its solubility limit,

$$Ca^{2+}(aq) + 2OH^-(aq) \rightarrow Ca(OH)_2(s). \quad (4)$$

Most cement studies are concerned with the C-S-H gel but in this report we focus on the CH phase and in particular on the rate at which it is formed. It is generally accepted that immediately after mixing water and C3S there is a brief burst of activity which is followed by a dormant period when the reaction rate decreases greatly. The dormant or induction period is thought to arise due to a surface layer of initial products coating the C3S grains and inhibiting further reaction. The rate stays very low for a few hours (depending on temperature), after which the coatings apparently rupture. It is known that the onset of CH formation coincides roughly with the end of the

induction period. However it is still not clear how the two events are causally linked.

The sample preparation, which involves the mixing of water with the C3S powder, is explained in detail in Ref. 1. The technique used to probe the CH formation is that of inelastic neutron spectroscopy. Measurements performed using the BT-4 filter analyzer spectrometer reveal a characteristic mode, centered at 40.5 meV, which is associated with the Ca-OH stretch. By continually monitoring the intensity of this mode we are able to determine the CH concentration throughout the hydration process.

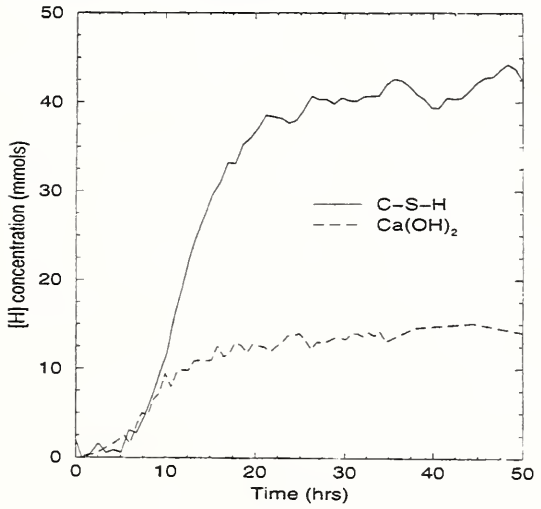

Fig. 13. Hydrogen content of both calcium hydroxide and C-S-H as a function of hydration time. The sample is cured at 20°C with a water to C3S ratio of 0.4 by mass.

Figure 13 shows the first two days of data for a sample cured at 20 °C. Significant amounts of CH are first formed three to five hours after mixing. The rate of formation remains high until roughly 15 hours have elapsed, and by 50 hours the CH concentration has almost become constant.

Combining the CH results with those from the FWI technique (which measures the fraction of initial water that is still mobile) we have been able to determine the hydrogen content in the C-S-H phase as a function of time. The most striking feature of the two curves is that their time dependences are so similar. Both curves increase from zero after the same delay time, reach a maximum rate at roughly the same hydration time and finally level off to a near constant value. The most likely explanation for this behavior is that throughout the hydration process the rate-limiting step is the dissolution of C3S outlined in Eq. 2.

Figure 14 shows the ratio of the hydrogen content in the C-S-H gel to that in CH as a function of hydration time. For times earlier than 5 hours neither concentration is high enough for us to obtain an accurate result. Between 10 and 20 hours the ratio rises steadily from 1 to 3. This may be the result of slight differences in the rates and or delay times between C-S-H and CH formation. The ratio is most sensitive to differences during this acceleratory period. An alternate explanation is that the increase arises from an increase in y, the hydrogen content of the C-S-H phase. Whether this increase is due to hydroxyl ion or bound water molecules incorporated into the C-S-H is unknown. A final point to be made with reference to Fig. 14 is that at long hydration times the ratio appears to be asymptotically approaching 3. This number is quite significant in that it allows us to determine the ratio of y/(3-x) in Eq. 1. A value of 3 is consistent with a theoretically predicted form of the equation which has y = 4.0 and x = 1.7.

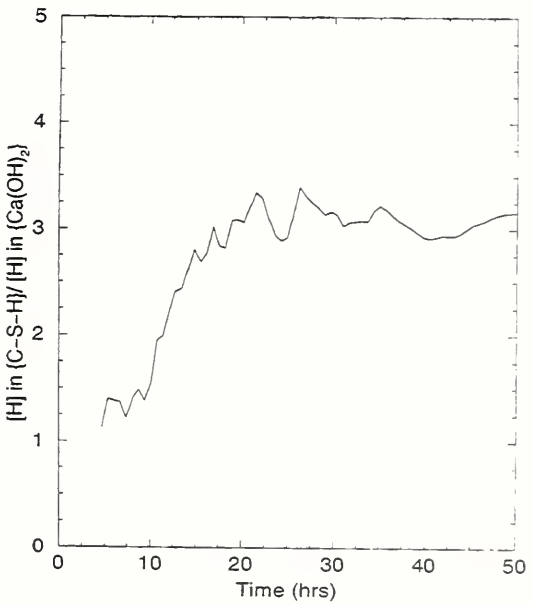

Fig. 14. Ratio of hydrogen content in the C-S-H phase to that in the CH phase as a function of hydration time.

Future work will focus on repeating the CH measurements over a range of temperatures. Combining these results with those of the FWI measurements at the same temperatures will allow us to determine the degree to which the stochiometry of the product phases is temperature dependent.

Neutron Scattering Studies of Alkali-Doped Polyacetylene

Polyacetylene $(CH)_x$ is structurally the simplest conjugated polymer, i.e., a polymer with all carbons sp^2 hybridized. The interest in polyacetylene and other conjugated systems was prompted by the discovery that the electrical conductivity of $(CH)_x$ films increases by several orders of magnitude upon doping with various electron donors or acceptors. The surprising new properties of conjugated polymers have been well described by a model proposed by Su, Schrieffer and Heeger [10], which considers electron-phonon coupling, and predicts self-localized non-linear excitations -- solitons, polarons, and bipolarons. Today, several technological applications of these materials have been developed, such as processable conducting films, electrode materials, light-emitting devices and electrochemical cells.

Although the applicability of polyacetylene itself is limited due to its brittleness and air sensitivity, polyacetylene has been widely studied during the past two decades as the prototypical conjugated polymer. Furthermore, doped $(CH)_x$ derivatives are also interesting from the structural point of view, because they represent anisotropic guest-host systems. The herringbone interchain configuration of pristine $(CH)_x$ transforms upon alkali metal doping to a triangular or square arrangement,with planar symmetry motifs depending on dopant size.

Vibrational spectroscopy has played an important role in the study of polyacetylene and other conjugated polymers. However, until recently little was known about the acoustic modes and the interchain phonons which are located in the low-frequency region not accessible by the optical methods (IR and Raman). Inelastic neutron scattering is well suited for the study of these phonons, as was demonstrated in our earlier results for pristine *cis*- and *trans*-$(CH)_x$. We have now carried out neutron scattering experiments also for alkali-doped samples [11].

Polyacetylene films were prepared using the solvent evaporation method. After the synthesis, the $(CH)_x$ films were cut to small strips and stretched up to five times their original length. This stretching procedure induces the alignment of polymer chains along the stretch direction, with the distribution of chain orientations of less than 15° FWHM. The use of highly oriented samples allows us to obtain not only frequency but also polarization information on the vibrational modes. The doping was carried out using the solution method in which the doping level is controlled by the redox potential of the dopant (alkali-metal salts of naphthalene). We have chosen two doping levels (1 and 14 mole %) in order to investigate the effects of light and heavy doping on the vibrational density of states.

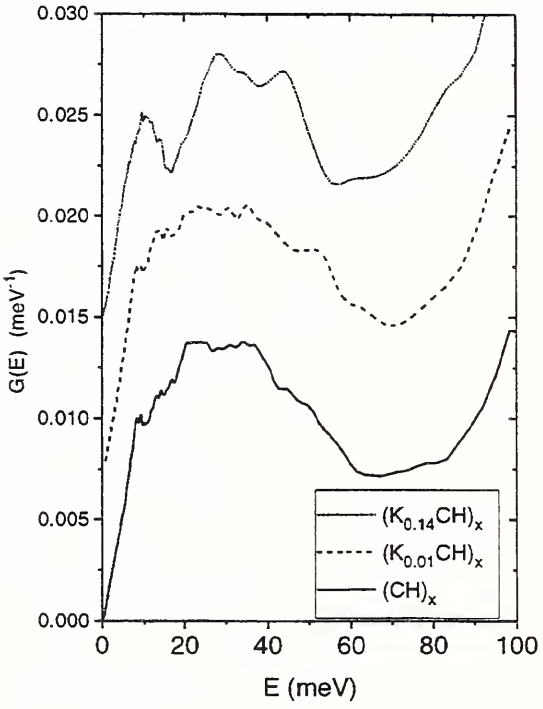

Fig. 15. The evolution of $G_\perp$ (E) of $(CH)_x$ upon doping with potassium, measured by the time-of-flight method in the $Q \perp c$ geometry. The data are offset for clarity.

Two complementary scattering techniques were used in this work, namely the time-of-flight (TOF) method and the filter-analyzer neutron spectrometry (FANS). TOF experiments were performed using the Fermi Chopper Spectrometer in NIST and the multichopper instrument MiBeMol in Saclay, France. Figure 15 shows the evolution of the polarized phonon density of states from pristine through 1% and 14% K-doped $(CH)_x$, derived from the TOF measurements. The data were collected in a particular scattering geometry, denoted $Q \perp c$ (where c is the polymer chain axis), in which only phonon modes with polarization vectors perpendicular to chain axes contribute strongly to the inelastic scattering. We see that there are only small differences between the pristine and the lightly doped $(CH)_x$; in particular, the singularities at 13 meV and 51 meV are better defined in the lightly doped polymer. After heavy doping, we observe a small energy shift of the lowest perpendicular singularity from 8 to 10 meV. This peak corresponds to an inter-

chain lattice phonon (whole-chain vibrations perpendicular to chain axis), and the stiffening of these modes in doped $(CH)_x$ is understandable, since Coulomb interactions become more important due to the charge transfer between dopants and $(CH)_x$ chains. However, the most prominent feature found in the heavily doped sample is the well defined gap in $G_\perp(E)$ at 16 meV. This gap was also observed in Na-doped samples. Further changes include a frequency shift of the broad maximum. These results confirm that doping (i.e., charge transfer) significantly affects the low-frequency intrachain modes as well, especially the chain torsional vibrations.

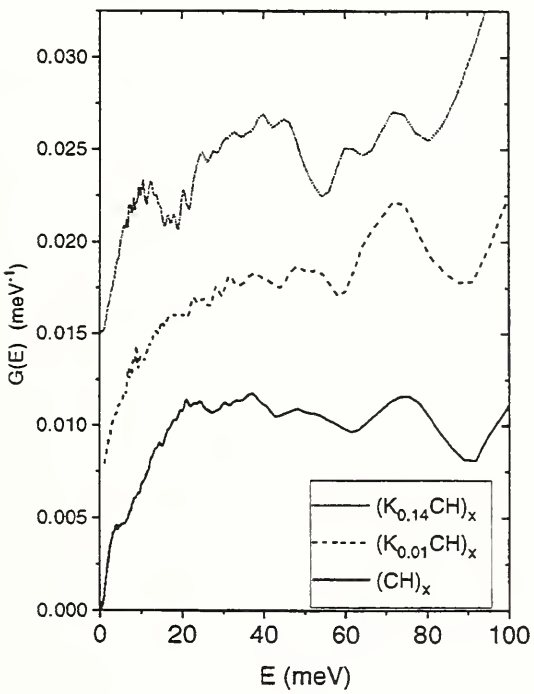

Fig. 16. The evolution of $G_{||}(E)$ of $(CH)_x$ upon doping with potassium, measured by the time-of-flight method in the Q||c geometry. The data are offset for clarity.

The evolution of the parallel component of the vibrational density of states $G_{||}(E)$ upon doping is shown in Fig. 16. Here we notice changes between the lightly doped and the pristine polymer. Firstly, the lowest parallel singularity at 3.5 meV has vanished from $G_{||}(E)$ of the lightly doped $(CH)_x$. Based on the results of molecular-dynamics simulations, this singularity was assigned to chain shearing modes. The strong influence of doping on these modes is not fully understood, but might be partially explained by the pinning of $(CH)_x$ chains to the dopants. Secondly, the well defined parallel peak at 76 meV in pristine $(CH)_x$ is slightly down-shifted in the 1% K-doped sample, and upon further doping this peaks develops a shoulder at 60 meV. We note that the 10-40 meV features are projections of the strong perpendicular peaks due to sample mosaicity. The inelastic scattering from the heavily K-doped $(CH)_x$ was measured again using the FANS spectrometer at NIST. The spectra were recorded for both polarizations and are shown in Fig. 17. The broad perpendicular maximum is now resolved as a blunt peak between 24 and 36 meV, and a second split peak near 50 meV. The gap at 16 meV is also confirmed by the FANS experiments. The Q||c spectra show several sharp peaks separated by smaller gaps, particularly in the energy region near 76 meV, where a pronounced longitudinal peak is located in pristine $(CH)_x$. The splitting of this peak (which corresponds to a longitudinal acoustic mode) can be explained by the existence of a charged soliton lattice in doped $(CH)_x$.

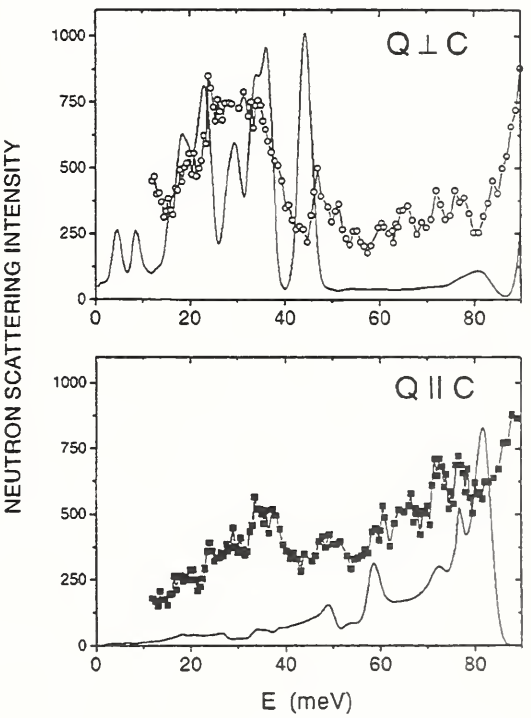

Fig. 17. The FANS spectra of 15% K-doped (CH)x. Upper figure: scattering measured om $Q_\perp$ c; lower figure: scattering measured in Q || c. The solid lines represent the AM1 calculated polarized density of states for a charge polyacetylene chain.

The solid lines in Fig. 17 represent calculated scattering for a single, negatively charged polyacetylene chain. Both *ab initio* and semiem-

pirical AM1 calculations predict the formation of a soliton lattice in which the soliton is spread over seven carbon sites (corresponding to 14% doping). The much larger translational period results in the typical folding of phonon lines in the Brillouin zone, and the modification of force constants causes the phonon branches to become discontinuous and separated by gaps that also emerge in the phonon density of states. Although the quantitative agreement with experimental data is not very good, the qualitative features of the scattering are reproduced quite well. We note that the nature of heavily doped, metallic $(CH)_x$ has been intensely debated for some time. Several theories explained the observed onset of temperature-independent spin susceptibility and rapid increase of electrical conductivity by the disappearance of dimerization and a transition to a simple metal. Our scattering experiments provide additional compelling evidence against this simple metal picture, since the observed features cannot be explained by an undimerized lattice with all carbon-carbon bonds equal. The concept of a soliton lattice persisting into the metallic state has been invoked in recent theories which consider quantum lattice fluctuations and interchain interactions in order to explain the closing of the Peierls gap. Further experimental work on the derivatives of poly(p-phenylene vinylene) is in progress.

Reference

[1] P. E. Eaton and T. W. Cole, Jr., J. Am. Chem. Soc. 86, 962 (1964).

[2] T. Yildirim, P. M. Gehring, D. A. Neumann, P. E. Eaton, and T. Emrick, Phys. Rev. Lett. **78**, 4938 (1997).

[3] J. J. Rush, T. J. Udovic, Hempelmann, D. Richter, and G. Driesen, J. Phys. Condens. Mat. **1**, 1061 (1989).

[4] D. Richter, G. Driesen, R. Hempelmann, and I. S. Anderson, Phys. Rev Lett. **57**, 731 (1986).

[5] J. N. Huiberts, R. Griessen, J. H. Rector, R. J. Wijngaarden, J. P. Dekker, D. G. deGroot, and N. J. Koeman, Nature 380, 231 (1996).

[6] T. J. Udovic, Q. Huang, and J. J. Rush, J. Phys. Chem. Solids 57, 423 (1996).

[7] R. G. Barnes, B. J. Beaudry, D. R. Toregeson, C. T. Chang, R. B. Creel, J. Alloys Comp. 253, 445 (1997).

[8] S. A. FitzGerald, D. A. Neumann, J. J. Rush, D. Bentz, R. A. Livingston, Chem. Mat. **10**, in press.

[9] Cement-chemistry notation: C = CaO, S = SiO_2, H = H_2O.

[10] W. P. Su, J. R. Schrieffer, and A. J. Heeger, Phys. Rev. Lett. 42, 1698 (1979).

[11] J. L. Sauvajol, P. Papanek, J. E. Fischer, A. J. Dianoux, P. M. McNeillis, C. Mathis, and B. Francois, Synth. Met. 84, 941 (1997).

Research Topics

Hydrogen Dynamics in $ZrBeH_{1.5}$

F. Altorfer[30,49], T. J. Udovic[30] and B. Hauback[19]

Hydrogen Dynamics in C_{24} and C_{15} Laves Phase Intermetallics

A. V. Skripov[24], J. C. Cook[30], C. Karmonik[30] and D. A. Neumann[30]

Proton Dynamics in Strontium Cerate Cramics

C. Karmonik[30], T. Yildirim[30], R. L. Paul[28], T. J. Udovic[30], J. J. Rush[30] and K. Lind[40]

Neutron Scattering Study of the Dynamics of Hydrogen and Deuterium Solved in Crystalline Pd_9Si_2

C. Karmonik[30], T. J. Udovic[30], Q. Huang[30,49], J. J. Rush[30], Y. Andersson[57], T. B. Flanagan[55]

Hydrogen Dynamics in K_3MnH_5 and Rb_3MnH_5 by means of Quasielastic Neutron Scattering

G. Auffermann[41], T. J. Udovic[30], C. Karmonik[30], J. J. Rush[30]

Proton Dynamics in LaH_{3-x} Investigated by Quasielastic Neutron Scattering

C. Karmonik[30], T. J. Udovic[30], J. J. Rush[30]

Inelastic Neutron Scattering Study of $La(H_yD_{1-y})_x$ ($2 \le x \le 3$)

T. J. Udovic[30], Q. Huang[30,49], J. J. Rush[30] and I. S. Anderson[18]

Electric Field Gradients Probed by μ^+SR in Sc and α-ScH_x Solid Solutions

F. N. Gygax[13], A. Amato[13], M. Pinkpank[13],A. Schenck[13], I. S. Anderson[18], G. Solt[18] and T. J. Udovic[30]

Inelastic Neutron Scattering Study of Rare Earth Trihydrides and Trideuterides

T. J. Udovic[30] and J. J. Rush[30]

Inelastic Neutron Scattering Study of the Nb-H(D) Phase Diagram

B. Hauer[40], R. Hempelmann[40], D. Richter[15], T. J. Udovic[30], J. J. Rush[30], W. Kockelmann[17], E. Jansen[17], and W. Schäfer[15]

Investigation of Nanocrystalline Ni

C. Karmonik[30], J. Barker[30], T. J. Udovic[30], J. J. Rush[30], M. Schmelzer[40], R. Hempelmann[40]

Diffusivity of Ga Confined in Nanostructured Alumina

H. Konrad[40], C. Karmonik[30], J. Weissmüller[40], J. C. Cook[30], H. Gleiter[40], R. Birringer[40], R. Hempelmann[40]

Inelastic Neutron Scattering Study of Aluminum Charged with Hydrogen

T. J. Udovic[30], J. J. Rush[30] C. Buckley[47] and H. K. Birnbaum[47]

The Dynamics of H_2 in Carbon Nanofibers

N. Rodriguez[32], P. Anderson[32], T. Sanders[32] and S. F. Trevino[30,7]

Hydrogen in Vycor

S. A. FitzGerald[30], D. Brown[53] and P. E. Sokol[53]

Dynamics of Interstitial Hydrogen in C_{60}

S. A. FitzGerald[30], D. A. Neumann[30], L. Santodonato[30], J. R. D. Copley[30], T. Yildirim[30] and J. J. Rush[30]

Dynamics of Interstitial H_2 in the Octahedral Site of Na_2C_{60}: An Inelastic Neutron Scattering Study

S. A. FitzGerald[30], T. Yildirim[30,49], L. Santodonato[30] and D. A. Neumann[30]

OH Dynamics in Sr(OH)Br

F. Altorfer[30,49], S. Peter[54] and H. D. Lutz[54]

Hydrogen Dynamics in $NaNH_2$

F. Altorfer[30,49], J. Senker[46] and H. Jacobs[46]

NH_3 Dynamics in Metal-Ammonia Halides

F. Altorfer[30,49] and R. Essmann[47]

Quasielastic Neutron Scattering of the Dynamics of NH_3in $(NH_3)_2Na_3C_{60}$

M. Green[52], D. A. Neumann[30], T. Yildirim[30] and M. J. Rosseinsky[52]

Pressure-Dependence of Methyl Group Tunneling in 4-Methyl Pyridine

S. F. Trevino[30, 7], J. C. Cook[30], D. A. Neumann[30] and L. Santodonato[30]

Measurement of the Phonon Density of States in Various Energetic Materials

S. F. Trevino[7] and L. Fried[23]

The Hydration of Cementitious Materials

S. A. FitzGerald[30], D. A. Neumann[30], J. J. Rush[30] and R. A. Livingston[33]

Inelastic Neutron Scattering Study of $H_5O_2^+$ Ions and their Partially Deuterated Analogs in $(H_5O_2)_3PW_{12}O_{40}$

N. C. Maliszewskyj[30] and T. J. Udovic[30]

Dynamics of Trioxane in Silica Sodalite

F. Altorfer[30,49], W. Buehrer[22] and C. Braunbarth[45]

Dynamics of Templating Molecules in CIT 1 Zeolite

B. H. Toby[30], N. C. Maliszewskyj[30], D. A. Neumann[30] and M. Davis[9]

Dynamics of Benzene in Si-Y Zeolite

L. Bull[43], R. Morris[43], A. K. Cheetham[43], D. A. Neumann[30] and J. M. Nicol[26]

Vibrational Spectroscopy of Hydrofluorocarbons Encaged in NaX and NaY Zeolites

N. C. Maliszewskyj[30], T. J. Udovic[30], R. R. Cavanagh[31], J. J. Rush[30], M. K. Crawford[12] and D. R. Corbin[12]

Quasielastic Scattering Study of Hydrofluorocarbons Encaged in NaX and NaY Zeolites

N. C. Maliszewskyj[30], C. Karmonik[30], T. J. Udovic[30], M. K. Crawford[12], R. R. Cavanagh[31], J. J. Rush[30] and D. R. Corbin[12]

Orientational Dynamics of P_4 Molecules in White Phosphorus

W. A. Kamitakahara[30], D. A. Neumann[30], F. Gompf[20] and Q. Huang[30,49]

X-ray and Neutron Study of the Temperature and Pressure Dependence of the Orientational Phase Transition in Solid Cubane

T. Yildirim[30,49], P. M. Gehring[30], D. A. Neumann[30], P. E. Eaton[44] and T. Emrick[44]

Neutron Investigation of Molecular Reorientations in Solid Cubane

T. Yildirim[30,49], P. M. Gehring[30], D. A Neumann[30], P. E. Eaton[44] and T. Emrick[44]

First-Principles Calculations of the Structural and Electronic Properties of Cubane and Various Cubane Derivatives

T. Yildirim[30,49], P. M. Gehring[30] and D. A. Neumann[30]

First-Principles and Inelastic Neutron Scattering Studies of Vibrational Modes in Cubane

T. Yildirim[30,49], P. M. Gehring[30] and D. A. Neumann[30]

Solid Cubane Dynamics, a MD Simulation

D. J. Tobias[30,53], M. L. Klein[53] and M. Tarek[30,53]

Electron-Phonon Coupling in Potassium Cryptand Complexes

N. C. Maliszewskyj[30], D. A. Neumann[30], D. J. Gilbert[25] and J. L. Dye[25]

Calculation of Bragg and Diffuse Scattering in C_{60}

J. R. D. Copley[30] and K. H. Michel[42]

Orientational Coordinates and Mode Coupling in C_{60}

K. H. Michel[42] and J. R. D. Copley[30]

Multiple Order Parameter Description of the First Order Phase Transition in C_{60}

K. H. Michel[42] and J. R. D. Copley[30]

Towards a Microscopic Approach to the Intermolecular Interaction in Solid C_{60}

S. Savin[53], A. B. Harris[53] and T. Yildirim[30]

Neutron Scattering Study of Na_2C_{60} in the (P,T)-Plane

T. Yildirim[30], D. A. Neumann[30], S. F. Trevino and J. E. Fischer[53]

Lattice Dynamics and Diffraction of K_1C_{60} in the Orthorhombic Phase: A Neutron Scattering Study

R. L. Cappelletti[34], H. M. Guerrero[34], T. Yildirim[30] and D. A. Neumann[30]

Synthesis and Properties of Mixed Alkali-Metal-Alkaline-Earth Fullerides

T. Yildirim[30], J. E. Fischer[53], P. W. Stephens[36] and P. Petit[16]

Fulleride Superconductors: Dependence of T_c on Average Molecular Valence

T. Yildirim[30], L. Barbedette[53], J. E. Fischer[53], C. L. Lin[36], J. Robert[16] and P. Petit[16]

Lattice Dynamics and Diffraction of Na_4C_{60}: A Neutron Scattering Study

T. Yildirim[30,49], S. A. FitzGerald[30] and D. A. Neumann[30]

Low Frequency Phonon Modes in Single Wall Carbon Nanotubes and Nanotube Ropes

P. Papanek[30,53], Z. Benes[53], P. Bernier[51] and J. E. Fischer[53]

Dynamics of Li-Doped Carbon Electrode Materials

P. Papanek[30,53], P. Zhou[53], Y. Sorek[53], W. A. Kamitakahara[30] and J. E. Fischer[53]

Structure and Dynamics of Amorphous Carbons

P. Zhou[53], P. Papanek[30,53], W. A. Kamitakahara[30] and J. E. Fischer[53]

Dynamics of Oxygen-Deficient Silica Glass

S. Das[4] and W. A. Kamitakahara[30]

Vibrational Densities of States for Cubic and Hexagonal Boron Nitride

W. A. Kamitakahara[30], D. A. Neumann[30], G. Doll[14], B. Sweeting[14] and A. W. Moore[1]

Neutron Scattering Study of Poly(p-phenylene vinylene) Derivatives

P. Papanek[30,53], J. E. Fischer[53], J. L. Sauvajol[51], A. J. Dianoux[18] and F. E. Karasz[50]

Low Energy Dynamics of Doped Poly(p-phenylene vinylene)

P. Papanek[30,53], J. E. Fischer[53], J. L. Sauvajol[51], A. J. Dianoux[18], G. Mao[56], M. J. Winokur[56] and F. E. Karasz[50]

Neutron Scattering Study of Hydrogen Bonding in Various Phases of Nylon Polymers

P. Papanek[30,53], N. S. Murthy and J. E. Fischer[53]

Polarized Vibrational Density of States of Alkali-Doped Polyacetylene

P. Papanek[30,53], J. E. Fischer[53], J. L. Sauvajol[51], P. McNeillis[16] and C. Mathis[16]

Intramolecular Dynamics of Kevlar

N. C. Maliszewskyj[30], T. J. Udovic[30] and M. L. Crawford[12]

Low Energy Dynamics of Isotopically Substituted Nylon 6.6

N. C. Maliszewskyj[30], T. J. Udovic[30], M. K. Crawford[12] and A. English[12]

Molecular Dynamics Studies of the Structure and Dynamics of Lipid Bilayers

D. J. Tobias[30,53], K. Tu[53] and M. L. Klein[53]

Molecular Dynamics Simulations of a SAM/DPPC Bilayer

D. J. Tobias[30,53], K. Tu[53], M. L. Klein[53] A. Plant[29,53] and M. Tarek[30,53]

Molecular Dynamics Simulations of the Temperature Dependence of Protein Dynamics

D. J. Tobias[30,53], M. L. Klein[53] and M. Tarek[30,53]

Dynamics of Layered Silicates-Influence of Intercalated Water and Cation Substitution

N. Wada[38] and W. A. Kamitakahara[30]

Layer Shearing Modes in Li-Graphite Compounds

W. A. Kamitakahara[30], C. Bindra[53] and J. E. Fischer[53]

Lattice Dynamics of $ZrSiO_4$

J. Nipko[6], C. K. Loong[6] and J. W. Lynn[30]

Soft Mode Dynamics in the Relaxor Ferroelectric $PbMg_{1/3}Nb_{2/3}O_3$

P. M. Gehring[30], G. Shirane[8], S. B. Vakhrushev[2] and S. M. Shapiro[8]

Pressure and Temperature Dependence of Fundamental Excitations in Liquid He

J. C. Cook[30], K. H. Andersen[18] and J. Bossy[10]

Affiliations

[1] Advanced Ceramics Corporation
[2] F. Ioffe Physioko-Technical Institute, Russia
[3] Allied Signal Inc.
[4] American University
[5] Ames Laboratory
[6] Argonne National Laboratory
[7] Army Research Laboratory
[8] Brookhaven National Laboratory
[9] California Institute of Technology
[10] Center for Advanced Research in Biology
[11] Drexel University
[12] E. I. DuPont
[13] Eidg. Technische Hochschule Zurich, Switzerland
[14] General Motors
[15] Institut für Festkörperforschung, Germany
[16] Institute Charles Sadron, France
[17] Universität Bonn, Germany
[18] Institute Laue-Langevin, France
[19] Institutt for Energiteknikk, Norway
[20] Karlsruhe Nuclear Research Center, Germany
[21] Laboratoire Lèon Brillouin, France
[22] Laboratory for Neutron Scattering, Switzerland
[23] Lawrence Livermore National Laboratory
[24] Metal Physics Institute
[25] Michigan State University
[26] Moltech Corporation
[27] Montgomery Blair High School
[28] NIST, Analytical Chemistry Division

[29] NIST, Biotechnology Division
[30] NIST Center for Neutron Research
[31] NIST, Surface and Microanalysis Division
[32] Northeastern University
[33] Federal Highway Administration
[34] Ohio University
[35] Paul Scherrer Institut, Switzerland
[36] State University of New York at Stony Brook
[37] Temple University
[38] Tohoku University, Japan
[39] Toyo University, Japan
[40] Universität des Saarlandes, Germany
[41] University of Aachen, Germany
[42] University of Antwerp, Belgium
[43] University of California at Santa Barbara
[44] University of Chicago
[45] University of Constance, Germany
[46] University of Dortmund, Germany
[47] University of Illinois
[48] University of Mainz, Germany
[49] University of Maryland at College Park
[50] University of Massachusetts
[51] Universitè Montpellier II, France
[52] University of Oxford, United Kingdom
[53] University of Pennsylvania
[54] University of Siegen, Germany
[55] University of Vermont
[56] University of Wisconsin
[57] Uppsala University, Sweden
[58] Yamanashi University, Japan

Magnetism and Superconductivity

Research in this area covers a rather diverse range of subjects this year, and the research topics section provides an overview of the breadth of the ongoing work. Following are some highlights of a number of interesting problems.

Exchange Biasing

In a variety of ferromagnetic/antiferromagnetic layered systems, field cooling through the antiferromagnetic Néel temperature results in a shift of the ferromagnetic hysteresis loop along the field axis. The ferromagnetic response is thus biased due to exchange interactions with the antiferromagnetic layer. This "exchange-biasing" effect has been the subject of much recent experimental and theoretical work. While the effect is being used to improve magnetic storage devices, the magnitude of the effect and its dependence on specific material properties (growth morphology, layer thickness, interfacial roughness, etc.) are still not well understood. In particular, there is still considerable discussion concerning the governing microscopic mechanisms.

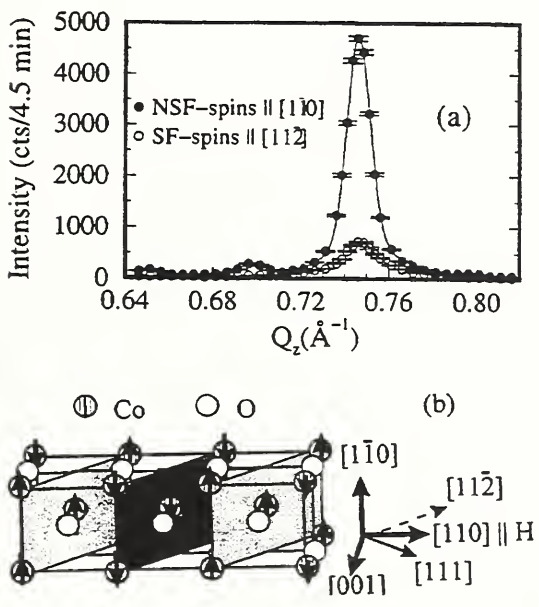

Fig. 1. (a) Polarized neutron diffraction scan along the [00l] direction through the (111) reflection for the superlattice $[Fe_3O_4(100Å)|CoO(30Å)]_{50}$ after cooling to 78 K in a field of 1.4 T applied along the [110] direction. Small amount of spin flip scattering is at the efficiency limit. (b) Corresponding spin structure and sample orientation.

In order to understand the specific role of the antiferromagnet, we have performed a series of neutron diffraction experiments on exchange-biased (001) Fe_3O_4/CoO superlattices [1]. The samples were grown at Philips Laboratories by molecular beam epitaxy. Despite differences in the crystal structures of the spinel Fe_3O_4 and the rocksalt CoO, the oxygen sublattices match to within 1.5%, such that single crystal superlattices can be grown. Thus, for these two oxides, it is possible to study very thin layers (17 Å to 100 Å) as the CoO antiferromagnetic order is long range and propagates coherently across intervening ferrimagnetic Fe_3O_4 layers.

In these superlattices, we have found that, as in bulk CoO, the Co spins order in ferromagnetic sheets that are coupled antiferromagnetically along the four possible <111> propagation directions. However, as illustrated in Fig. 1, polarized neutron diffraction results have shown that within the sheets the spins lie along new <110> easy axes which are in the film growth plane. The spins remain pinned to these directions for a variety of temperature and magnetic field conditions.

Instead of changes to the easy axis directions associated with each {111} domain, we have found that in response to different Fe_3O_4 magnetization conditions, the {111} domain populations change as shown in Fig. 2. In the figure, we note that the (111) intensity is much reduced after field cooling in the [1$\bar{1}$0] direction, but significantly increased for field cooling in the [110] direction. Field cooling in the [100] direction leads to an evening out of the domain populations.

A similar experiment was conducted on a $[CoO(30 Å)/MgO(30 Å)]_{333}$ superlattice which showed less than a few percent change for different field directions, despite having again these constrained in-plane <110> easy axes. The population changes thus stem from interactions with the Fe_3O_4 layers and are not just the direct response of CoO to an applied field. In addition, the magnitude of the change and its temperature dependence are correlated to the ferrimagnetic biasing behavior. In examining the orientation of the spins as illustrated in figure 1(b), we find that the CoO spins reorient to favor those domains

with easy axes *perpendicular* to the net Fe_3O_4 moment.

Thus, we have demonstrated the presence of perpendicular coupling between the Fe_3O_4 and CoO layers in this unique exchange-biasing system. This coupling has been part of recent theory to explain biasing. We are currently investigating whether we can gain further insight into the mechanism for the biasing by looking for domain wall motion as evidenced by linewidth changes. We have also begun to consider more industrially applicable systems, such as the polycrystalline NiO/NiFe bilayer system.

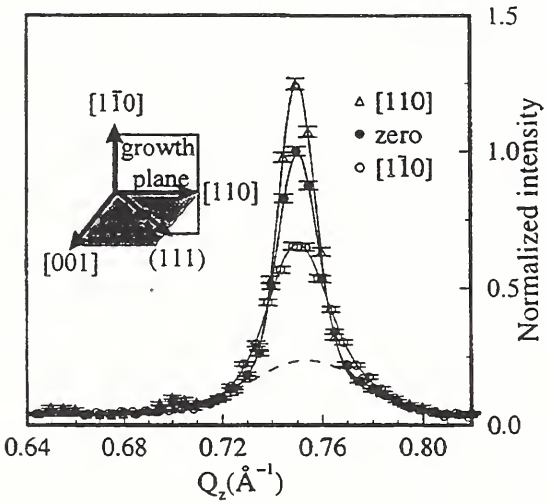

Fig. 2. Neutron diffraction scans along the [00l] direction for the superlattice $[Fe_3O_4(100Å)|CoO(30Å)]_{50}$. The sample was cooled to 78 K in 1.4 T field applied along the [110] and [$1\bar{1}0$] directions as well as zero field cooled. Dashed line indicates a broadened, field-independent Fe_3O_4 contri-bution. Inset illustrates the scattering geo-metry.

Magnetoresistive Materials

Interest in the magnetic properties of the doped $LaMnO_3$ class of materials has been renewed recently with the discovery of a dramatic increase in the conductivity when the spins order ferromagnetically, either by lowering the temperature or applying a magnetic field. This large variation in the carrier mobility originates from a metal-insulator transition that is closely associated with the magnetic ordering. To understand the basic physics of this problem, we start with the electronic configuration of the magnetically active Mn ions, which has three d electrons in a t_{2g} orbital. The spins of these electrons are rigidly aligned by a strong Hund's rule exchange coupling to form a core spin (S=3/2) on each Mn ion. On the Mn^{3+} ions such as found in the undoped $LaMnO_3$ compound, there is another d electron, which goes into a higher-energy e_g level. The on-site Hund's rule coupling again favors the parallel alignment of the spin of this extra electron with the core spin. Doping of the La^{3+} with divalent ions then removes some of these e_g electrons, creating Mn^{4+} with empty e_g levels. The remaining e_g electrons may then hop from site to site, forming a conduction band. The on-site exchange interaction is believed to be strong enough in this class of materials to completely polarize the (e_g) conduction electrons in the ground state, forming a "half-metallic ferromagnet". However, hopping, and hence conduction, may only occur if the Mn core spins are parallel, which then directly couples ferromagnetic order with the electrical conductivity at elevated temperatures.

The discovery of these half-metallic ferromagnets provides an extraordinary opportunity to elucidate the magnetic excitations of this unique class of systems, and we have been carrying out inelastic neutron studies on the Ca, Ba, and Sr doped materials to probe the spin dynamics as a function of temperature and field. The ground state spin dynamics for a half-metallic ferromagnet was not expected to differ much from the conventional picture of well-defined spin waves. We found [2] that the long wavelength magnetic excitations were in fact the usual spin waves, with a dispersion relation given by $E=\Delta+D(T)q^2$ where Δ represents the spin wave energy gap and the spin stiffness coefficient D(T) is directly related to the exchange interactions. For the optimal doping concentration of x=1/3 the spin wave gap Δ was too small (< 0.02 meV) to be determined, which demonstrates that these are "soft" isotropic ferromagnets, comparable to very soft amorphous ferromagnets. Measurements in single crystal samples of $La_{0.85}Sr_{0.15}MnO_3$, on the other hand, show that at large q the spin waves in the ground state are heavily damped, indicating a strong magnon-electron interaction. Such an interaction is forbidden in the ground state of a half-metallic ferromagnet, and the large observed damping suggests that hybridization effects in a multiband model must be included in the description of these materials.

With increasing temperature the spin wave linewidths increase rapidly, which again is associated with the itinerant nature of the e_g electrons. More interesting, though, was the discovery of a

quasielastic component of the scattering that develops rapidly as the Curie temperature is approached. Systematic results as a function of Ca doping reveal that this feature is strongest at optimal doping (x~1/3), where it becomes the dominant feature in the spectral weight function as $T \rightarrow T_C$. The width of this scattering is proportional to q^2, indicating that it represents spin diffusion. The correlation length, on the other hand, is anomalously small (~10 Å) and only weakly temperature dependent.

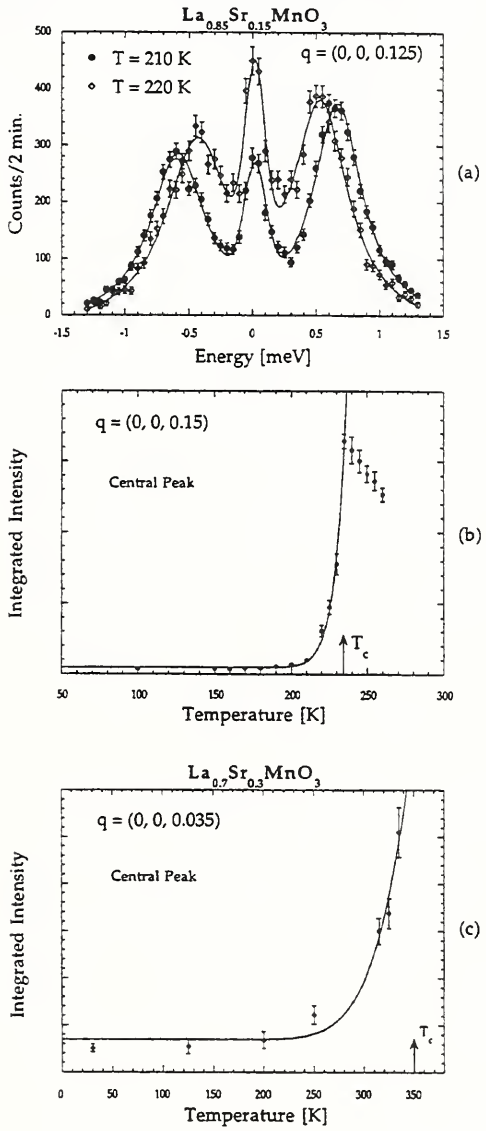

Fig. 3. (a) Constant-q magnetic inelastic spectra collected at 210 and 220 K for $La_{0.85}Sr_{0.15}MnO_3$ (T_C = 235 K), and (b) temperature dependence of the integrated intensity of the quasielastic central com-ponent. (c) T dependence of the quasielastic component for $La_{0.70}Sr_{0.30}MnO_3$ (T_C = 350 K). At this concentration we see that the central component is observable over a much wider temperature range than for the x=0.15 doping.

These results suggest that this quasielastic component is associated with the localization of the e_g electrons on the Mn^{3+}/Mn^{4+} lattice, and may be related to the formation of spin polarons in the system. It is this spin diffusion that drives the ferromagnetic phase transition rather than the thermal population of conventional spin waves.

To further investigate the nature of this spin diffusion component, we have been carrying out additional measurements on the Sr and Ba-doped systems, on polycrystalline samples as well as single crystals. Figure 3(a) shows some inelastic data on $La_{0.85}Sr_{0.15}MnO_3$ (T_C = 235 K), collected at 210 and 220 K for a reduced wave vector q = 0.125 away from the (002) reciprocal point. We see the development of the quasielastic component, and the strength of this scattering is shown in Fig. 3(b) as a function of temperature. We observe a significant intensity starting at 210 K (~25K below T_C,) and the scattering peaks at T_C . At and above T_C all the scattering is quasielastic. For the more heavily doped $La_{0.70}Sr_{0.30}MnO_3$ crystal we find that the central component becomes evident much further away (~100K) from the Curie temperature, as shown in Fig. 3(c). Similar data have been obtained on both polycrystalline and single crystal samples of the Ba-doped system. It thus appears that the coexistence of spin-wave excitations and spin diffusion is a common characteristic for these manganites, and is directly related to the colossal magnetoresistance properties observed in the vicinity of T_C.

Magnetic Resonance Gap

The "magnetic resonance peak" is a strikingly sharp collective magnetic excitation first observed in inelastic neutron scattering experiments on $YBa_2Cu_3O_7$ [3]. The excitation is localized in energy (41 meV) and momentum ($\mathbf{q} = \pi,\pi$), the antiferromagnetic ordering wave vector in the undoped parent compound, and is present only in the superconducting state. As this mode is a novel signature of the superconducting state in the cuprates, proponents of all major theories of high temperature superconductivity have proposed explanations of this phenomenon. These theories can be classified into two basic mechanisms. In the first model, the resonance peak is due to electron-hole pair production across the superconducting energy gap. Interestingly, this

model requires d-wave symmetry of the gap function. While neutron data cannot be reproduced in a generic noninteracting electron model, band structure singularities, spin fluctuations, or interlayer pair tunneling effects have been held responsible for the sharpness of the peak in both energy and momentum. In the second model, the peak originates from a particle-particle resonance which appears in correlated-electron models often used to describe the electronic state in the cuprates. The matrix element coupling this resonance to the magnetic neutron cross section vanishes in the normal state, but is nonzero in the superconducting state. This explanation of the neutron data is also the cornerstone of the recent "SO(5) theory" linking antiferromagnetism and d-wave superconductivity which is generating much attention in the theoretical community. Both of these models are consistent, at least on a qualitative level, with all of the presently available neutron data, including the functional form of the cross section in energy and momentum, the temperature and doping dependencies, and the absolute spectral weight.

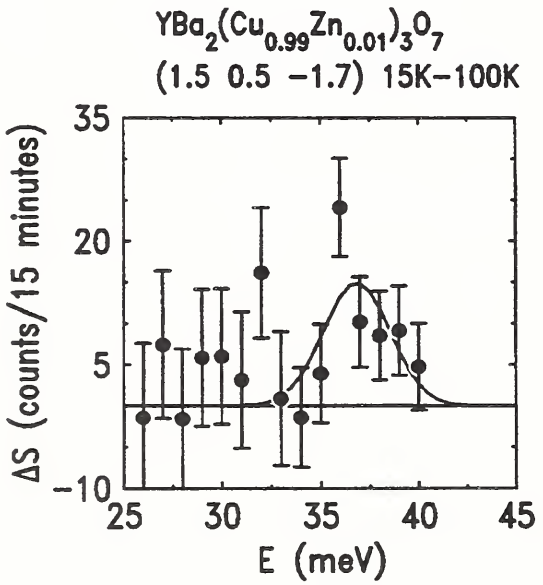

Fig. 4. Difference in the scattering observed above and below the superconducting transition temperature.

The idea behind the Zn substitution experiments is straightforward. Because of the fundamentally different mechanisms responsible for the resonance in both models, the energy at which the resonance occurs is determined by different physical parameters. In the "gap model", the resonance energy is essentially equal to $2\Delta_{max}$, where Δ_{max} is the maximum superconducting energy gap which in turn is proportional to the superconducting transition temperature T_c. In the SO(5) model of Zhang and collaborators, on the other hand, the resonance energy does not depend on the gap, but is instead proportional to the doping level. In previous neutron experiments which showed that the resonance energy decreases as the oxygen level x in $YBa_2Cu_3O_{6+x}$ is decreased, both T_c and the doping level were decreased simultaneously, so that these experiments did not discriminate between the two rival theories. By contrast, Zn substitution suppresses T_c (and thus the gap) dramatically while leaving the carrier concentration almost unaffected. Thus, if the resonance energy decreases significantly with Zn substitution, Zhang's explanation, and with it the entire SO(5) theory, would be disproven.

In the triple-axis experiment, a large single crystal of composition $YBa_2Cu_{2.97}Zn_{0.03}O_7$ was investigated, and evidence for a resolution-limited resonance peak centered at 37 meV was found as shown in Fig. 4. If confirmed and extended in future studies on more heavily Zn-substituted crystals, the observed substantial renormalization of the resonance energy would provide strong support for the gap interpretation of the resonance peak.

Magnetic Theory for R_2CuO_4

Magnetic interactions in rare earth (R) cuprate R_2CuO_4 systems (which become superconducting under electron doping) have been the subject of extensive study. This is mainly due to their simpler structures compared to the hole-doped superconducting cuprates and their novel magnetic properties involving both the Cu- and R-subsystems. In the case of Ce-doped Sm_2CuO_4, coexisting rare earth magnetism and superconductivity has also been observed. Therefore the nature of magnetic interactions which determine the 3 dimensional (3D) magnetic structure and the correlation between rare earth magnetism and superconductivity are both of fundamental importance.

Recently we have developed a theory [4] in which the various novel anisotropic magnetic interactions in the cuprates can be given a microscopic explanation. From these interactions it was possible to have a global understanding of the 3D spin structure of various layered magnetic systems, but many magnetic properties of Nd_2CuO_4 remained unexplained. Among these unexplained properties are the following: 1) Although it is now understood that the R ions exhibit magnetic

moments that are mainly induced by the exchange field of the Cu ions, the role of the R-R interactions is less well quantified. 2) Unlike La_2CuO_4 and $Sr_2CuCl_2O_2$, in R_2CuO_4, the Cu spins prefer a noncollinear arrangement as shown in Fig. 5. A detailed analysis of the energetics of these noncollinear structures on the basis of a microscopic model has not yet been given. 3) In particular, the sequence of spin reorientation phase transitions in Nd_2CuO_4 shown in Fig. 5 (and the absence of such reorientations in Pr_2CuO_4) has not been explained in terms of a microscopic model. It is the purpose of the present work to explain some of these issues. Our conclusions are summarized below.

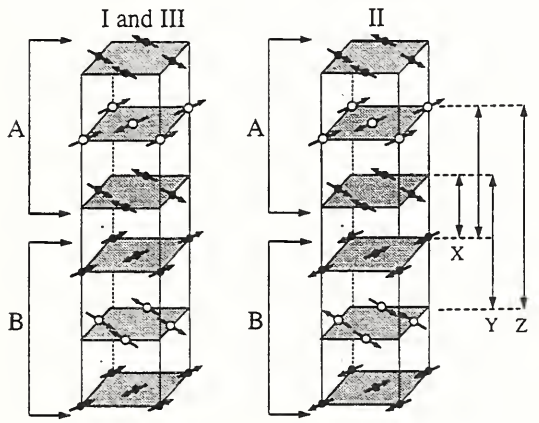

Fig. 5. The magnetic unit cell for the noncollinear phases I, II, and III of Nd_2CuO_4. The open circles are Cu ions and the filled ones Nd ions. Note that in all phases each set of three planes (one Cu plane together with its two neighboring Nd planes) forms a rigid unit (here labeled A and B) within which the relative spin orientations remain fixed. In passing from one phase to another the relative orientations of one rigid unit

We show that due to the exchange field acting on the rare earth ion and crystalline electric field interactions, there is a strong single ion anisotropy which aligns the Cu and R=Pr, Nd magnetization along the [100]-axis, as observed. This same type of calculation also indicates that for Sm in Sm_2CuO_4 the easy axis lies along [001], again in agreement with observations.

Crystalline electric field theory with a Cu-R exchange interaction and an exchange field of the order 0.080 meV for Nd (corresponding to a splitting of the lowest doublet of 0.3 meV), and 0.139 meV for Pr, successfully explains many properties, such as the induced R magnetization, and the splitting of the Kramers doublet, etc., at all temperatures.

We propose a model involving Nd-Nd (X), Nd-Cu (Y), and Cu-Cu (Z) interactions between neighboring tightly bound units A and B due to interactions between the Cu plaquette and the Nd ions adjacent to it as shown in Fig. 5. In view of the frustration, only pseudodipolar interplanar interactions effectively contribute. Then the mean-field free energy is proportional to

$$F \approx \sigma[XM_{Nd}(T)^2 + YM_{Nd}(T)M_{Cu}(T) + ZM_{Cu}(T)^2] = \sigma\Psi(T) \quad (1)$$

where σ is +1 in phases I and III and is -1 in phase II. We find that due to the strong temperature dependence of $M_{Nd}(T)$, the interactions X,Y,

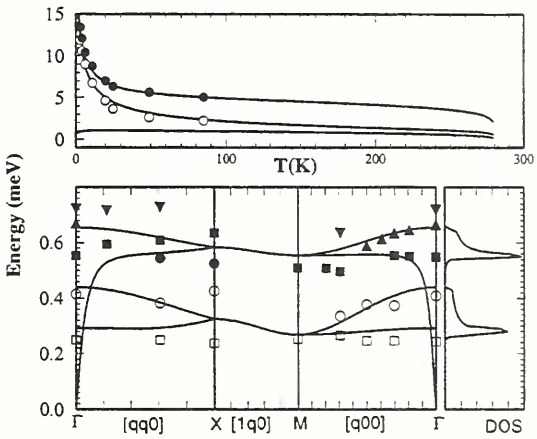

Fig. 6. Top Panel: Temperature dependence of the three spin-wave modes at zero wave vector which involve motion of the Cu spins. The experimental points of Ivanov for two of these modes are shown by filled and open circles. The bottom curve is $200\omega_{ac}$. Bottom Panel: Nd-spin-wave spectrum along various high-symmetry directions. The squares, circles, and triangles are mode energies determined by the inelastic neutron experiments. Note that the calculations (solid line) predict a strong dispersion of the acoustic mode at small wave vector. At the far right we show the density of states.

and Z compete and thus $\Psi(T)$ changes sign twice, leading to the observed successive phase transitions. For Pr_2CuO_4, $M_{Pr}(T)$ is weakly temperature dependent. Therefore $\Psi(T)$ does not change sign with temperature and thus there is no phase transition. This is the simplest model that explains both the three consecutive phase transitions observed in Nd_2CuO_4 as well as the absence of such phase transitions in Pr_2CuO_4.

The final phenomenon which we address is the spin-wave spectrum of Nd_2CuO_4. There are two new ingredients in Nd_2CuO_4 which are not present in, say, La_2CuO_4. The first of these is the existence of low energy excitations on the rare earth sublattices. These excitations will give rise to nearly flat optical magnon modes, reminiscent of the analogous rare earth excitations in the rare earth iron garnets. The second new feature of Nd_2CuO_4 is the noncollinearity of both the Cu and Nd moments. We have calculated the spin-wave spectrum of Nd_2CuO_4 within a simplified three-plane model which qualitatively reproduces the spectrum obtained from inelastic neutron scattering, as is shown in Fig. 6. The resulting Cu-Nd optical modes have a temperature dependence which agrees quite well (see top panel in Fig. 6) with the experimental results. Another interesting feature of this system is the existence of a Goldstone mode which reflects a symmetry of the dipolar interactions with respect to a suitable rotation of the moments in the easy plane. When the four-fold tetragonal anisotropy is taken into account, this mode develops a small gap. The energy of the acoustic spin-wave mode at zero wave vector is predicted to be $\approx(2k_4\Delta)^{1/2} \approx 5$ μeV, where k_4 is the small four-fold anisotropy in the plane and Δ is the splitting of the lowest Nd doublet in the Cu exchange field. This mode has not yet been observed, but clearly its observation is highly desirable.

Spin Ladders

Not only can copper oxides superconduct, but they are also the basis for a number of interesting quasi-one-dimensional S=1/2 quantum magnets. In particular, materials have been synthesized that are experimental realizations of spin-chains (Sr_2CuO_3), spin ladders with two ($SrCu_2O_3$, $Sr_{14}Cu_{24}O_{41}$) and three ($Sr_2Cu_3O_5$) rungs, and spins in a zig-zag chain ($SrCuO_2$). The main exchange interaction in all of these systems comes from the covalent 180° Cu-O-Cu bond and is of order J/k_B ~2000 K (single bond energy). However, because J in these orthorhombic materials only acts in one direction, the systems are magnetically quasi-one-dimensional and Néel order is absent down to very low temperatures. The combination of low dimensionality and the ability to accept hole carriers from off-chain dopants makes these materials unique model systems in which to explore charge transport through a strongly fluctuating magnetic state.

One of the copper-oxide spin chains that we have studied is $SrCuO_2$ [5]. The Cu ions in this material form zig-zag chains along the c-axis as shown in Fig. 7. Susceptibility measurements indicate that $J_2 \approx 180$ meV, while the nearest neighbor 90° Cu-O-Cu exchange interaction is expected to fall in the range -10 meV < J_1 <10 meV, and interchain coupling should be weaker still.

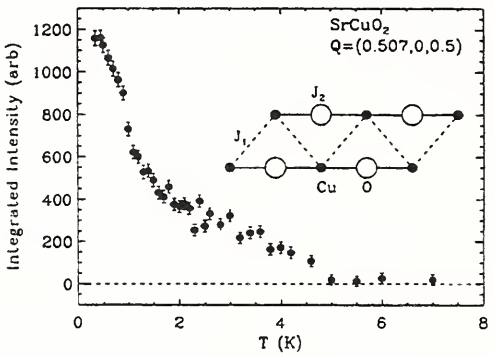

Fig. 7. Temperature dependence of the integrated intensity of the magnetic Bragg peak close to (0.5,0,0.5) in $SrCuO_2$. The data were taken with the crystal oriented in the (*h0l*) zone and thus the coarse vertical resolution is oriented along the b direction where the magnetic correlation length is short. The energy resolution is 0.24 meV. Also shown is a schematic of the zig-zag chain structure.

The zig-zag spin chain with antiferromagnetic next-nearest neighbor interactions, $J_2>0$, is interesting because J_1 and J_2 compete and produce a frustrated one-dimensional magnet. For classical spins (S→∞) and -4< J_1 / J_2 <4 the compromise between these interactions is an incommensurate spiral with $l_m = (1/\pi)/\cos^{-1}(J_1/4J_2)$ where l_m c* is the magnetic wave vector. In the quantum limit (S=1/2), on the other hand, frustration favors dimerization, which always lurks in one dimension, and produces a gap in the excitation spectrum for - 4< J_1 / J_2 < 4.14650. This phase is commensurate with l_m =1 for 2< J_1 / J_2 < 4.14650, but outside this range spin correlations are incommensurate with $l_m \rightarrow 0.5$ for $J_1 / J_2 \rightarrow 0$. The limit corresponds to Néel-like order in decoupled J_2 spin chains. For a pure one-dimensional system, the correlation length at $T=0$ is expected to be finite in the dimerized phase and to vary as $\xi/c \approx 1/(4l_m-2)$ for $J_1/J_2 \rightarrow 0$. The gap should then vary as $\Delta \approx \pi J_2 (2l_m-1)$.

In real materials, the interchain coupling could significantly modify the low temperature behavior, especially when the gap is small, and

this appears to be the case in $SrCuO_2$. Our neutron measurements reveal weak elastic magnetic Bragg scattering developing at $Q_m \approx (0.5,0,0.5)$ for $T_N < T \sim 2$ K, in agreement with indications of magnetic order seen in μ^+SR, specific heat, and susceptibility measurements. Fig. 7 shows the temperature-dependent integrated intensity, where a very unusual order parameter curve is observed, as well as an unusually small ordered moment ($<0.1\ \mu_B$).

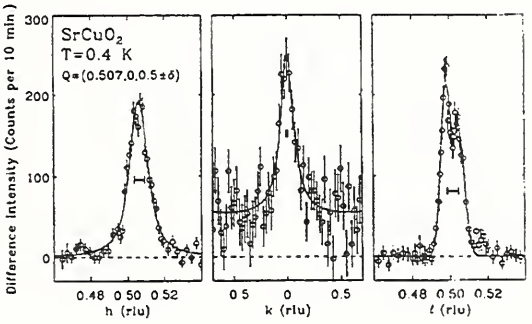

Fig. 8. Diffraction scans through the magnetic elastic scattering close to (0.507, 0, 0.5) in $SrCuO_2$. In all cases a non-magnetic high-temperature background has been subtracted. The energy resolution in these scans was 0.24 meV for (a) and (c) and 0.8 meV for (b). The wave vector resolution is shown by horizontal bars.

Bragg scans through the magnetic diffraction peak are shown in Fig. 8. Along the chain direction, c*, there are in fact two incommensurate peaks with $l_m = 1/2 \pm 0.0036(2)$. Using this value for the incommensurability, the theoretical results above predict $\Delta \approx 4$ meV and $\xi \approx 63\ c$. Experimentally, however, the peaks are resolution limited along the zig-zag spin chains, corresponding to an experimental lower bound on the correlation length $\xi > 500\ c$. Moreover, inelastic scattering clearly shows that the low temperature magnetic excitation spectrum is gapless ($\Delta < 0.1$ meV) close to (0.5,0,0.5), which suggests that the zig-zag chains are coupled with an exchange interaction $zJ' \approx \Delta \approx 4$ meV, where z is the coordination number in the off-chain directions. Under these circumstances, it is reasonable to use the classical expression for l_m to extract an estimate for nearest neighbor interaction $|J_1| = 4\ J_2\ |\cos\ l_m\pi| \approx 8$ meV.

Diffraction scans along directions perpendicular to the chain reveal that the spin order is also incommensurate along a, with a correlation length $\xi \approx 36(2)a$. Most surprising, however, is the very broad peak along the **b** direction, which spans the better part of the Brillouin zone and corresponds to a correlation length $\xi \approx 2.2(5)b$. There is even a temperature-dependent rod of magnetic scattering along this direction, suggesting that the frozen spin structure in $SrCuO_2$ actually consists of nearly perfectly ordered incommensurate two-dimensional layers, which are then stacked with little regard for inter-plane phase coherence along the **b** direction. It remains to be seen whether this is an intrinsic frustration and quantum-fluctuation-induced glassy structure, or whether chemical disorder plays an important role as well.

References

[1] Y. Ijiri, J. A. Borchers, R. W. Erwin, S.-H. Lee, P. J. van der Zaag, and R. M. Wolf, Phys. Rev. Lett., (in press).

[2] J. W. Lynn, L. Vasiliu-Doloc, R. W. Erwin, J. A. Borchers, Q. Huang, A. Santoro, Y. Mukovskii, A.M. de Leon-Guevara, A. Revcolevschi, J.-L. Peng, K. Ghosh, and R. L. Greene (preprints).

[3] H. F. Fong, B. Keimer, and R. W. Erwin (preprint); H.F. Fong, B. Keimer, F. Dogan, and I.A. Aksay, Phys. Rev. Lett. 78, 713 (1997).

[4] T. Yildirim, A. B. Harris, O. E. Wohlman, and A. Aharony, Phys. Rev. Lett. **72**, 3710 (1994); S. Skanthakumar, J. W. Lynn, and I. W. Sumarlin, Phys. Rev. Lett **74**, 2842 (1995); R. Sachidanandam, T. Yildirim, A. B. Harris, and A. Aharony, Phys. Rev. B **56**, 260 (1997).

[5] I. A. Zaliznyak, M. Kibune, H. Takagi, and C. Broholm (preprint).

Research Topics

Analysis of Single Crystals of $Cu(NO_3)_2 \cdot 2.5D_2O$
G. Xu[11], C. Broholm[11] and D. H. Reich[11]

Anisotropic Spin Hamiltonians Due to Spin-Orbit and Coulomb Exchange-Interactions
T. Yildirim[21,42], A. B. Harris[45], A. Aharony[33] and O. Entin-Wohlman[33]

Antiferromagnetic Ordering of $La_{0.33}Ca_{0.66}MnO_3$ Thin Films
Y. Ijiri[21], J. A. Borchers[21], J. W. Lynn[21,42], R. W. Erwin[21], M. Rajeswari[42], M. C. Robson[42], R. Ramesh[42] and V. Venkatesan[42]

Crystal and Magnetic Structures of NiF_3
L. Chacon[37], N. Rosov[21] and J. W. Lynn[21,42]

Crystal Structure and Magnetic Ordering in $CoMoO_3$
Q. Huang[21,42], J. W. Lynn[21,42], R. W. Erwin[21] and M. Crawford[6]

Crystal Structure and Magnetic Order in the Nd-based CMR Compounds

W.-H. Li[19], K. C. Lee[19], R. S. Liu[25], C. Y. Huang[25] and J. W. Lynn[21,42]

Determination of Exchange Interactions Through Spin-pair Scattering in $Zn(Cr_{1-x}Ga_x)_2O_4$

S.-H. Lee[42,21], S.-W. Cheong[14] and C. Broholm[11,21]

Effect of Superconductivity on the Lattice Dynamics of $Ba_{0.6}K_{0.4}BiO_3$

S. Skanthakumar[21,42], J. W. Lynn[21,42] and S. N. Barilo[3]

Effect of Zn Substitution on the Magnetic Resonance Peak in $YBa_2Cu_3O_7$

H. F. Fong[29], B. Keimer[29] and R. W. Erwin[21]

Effects of Si-doping on Magnetic Excitations in the Spin-Peierls System, $CuGeO_3$

S.-H. Lee[21,42], G. Shirane[4], P. Gehring[21] and K. Hirota[34]

Finite-size Effects on Magnetic Ordering in Thin Film Antiferromagnetic CoO Layers

Y. Ijiri[21], S.-H. Lee[21,42], R. W. Erwin[21], C. F. Majkrzak[21], T. Ambrose[11] and C.-L. Chien[11]

Ground-State Selection in FCC and FCT Antiferromagnets Due to Quantum Disorder

T. Yildirim[21,42], A. B. Harris[45] and E. F. Shender[37]

High-Frequency Phonon Dispersion in $La_{1.85}Sr_{0.15}CuO_4$

A. H. Moudden[13], P. M. Gehring[21], L. Vasiliu-Doloc[21,42], B. Hennion[13], M. Matsuda[4], G. Shirane[4], Y. Endoh[34], I. Tanaka[49] and H. Kojima[49]

Incommensurate and Commensurate Magnetic Structures in the Magnetoresistive $R_2Ni_3Si_5$ Materials

S. Skanthakumar[21,42], J. W. Lynn[21,42] and L. C. Gupta[32]

Incommensurate Spin Fluctuations and Structural Transitions in Excess Oxygen-doped La_2CuO_{4+y}.

R. J. Birgeneau[17], Y. S. Lee[17], R. J. Christianson[17], M. A. Kastner[17] and R. W. Erwin[21]

The Invar Effect in $Fe_{65}Ni_{35}$

N. Rosov[21], J. W. Lynn[21,42] and M. Acet[40]

Laue Focussing and Its Applications

V. K. Kuardakov[12], V. A. Somenbow[12], S. Shilstein[12], J. W. Lynn[21,42], D. R. Mildner[23] and H. Chen[23]

Magnetic Correlations in the Bilayer Manganite $La_{1.2}Sr_{1.8}Mn_2O_7$

S. Rosenbranz[2], L. Vasiliu-Doloc[42,21], R. Osborn[2], S. K. Sinha[2], J. W. Lynn[21, 42] and J. F. Mitchell[2]

Magnetic Field Effects on Antiferromagnetic Ordering in a Fe/FeF_2 Bilayer

Y. Ijiri[21], J. A. Borchers[21], R. W. Erwin[21], M.–C. Cyrille[39], I. K. Schuller[39], J. Nogués[36] and D. Lederman[48]

Magnetic Order and Fluctuations in a Zig-Zag Spin-1/2 Chain

I. A. Zaliznyak[11,21], C. Broholm[11,21], M. Kibune[46] and H. Takagi[46]

Magnetic Ordering and Structure of $PrBa_2Fe_3O_8$

N. Rosov[21], J. W. Lynn[21, 42], M. Seyedahmadian[14] and T. Yeun[14]

Magnetic Ordering in $Dy_5Os_4Ge_{10}$

S. Skanthakumar[21,42], J. W. Lynn [21,42], L. C. Gupta[32], M. Lin[8] and S. K. Sinha[2]

Magnetic Order in Pr-containing Cuprate Superconductors

W.-H. Li[19], K. C. Lee[19], H. C. Ku [26] and J. W. Lynn [21,42]

Magnetic Order in Tb-containing Cuprate Superconductors

W.-H. Li[19], K. C. Lee[19] and H. D. Yang[24] and J. W. Lynn [21,42]

Magnetic Order in the Superconductor RNi_2B_2C

J. W. Lynn[21, 42], S. Skanthakumar[21, 42], Z. Hossain[32], L. C. Gupta[32], R. Nagarajan[32] and C. Godart[5]

Magnetic Ordering of Fe_3O_4/NiO Superlattices

J. A. Borchers[21], R. W. Erwin[21], Y. Ijiri[21], D. M. Lind[9], K. A. Shaw[9] and P. Stoyanov[9]

Magnetic Order, Structure, and Spin Dynamics of $(La_{1-x}Ca_x)MnO_3$

R. W. Erwin[21], J. A. Borchers[21], J. W. Lynn[21,42], Q. Huang[21,42], A. Santoro[21], J. L. Peng[42], K. Ghosh[42] and R. L. Greene[42]

Magnetic Properties of Doped $CuGeO_3$

P. Anderson[38], R. N. Shelton[42], S.-H. Lee[21,42], C. Broholm[11] and J. W. Lynn[21,42]

Magnetic Properties of $HoVO_4$

C. K. Loong[2], S. Skanthakumar[21,42], J. W. Lynn[21,42] and G. K. Liu[42]

Magnetic Properties of Ru in $SrRuO_3$ and $Sr_3Ru_2O_7$

S. Skanthakumar[21,42], J. W. Lynn[21,42], G. Cao[9] and J. E. Crow[9]

Magnetism Above the Critical Field in the S=1 One Dimensional Antiferromagnet TMNIN

I. A. Zaliznyak[11,21], D. H. Reich[11] and C. Broholm[11,21]

Neutron Diffraction Studies of Antiferromagnetic Ordering in Thin Film MgO/CoO Superlattices

Y. Ijiri[21], J. A. Borchers[21], R. W. Erwin[21], S.-H. Lee[21,42], P. J. van der Zaag[30] and R. M. Wolf[30]

Neutron Powder Diffraction Determination of $Sr_3Ru_2O_7$
Q. Huang[21,42], J. W. Lynn[21,42], R. W. Erwin[21], A. Santoro[21] and R. J. Cava[29]

Neutron Powder Diffraction Study of the Crystal Structure and Magnetic Ordering of $Y_2Ca_2Cu_5O_{10}$
Q. Huang[21,42], J. W. Lynn[21,42], T. Fong[29], R. J. Cava[29] and B. Keimer[29]

Neutron Powder Diffraction Study of the Crystal and Magnetic Structures in $Ba_3MRu_2O_9$(M=In, Co, Ni, Fe)
Q. Huang[21,42], A. Santoro[21], J. W. Lynn[21,42], R. W. Erwin[21] and R. J. Cava[29]

Observation of Pr Magnetic Order in $PrBa_2Cu_3O_7$
S. Skanthakumar[21,42], J. W. Lynn[21,42], N. Rosov[21], G. Cao[9], J. E. Crow[9], S. Uma[15] and A. Erb[41]

Polarized Neutron Diffraction Studies of Antiferromagnetic Ordering in Exchange-biased Fe_3O_4/CoO Superlattices
Y. Ijiri[21], J. A. Borchers[21], R. W. Erwin[21], S.-H. Lee[21,42], P. J. van der Zaag[30] and R. M. Wolf[30]

Search for Orbital Moments in $La_{2-x}Sr_xCuO_4$
S.-H. Lee[21,42], C. F. Majkrzak[21], S. K. Sinha[2], C. Stassis[10], H. Kawano[35], K. Yamada[34], S.-W. Cheong[14], S. Ueki[34] and Y. Endoh[34]

Single-Ion Anisotropy and Crystal Field Effects in R_2CuO_4 (R=Nd, Sm, Pr, ...)
T. Yildirim[21,42], R. Sachidanandam[33], A. Aharony[33] and A. B. Harris[45]

Spin Chain Direction in Copper Pyrazine Nitrate
M. Stone[11], D. H. Reich[11] and C. Broholm[11,21]

Spin Dynamics of Er^{3+} in $ErBa_2Cu_3O_7$
S. Skanthakumar[21,42], J. W. Lynn[21,42] and F. Dogan[47]

Spin Dynamics of the Mn Ions in $La_{1-x}Ba_xMnO_3$
S. Skanthakumar[21,42], J. W. Lynn[21,42], J. L Peng[42], R. L. Greene[42] and S. Barilo[3]

Spin-flop Tendencies in Exchange-biased Co/CoO Thin Films
J. A. Borchers[21], Y. Ijiri[21], S.-H. Lee[21,42], C. F. Majkrzak[21], G. Felcher[2], R. Kodama[39], K. Takano[39] and A. E. Berkowitz[39]

Spin Freezing in a Geometrically Frustrated Antiferromagnet, $Y_2Mo_2O_7$
J. Gardner[16], B. Gaulin[16], C. Broholm[11] and S.-H. Lee[21,42]

Spin Wave Dispersion Relations in the Magnetoresistive Pyrochlore $Tl_2Mn_2O_7$
J. W. Lynn[21,42], L. Vasiliu-Doloc[21,42] and M. A. Subramanian[6]

Static and Dynamic Properties of Spin and Charge Ordering in $La_{2-x}Sr_xNiO_4$
S.-H. Lee[21,42], S-W. Cheong[14] and G. Aeppli[27]

Structural Phase Transition and Magnetic Order in Heavy Fermion Compounds Ce_3M with M=Al, In, and Sn
W.-H. Li[19], K. C. Lee[19] and Y. Y. Chen[1]

Structure and Dynamics of (La-Sr)MnO_3
L. Vasiliu-Doloc[21,42], J. W. Lynn[21,42], A. H. Moudden[5,13], A. M. de Leon-Guevara[17] and Y. Mukovskii[17]

Structure and Spin Dynamics of the Magnetoresistive Materials $(Sr_{1-x}La_x)_2MoMnO_6$
J. W. Lynn[21,42], Q. Huang[21,42], G. Cao[9] and J. E. Crow[9]

Study of the Origin of Incommensurate Spin Fluctuations in $La_{2-x}Sr_xCu_{1-y}Zn_yO_4$
H. Kimura[34], S. Wakimoto[34], K. Yamada[34], S.-H. Lee[21,42], C. F. Majkrzak[21], R. Erwin[21], G. Shirane[4], Y. Lee[21,42] and R. Birgeneau[17]

Temperature Dependence of Spin Correlations in Y_2BaNiO_5
G. Xu[11], T. Ito[7], H. Takagi[46], K. Oka[7], C. Broholm[11,21] and G. Aeppli[27]

Three-dimensional Spin Structure of $Sr_2CuO_2Cl_2$: Field Dependent Neutron Scattering Study
T. Yildirim[21,42], S. Skanthakumar[21,42] and J. W. Lynn[21,42]

Vortex Lattice and Melting in Nb
J. W. Lynn[21,42] and N. Rosov[21]

Vortex Lattice Structure and Melting in $Ba_{0.6}K_{0.4}BiO_3$
J. W. Lynn[21,42], N. Rosov[21] and S. N. Barilo[3]

Affiliations

[1] Academia Sinica, Taiwan
[2] Argonne National Laboratory
[3] Belarus Academy of Sciences, Belang
[4] Brookhaven National Laboratory
[5] Centre National de Recherche Scientific, France
[6] Dupont Company
[7] Electrotechnical Laboratory, Japan
[8] Exxon Research & Engineering Company
[9] Florida State University
[10] Iowa State University
[11] Johns Hopkins University
[12] Kurchatov Institute, Russia
[13] Laboratoire Léon Brillouin, France
[14] Lucent Technologies, Bell Laboratories
[15] Max Plank Institute, Germany
[16] McMaster University, Canada

[17] Massachusetts Institute of Technology
[18] Moscow Steel and Alloys Institute, Russia
[19] National Central University, Taiwan
[20] National Institute for Research in Inorganic Materials, Japan
[21] NIST, Center for Neutron Research
[22] NIST, Ceramics Division
[23] NIST, Nuclear Methods Group
[24] National Sun Yat-Sen University, Tawain
[25] National Taiwan University, Tawain
[26] National Tsing Hua University, Tawain
[27] NEC Research Institute Inc.
[28] Pennsylvania State University
[29] Princeton University
[30] Philips Research Laboratories, The Netherlands
[31] Shanghai Institute of Metallurgy, China
[32] Tata Inst. Of Fundamental Res., India
[33] Tel Aviv University, Israel
[34] Tohoku University, Japan
[35] Tokyo University, Japan
[36] Universitat Autònoma de Barcelona, Spain
[37] University of California at Berkeley
[38] University of California at Davis
[39] University of California at San Diego
[40] Universität Duisberg, Germany
[41] University of Geneva, Switzerland
[42] University of Maryland at College Park
[43] University of Oslo, Norway
[44] University of Paris, France
[45] University of Pennsylvania
[46] University of Tokyo, Japan
[47] University of Washington
[48] West Virginia University
[49] Yamanashi University, Japan

Crystallography

The World Wide Web (WWW) based proposal and beam time request system was fully implemented for the 32-detector high-resolution powder diffractometer at BT-1 in FY97. Approximately 120 proposals were received and scheduled in the system's first year of operation. Over 1000 data sets were collected on approximately 320 different materials under various experimental conditions. A few examples of the wide range of studies are highlighted in this section; many other crystallographic contributions are included in the sections on Chemical Physics of Materials and Magnetism and Superconductivity.

A materials screening program with a WWW interface was also implemented, so that a researcher may anticipate potential difficulties before scheduling an experiment. Input of chemical formula and sample density is used to calculate beam attenuation, due to either neutron absorption and/or incoherent scattering and an estimate of neutron activation assuming a 24 h irradiation. The program alerts researchers to samples with high beam attenuation ($\mu R > 1$), considerable gamma radiation while in the beam, or significant immediate or long-term neutron activation. It is planned to expand these capabilities to allow for more accurate estimation of neutron activation based on the actual sample irradiation history. This WWW page may be accessed from http://rrdjazz.nist.gov/~toby.

Instrumentation

- **Ge(311) Monochromator**

The available data collection options were greatly enhanced with the installation of a new Ge(311) monochromator at the 75° take-off angle position, replacing the old Cu(220) monochromator. The five Ge crystals were hot-pressed to give a mosaic spread of 0.25° and placed in the focusing holder and aligned. The Ge(311) wavelength of approximately 2.08 Å is ideal for the study of zeolites and other materials with large unit cells and also for structures with magnetic reflections for which the complete absence of $\lambda/2$ intensities greatly facilitates the identification of superstructure peaks. Additionally, the greater diffracted intensity provided by the longer wavelength permits the study of smaller samples in a reasonable data collection time. The characteristics of the three monochromator options are summarized in Table 1.

Table 1. BT-1 Monochromator Options

Mono-chromator	Take-off Angle (°)	Wavelength (Å)	Relative Intensity
Ge(311)	75	2.079	3.34
Cu(311)	90	1.540	1.00
Si(531)	120	1.590	0.33

- **Incident Collimation**

A new 7′ in-pile collimator was installed in place of the original one that had been damaged. Instead of using aluminum blades, the new collimator has stretched film ("PEEK", poly ether ether ketone) coated with Gd_2O_3. The resultant neutron flux is approximately twice that which was obtained with the Al-blade collimator, even when initially installed. The ratio of diffracted intensities using the 7′ and 15′ in-pile collimators ranges from 0.55 to 0.70 for the three monochromators. This is significantly greater than the theoretical value of 0.47, indicating that a PEEK film 15′ collimator might give increased intensity over that obtained with the current Al collimator. A new 15′ collimator has been ordered. The neutron flux was measured at the sample position using Au foil and was found to be 7×10^5 n/cm^2/s for the Ge(311) monochromator at 15′ in-pile collimation.

- **Background Reduction**

The low-angle background was significantly reduced through the addition of an incident slit system that eliminates much of the fast neutron background. Incident beam widths up to 16 mm (5/8 in) are allowed. The difficulties with fast neutron background at high angles have yet to be resolved, but are much less important.

Crystal Structures

- **A New Phase of ReO_2**

Rhenium oxides are often used to improve supported metal catalysts used in hydrogenation reactions. Under the conditions of plant operation, it has generally been assumed that the rhenium oxide is reduced to rhenium metal. However, there has been some speculation that partially oxidized Re may also be present. Thus,

XANES/EXAFS experiments were carried out at the APS to determine both the oxidation state and the coordination geometry around the Re atoms. As part of this experiment, the spectra of a number or rhenium oxide standards were measured and analyzed. The spectrum of ReO_2 (obtained commercially), however, proved to be problematic; the observed spectrum did not match with that calculated from the orthorhombic crystal structure reported in 1957. Since the reported structure determination was not of high quality, it was decided to re-refine the structure using neutron powder diffraction in order to obtain more accurate oxygen positions.

An examination of the neutron powder pattern revealed that the known orthorhombic ReO_2 phase made up only a small fraction of the material. Matching the unknown lines against other known phases of rhenium oxides demonstrated that the material was contaminated with a significant amount of ReO_3, in addition to yet another unknown phase. A general search matching the major d-spacings of the unknown phase hit upon one form of MoO_2 with slightly different monoclinic unit cell parameters. The structure of this new monoclinic form of ReO_2, along with that of the orthorhombic ReO_2 and the cubic ReO_3 phases, was refined in a simultaneous refinement of the neutron powder data and synchrotron x-ray data collected at the APS.

The results show that the commercial sample of ReO_2 consisted of the following three phases: (a) the known orthorhombic phase of ReO_2 (14.5%), space group *Pbcn*, a = 4.8084(5), b = 5.6318(6), c = 4.6118(4) Å; (b) the previously unknown monoclinic phase of ReO_2 (61.3%), space group $P2_1/c$, a = 5.6149(2), b = 4.8117(2), c = 5.5552(4) Å, β = 120.554(4)°; and (c) the known cubic phase of ReO_3 (25.2%), space group *Pm3m*, a = 3.7483(1) Å. The reason for the poor fit between the observed and calculated EXAFS patterns is now clear. The ReO_2 "standard" is actually a mixture of three phases in which the rhenium has two different oxidation states.

- **$Ba_3Fe_{21}Ti_8O_{53}$**

The desire to produce smaller and lighter radio devices, such as cellular telephones, has driven research efforts to identify new materials with high dielectric constants and to attempt to understand the factors that cause some materials to have high dielectric constants while similar related materials do not. The barium-iron titanates are being systematically studied by the NIST Ceramics Division due to the wide variation in electronic properties seen in this phase field.

The crystal structure of one new material in this series was first investigated by single crystal x-ray diffraction. The unit cell was found to be monoclinic, space group *C2/m*, with approximate dimensions a = 19.41, b = 20.28, c = 10.08 Å; β = 105.27°. The single crystal study was able to demonstrate that the asymmetric unit for this material consists of 54 atomic sites: three occupied by Ba atoms, 33 by O atoms and 18 shared by Fe and Ti atoms. If all sites are fully occupied, the chemical formula would be $Ba_3Fe_{31-x}Ti_xO_{53}$; however, valence arguments predict a formula of $Ba_3Fe_{21}Ti_8O_{53}$ with a vacancy level of ~3% for the Fe/Ti atomic sites. Analysis of the x-ray data could not determine the distribution of Fe and Ti atoms among the shared sites and gave no information about likely vacancy locations.

The structure was next refined using Rietveld refinement of combined x-ray synchrotron and neutron powder diffraction data. The atomic coordinates for the atoms on all 54 sites were refined, as well as the Ti and Fe atom occupancies for all 18 shared sites with no chemical or physical constraints. Since no constraints on bond distances or on occupancies were used, the reliability of the results can be evaluated from the refined site occupancies and chemical composition: the smallest observed occupancy was 0.01(4) and the largest total site occupancy was 1.01(9). The net chemical composition was determined to be $Ba_3Fe_{21.1}Ti_{7.9}O_{53}$ in excellent agreement with the predicted formula. A large portion of the vacancies were demonstrated to occur on one crystallographic site with Fe occupancy of 0.66(3) and Ti occupancy of 0.08(4). It is very likely that the remainder of the vacancies are distributed over several other sites.

- **Structure and Magnetic Order in $La_{1-x}Ca_xMnO_3$**

Interest in rare-earth manganites has been recently stimulated by the observation of "giant" (and even "colossal") magnetoresistance. These compounds have the basic perovskite structure and display numerous and complex magnetic and structural transitions, some of which are strongly coupled with changes of electrical conductivity. Since the magnetic structures of these materials depend on the coupling of Mn^{3+} and Mn^{4+} cations, methods have been devised to change the relative

concentrations of these cations. The system $La_{1-x}Ca_xMnO_3$ has been studied extensively because it offers the possibility of varying the Mn formal valence over the entire range between +3 and +4, without significant change of the La/Ca size, due to the fact that the ionic radii of La^{3+}(XII) and Ca^{2+}(XII) are almost identical (1.36 and 1.34 Å, respectively).

In order to establish the relationship between crystal structure and magnetic and electronic properties in rare-earth manganites, the nuclear and magnetic structures of $La_{1-x}Ca_xMnO_3$ have been studied by neutron powder diffraction methods for the compositions x = 0.06, 0.15, 0.175, 0.25 and 0.33. At low concentrations of Ca (x = 0.06) the oxidized sample contains cation vacancies and the structure is ferromagnetic, while in reduced samples all atomic sites are fully occupied and the structure is antiferromagnetic. This result explains the discrepancies found in published phase diagrams. In the samples with compositions $x \geq 0.15$ the structural distortions associated with the magnetic and electronic transitions increase with increasing Ca content. These distortions consist mainly of an increase in the tilting of the MnO_6 octahedra and a consequent sharp decrease of the Mn-Mn separations as the system becomes metallic and ferromagnetic. These readjustments of the structure may be responsible for the metallic character of the bonds at the transition from insulating to metallic behavior. The magnetic field dependence of the lattice parameters, studied in sample x = 0.33 at two fixed temperatures (270 and 240 K), demonstrates that there is strong coupling between the magnetization and the structural properties in this system.

- **Template Location in Zeolite CIT-1**

The CIT-1 zeolite is unique in that when synthesized using a N,N,N-trimethyl-(-)-cis-myrtanylammonium cation as a structure directing agent (SDA), the zeolite grows nearly free of stacking faults. Several other similar organic amines can be used as SDAs to produce a version of the same zeolite that is heavily faulted, SSZ-33. Relatively little is understood about the interactions between SDAs and zeolites. Stacking faults occur in many zeolite systems; this particular system provides an opportunity for the study of the effect of the SDA on zeolite structure as well as the genesis of stacking faults.

Metropolis Monte-Carlo docking techniques were used to identify possible locations where the SDA molecules can be accommodated by the CIT-1 pore structure at high loading levels. Only three such locations were found from 12 attempts. Rietveld refinement using both neutron and synchrotron x-ray powder diffraction data from a sample of CIT-1 containing a partially deuterated SDA and a non-deuterated SDA demonstrated that the molecules are sited in two of these locations, but not the third. The SDA molecules pack tightly in the CIT-1 pores demonstrating how these molecules provide a scaffolding that the zeolite crystallizes around (see Fig. 1). Additional molecular mechanics analysis is in progress to study the energetics of SDA packing for different template molecules in several configurations.

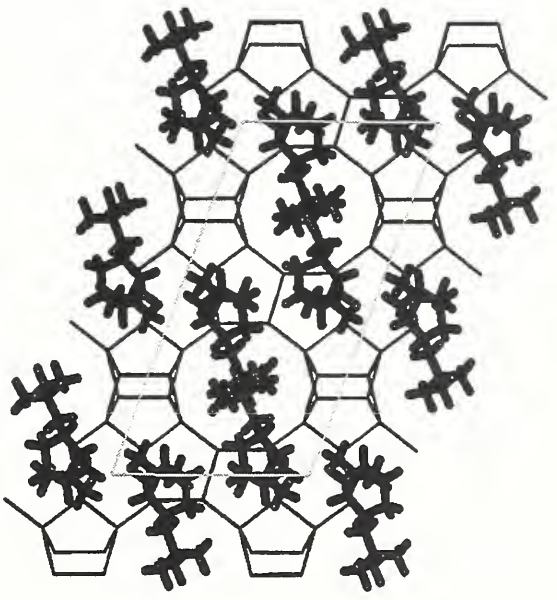

Fig. 1. A view of the CIT-1 tetrahedral atoms comprising the zeolite framwork (thin lines) viewed down the *b* axis. The packing of structure-directing organic molecules as determined by Rietveld refinement and molecular mechanics is shown with thick lines.

- **Template Mediated Growth of Rare Earth Carbides**

Highly oriented pyrolytic graphite (HOPG) consists of an array of grains that share a common *c* axis, but which are randomly oriented in the *a*—*b* plane. When reacted with thulium in the solid state, wafers of pure HOPG form highly oriented carbide samples. This reaction destroys the graphitic layers and disperses the carbon atoms throughout the interstitial sites of a new lattice formed by rare-earth atoms. Even though the

graphite is completely consumed during the reaction, its texture and morphology are inherited by the carbide product. The graphite thus provides a template for the growth of the carbide sample.

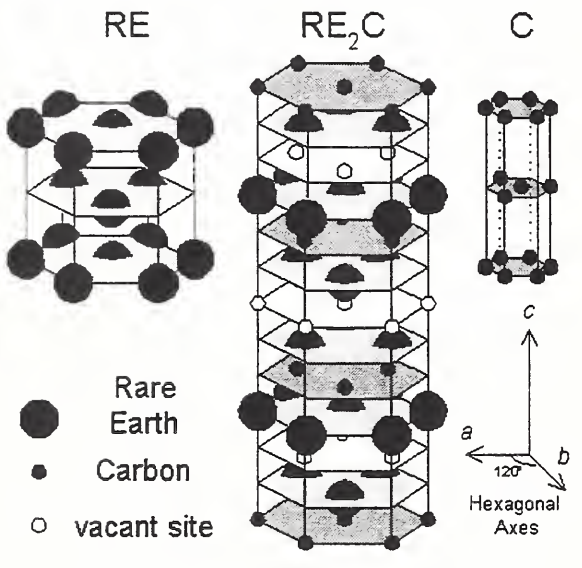

Fig. 2 A comparison, drawn to scale, of the typical rare earth metal (RE), trigonal hypocarbide (RE_2C) and graphite (C) crystal structures. Note the hypocarbide's similarity to the pure metal and its dissimilarity (particularly in lattice spacing) to graphite.

When thulium metal vapor was reacted with HOPG, the increased mass of the HOPG wafers indicated the formation of the previously unreported hypocarbide Tm_2C. Neutron diffraction data were obtained on triple axis spectrometers. The observed intensities were independent of sample rotations about the *c* axis, but revealed a *c*-axis mosaic of about 3°, approximately 30% larger than that of the HOPG reactant. The space group was identified as $R\bar{3}m$, the same as for all other RE_2C compounds, with unit cell parameters a = 3.56(1) and c = 17.45(2) Å comparable to those of the RE_2C phases of the neighboring rare earth hypocarbides. Whereas a perfectly ordered RE_2C compound has one fully occupied carbon 3*a* site (0,0,0) at z = 0, this material was found to have two partially occupied carbon sites at z = 0 and ½ (site 3*b*) with fractional occupancies of 0.76(5) and 0.16(4), respectively. The thulium atoms fully occupy the 6*c* sites at 0,0,z with z = ¼ + δ, where δ represents a slight shift of a thulium layer toward the higher density interstitial carbon layer.

Figure 2 shows a comparison of the structures of the rare earth metals, RE_2C and graphite. In spite of the dissimilarities between the graphite and hypocarbide lattices, the hypocarbide adopts the same orientational texture and morphology as the parent HOPG material. A growth mechanism is proposed where the hypocarbide forms between two distinct interfaces, one with the thulium vapor which is commensurate and the other with the graphite which is incommensurate. The low corrugation potential provided by the graphite allows the hypocarbide to grow to macroscopic thickness without destroying the texture and morphology which the graphite imparts to the hypocarbide. This is believed to be the first observation of a complete template-mediated reaction on a macroscopic scale.

NIST Crystallographic Data Center

In FY97 the NIST Crystallographic Data Center initiated a new collaborative project on full structural crystallographic descriptions of inorganic materials. Two new partnerships have been formalized, one with FIZ Karlsruhe and the Gmelin Institute in Germany (Inorganic Crystal Structure Database), and a second with Toth Information Systems in Canada (Metals and Intermetallics Database). The participants will work together to develop and maintain a collection of evaluated data, with full structural information on non-organic crystalline substances, and to disseminate these data in computerized formats to researchers and software developers worldwide. These collaborations will form the basis for future Data Center activities.

The existing NIST Crystal Data database, which contains evaluated crystallographic data such as unit cell parameters but does not contain atomic coordinates, has also continued to be developed and upgraded. A major effort was made this year to reorganize, restructure, and document Data Center operations so that these operations can be continued while new products are created by the same staff. As part of this modernization effort, a new version of the Master Database, containing approximately 240,000 entries, was implemented using a modern database management software package. Also during this year, several scientific evaluation and processing routines were revised, and approximately 20,000 inorganic entries were reevaluated and edited. Concurrent with these efforts, the two distribution databases, NIST

Crystal Data and the Electron Diffraction Database, were produced for distribution to the scientific community.

Research Topics

Template Mediated Growth of Rare Earth Carbides
L. J. Santodonato[26], D. A. Neumann[26] and R. W. Erwin[26]

Proton Sites in ZSM-5
A. Peters[11], R.-H. Hu[57], S. Purnell[57] and B. H. Toby[26]

High Dielectric Ba-Fe Titanate Ceramics
T. Siegrist[18], T. A. Vanderah[27], W. Wong-Ng[27], L. Bendersky[28] and B. H. Toby[26]

High Dielectric Ba-Lanthanide Titanate Perovskites
T. Negas[39], C. Rawn[30], N. Khosrovani[37,26] and B. H. Toby[26]

Cation Ordering in $(Pb,Ca)TiO_3$ Perovskites
B. Burton[27], E. K. Goo[53], L. Schioler[23] and B. H. Toby[26]

Determination of Amorphous Content in Alumina SRM676
J. Cline[27] and B. H. Toby[26]

Template Siting in Zeolite CIT-1
N. Khosrovani[37,26], M. Davis[9] and B. H. Toby[26]

A Search for Orthorhombic Forms of Faujasite
J. B. Higgins[3], J. E. MacDougall[3] and B. H. Toby[26]

High Temperature Structure Characterization of Metal Oxides
J. B. Higgins[3] and R. Hamilton[3]

Structural Studies of Zeolites for Gas Separations
J. B. Higgins[3]

Magnetic Scattering Studies of $Tl_2Mn_2O_7$
J. Greedan[20], M. Subramanian[12] and B. H. Toby[26]

Combined X-ray and Neutron Crystal Structure of $Ba_4Ti_{10}M_2O_{27}$ (M = Al, Mg, Zn)
J. Kaduk[4], B. H. Toby[26], W. Wong-Ng[27] and W. Greenwood[50]

Crystallographic Studies of BaR_2ZnO_5 (R = La, Nd, Dy, Ho, Er, Y)
W. Wong-Ng[27], B. H. Toby[26] and W. Greenwood[50]

Neutron Diffraction Study of Li Siting in Zeolites
R. Lobo[46], M. Feuerstein[46] and A. Burton[46]

Neutron Diffraction Study of a ReO_2 Catalyst
R. Harlow[12] and B. H. Toby[26]

In-Situ Dehydration Studies of the SRM2851 (NaA) Zeolite
N. Khosrovani[37,26] and B. H. Toby[26]

In Situ Studies of CFC Loading of Zeolites
J. B. Parise[37], Y. Lee[37], N. Khosrovani[37,26] and B. H. Toby[26]

Structural Studies of Fast-Ion Conductors $Y_2(Sn,Ti)_2O_7$, $(Y,Ca)_2Ti_2O_7$, $(Yb,Ce)_2Ti_2O_7$ and $(La,Ca)_2Sn_2O_7$
K. Eberman[19], B. J. Wuensch[19] and J. K. Stalick[26]

Neutron Investigation of the Crystal Structure of Zr_9Pd_{11}
J. K. Stalick[26] and R. M. Waterstrat[28]

Quantitative Phase Analysis of ZrO_2 Powders
J. K. Stalick[26] and J. Ilavsky[2]

Effect of Annealing on Phase Composition and Yttria Content of Plasma-Sprayed YSZ Coatings
J. Ilavsky[2] and J. K. Stalick[26]

Phase Analysis of Sintered Yttria-Stabilized ZrO_2 for Potential SRM
J. Wallace[27] and J. K. Stalick[26]

Neutron Powder Diffraction Study of $BaNd_2O_4$
W. Wong-Ng[27] and J. K. Stalick[26]

Structural Studies of Templated and Calcined SSZ-35 and CIT-5
P. Wagner[9] and M. Davis[9]

Structure of the Frustrated Magnet $Y_2Mo_2O_7$
J.Gardner[20], S.-H. Lee[50], B. D. Gaulin[20] and C. Broholm[15]

Magnetic Ordering in the System $La_{1-x}Pr_xBaCuFeO_5$
A. W. Mombru[40], F. Araujo-Moreira[50] and L. Suescun[40]

Neutron Diffraction Study of the Electrostriction in PMN Based Relaxor Ferroelectrics
Q. Zhang[34] and J. Zhao[34]

Neutron Diffraction Studies of Intercalated Poly(ethyleneoxide)/Layered Silicate Nano-composites
R. Krishnamoorti[48], R. A. Vaia[58], E. P. Giannelis[10] and N. C. Maliszewskyj[26]

Structure of Deuterated Kevlar
N. C. Maliszewskyj[26], M. Crawford[12] and T. J. Udovic[26]

Effect of Residual Stress and Particle Size of Ni,Fe in Tungsten
S. F. Trevino[26.6] and W. Bruchey[6]

High Pressure Phase Transitions and Structure of $Ba_{1-x}Sr_xRuO_3$
Q. Huang[26,50], A. Santoro[26], R. J. Cava[35] and S. F. Trevino[26.6]

High Pressure Neutron Diffraction Study of

Deuterated γ-Picoline
J. Cook[26,50], S. F. Trevino[26,6] and D. A. Neumann[26]

Search for a High Pressure Phase Transition in Dipicrylresorcinol
S. F. Trevino[26,6], J. Cook[26,50] and D. A. Neumann[26]

Location of H_2 in Graphite Nanofibers
S. F. Trevino[26,6] and N. Rodriguez[29]

Neutron Diffraction Study of Ropes of Carbon Nanotubes
Z. Benes[52], J. E. Fischer[52], P. Papanek[26,52] and D. A. Neumann[26]

Neutron Diffraction Study of Interstitial Hydrogen in C_{60}
S. A. FitzGerald[26], D. A. Neumann[26], L. J. Santodonato[26], J. R. D. Copley[26], T. Yildirim[26,50] and J. J. Rush[26]

Neutron Diffraction Study of Na_2C_{60} as a Function of Temperature and Pressure
T. Yildirim[26,50], S. F. Trevino[26,6], D. A. Neumann[26] and J. E. Fischer[52]

Neutron Diffraction Study of KC_{60}
H. Guerrero[31], R. L. Cappelletti[31], T. Yildirim[26,50] and D. A. Neumann[26]

Neutron Diffraction Study of Na_xC_{60}
T. Yildirim[26,50], S. A. FitzGerald[26], L. Santodonato[26] and D. A. Neumann[26]

Neutron Diffraction Determination of the Phase Diagram of $Ni_2Mn_{1+x}Ga_{1-x}$
R. Overholser[50], M. Wuttig[50] and D. A. Neumann[26]

Neutron Diffraction Study of Ba_3NiNbO_7 and Sr_3NiNbO_7
M. Green[33], M. Rosseinsky[33] and D. A. Neumann[26]

Neutron Diffraction Study of $(LaSr)NiO_4$
M. Green[33], M. Rosseinsky[33] and D. A. Neumann[26]

Characterization of Candidate Materials for Ceramic Membranes
H. J. Prask[26] and P. C. Brand[26]

Determination of Percent Retained Austenite in Steel
H. J. Prask[26], P. C. Brand[26], C. S. Choi[26], G. Hicho[28] and W. Sharpe[5]

Structural and Magnetic Phase Transitions in $KMnF_3$
P. M. Gehring[26], S. M. Shapiro[8] and A. Gibaud[49]

Crystal Structure of the Semiconductor $ZnGa_2Se_4$
F. Izumi[22], Q. Huang[26,50] and A. Santoro[26]

Neutron Powder Diffraction Study of the Structure of the Superconductor $Nd_{1.62}Ba_{2.28}Cu_{3.30}O_y$
Q. Huang[26,50] and C. Chongbin[36]

Crystal and Magnetic Structure Transitions in Fe_2TiO_4
Q. Huang[26,50]

Neutron Investigation of the Crystal and Magnetic Structures of $NdBaFe_2O_{5.13}$
Q. Huang[26,50], P. Karen[51], A. Santoro[26], V. L. Karen[26] and A. D. Mighell[26]

Study of Carbon in $YBa_2Cu_{2.7}C_{0.3}O_{7.12}$
Q. Huang[26,50], P. Karen[51], A. Santoro[26], V. L. Karen[26] and A. D. Mighell[26]

Neutron Powder Diffraction Studies of the Crystal and Magnetic Structures of $Ba_3MRu_2O_9$ (M = In, Co, Ni, Fe)
Q. Huang[26,50], A. Santoro[26], J. W. Lynn[26,50], R. W. Erwin[26] and R. J. Cava[35]

Neutron Powder Diffraction Determination of the $Sr_3Ru_2O_7$ Layer Structure
Q. Huang[26,50], J. W. Lynn[26,50], R. W. Erwin[26], A. Santoro[26] and R. J. Cava[35]

Nuclear and Magnetic Structures of $La_{1-x}Ca_xMnO_3$ (x = 0.25 and 0.33)
Q. Huang[26,50], J. W. Lynn[26,50], R. W. Erwin[26] and A. Santoro[26]

Structures of the Solid Solution of Pb-Ba-Na-K-Na-Sr-Nb-O
Q. Huang[26,50] and R. Guo[34]

Crystal Structure and Magnetic Ordering in $CoMoO_{4-\delta}$
Q. Huang[26,50], J. W. Lynn[26,50], R. W. Erwin[26] and M. Crawford[12]

Neutron Powder Diffraction Study of the Crystal Structure and Magnetic Ordering of $Y_2Ca_2Cu_5O_{10}$
Q. Huang[26,50], J. W. Lynn[26,50], R. W. Erwin[26], H. F. Fong[35], R. J. Cava[35] and B. Keimer[35]

Neutron and X-ray Diffraction Study of the Crystal Structure of $Bi_{11}Sr_9O_x$
Q. Huang[26,50] and W. Wong-Ng[27]

Neutron and X-ray Diffraction Study of the Crystal Structure of $CuGe_{1-x}(Al,B)_xO_3$
Q. Huang[26,50] and W. Wong-Ng[27]

Structure Characterization of the Proton Conductor $Ba_3Ca_{1.18}Nb_{1.82}D_{0.9}O_{9-y}$
Q. Huang[26,50], C. Karmonik[26], T. J. Udovic[26] and J. J. Rush[26]

Phase Analysis of TiO_2 - Al_2O_3 - Co
Q. Huang[26,50] and M. Lin[13]

Crystal Chemistry of Perovskites: Study of Mixed Cubic-Hexagonal Closest-Packed Stackings
A. Santoro[26]

Neutron Powder Diffraction Study of the Temperature-Dependent Site Occupation of D

in YD_2
T. J. Udovic[26], Q. Huang[26,50], F. Altorfer[26,50] and J. J. Rush[26]

Neutron Powder Diffraction Studies of MD_{3-x} (M = Y, Lu, Tb, Dy, Ho)
T. J. Udovic[26], Q. Huang[26,50] and J. J. Rush[26]

Neutron Powder Diffraction Studies of LaD_{2+x}
T. J. Udovic[26], Q. Huang[26,50] and J. J. Rush[26]

Neutron Powder Diffraction Study of $Pd_9Si_2D(H)_x$
T. J. Udovic[26], Q. Huang[26,50], C. Karmonik[26], J. J. Rush[26], Y. Andersson[55] and T. B. Flanagan[56]

Neutron Powder Diffraction Study of Isotope Effects in $La(H_yD_{1-y})_{2.50}$
T. J. Udovic[26], Q. Huang[26,50] and J. J. Rush[26]

Neutron Powder Diffraction Study of $NbD(H)_x$ ($0.72 \leq x \leq 0.92$)
B. Hauer[16], R. Hempelmann[41], D. Richter[16], T. J. Udovic[26] and J. J. Rush[26]

Absorption Corrections for Diffraction from Cylindrical Shells
N. Rosov[26] and J. W. Lynn[26,50]

Structure and Magnetic Order In Undoped Lanthanum Manganite
Q. Huang[26,50], A. Santoro[26], J. W. Lynn[26,50], R. W. Erwin[26], J. A. Borchers[26], J. L. Peng[50] and R. L. Greene[50]

Magnetic Ordering and Structure of $PrBa_2Fe_3O_8$
N. Rosov[26], J. W. Lynn[26,50], M. Seyedahmadian[38] and T. Yuen[38]

Structure and Magnetic Order in Ca-Doped Lanthanum Manganite
Q. Huang[26,50], A. Santoro[26], J. W. Lynn[26,50], R. W. Erwin[26], J. A. Borchers[26], J. L. Peng[50], K. Ghosh[49] and R. L. Greene[50]

Crystal and Magnetic Structure of $Sr_3Ru_2O_7$
S. Skanthakumar[26,50], J. W. Lynn[26,50], G. Cao[14] and J. E. Crow[14]

Magnetic Order in $Y_{2-x}Ca_{2+x}Cu_5O_{10}$
B. Keimer[35], H. F. Fong[35] and J. W. Lynn[26,50]

Crystal Structure of $TlSr_2RECu_2O_7$ and Related Compounds
W.-H. Li[21], K. C. Lee[21], J. W. Lynn[26,50], C. C. Lai[25], H. C. Ku[25] and S. Y. Wu[21]

Crystal Structure of $TbBa_2Cu_3O_7$
W.-H. Li[21], K. C. Lee[21], J. W. Lynn[26,50], C. C. Lai[25], H. C. Ku[25] and S. Y. Wu[21]

Crystal Structures of Nd-Based CMR Compounds
W.-H. Li[21], K. C. Lee[21], R. S. Liu[24] and C. Y. Huang[24]

Structural Phase Transition and Magnetic Order in Heavy Fermion Compounds Ce_3M (M = Al, In, Sn)
W.-H. Li[21], K. C. Lee[21] and Y. Y. Chen[1]

Magnetic Ordering and Structure of $(Pr,Nd)_{1-x}Ce_xSr_2Cu_2(Nb,Ta)O_{10}$
N. Rosov[26], J. W. Lynn[26,50], T. Goodwin[44], R. Shelton[44] and H. Radousky[17]

Neutron and X-ray Powder Diffraction Study of $REBa_2Fe_3O_{8+w}$ Phases
P. Karen[51], A. Kjekshus[51], I. Natali Sora[42], Q. Huang[26,50], V. L. Karen[26], A. D. Mighell[26], J. W. Lynn[26,50], N. Rosov[26] and A. Santoro[26]

Charge and Magnetic Ordering in NiF_3
L. Chacon[43], N. Rosov[26] and J. W. Lynn[26,50]

The NIST Crystal and Electron Diffraction Data Center
V. L. Karen[26] and A. D. Mighell[26]

International Tables for Crystallography, Volume C, Revised Edition
E. Prince[26,50]

Quasi-Laue Neutron Diffraction
E. Prince[26,50] and I. G. Schroder[26]

Titanium Doping and Cation Vacancies in Fe_2O_3
A. Drews[26] and T. A. Vanderah[27]

Investigations of High Temperature Furnace Materials
A. Drews[26] and B. H. Toby[26]

Structure of $Bi_2Ti_2O_7$
A. W. Sleight[32] and T. Vogt[8]

$M_2Cu_2CoO_2S_2$ (M = Sr, Ba): A Novel Example of a Square-Planar CoO_2 Layer
W. H. Zhu[48], P. H. Hor[48], A. J. Jacobsen[48], G. Crisci[48], T. A. Albright[48], S. H. Wang[48] and T. Vogt[8]

The Effect of Co in MB_5 and MB_5D_x Alloys: The Use of Isotopical Substitution in Neutron Powder Diffraction
T. Vogt[8], J. Reilly[8] and J. Johnson[8]

Incipient Charge Order in $La_{0.25}Nd_{0.25}Ca_{0.5}MnO_3$
P. M. Woodward[8], T. Vogt[8], D. E. Cox[8], C. N. Rao[7] and A. K. Cheetham[45]

Ruthenium Containing Double Perovskites
B. J. Kennedy[54], P. M. Woodward[8] and T. Vogt[8]

The Structure of $Sr_2Ru_{1-x}Rh_xO_4$
B. J. Kennedy[54], T. Vogt[8], P. M. Woodward[8] and D. J. Buttrey[46]

Structure of D-Mordenite
B. Campbell[45], A. K. Cheetham[45] and T. Vogt[8]

Structures in the System Li-B and Li-B-D
B. Albrecht[47] and T. Vogt[8]

The Structure of $Pr_4Ni_3O_{10}$
D. J. Buttrey[46] and T. Vogt[8]

Powder Measurements of Single Crystals: A

Neutron Gandolfi Camera
T. Vogt[8]

Affiliations

[1] Academia Sinica, Taiwan
[2] Academy of Sciences, Czech Republic
[3] Air Products and Chemicals, Inc.
[4] Amoco Corporation
[5] Army Armament Research, Development and Engneering Center
[6] Army Research Laboratory
[7] Bangalor Institute of Science, India
[8] Brookhaven National Laboratory
[9] California Institute of Technology
[10] Cornell University
[11] Davidson Chemical
[12] E. I. DuPont de Nemours and Company
[13] Exxon Research and Engineering Company
[14] Florida State University
[15] Johns Hopkins University
[16] KFA Jülich , Germany
[17] Lawrence Livermore Laboratory
[18] Lucent Technologies, Bell Laboratories
[19] Massachusetts Institute of Technology
[20] McMaster University, Canada
[21] National Central University, Taiwan
[22] National Institute for Research in Inorganic Chemistry, Japan
[23] National Science Foundation
[24] National Taiwan University
[25] National Tsing Hua University, Taiwan
[26] NIST Center for Neutron Research
[27] NIST, Ceramics Division
[28] NIST, Metallurgy Division
[29] Northeastern University
[30] Oak Ridge National Laboratory
[31] Ohio State University
[32] Oregon State University
[33] Oxford University, United Kingdom
[34] Pennsylvania State University
[35] Princeton University
[36] Shanghai Institute of Metallurgy, P. R. China
[37] State University of New York at Stony Brook
[38] Temple University
[39] Trans-Tech
[40] Universidad de la Republica, Uruguay
[41] Universität des Saarlands, Germany
[42] University of Bressica, Italy
[43] University of California, Berkeley
[44] University of California, Davis
[45] University of California at Santa Barbara
[46] University of Delaware
[47] University of Giessen, Germany
[48] University of Houston
[49] University of Le Mans, France
[50] University of Maryland at College Park
[51] University of Oslo, Norway
[52] University of Pennsylvania
[53] University of Southern California
[54] University of Sydney, Australia
[55] University of Uppsalla, Sweden
[56] University of Vermont
[57] W. R. Grace and Company
[58] Wright-Patterson Air Force Base

Surface and Interfacial Studies

This past year has been a very productive one for neutron reflectometry studies. A number of important experiments in polymer science, magnetism, Langmuir-Blodgett films, and other topical areas were successfully performed. A sampling of this research is highlighted in the following subsections.

Studies of Wetting of d-Pentane on Water

Spreading of alkanes on water is an important problem both from both fundamental and applications point of view. Applications of this problem lie in petroleum engineering, where the hydrodynamic flows and the subsequent recovery rates of oil and gas are closely related to the spreading characteristics of oil on the water rich phase [1]. Therefore, it is important to understand the wetting of "model" oils, namely alkanes, on water under different conditions.

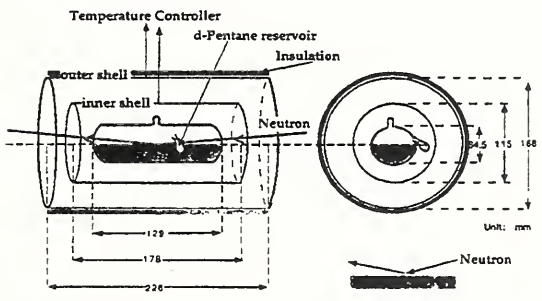

Fig. 1. Sample cell and temperature control assembly used in the wetting experiments.

Until a few years ago it was known that alkanes higher than octane do not wet water at room temperature, instead forming well defined lenses on the surface of water, whereas lower alkanes were thought to spread on water. More recent experiments, however, show that heptane and hexane also form lenses on the water surface and thus are nonwetting [2]. The case of pentane is still somewhat controversial. In a recent paper Ragil et. al. report the observation of continuous wetting of pentane on water as the temperature is increased [3]. They observed with ellipsometry, a continuous increase in the thickness of the pentane film on water as a function of increasing temperature at the saturated vapor pressure of pentane. Fitting of ellipticity data, however, involves the assumption that both water/pentane and pentane/vapor interfaces are sharp.

We have carried out neutron reflectivity experiments on the pentane-water system in order to elucidate the density profile of these wetting films. Since precise temperature control is important for these studies, a special temperature control device was built to control the temperature of the cell to better than a mK from room temperature to 75°C. The sample cell contains two reservoirs, the larger one made from a 6 cm dia., 12 cm long fused quartz tube is filled with water. The smaller reservoir for pentane is attached as a side to the larger reservoir. The cell is contained within two aluminum shells. The outer shell is insulated from the outside by ¼ inch thick foam insulation. The outer shell is maintained at a temperature of T +/- .005°C, the inner shell is kept at T+dT+/- .001°C. The value of dT was typically kept to be 0.05°C. With this arrangement the cell could be maintained with a short term (2-3 hrs) temperature stability of 0.2-0.3 mK and longer term (24 hours) stability of 1-1.5mK.

In order to avoid a rising meniscus of water along the cell walls, the cell was coated with OTS using a standard literature procedure. The OTS film renders the cell walls hydrophobic and is known to be a robust film. About 150 cc of deionized water was placed in to the cell and degassed under vacuum by freezing and thawing. Deuterated pentane [2 cc] was transferred under vacuum into the cell. The cell was subsequently sealed under vacuum. Prior to putting the sealed cell in the temperature control assembly, all of the pentane was distilled into the smaller pentane reservoir.

The cell was then equilibrated at slightly higher than room temperature [in our case 25C] for a period of two days before being transferred to the neutron reflectometer. A series of reflectivity scans were performed as a function of time, which showed that reflectivity reached equilibrium in 16-18 hours. In fact, at each change of temperature it typically took 10-20 hours to reach equilibrium reflectivity profiles. Such profiles at various temperatures are shown in Fig. 2.

At 25°C the reflectivity profile shows a clear minimum at ca. 0.1 $Å^{-1}$, meaning that there is well defined film of d-pentane on water whose thickness is 63 Å.

Movement of the reflectivity minimum to higher Q on increasing the temperature clearly shows that the equilibrium film thickness is decreasing at higher temperatures. The film thickness at the highest temperature we measured [65°C] is only 35 angstroms. While the film thickness at 25°C is in reasonable agreement with that measured with ellipsometry by Ragil *et. al.* [3], temperature dependence of film thickness in our measurement is completely opposite to the ellipsometry result.

The reason for this discrepancy is not

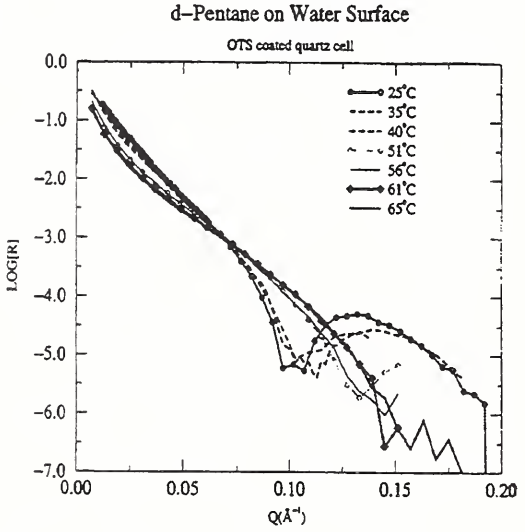

Fig. 2. Equilibrium neutron reflectivity profiles at various temperatures for the d-pentane water system. Note the decrease in film thickness as the temperature is increased.

clear at present. One reason the difference can be the use of d-pentane in our study which is needed to have a neutron contrast. Ragil *et. al.* calculated the Hamaker constant for h-pentane-water system and showed that the Hamaker constant changes sign at 51°C, very close to their experimentally determined wetting temperature. A similar calculation of Hamaker constant for d-pentane-water system shows that the wetting temperature for this system should be 42°C, clearly not what we observe in our study. Another reason for the discrepancy can be thedeterioration of the OTS coating on the walls of the cell. Surface phenomena are typically very sensitive to very small amount of impurities. However, the fact that we have been able to reproduce our results, quantitatively, in three different cells argues against such an explanation.

Effects of Copolymer Additives on the Phase Behavior of Polymer Blend Films

Studies of finite size effects on the equilibrium properties and kinetic precesses of materials confined to thin films provide important insight into the processing of materials in thin film coating applications. Many recent experimental and theoretical investigations have focused on fundamental understanding of the phase behaviors resulting from varying film thickness. Modification of the interparticle or interfacial interactions near the boundaries of confined materials can lead to essentially new phenomena which may provide useful technologic applications. Moreover, quantitative changes in blend morphology and interfacial tension that occur become more interesting with addition of block copolymer. These results have direct importance in thin film coatings. In the present study, we use state-of art neutron reflection, optical and atomic force microscopy techniques to characterize the interfacial activity of diblock copolymer, and quantify phase separation (macrophase) and microphase separation of polymer blend films.

In the bulk state (thickness of 40 μm to 500 μm) of a binary mixture of deuterated polystyrene (PSD)/hydrogenated polybutadiene (PB), small angle neutron scattering (SANS) and temperature jump light scattering (TJLS) experiments have demonstrated that a small amount of PSD-PB diblock copolymer additives suppresses the concentration fluctuations near the transition temperature of a binary blend, and shifts the phase boundaries downward linearly with increasing copolymer content. As copolymer concentration increases, micelle formation is evident in the scattering function, as are the competing effects of concentration fluctuations (macrophase separation) and ordering (microphase separation) between different types of polymers. Moreover, at a constant, shallow quench depth, the kinetics of phase separation were greatly retarded by the presence of the copolymer (greater than 1.6% copolymer additives).

To investigate the effects of block copolymer additives on the phase behavior of polymer blend films (thickness less than 2000 Å), blends of fixed binary composition (near its critical composition) with various copolymer concentrations were studied as a function of time by neutron reflection (NR), optical (OM) and atomic force (AFM) microscopy measure-

ments on the thin polymer blend films at different film thickness, and different homopolymer/diblock deuteration matches. Thin blend film samples were cast on a 5 cm dia. X 5mm thick polished silicon substrate by spin coating from toluene solutions of the blend. Variations in film thickness were achieved by varying the solution concentration and spinning speed. As cast (t=0), all films appeared homogeneous and uniform under the optical

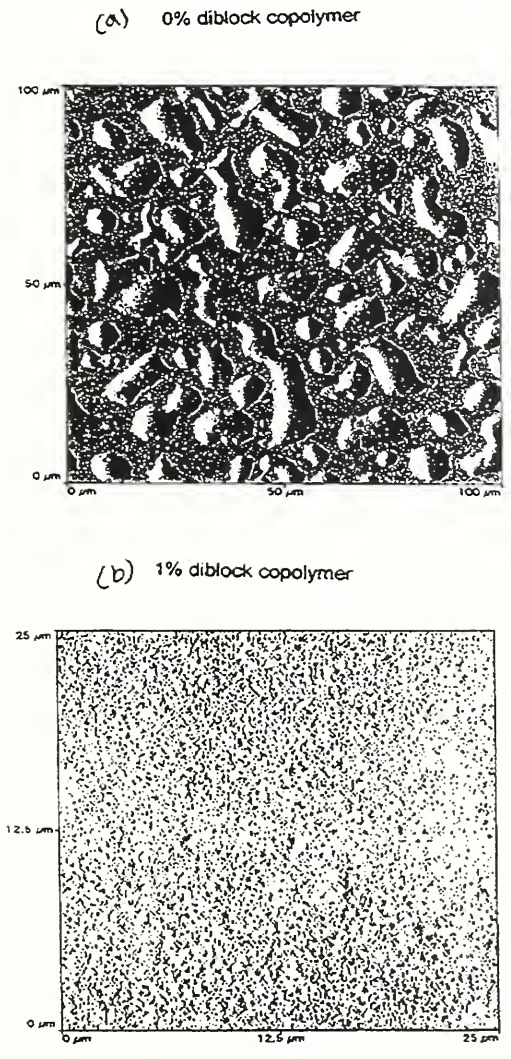

Fig. 3. Atom force micrographs of polymer blend films films (1000) of PSD/PD (75:25) with (part b)/without (part b) 1% PSD-PB copolymer additives.

microscope. Each film was placed under quiescent conditions at ambient (~25°C) temperature, and the temporal pattern evolution at the free boundary observed and imaged by OM and AFM. The time-development optical micrographs of the surface pattern formation associated with the phase separation in the blend film were studied and compared to the previous study of the kinetics of bulk phase separation for this PSD/PB blend using TJLS.

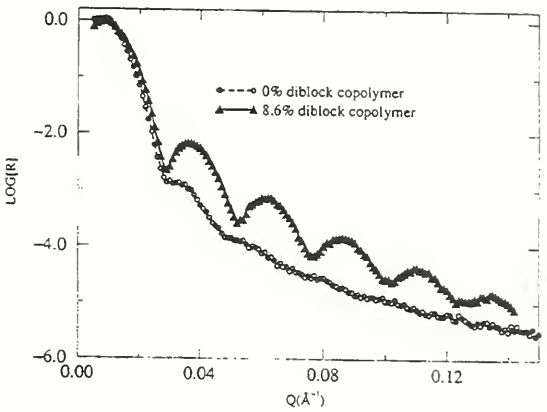

Fig. 4. Neutron reflectivity data of PSD/PB blend films with/without diblock copolymer additives (400 Å) as a function of Q vector in a semi-log plot. Different copolymer contents are shown by different symbols as indicated in the legend.

Preliminary microscopy results have shown that, with addition of small amounts (less than 0.1%) of PSD-PB diblock copolymer into the blend, the time-development of morphology is very different from that of the pure binary blend film. Fig. 3 shows AFM micrographs of film samples with (Fig. 3a) and without (Fig. 3b) 1% diblock copolymer. These two samples were both spun cast on at the same substrate, at the same thickness (1000 Å), and captured at equal time (t~24 hrs). The dramatic alteration of the surface pattern formation in thin film upon addition of 1% symmetric PSD-PB diblock copolymer is a quite different result from kinetics results of TJLS measurements in the bulk state, where there is no significant change in the phase separation kinetics via spinodal decomposition with addition of 1.6% diblock copolymer.

Neutron reflectivity measurements were conducted to study the density profile of block copolymer blend normal to the silicon solid interface in the early stages of phase separation. Fig. 5 shows the reflectivity data (1 hour after casting) as a function of wavevector Q in a semi-log plot for polymer blend (400Å with/without diblock copolymer additives). Note that the kinetics of phase separation in the

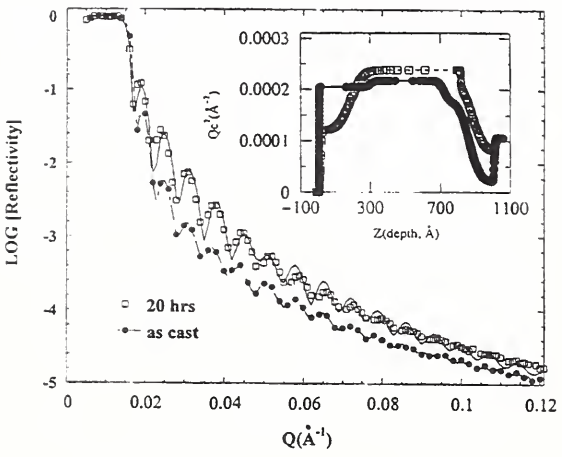

Fig. 5. Neutron reflectivity data of PSD/PB blend with 8.6% PSD-PB diblock copolymer additives (1000 Å) for different time after spun cast. Insert is the scattering profile for the best fit tot the data.

pure binary blend film is very fast, the spinodal decomposition surface pattern develops after 2 two hours and the surface becomes rough. However, the air-polymer surface remains smooth for more than 3 days after being spun cast for blend film with 8.6% diblock copolymer. The phase separation kinetics slows down dramatically upon addition of the diblock copolymer. Further investigation on the kinetics of phase separation in blend films with various copolymer concentrations of film thickness from 2000 Å to 400 Å is in progress. Figure 5 shows how the scattering density profile evolves as a function of time for a blend film (1000 Å) with 8.6% diblock copolymer. Evidently, a bilayer profile is formed and a smooth surface pattern is observed as shown in part (b) of Fig. 3.

In conclusion, neutron reflectivity measurements provide complementary results on the effect of copolymer additives to slow down phase separation kinetics in thin blend films and time evolution of the scattering density profile of polymers normal to the silicon surface during the early stage of the polymer blend films.

Ordering vs. Microphase Separation in Thin Diblock Copolymer Films

An interesting question with regard to block copolymer thin films is the nature of the order disorder transition (ODT) or microphase-separation transition (MST), and how it differs from bulk transition. However there has been little work on this subject since the studies of Menelle et al, which found evidence for an upward shift in the transition temperature with decreasing film thickness. We here present highlights of a more detailed study of this question, made possible in part by the recent increases in flux and resulting faster data acquisition times. We here describe studies of P(dS-b-nBMA) thin films, but have observed similar results for more familiar systems such as P(dS-b-I) and P(dS-b-MMA). P(dS-b-nBMA) has an unusual inverted ODT, becoming more ordered with increasing temperature. This behavior is associated with large volume-of-mixing effects.

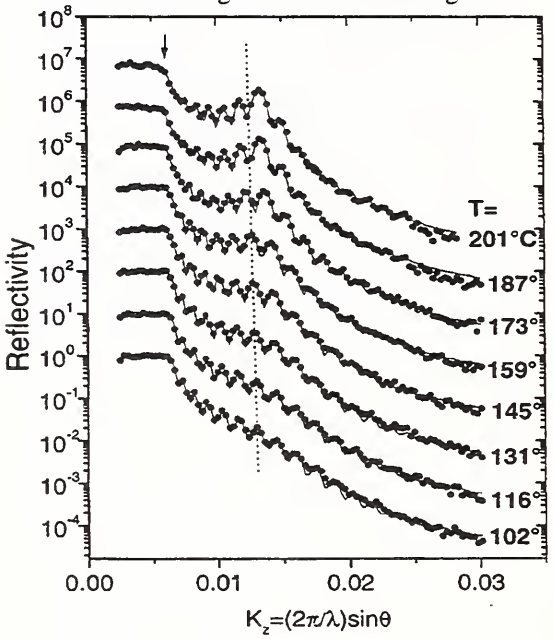

Fig. 6a. Neutron reflectivity profiles for P(dSbnBMA) film as a function of temperature.

Figure 6a shows neutron reflectivity profiles (points) taken for a P(dS-b-nBMA) film (Mw=68,000) at a series of temperatures from 100 to 200°C. The sample was contained in a diffusion-pumped heater cell during the measurements, and the temperature was increased from one scan to the next. Best-fit scattering length densities are shown in Fig. 6b. Annealing leads to partial ordering at the film surfaces, characterized by a damped cosine volume fraction profile with period L and decay length ξ. These composition oscillations give rise to the broad quasi-Bragg peak in the reflectivity data. ξ grows as the temperature is raised, and the Bragg peak intensifies and sharpens. A steady contraction of the Kiessig fringes is also appar-

ent with increasing temperature, due to thermal expansion. This polymer has a bulk LODT at 225-250°C, and is thus "disordered" at the temperatures of the data in Fig. 6, consistent with the lack of any sudden sharpening of the Bragg peak.

A number of subtle but distinct changes occur in the reflectivity data at approximately 160°C, however, which are associated with the onset of film thickness discretization (island formation).

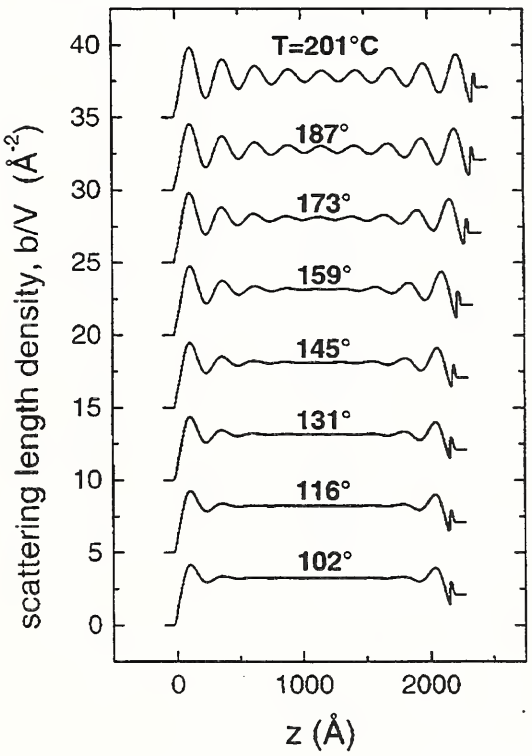

Fig. 6b. Fitted scattering length density profiles at various temperature for the P(dS-bnBMA) film.

There is a pronounced drop in the magnitude of the reflectivity just below the critical temperatuure (Fig. 7a), due to the sudden increase in surface roughness and off specular scattering. There is also a large downward shift of the Kiessig fringes (dotted lines, Fig. 6a), corresponding to an apparent increase in the film thickness beyond the trend due to thermal expansion. The best-fit thickness t, normalized by the fit period L, is plotted against temperature in Fig. 7b, and is seen to undergo a seemingly discontinuous jump from and incommensurate value (t/L=8.6) to a commensurate value (t/L=9). (in fact, only about 70% of the film has thickenss t=9L, while the remainder has thickness t=8L, as was confirmed by examination of the sample following the experiments; however the 9L thickness dominates the Kiessig fringes and "pulls" the fit).

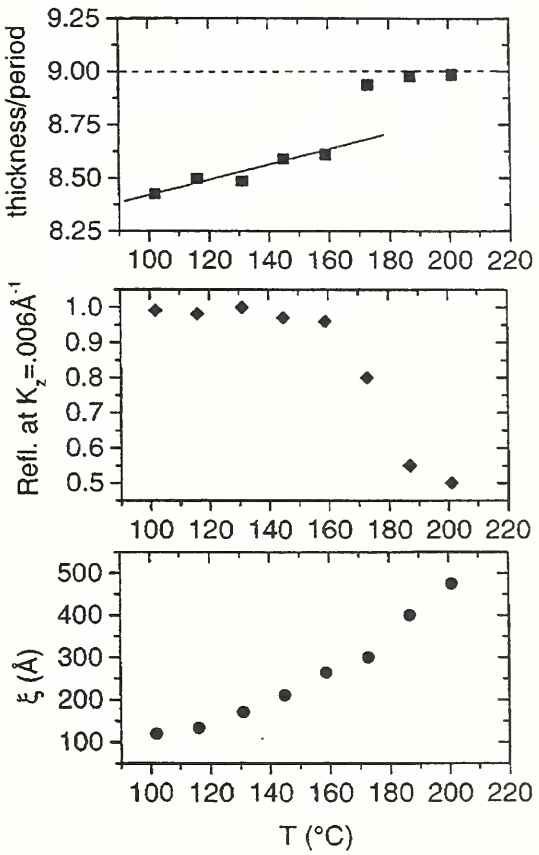

Fig. 7. Decay length, reflected intensity at k_z=.006 and t/l as a function of temperature for P(dS-bnBMA) film.

What is remarkable is that the overlap between the surface-ordered regions is extremely weak at the temperature where island formation begins to occur (Fig. 6b). The film thickness is approximately eight times the decay length of ξ=300 Å. The onset of island formation is an indisputable sign that the order parameter is *phase coherent* across the entire film, despite the fact that it is only *weak microphase separated* in the center of the film (the temperature is 50-75°C below the bulk microphase separation temperature). "Ordering" and "microphase separation" have thus been decoupled due to wetting and finite size effects.

The question then arises as to what vestige of the bulk MST remains when that temperature is reached. Fig. 8 shows the intensity of the first order Bragg peak reflection vs. temperature, for films of several different thicknesses.

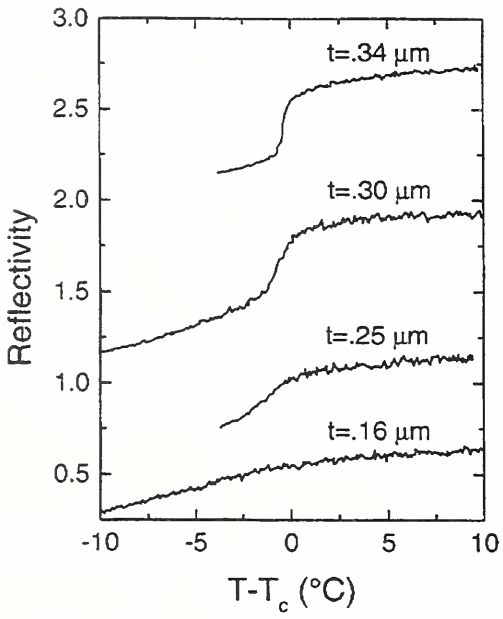

Fig. 8. Intensity of first order Bragg peak for films of various thicknesses of P(dS-bnMA).

The polymer in this case is P(dS-b-nBMA) with Mw=85,000, and the bulk MST occurs at approximately 155°C. The thickest film has a sharp, bulk-like MST – the width is approximately 1°C – indicating a large discontinuous jump in ξ. As the film thickness is reduced the transition becomes broader and less distinct, until only a change in slope marking the onset of the transition remains.

Thus one must consider two separate processes in block copolymer thin films – the ODT and the MST. For sufficiently thick films, the two coincide – microphase separation and phase coherence (ordering) occur in the center of the film at the same temperature. For thinner films, however, phase coherence can be established at temperatures far removed from the bulk MST, resulting in island formation. Residual microphase separation still occurs near the bulk MST, but becomes increasingly weaker as the film thickness is reduced and the film is more ordered.

Polymer Interdiffusion Near the Polymer/Solid Interface

The performance of materials in many technological applications such as electronics packaging and adhesives is often dependent upon knowledge about polymer chain mobility near the polymer/solid interface. Measurements of bulk polymer properties are not helpful because the properties of the interfacial polymer are different from those of the bulk polymer. Geometric constraints on the chain conformations by and enthalpic interaction energies with the solid surface both perturb the polymers from the bulk state. For example, it has been observed that ultrathin polymer films of polystyrene on different substrates (or no substrate) show increased or decreased apparent glass transition temperatures depending upon the nature of the polymer/solid interaction energy and the degree of chain confinement. To date, experimental data for polymer chain mobility near the polymer/solid interface are limited, particularly for polymer melt systems where buried interfaces must be probed.

In this study, polymer mobility near a solid surface is measured using neutron reflectometry by monitoring the interdiffusion between deuterated poly(methyl methacrylate) (PMMA) and hydrogenated PMMA layers on a silicon substrate. Neutron reflectometry is an ideal technique to study this problem because of the very high resolution and the strong contrast between the deuterated and hydrogenated components. The short-range polymer chain movement (interdiffusion distances <150Å) at different distances from the substrate surface are measured from bilayer samples with lower deuterated layers of varying thicknesses, h, with a hydrogenated polymer layers top layer. From a series of samples, an estimate of the effective distance the solid substrate perturbs the polymer diffusive dynamics from those of the bulk polymer can be determined and correlated with the conformational characteristics of the chains. Previous interdiffusion experiments have focused on either diffusion free from substrate effects or monitoring the overall chain movement from a solid surface.

The bilayer samples are prepared with lower deuterated thicknesses ranging from 35 Å to 669 Å with hydrogenated overlayers (800 Å to 1500 Å thick) floated onto the lower layers from deionized water. Two different relative molecular mass pairs are used: deuterated PMMA M_n = 143,000 and deuterated PMMA M_n=260,000 and hydrogenated PMMA M_n=262,000. The samples are annealed at 150°C, 35°C above the bulk glass transition temperature in a vacuum oven and periodically removed to measure the reflectivity. The measurements were performed at the National Institute of Standards and Technology NG7 reflectometer.

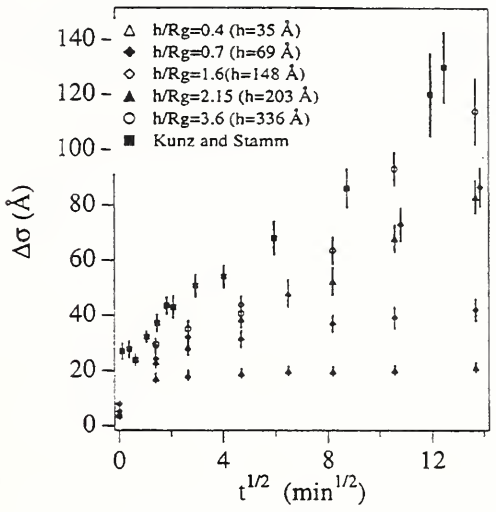

Fig. 9. The measured interfacial width plotted as a function of the square root of time for the deuterated PMMA M_n=135,000 bilayer samples. The error bars represent the standard uncertainty in the measurement.

Changes in the concentration profiles with annealing time were determined from fits to the reflectivity profiles. The interfacial width, $\Delta\sigma$, is characterized from the second moment of the derivative of the concentration profile between the two polymer layers. The initial roughness from the as cast film is quadratically substracted throught the expression $\Delta\sigma = \sqrt{\sigma^2 - \sigma_o^2}$, where σ is the interfacial width from the measurement and σ^2 is the initial roughness. In Fig. 9, the interfacial width for the deuterated PMMA M_n=135,000 series is plotted as a function of the square root of time. From Fig. 9, it is clear that the rate of interdiffusion depends strongly on the initial size do the deuterated layer. After several hours of annealing, $\Delta\sigma$ for the thinnest layer is a factor of five smaller than $\Delta\sigma$ of the thickest bilayer sample. Similar data are obtained from the higher molecular weight series. The interdiffusion rate for each sample is characterized by a linear fit to the data in Fig. 9. For Fickian diffusion, the slope of the linear fit is proportional to the bulk diffusion constant. It is important to note that the diffusion coefficient determined here is not the bulk diffusion coefficient, but an effective monomer diffusion coefficient. The Fickian limit is not clearly reached here as the diffusion distances are less than the bulk radius of gyration, R_g of the polymer. Nevertheless, such a fit provides a good measure of the interdiffusion rate over the time scale of the experiment. The effective diffusion coefficients are shown as a function of the lower film size normalized on the polymer bulk R_g in Fig. 10. From Fig. 10, the thinnest layer shave an effective diffusion constant almost two orders of magnitude smaller than that of the thickest films which gradually approaches that of the substrate-free value as the lower film size increases. The effective range of the substrate on the polymer dynamics is approximately $3R_g$. The larger molecular weight series also shows decreased chain segment mobility $3R_g$ from the substrate surface.

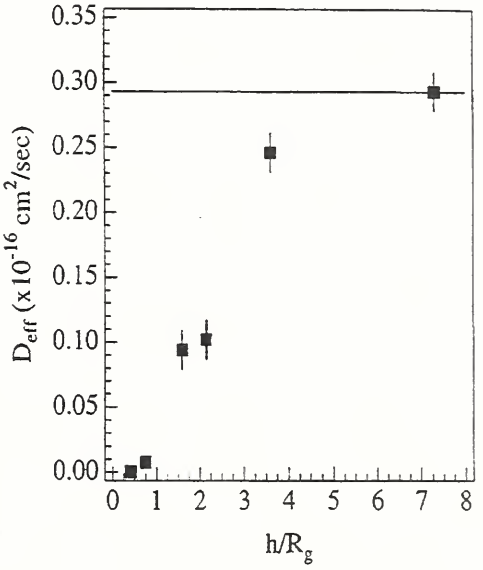

Fig. 10. The effective diffusion coefficient for the deuterated PMMA M_n=135,000 bilayers as a function of the lower film thickness normalized on the bulk radius of gyration of the polymer (R_g=93 Å). The effective range of the interface is approximately $3R_g$. The error bars represent an estimate of the standard uncertaintly in the measurement.

The decrease in the interdiffusion rate can be related to the polymer chain conformations near the substrate surface and the attractive enthalpic interaction energy between PMMA and silicon oxide. For the thinnest layers ($h<R_g$), the chains in the lower film have conformations that are extended parallel to the substrate from geometric constraints and have numerous contacts with the substrate. From a large number of contact points, only a small attractive interaction energy is needed to effec-

tively fix the polymer chains to the surface. The result is a large decrease in the observed interdiffusion constant. For intermediate lower film sizes ($R_g<h<3R_g$), polymer chains at the polymer-polymer interface are affected by the reduced mobility of the adsorbed layer structure with chains pinned to the surface. For the thickest layers ($h>3R_g$), the polymer chains are not affected by from the substrate. These results show that the polymer dynamics at temperatures well above the T_g of the bulk polymer are altered at distances more than R_g from the surface. Work is currently under way utilizing different molecular weights as well as varying polymer-substrate interaction energies to better understand the dynamics near the polymer-solid interface.

Interfacial Width Determination in Immiscible Homopolymer/Random Copolymer Bilayers

Many important practical applications of polymer blends utilize blends of homopolymers with random copolymers, where the copolymers act as reinforcing agents at the interfaces. Thus, a knowledge of the interface width between a homopolymer and a copolymer is useful. In this study we investigate one such system, deuterated polyphenylene oxide (dPXE) and a random copolymer styrene acrylonitrile (SAN), in which there is no chemical or grafting reaction, but only a favorable interaction. The interface toughness of such systems depend primarily on the number of effective entanglements across the immiscible interface and how far one phase penetrates into the other. Here we have used neutron reflection to investigate the interface width between dPXE and SAN for varying AN composition, ϕ_{AN} between 0.15 to 0.40 weight fraction.

For this experiment bilayer samples of the two polymers were prepared as follows. Thin layers of dPXE were spun cast from dilute toluene solution onto acid-cleaned polished silicon wafers that were typically 10 cm in diameter and 5 mm thick. The thickness of this first layer was approximately 40 nm thick. SAN layers of different AN compositions were then spin coated from methyl ethylketone (MEK) solutions onto glass slides and subsequently floated off onto water. The silicon substrate with the previously coated dPXE layer was used then to pick up the floating SAN film to make a bilayered sample with the construction Si/dPPO/SAN. Samples were placed in vacuum at room temperature for several hours to remove any residual water or solvent molecules.

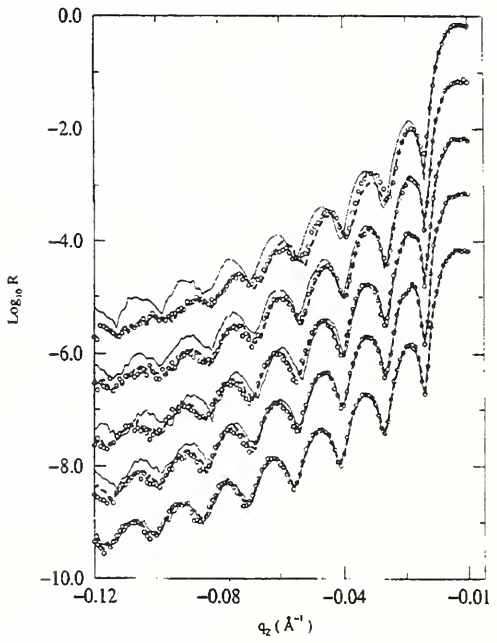

Fig. 11. Neutron reflection through silicon from a series of Si/dPXE/SAN bilayer films, for different AN content. For reflectivity sets from top to bottom, ϕ_{AN} = 0.15, 0.20, 0.25, 0.31 and 0.40. The thin solid line in each set shows reflectivity from as-cast samples, while dashes and circles correspond to the reflectivity after annealing for 1.5 hours and 9 hours at 140 °C respectively. A progressive damping with decrease ϕ_{AN} is predicted from theory, but quantitative values of the experimental widths are substantially larger.

Neutron reflection measurements with the incident beam entering through the silicon wafer were performed on the samples as-cast and after annealing at elevated temperatures.

Figure 11 shows a set of neutron reflection measurements, off-set from each other for clarity, for the series of Si/dppoE/SAN samples having ϕ_{AN} = 0.15, 0.20, 0.25, 0.31 and 0.40, both as-cast and following annealing at 140 °C for 1.5 hours and 9 hours. It is observed that all the as-cast samples have roughly similar undamped oscillations which correspond to an interface width of ~1 nm. However, upon annealing, the oscillation damping varies in inverse relationship to ϕ_{AN}. Annealing longer at 140 °C, or at the higher temperature of 180 °C did not significantly alter the reflectivity pro-

files. This trend is expected from calculations using the interaction parameter, $\chi_{dPPO/SAN}$ for this system. For sufficiently low ϕ_{AN}, the homopolymer and random copolymer become miscible. Neutron reflection measurements on a dppo/PS (ϕ_{AN} = 0) system confirm that the system is miscible, since the oscillations get progressively damped with annealing time and eventually no oscillations in the reflectivity profile are observed. Preliminary fits to the data in Fig. 11 indicate that the interface widths are larger than the calculated value from theory for low values of ϕ_{AN}. Additional broadening arising from capillary waves may thus be important as well in thin film geometry.

Field History of the Magnetic Structure in GMR Co/Cu Multilayers

Giant magnetoresistance (GMR) has recently been observed in magnetic multilayers composed of alternating ferromagnetic and nonmagnetic layers, such as Fe/Cr and Co/Cu. Specifically, the magnetoresistance, MR, is defined as $MR(0) = [R(0)-R(H_{sat})]/R(H_{sat})$, where the zero-field resistance, R(0), of these materials is larger than that measured in saturating fields, $R(H_{sat})$. The largest GMR is generally associated with an antiparallel alignment of the ferromagnetic layers across the nonmagnetic interlayers, as determined by neutron reflectivity, bulk magnetization and related techniques. In most multilayer systems, the strength of the antiferromagnetic interlayer coupling and the magnitude of the GMR oscillate and decay exponentially with increasing thickness of the nonmagnetic layer.

For magnetic sensor applications, the challenge is to maximize MR while reducing the saturation field. High field sensitivity can be achieved in Co/Cu multilayers in which thick Cu layers (> 5 - 6 nm) give rise to weak interlayer coupling. For example, (111) Co(6 nm)/Cu(6 nm) multilayers grown by sputtering techniques have saturating fields smaller than 200 Oe and yield an MR(0) of several percent. After saturation, a maximum in MR occurs at the coercive field, H_c, where the net magnetization of the sample is zero. However, the MR obtained in the coercive state is not nearly as large as that obtained in the as-prepared state. Even after demagnetizing the sample, the MR never exceeds the as-prepared value.

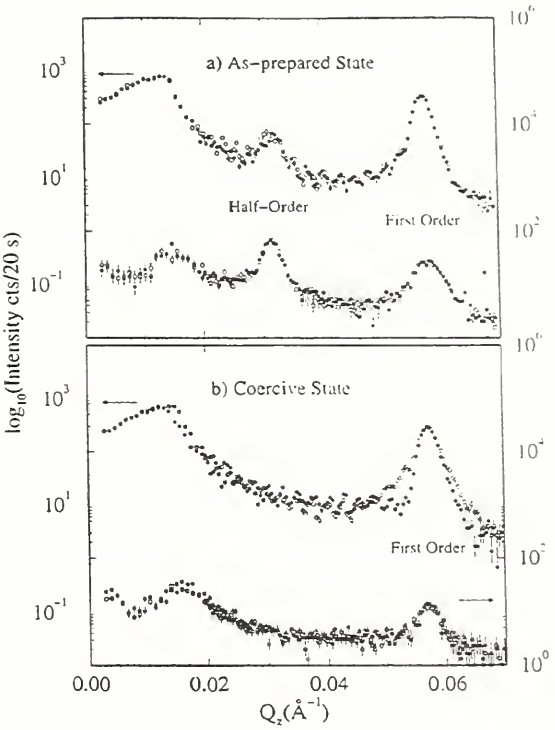

Fig. 12 Specular polarized neutron reflectivity for $[Co(6nm)/Cu(6nm)]_{20}$ multilayer at room temperature in (a) the as-prepared state and (b) the coercive state (H_c=54 Oe). The data have not been corrected for background, sample footprint or polarization efficiencies. The open and shaded circles correspond to the (--) and (++) cross sections respectively. The open and shaded squares designate the (++) and (-+) cross sections. The arrow point to the appropriate vertical axis for each set of cross sections.

Using specular and off-specular polarized neutron reflectivity (PNR), we have examined several Co(6 nm)/Cu(6 nm) multilayers to determine the difference between the Co magnetic structure in the as-prepared and coercive states. These experiments were performed at room temperature on the NG-1 reflectometer. Specular PNR provides a depth profile of the magnetic moment if the in-plane magnetic domains are large (of order 100 μm), while off-specular PNR is sensitive to smaller in-plane domains. All four spin cross sections, (+ +), (- -), (+ -) and (- +), were measured in each configuration to determine the orientation of the Co moments within the sample growth plane.

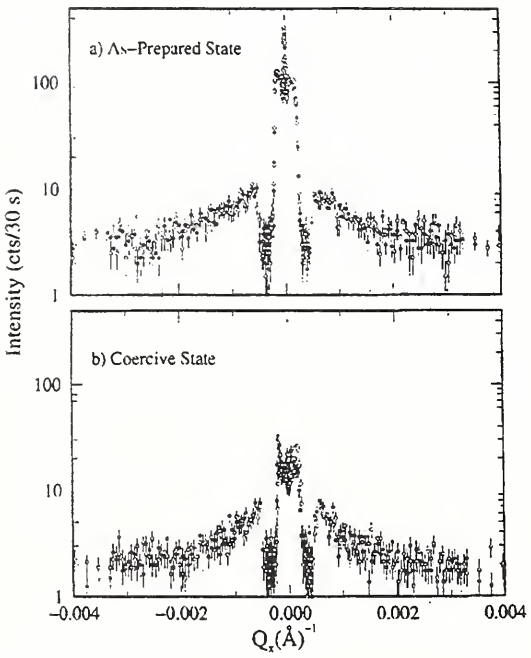

Fig. 13. Transverse Q_x scan at the half-ordered position (Q_z=0.031 A^{-1}) for [Co(6 nm)/Cu(6 nm)]$_{20}$ at room temperature for the (a) as-prepared state and (b) the coercive state (H_c=54Oe). Only the (+-) and (-+) spin-flip cross sections are shown (shaded and open circles respectively). The data have not been corrected for background or polarization efficiencies, which are greater than 98%.

We first characterized each sample in the as-prepared state in a small field of 1.5 Oe. Figure 1(a) shows specular scans along the Q_z direction for a Co(6 nm)/Cu(6 nm) multilayer with 20 repeats.

The (+ +) and (- -) cross sections are effectively equal through the critical region and at the first-order superlattice peak position (Q_z = 0.058 A^{-1}) indicating that there is no ferromagnetic component of the Co moment parallel to the field direction. However, a pronounced peak is evident in all four cross sections at the half-order position (Q_z= 0.031 A^{-1}). Most of the Co moments are thus aligned antiparallel across the intervening Cu layers in the as-prepared state. The narrow width of this reflection indicates that the antiferromagnetic order in this sample is coherent through many superlattice bilayers. Similar half-order peaks were observed for other comparable samples in the as-prepared state, but the intensities were typically smaller and the widths were broader. A smaller fraction of the Co moments are aligned antiparallel in these samples, and the growth-axis coherence is limited to only a few bilayers. The characteristics of this initial antiferromagnetic spin state are apparently sensitive to growth conditions and/or sample storage time and environment.

This antiferromagnetic order is irreversibly destroyed by the application of a field. After saturation in a -200 Oe field, the PNR data for the coercive state (H_c = 54 Oe) differ substantially from the as-prepared data, as demonstrated in Fig. 12(b). The half-order magnetic reflection is absent, and no other magnetic scattering is apparent in these specular data. The Co moments are not correlated along the growth axis direction.

Additional details of the Co spin structure can be gained from off-specular Q_x scans centered at the half-order peak position (Q_z = 0.031 A^{-1}). Only the (+ -) and (- +) spin-flip off-specular data are shown in Fig. 13, because they are entirely of magnetic origin. The qualitative features of the (+ +) and (- -) non-spin-flip data are similar. Figure 13(a) for the as-prepared state shows a narrow specular peak at Q_x = 0.0 A^{-1} on top of a broad diffuse feature. (These data are among the best examples of magnetic diffuse scattering currently available.) Pronounced dips occur symmetrically at angular scattering positions where the incident (or scattered) neutron beam is exactly parallel to the sample face and is thus reflected out of the detector. These features can be ignored in a qualitative treatment of the data, but must be considered in a full dynamical model.

The presence of specular intensity indicates that a small portion of the Co moments order in in-plane domains larger than approximately 100 μm. The observation of diffuse intensity suggests that the remaining Co moments align in substantially smaller domains. (We note that some of the diffuse scattering may originate from macroscopic roughness between the Cu and ferromagnetic Co layers at the interfaces, but x-ray characterization of this sample indicates that this contribution is reasonably small.) From the inverse of the width of the diffuse scattering, we can roughly estimate that the in-plane domain size is 0.2 – 1.0 μm.

This magnetic diffuse scattering completely disappears in saturating fields as the Co in-plane domains coalesce, but it is recovered at the coercive field where the smaller domains reform [Fig. 13(b)]. The width of this scattering is comparable to that of the as-prepared data, indicating that the in-plane domain size is again 0.2 – 1.0•μm. The overall appearance of the data differs, however, and the central specular reflection is absent.

From both the specular and off-specular PNR data in Figs. 12 and 13, we conclude that the larger MR for as-prepared Co/Cu multilayers arises from long-range antiferromagnetic order along the growth axis among in-plane domains of various sizes. This antiferromagnetic order is present only after growth and cannot be recovered after field cycling. The smaller MR at the coercive field is associated with the lack of correlation among the Co domains along the growth axis and within the sample plane. In our future studies of these materials, we hope to determine the physical mechanism responsible for this irreversibility and thus attempt to isolate the antiferromagnetic state that exhibits maximum MR. In addition, we are developing a dynamical model of the off-specular data in order to extract information about the in-plane domain structure that can not be obtained from other measurement techniques.

Antiferromagnetic Phase Transition and Interlayer Spin Coherence in Short-period EuTe/PbTe Superlattices (SLp) [4]

EuTe and PbTe are both NaCl-type and well lattice-matched (a_{EuTe}=6.59 Å, a_{PbTe}=6.46 Å). EuTe/PbTe SLs prepared by MBE on(111) BaF_2 are of very high structural quality, showing many orders of satellites to X-ray Bragg reflections. Neutron diffraction reveals details of spin ordering in the EuTe layers at low *T*. Bulk EuTe is a Type II FCC antiferromagnet — below T_N=9.6 the Eu^{2+} spins form ferromagnetic (FM) "sheets" on (111)-type planes, with adjacent sheets antiferromagnetically (AFM) correlated. This structure is preserved in the EuTe/PbTe systems — however, while in bulk four equvailent domain types are possible corresponding to four families of (111) planes, in the SLs the small mismatch strain in EuTe always selects a *single* arrangement with the FM sheets *parallel* to the layers. The dependence of the T_N on the EuTe

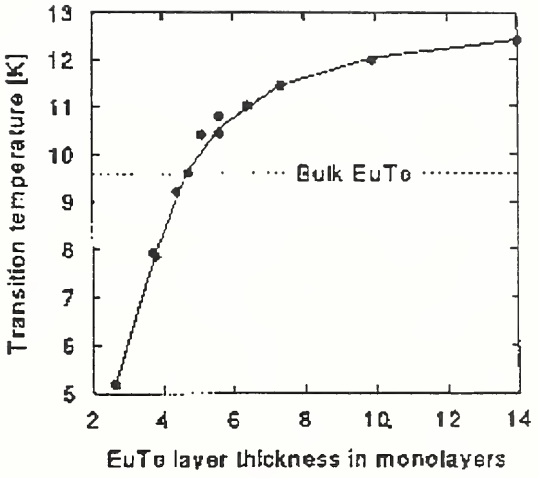

Fig. 14. The dependence of the transition temperature T_N on the EuTe layer thickness observed in a series of EuTe/PbTe SL samples.

layer thickness D_{EuTe} obtained from *ac* χ(T)$ measurements (with *f*=10 Hz, and 5 Gs in-plane field amplitude) on a series of 12 samples is displayed in Fig. 14 (with neutron T_N data being in excellent agreement). While the low T_N values for small D_{EuTe} apparently reflect the proximity of the 3D→2D transition, the increase above the bulk T_N level for larger thicknesses is associated with the increasing in-plane strain that changes the Eu-Eu distances and thus the exchange constants.

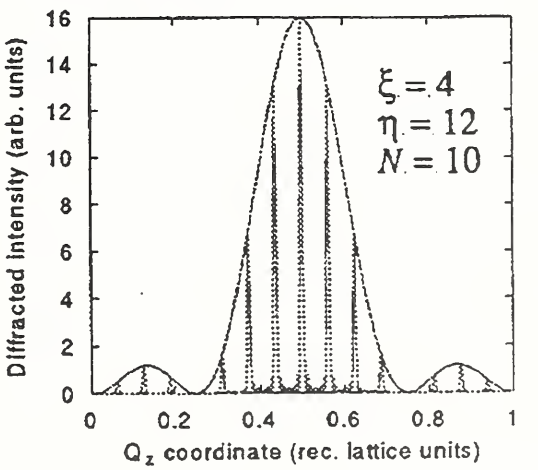

Fig. 15. Simulated diffraction data from: (a) an uncoupled SL – the broad maximum, (b) coupled SL – the multi-peaked curve.

Neutron diffraction also allows one to distinguish states in which successive EuTe layers are magnetically *correlated* or *uncorre-*

lated. In the total absence of correlations, the shape of the AFM reflections in Q-scans parallel to the SL growth axis z essentially repro-

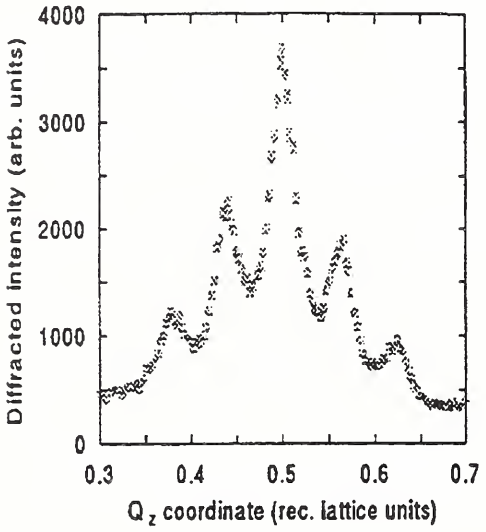

Fig. 16. Magnetic diffraction data from a $[(EuTe)_4|(PbTe)_{12}]_{300}$ SL specimen at 4.2 K.

duces the shape of the *single layer structure factor* $|F_{s.l.}(Qz)|^2 \propto \sin^2(\xi\ dQ_z/2)/\sin^2(dQ_z/2)$ where d is the distance between the spin "sheets" (Fig 15a). In contrast, in the case of spin coherence in successive layers, the spectrum exhibits sharp "satellite" peaks at $\Delta Q_z=2\pi/D$ intervals (where D = the SL period), with heights "modulated" by the $|F_{s.l.}\}|^2$ function (Fig. 15b). In our experiments, distinct satellite peak patterns were observed in almost all investigated samples with thicknesses of the PbTe spacers $D_{PbTe}\leq 60$Å (an example is shown in Fig. 16). These results clearly attest to the existence of some kind of a long-range spin-spin interaction force in the system. Exchange transfer across non-magnetic spacers of similar thicknesses occurs in many *metallic* SL systems with FM layers. It is well established that *conduction electrons* play a crucial role in this process [5]. However, EuTe is a wide-gap semiconductor with virtually no mobile carriers at low T, and in PbTe, a narrow-gap semiconductor, the carrier concentration is only $n\sim 10^{17}$ cm^{-3} — several orders of magnitude less than in typical metals. Moreover, the increase of carrier concentration in the PbTe layers to $n\sim 10^{20}$ cm^{-3} (through doping with Bi) does not enhance the coupling effects — on the contrary, in all such samples investigated by us the satellite lines were either totally absent, or their sharpness visibly deteriorated in comparison with those seen in equivalent undoped samples. Thus, the observed coupling cannot be explained on the grounds of the carrier-mediated mechanism that applies to metallic SLs. Another "easy" explanation of this effect be coupling maintained by internal magnetic fields associated with thickness fluctuations of the EuTe layers — as shown by computer simulations, such fields may be as strong as Bi_{nt} ~20 –50 Gs. However, the formation of such correlations should be impossible if the sample is cooled through T_N at external B of the same strength as Bint, whereas in several samples the satellites were still observed when the cooling occurred at Bext considerably stronger than Bint (Fig. 17).

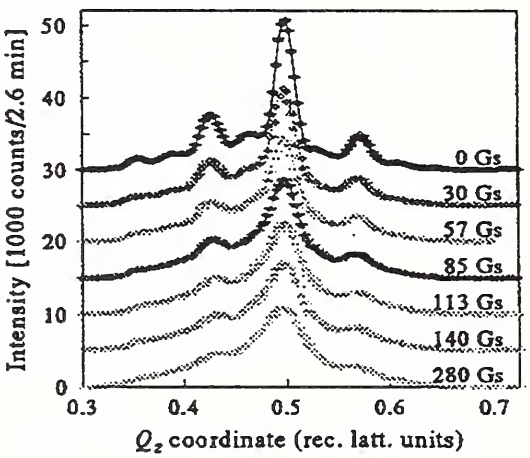

Fig. 17. Magnetic diffraction data from a $[(EuTe)_5|(PbTe)_8]_{400}$ SL cooled through the T_N at different external magnetic fields.

In view of the above, our results strongly suggest that in the EuTe/PbTe system there is a long-range magnetic interaction mechanism not yet taken into consideration in theoretical analyses. Most theoretical studies of magnetic interactions in Eu chalcogenides and related systems were done in 1970's and 80's in context of research on bulk systems, in which only interactions within the nearest few coordination shells are relevant, and weak interactions of longer range can be ignored. However, in SLs where the situation is changed, such interactions may become of importance. The results of our experiments on EuTe/PbTe systems provide a strong motivation for undertaking new theoretical insight into this issue.

Neutron Reflectivity, X-ray Reflectivity, and Spectroscopic Ellipsometry Characterization of SiO_2 on Si (100) [6].

Improved metrology methods are critically needed for the characterization and process control of the ultrathin gate dielectrics of today's and tomorrow's technology. Optical techniques such as ellipsometry are generally used to monitor gate dielectric production. Unfortunately, for very thin films, the accuracy of these optical methods degrades because they are model dependent [6], and use wavelengths of radiation that are very large compared to the film thickness. Neutron and x-ray reflectivity are nondestructive, short wavelength techniques (we use λ=0.475 nm, and λ=0.154 nm, respectively). X-ray reflectivity is a relatively common analytical tool. However, it is not well suited for the case of SiO_2 on Si because the x-ray contrast between them (or difference in scattering length density, SLD) is relatively low, 7.6%. Neutron reflectivity is better suited for the study of the SiO_2/Si system because there is a large contrast, 65% [6]. We show here that the dynamic range of neutron reflectivity, $>10^8$, has been brought to a level on par with that of laboratory x-ray reflectivity measurements.

The sample is a nominally 10 nm thick thermal oxide film on silicon (100). This moderate thickness was chosen to increase our confidence in the results of the various characterization methods, while remaining thin enough that the results are revelent.

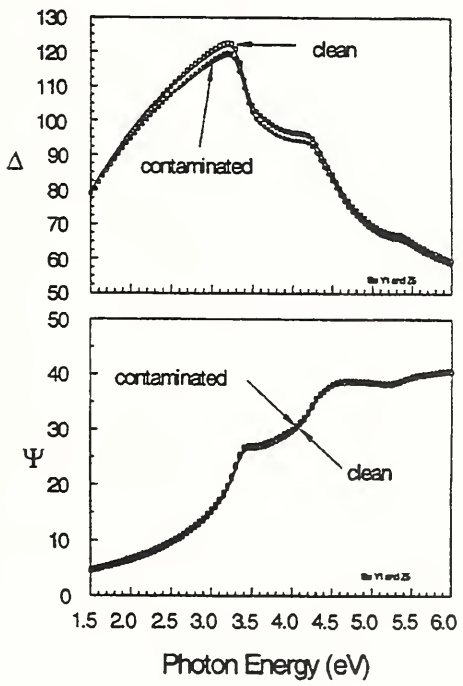

Fig. 18. Spectroscopic ellipsometry data and fits.

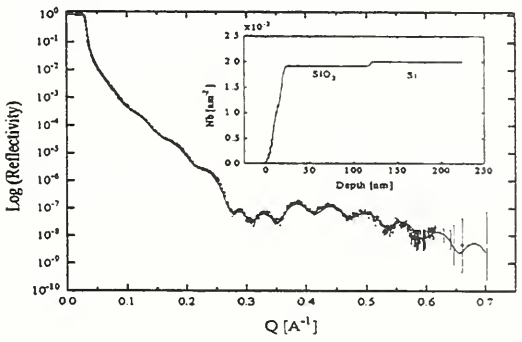

Fig. 19. X-ray reflectivity data and fit. The inset is the SLD profile determined by the fit.

Single-wavelength ellipsometry done before and after the neutron scattering indicated that a contamination layer formed on the sample sometime during the transit, handling, and/or measurement of the sample. This contamination layer was also present on the sample's surface during subsequent x-ray and spectroscopic ellipsometry, SE measurements. An aggressive organic clean was performed and SE was repeated. The results of the SE are shown in Fig. 18. Simple, one-layer analysis indicates that the clean sample is 10.8 nm thick, and the contaminated sample is 0.9 nm thicker. The missing material can be interpreted as the contamination layer. The x-ray reflectivity data in Fig. 19, confirms the presence of this The missing material can be interpreted as the contamination layer. The solid line is the best fit to the data, and corresponds to the profile shown in the inset. There are two periods of oscillation observed in these data, a high frequency period corresponds to 2π divided by the 10.14 nm thickness of the SiO_2 film, and a low fre-

Table 1 . Parameters used in the best fits to the data from the three techniques. NA indicates a parameter not inclued in the model, ND, a parameter not determined by fitting, rather a bulk, or standard value was used. Roughness is the full width at half max of the derivative of the profile about the interface above the given layer. Thicknesses are measured between the middle of adjacent interfaces [8].

Tecnique/ Sample State		Ellipsometry Clean	Ellipsometry Contaiminated	X-Ray Reflectivity	Neutron Reflectivity
Contamination layer	Roughness [nm]	NA	NA	0.93	0.13
	Thickness [nm]	NA	NA	1.03	0.69
SiO_2	Roughness [nm]	NA	NA	0.63	0.94
	Thickness [nm]	10.8	11.7	10.14	10.27
	Density [gm/cm^3]	ND	ND	2.24	2.21
Si	Roughness [nm]	NA	NA	0.24	0.24

quency modulation due to the 1.03 nm thick contamination layer. The parameters used in the fits are shown in Table 1.

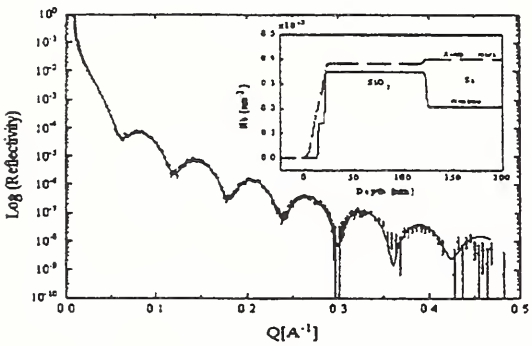

Fig. 20. Neutron reflectivity data and fit. The inset is the SLD profile determined by the fit.

Figure 20 shows the neutron reflectivity data, preliminary fit, and, in the inset, the corresponding SLD profile compared to that from the x-ray data. The fitted parameters are very close to those from the x-ray fits The inset is the SLD profile determined by the fit. In Table 1 we compare the structural profiles obtained from the 3 different analysis techniques. With x-ray reflectivity we gain a direct sensitivity to the surface contamination layer. The x-ray measured value of 1.03 nm agrees well with the 0.9 nm difference in thickness measured but spectroscopic ellipsometry before and after cleaning. The thickness of surface contamination as measured by neutron reflectivity was 0.34 nm thinner. Part of this difference may be explained by the assignment of an additional 0.13 nm to the SiO_2 layer, and the rest can be explained by additional contamination received after the neutron measurements were completed By comparing the structural profiles obtained by three different techniques, which arise from three different scattering length densities we are able to gain multiple perspectives on the interfacial structure of a thin SiO_2 film on Si. While the ellipsometry measurements give quick and reproducible results they do not have the resolution to distinguish various layers. X-ray reflectivity is better able to distinguish the ~1nm surface contamination layer. With neutron reflectivity there is a much higher contrast between SiO_2 and Si than in x-ray reflectivity, thus we are better able to describe the interface between SiO_2 and Si.

Neutron and X-ray reflectometry studies of rough interfaces in a Langmuir-Blodgett film

Langmuir-Blodgett (LB) films have been studied extensively with neutron and x-ray reflectometry. Diffuse scattering data show that their interlayer interfaces are typically self-affine, though the exact nature of this roughness varies significantly with the film composition. Self-affine interfaces have also been found in many different metallic films, where their presence can be related to growth processes.

In this report, we describe neutron and x-ray reflectometry studies of a 20-bilayer barium stearate LB film grown on a silicon substrate with alternating hydrogenated and deuterated bilayers. The large number (35) of Bragg peaks in the x-ray specular reflectivity permits the accurate use of diffuse peak width data to characterize the interlayer roughness.

By examining Kiessig fringes in the neutron and x-ray specular reflectivities, we also study islanding in the film, and find support for a mechanism of islanding related to the film preparation. Incomplete transfer during the

study islanding in the film, and find support for a mechanism of islanding related to the film preparation. Incomplete transfer during the deposition process is likely responsible for the islanding.

X-ray reflectometry experiments were performed at NIST with a double-axis diffractometer using CuK_a radiation. Transverse and longitudinal scans were made with the sample in two orientations. A miscut angle of 0.22 degree was measured relative to the Si (111) surface, and the sample was first oriented so the scattering plane was perpendicular to the miscut steps, and later so it was parallel to the steps. Neutron reflectivity was measured with the NG-1 reflectometer at the NIST Center for Neutron Research.

A detailed analysis of diffuse lineshapes using more extensive data than has been previously considered was performed. The large number of Bragg peaks in the x-ray specular reflectivity suggests that the interlayer roughness in the LB film is highly conformal.

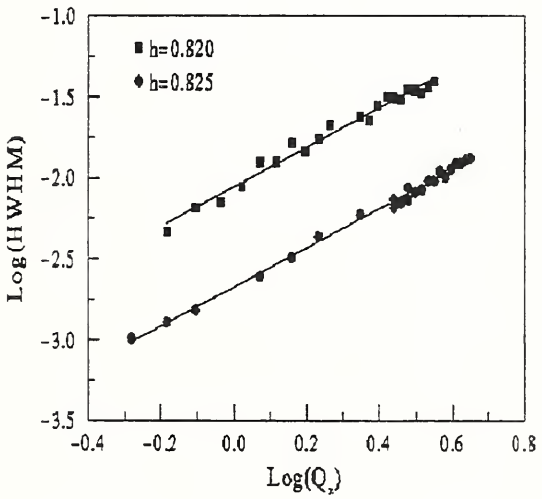

Fig. 21. Log-log plot of the HWHM of the diffuse peaks vs. q_z, measured with the scattering plane parallel (squares) and perpendicular (circles) to the miscut steps. The difference in length scales over which the interlayer roughness is approximately self-affine, presumably a consequence of the steps.

The log-log plot of the HWHM of the diffuse peaks vs. q_z should be linear if the roughness is self-affine [9]. Fig. 21 is a log-log plot of two sets of HWHM data for our LB film. The circles are from transverse x-ray scans made with the sample oriented so the scattering plane was perpendicular to the miscut steps, and the squares are from scans with the scattering plane parallel to the steps. Best-fit lines for both sets of data are also shown. The slopes of the best-fit lines are in excellent agreement, yielding roughness exponents of $h \cong 0.820$ and $h \cong 0.825$, as indicated in the figure.

For both sample orientations, the transverse scans show a resolution broadened specular component, indicating finite length scales perpendicular and parallel to the steps at which the interlayer roughness no longer appears self-affine. The specular component is larger compared to the diffuse component and decays more slowly in the scans perpendicular to the steps than in the scans parallel to the steps. This suggests that the lateral correlation of the film is interrupted by the steps, which are approximately 3 Å high and 750 Å wide. Apparently, however, the steps do not affect the short-range correlation of the film, since a single roughness exponent characterizes the short-range height fluctuations across and along the steps. Intuitively, one expects that the steps may provide a sharp cutoff in the correlation of the film, so that points on the film are completely correlated if they are `above' the same step, and totally uncorrelated if they are above different steps. Without committing to a model for the correlation of the film along the steps, we can still obtain an approximate lower bound on the length scale over which the film no longer appears self-affine in this direction. In order for the steps to have the significant impact that they do on the correlation of the film, the film must be nearly self-affine at least at a length scale on the order of the step width, or 750 Å. The fact that the film appears self-affine over larger length scales along the steps than across them is also evidenced by the difference in intercepts of the best-fit lines in Fig. 21. It is interesting to note that if we assume the correlation of the film along the steps is described by the exponential cutoff model [10], we obtain lower bounds on the saturation rms roughness (σ) and correlation length (λ) of 5 Å and 1200 Å, respectively, which agree with the lower bound we obtain from comparing the HWHM data from scans across and along the steps. We can only obtain lower bounds on these parameters because the log-log plot of our data does not show significant deviations from linearity, which should occur at lower q_z.

The x-ray specular reflectivity for this film shows, apart from a large number of Bragg peaks, many clearly defined Kiessig fringes.

The most striking feature of the Kiessig fringes is their modulation. The modulation of the Kiessig fringes implies that the top bilayer of the film (and perhaps others) is not completely present. From the modulation has been inferred that only 40% of the twentieth bilayer is present.

Direct Inversion of Specular Reflectometry

The phase determination and inversion techniques developed at the NIST Center for Neutron Research have been applied to data obtained from neutron reflectivity experiments performed on thin film samples for the first time. The experiments were performed on the reflectometer located on guide tube NG-1 at an incident wavelength of 4.75 Å.

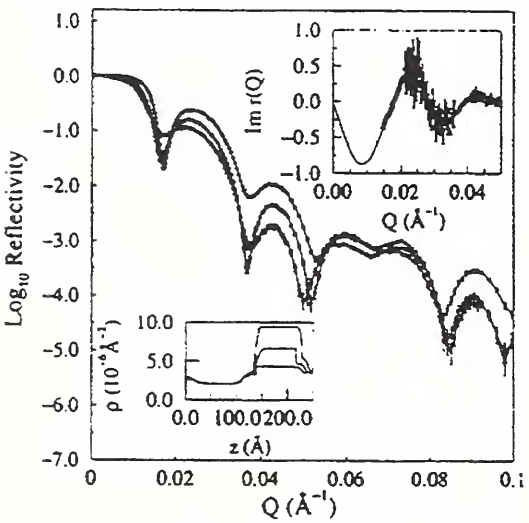

Fig. 22. Reflectivities of composite films of unknown with Ni, Cu, and Mo references (top to bottom at Q=0.03 Å). Measurements extended to Q=0.28 $Å^{-1}$. Lower inset: fitted reference potentials with Si cap. Upper inset: resultant Im r(Q) for the unknown part of the potential. Values below Q=0.015 were interpolated (see text).

Dynamical phase determination requires, in general, that the reflectivity of the film of interest be measured in proximity to three known films as references[11, 13]. (Other recent work has shown that two references suffice, but the analysis is more complicated.) The complex reflection amplitude r(Q) for the isolated unknown is extracted algebraically from these composite spectra. The phase of reflection from symmetric potentials is measurable without references[12].

The reference method of phase determination was applied to deuterated polystyrene on Si. Neutron reflectivities (not shown) were measured for Ni, Cu, and Mo reference layers approximately 2.5 cm wide on the same single crystalline silicon substrate of diameter approximately 10.2 cm.

The films were deposited by sputtering, and some Cr was added between the metal layers and the Si to inhibit interdiffusion and enhance adhesion. The three adjacent bands were covered with a Si "cap" layer, and a layer of deuterated polystyrene was deposited onto this.

Nonlinear least squares fitting of the reference reflectivities gave the scattering length density profiles appearing in the lower inset of Fig. 22. Finally, a deuterated polystyrene film was spin-coated onto the Si cap. The Si cap and polystyrene layer were treated together as the "unknown" potential for this study.

The reflectivities for the composite systems are given in Fig. 22. The upper inset shows the extracted Im r(Q) for the unknown. Values below the Si critical wavevector were interpolated to zero using a low-Q-fitted rectangular barrier. The data in Fig. 22 were obtained with the Si substrate as the fronting medium for the neutron beam. Measurements (not shown) also were made with air as fronting, which gave equivalent results.

The measured r(Q) was inverted for the reflecting potential using the Gel'fand-Levitan-Marchenko (GLM) method. The result is shown in Fig.23.

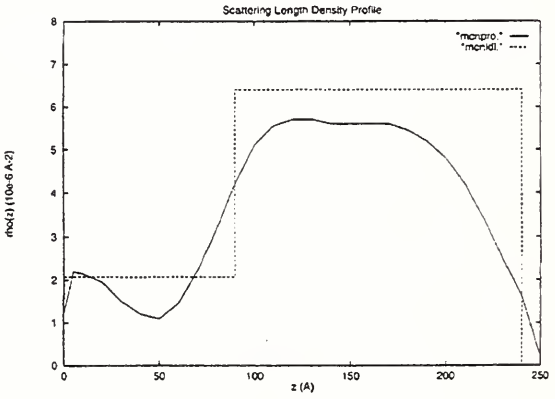

Fig. 23. Inverted potentials from the data in Fig. 1. The dashed line is the expectd profile.

The unknown film (as seen from the substrate side) is expected to be a uniform Si layer, approximately 90 Å, thick abutting a uniform layer of deuterated polystyrene, approximately 150 Å thick. This model fits the composite reflectivities.

The retrieved potential has the correct shape overall but is significantly distorted between 0 Å, and 120 Å. Tests with simulations indicate that these deviations are attributable to our choice of references, which caused two of the three composite reflectivities in Fig. 23 to coincide for Q between 0.05 Å-1, and 0.07 $Å^{-1}$ and thus precluded a reliable determination of r(Q) in this part of the spectrum.

A sample with a symmetric potential was prepared by spin-coating a deuterated polystyrene film onto a single crystalline Si substrate, which had been chemically treated to remove the native oxide layer. The film was placed in direct contact with an aqueous reservoir contrast matched to the substrate. This construction effectively ensured symmetric fronting and backing with smooth, conformal interfaces.

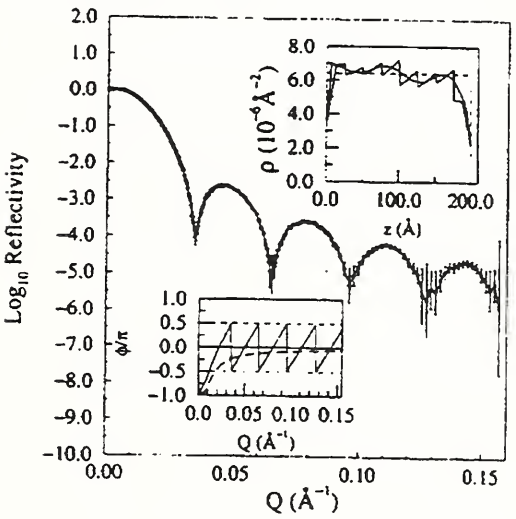

Fig. 24. Reflectivity from a symmetric polystyrene film. The sharp dips are interpreted as true zeros, which induce π-discontinuities in the phase. Lower inset: deduced phase of reflection. The long dashed line is the computed phase of transmission. Upper inset: the inverted potential.

Figure 24 shows the reflectivity data for this sample, measured as shown to Q= 0.16 $Å^{-1}$. The lower inset of Fig. 24 is the phase angle or r(Q), as deduced from the analysis described in ref. [12]. The dashed line in the inset is the phase of the transmission amplitude, t(Q)[12].

The upper inset of Fig. 24 depicts the potential inverted from Im r(Q), using the GLM method. Agreement generally is good between the profile determined by inversion and that expected from the fabrication.

We have presented examples designed to demonstrate the present experimental feasibility of phase determination and inversion of neutron reflectivity data. As seen in the first example, the choice of references can be important, but forethought and experience with the technique preempt such problems for a wide range of physically interesting films. The phase determination method for symmetric potentials can be extended to a wider range of films which are fabricated in symmetric configurations for the purpose. More detailed discussions of these results will be presented in a comprehensive report[4].

References

[1] F. Kalaydjian *et. al*, Soc. Pet. Eng., 26671 (1993).

[2] C. Del Cerro and G. J. Jameson, J. Colloid. Inter. Sci. **78**, 362 (1980).

[3] K. Ragil et. Al. Phys. Rev. Lett. **77**, 1532 (1996).

[4] Work performed by H. Kepa, K. I. Goldman, T. M. Giebultowicz, Oregon State Univ., Corvallis, OR; C. F. Majkrzak, National Inst. Of Stands. And Techn., Gaithersburg, MD; G. Springholtz, H. Krenn, S. Holl, F. Schinagl and G. Bauer, J. Kepler Universität Linz, Austria.

[5] See, e.g., P. Bruno, J. Appl. Phys. **76**, 6972 (1994)

[6] J. A. Dura, C. A. Richter, C. F. Majkrzak, work in progress.

[7] N.V. Nguyen and C.A. Richter, Thickness Determination of Ultra-Thin SiO_2 Films on Si by Spectroscopic Ellipsometry, Silicon Nitride and Silicon Dioxide Thin Insulating Films IV, M.J. Deen, W.D. Brown, S.I. Raider and K. Sundaram, Editors, PV 97-10, Montreal, Canada - May 1997.

[8] J. A. Dura, and C. F. Majkrzak, in Semiconductor Characterization: Present Status and Future Needs, eds.W.M. Bullis, D.G. Seiler, and A.C. Diebold (AIP Press, Woodbury, NY, 1996) pp. 549-55.

[9] H. Kepa, L. J. Kleinwaks, N. F. Berk, C. F. Majkrzak, T. S. Berzina, V. I. Troitsky, R. Antolini, L. A. Feigin - Neutron and x-ray reflectometry studies of rough interfaces in a Langmuir-Blodgett film, Physica B (in print)

[10] S. K. Sinha, E. B. Sirota, S. Garoff, H. B. Stanley, Phys. Rev. B 38 (1988) 2297.

[11] C. F. Majkrzak and N. F. Berk, Phys. Rev. B **15**, 10825 (1995)

[12] N. F. Berk and C. F. Majkrzak, J. Phys. Soc. Jpn. 65 Suppl. A, 107 (1996)

[13] V. O. deHaan, A. A. van Well, S. Adenwalla, and G. P. Felcher, Phys. Rev. B **15**. 10830 (1995).

[14] C. F. Majkrzak and N. F. Berk, to be published.

Research Topics

Adsorption of Surfactants at a Hydrophobic Surface Near the Solid-Liquid Interface
D. C. McDermott[59], R. Thomas[59], A. R. Rennie[49], S. K. Satija[22] and P. D. Gallagher[22]

Adsorption of Surfactants on Hydrophobic Surfaces
A. Rennie[49], P. Thirtle[59] and R. Thomas[59]

Antiferromagnetic Spin Ordering and Interlayer Magnetic Correlations in MnTe/CdTe Superlattices
T. M. Giebultowicz[7], W. Faschinger[55], G. Bauer[55], V. Nunez[56,22], P. Klosowski[22] and J. K. Furdyna[58]

Block Copolymers in Confined Geometries
P. Lambooy[10], T. P. Russell[10], G. Kellogg[16], A. Mayes[16], S. K. Satija[22] and P. D. Gallagher[22]

Branched Linear Polymer Blends
D. Walton[16] and A. Mayes[16]

Crosslinked Polymer Interdiffusion
W-L. Wu[26] and W. Wallace[26]

Development of Molecular Beam Epitaxy Chamber for Neutron Scattering
J. A. Dura[22]

Effect of Solvent on Surface Induced Diblock Copolymer Ordering
H. Lin[28], A. Steyrl[61], A. Karim[26], T. P. Russell[10], and S. K. Satija[22]

Effects of H Loading on Magnetic Properties of Fe/V Superlattices
J. A. Dura[22], B. Hjorvarrson[61], T. J. Udovic[22], T. Watanabe[41] and C. F. Majkrzak[22]

Effects of Field Cycling on Co/Cu and Co/Ag Multilayers
J. A. Borchers[22], J. A. Dura[22], T. Watanabe[41] and C. F. Majkrzak[22]

Exact Determination of the Giant Fe Moment in $Fe_{16}N_2$ Films
T. Watanabe[41], Y. Sugita[9], J. A. Borchers[22], J. A. Dura[22] and C. F. Majkrzak[22]

Fe/Si Supermirror Polarizer Efficiency
J. Wood[31] and C. F. Majkrzak[22]

Fe/Cr Superlattices: Polarized Neutron Study of Interlayer Coupling
A. Schreyer[34], J. F. Ankner[17], H. Zabel[34] and C. F. Majkrzak[22]

Interfacial Spin States in Magnetic Tunnel Junction Structures
C. Platt[48], A. Berkowitz[48], J. A. Borchers[22], J. A. Dura[22] and C. F. Majkrzak[22]

Interfacial Structures of Electrically Conducting Adsorbed Multilayers
G. Kellogg[16], A. Mayes[16], W. Stockton[10], M. Ferreira[16], M. F. Rubner[16] and S. K. Satija[22]

Lamellar Surfactant Phases at Solid-Liquid Interface
G. Salamat[2] and K. Wong[2]

Langmuir Films of Block Copolymers
M. Kent[36] and G. Smith[14]

Location of Peptides in Alkanethiol/Phospholipid Biomimetic Bilayer Membranes
S. Krueger[22], A. Plant[21], K. Meuse[21], C. F. Majkrzak[22], and J. A. Dura[22]

Magnetic Depth Profile of CMR Perovskite Films and Spin Values
Y. Ijiri[22], J. A. Borchers[22], J. W. Lynn[22], R. W. Erwin[22], C. F. Majkrzak[22], M. Robeson[56], R. Ramesh[56], V. Venkatesan[56] and R. Greene[56]

Magnetic Diffuse Scattering in Co/Cu and Co/Ag Multilayers
J. A. Borchers[22], J. A. Dura[22], T. Watanabe[41], C. F. Majkrzak[22], J. Bass[15], W. P. Pratt, Jr.[15], S. Y. Hsu[15] and R. Loloee[15]

Magnetic Homogeneity of a Fe_3O_4 Film Capped with Co
R. W. Erwin[22], J. A. Borchers[22], C. F. Majkrzak[22], D. Marguiles[48] and A. E. Berkowitz[48]

Magnetic Structure Determination in Annealed $Ni_{83}Fe_{17}$/Cu Multilayers
J. A. Borchers[22], P. M. Gehring[22], C. F. Majkrzak[22], J. F. Ankner[1757], A. M. Zeltser[3] and Neil Smith[3]

Magnetic Structure in Discontinuous Co-SiO_2 Mulilayers
S. Sankar[48], A. Berkowitz[48], J. A. Borchers[22], J. A. Dura[22] and C. F. Majkrzak[22]

Neutron Reflectivity Characterization of Thin SiO_2 SRMs Materials
J. A. Dura[22] and C. Richter[27]

Neutron Reflectivity Studies of Biological Membrane Films
K. Gawrisch[18], B. Koenig[13], S. Krueger[22], N. F. Berk[22] and C. F. Majkrzak[22]

Nickel Oxide Electrochemistry
R. Hillman[54]

NiC/Ti Supermirror Coating Reflectivity
J. Wood[31] and C. F. Majkrzak[22]

Origin of Low-Field Giant Magnetoresistance in $Ni_{80}Fe_{20}$/Ag Multilayers
J. A. Borchers[22], P. M. Gehring[22], J. F. Ankner[17], C. F. Majkrzak[22], T. L. Hylton[11], K. R. Coffey[11], M. A. Parker[11] and J. K. Howard[11]

Particle Size Determination of Metals in Ceramic Matrices
A. Gibaud[42], S. K. Satija[22], J. A. Dura[22], L. Sung[22,56]

Phase Determination and Inversion in Specular neutron Reflectometry
C. F. Majkrzak[22], N. F. Berk[22], J. A. Dura[22], S. K. Satija[22], A. Karim[26], J. Pedulla[20] and R. D. Deslattes[20]

Polarization of the Rh Layer in Fe/Rh Superlattices
J. A. Borchers[22], T. Watanabe[22,41], J. A. Dura[22], C. F. Majkrzak[22], G. R. Harp[29] and M. A. Tomaz[29]

Polyelectrolyte Brushes
D. Irvine[16] and A. Mayes[16]

Polyimide Foam Films
J. Fodor[56] and R. Briber[56]

Proteins in Thin Films
A. Liebmann[43], H. Wu[43], M. Foster[43] and C. F. Majkrzak[22]

Selective Solvation in Lamellar Block Copolymer Thin
R. Levicki[57], N. Koneripalli[57], M. Tirrell[57], F. S. Bates[57], and S. K. Satija[22]

Selective Transmutation Doping in Silicon Epilayers
J. A. Dura[22], T. Golding[52] and R. Lindstrom[22]

Structural Characterization and Magnetism of Fe/Tb Multilayers
N. S. Rosov[22], J. A. Borchers[22], A. Freitag[44] and A. R. Chowdhury[44]

Structure and Diffusion in Langmuir-Blodgett Films
L. A. Feigin[33], H. Kepa[30], N. Berk[22], L. Kleinwaks[25], C. F. Majkrzak[22] and J. A. Dura[22]

Structure of a Bimodal Polymer Brush
M. S. Kent[36], B. J. Factor[26], G. S. Smith[14], and S. K. Satija[22]

Studies of Magnetic Critical Scattering in Strained and
Lattice-Matched (Y/Lu)mid Homid (Y/Lu) Films
P. M. Gehring[22], C. F. Majkrzak[22], J. A. Dura[22], L. Doloc[22,56], L. D. Gibbs[1], A. C. Lake[59], J. Goff[59] and R. A. Cowley[59]

Surface and Phase Behavior of Thin Polymer Blend Films
T. Slawecki[22], S. K. Kumar[32], A. Karim[26] and S. K. Satija[22]

Surface Segregation in Thin Polymer Films
N. Singh[57], M. Sikka[57], F. S. Bates[57], S. K. Satija[22] and P. D. Gallagher[22]

Surface Segregation of Polymers
N. Pellgrini[60] and K. Winey[60]

UHV Ion-Beam Etching Investigations of the Origin of Two Length Scales
J. A. Dura[22], P. M. Gehring[22], C. F. Majkrzak[22] and G. Shirane[1]

Wetting on Polymer Surfaces by Critical Binary Fluids
P. D. Gallagher[22], S. K. Satija[22], A. Karim[26] and L. Fetters[5]

X-ray Characterization of Interfaces in Exchange-biased Trilayers
N. Gökemeijer[13], J. A. Borchers[22]

Affiliations

1 Brookhaven National Laboratory
2 CEN, Saclay, France
3 Eastman Kodak Company, San Diego
4 Eastman Kodak Company, Rochester
5 Exxon Research and Engineering Company
6 Florida State University
7 George Mason University
8 Georgetowm University
9 Hitachi, Japan
10 IBM Almaden
11 IBM Storage Systems Division
12 Institut Laue Langevin, France
13 Johns Hopkins University
14 Los Alamos National Laboratory
15 Michigan State University
16 Massachusetts Institute of Technology
17 Missouri University Research Reactor
18 National Institutes of Health
19 Naval Research Laboratory
20 NIST, Atomic Physics Division
21 NIST, Biotechnology Division
22 NIST Center for Neutron Research
23 NIST, Ceramics Division
24 NIST, Inorganic Analytical Research Division
25 NIST, Metallurgy Division
26 NIST, Polymers Division
27 NIST, Semiconductor Electronics Division
28 Oak Ridge National Laboratory
29 Ohio University
30 Oregon State University
31 Ovonics Company
32 Penn State University
33 Russian Academy of Science, Russia
34 Rühr University, Germany
35 Rutgers University
36 Sandia National Laboratory
37 Sandia University
38 Southwest Texas State
39 Texas Instruments

[40] Thomson-CSF, France
[41] Tohoku University, Japan
[42] Universite du Maine, France
[43] University of Akron
[44] University of Alaska
[45] University of Arizona
[46] University of Arkansas
[47] University of Bath, United Kingdom
[48] University of California at San Diego
[49] University of Cambridge, United Kingdom
[50] University of Delaware
[51] University of Florida
[52] University of Houston
[53] University of Illinois
[54] University of Leicester, United Kingdom
[55] University of Linz, Austria
[56] University of Maryland at College Park
[57] University of Minnesota
[58] University of Notre Dame
[59] University of Oxford, United Kingdom
[60] University of Pennsylvania
[61] University of Rhode Island
[62] Uppsala University, Sweden

Macromolecular and Microstructure Studies

Two, high resolution, 30 m long, small angle neutron scattering (SANS) instruments, and a moderate resolution 8 m SANS instrument, are the principal tools used at the NCNR to characterize the nanoscale structure (~1 to 400 nm) of a wide variety of materials including polymers, colloids and microemulsions, microporous media, biological macromolecular complexes, nanocrystalline metals and ceramics, molecular composites, and many others. Over 200 researchers from domestic and foreign universities, and industrial and government laboratories, carried out experiments on these instruments during the year covered in this report. The titles of the studies conducted in the past year, in these areas, are listed at the end of this section. Summarized below are highlights of some of this work in which NCNR staff scientists have played a leading role.

Polymerization of Rod-Like Surfactant Micelles

Surfactant molecules self-assemble into micellar aggregates at concentrations greater than their critical micelle concentration (CMC). A variety of aggregate structures can form such as spherical or rod-like micelles, vesicles, or lamellar phases. In particular, long, entangled, rod-like micelles display very rich rheological behavior, often at very low total surfactant concentrations (only a few mM). Such solutions show highly non-linear rheology, and can be highly viscous and viscoelastic. The equilibrium and dynamics of the micellar structures, however, are determined by a delicate balance of intermolecular forces that can be easily disrupted. For example, increasing the temperature or adding electrolyte can alter the micellar structure and have dramatic effects on the resulting solution viscosity. A method for "locking in" the micellar structure so that it is less sensitive to environmental changes would be advantageous for applications. One approach is the stabilization of surfactant structures by the use of polymerizable surfactants, and this technique has been applied to vesicular structures for possible application as drug delivery systems or model biological membranes.

We have attempted to capture the entangled network structure of rod-like micelles through the use of the polymerizable surfactant cetyltrimethylammonium vinyl benzoate (CTVB), prepared here at NIST [1]. Aromatic counterions bind tightly to the micellar surface and promote growth of the micelles into highly elongated structures at very low concentrations (CMC = 0.007 wt%). A solution of 0.1 wt% (2 mM) CTVB in D_2O is significantly more viscous than pure D_2O, and highly elastic. Although the total surfactant concentration is very low, polymerization is still possible since the polymerizable species (the counterions) are highly concentrated at the micellar surface. Initiation of the reaction with a free radical initiator (5 mol % based on surfactant) results in a fast reaction, completed within 15 minutes at 60°C.

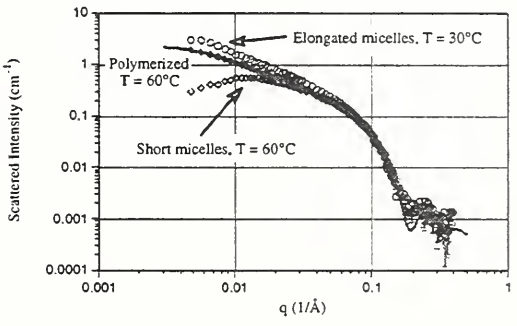

Fig. 1. SANS data for 0.1 wt% CTVB in D_2O before and after polymerization. There is a significant difference in the structure of the unpolymerized micelles at 30°C and 60°C evident from the change in the scattered intensity. The scattering from the polymerized micelles is insensitive to temperature, and is fit well with a model (solid line) of uncharged cylinders 40 Å in diameter and 420 Å long.

SANS data for the unpolymerized and polymerized micelles are shown in Fig. 1. The upper and lower data points are the unpolymerized micelles at 30°C and 60°C respectively. The reduction in the low-Q scattering at 60°C indicates a decrease in the micelle length at higher temperatures, in agreement with living polymer models. The middle data set is the same sample, after free-radical polymerization at 60°C. The increased low q scattering (compared to micelles at 60°C) and Q^{-1} dependence indicates cylindrical structures. The polymerized structures retain the same cylindrical cross-sectional structure of the micelles, as evident from the overlap of the SANS data at $Q > 0.08$ Å^{-1}. The polymerized solution, however, does not retain the viscoelastic properties of the parent micellar solution, but rather be-

comes as fluid as the pure D_2O solvent. The polymerized micelles are modeled well as non-interacting cylinders (solid line) of D = 40 Å and L = 420 Å at a volume fraction of f = 9.2 x 10^{-4}. Zimm analysis of a concentration series yielded a molecular weight of the surfactant-polymer complex of 300,000 g/mol, corresponding to an average length of 380 Å, in good agreement with the cylinder model that was used to model the full Q-range of the data.

These results show that the polymerized structures do retain some of the physical dimensions of the parent micelles, but none of the rheological properties. Future experiments will focus on polymerization conditions that retain the cylindrical microstructure as well as preserve the viscoelasticity of the original micellar solution.

Diblock Copolymer Mixtures under Shear

Block copolymers are widely used commercially as compatibilizers, adhesives and as thermoplastic elastomers due to their unique physical and mechanical properties. They are also model systems to examine the process of self assembly (found in surfactant and lipid membranes). In an effort to control microstructure, and hence physical and mechanical properties, mixtures of diblock copolymers have been the subject of several recent studies. Most of these studies have found that diblock mixtures obey, in general, mean-field theories and standard mixing laws.

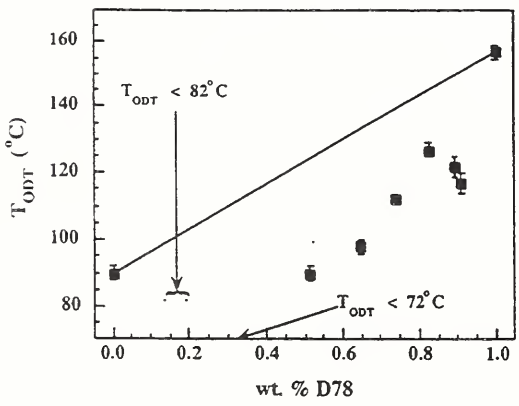

Fig. 2. Compositional dependence of the Order-Disorder Temperature for a series of styrene-isoprene diblock copolymer blends. The straight line is the simple mixing law prediction.

In the present study [2], we have examined blends of diblock copolymers of polystyrene (PS) and 1,4 polyisoprene (PI). The first diblock is nearly symmetrical (named D19), has an overall molecular weight of 19 K, and possesses an order-disorder temperature (ODT) of 90 ± 2°C. The second diblock (D78) is highly asymmetrical containing only 11 vol. % PS with an overall molecular weight of 78.5 K, and an ODT of 156 ± 2°C.

A series of mixtures of these two diblock copolymers were prepared spanning the entire range of compositions between the two pure components. The ODTs for the samples were determined by SANS as a function of temperature. These were further verified by dynamic mechanical rheological measurements as a function of temperature in a melt state rheometer. The ODT's determined by SANS and rheology agree within experimental error and are shown in Fig. 2.

The ODT for the blends is dramatically lowered from the values expected from a simple mixing law (straight line). Furthermore the ODT values near both limits of composition show an unexpected decrease. The correlation hole d-spacing ($2p/q_{max}$) obtained from the SANS peak intensity (at q_{max}) for the series of blends in the single phase region (at 90°C) shows considerable non-linearity as a function of blend composition (as shown in Fig. 3).

In order to probe the microstructure and alignment kinetics of these diblock copolymer mixtures, *in-situ* shearing experiments using the NIST Plate/Plate Shear Cell were undertaken. Scattering measurements were performed with the neutron beam along the velocity-gradient direction as well as along the neutral direction, so as to completely probe the microstructure as well as its evolution.

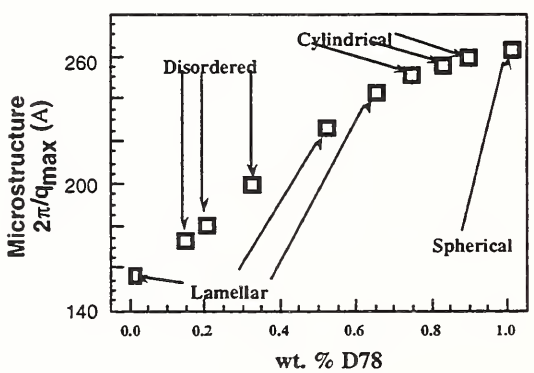

Fig 3. Dependence of the correlation hole d-spacing ($2p/q_{max}$) for a series of styrene-isoprene diblock copolymer blends at 90°C. Based on the SANS "spot patterns", a microstructure is determined

The *in-situ* shear SANS experiments revealed an interesting phase behavior (also shown in Fig. 3). No thermally-induced order-order

transitions were observed in the melt-state, although upon cooling to room temperature distortions to some of the aligned structures were observed. As expected the pure D19 sample is lamellar (at 82 and 85°C) and D78 possesses a spherical microstructure which arranges into a BCC crystal upon application of large amplitude shear at a temperature of 100°C. Upon cooling, D78 exhibits considerable strain in its packing with the reflections being slightly displaced. *In situ* shear experiments were also carried out on blends containing D78 as the majority component. Surprisingly, lamellar microdomains were observed for blends containing up to 65 wt. % D78 (i.e., a styrene volume fraction of 0.21). These could also be aligned "parallel" (with layer normals in the velocity gradient direction) and "perpendicular" (layer normals along the neutral direction), with the "perpendicular" aligned sample capable of being flipped to a predominately "parallel" state. Samples containing a higher level of D78 exhibited cylindrical microstructure during the *in-situ* alignment at high temperatures. However, a sample with 75 wt. % D78, exhibited a mixed microstructure upon cooling down to room temperature with a predominantly lamellar orientation near the stationary surface.

The phase behavior and microstructure of polystyrene-polyisoprene diblock copolymer blends (with a symmetric and an asymmetric component) is remarkably varied. The ODT was found to show significant deviations from a simple mixing law. Furthermore, the microstructures for these blends are considerably different from those observed for pure diblock copolymers with the same composition of the constituent chains. Moreover, a destabilization of the ordered lamellar (or spherical) phase is observed for a small addition of spherical (or lamellar) diblock, respectively.

Shear-Induced Micellar Crystal Structures in Triblock Copolymer Solutions

Amphiphilic triblock copolymers have attracted considerable interest recently both for their potential applications as novel surfactants and as model systems for the study of macromolecular self-assembly. In particular, triblocks of polyethylene oxide (PEO) and polypropylene oxide (PPO) have been found to possess rich structure in solution due to the increasing hydrophobicity of PPO with increasing temperature. Symmetric $PEO_nPPO_mPEO_n$ triblocks are soluble in water at low temperatures, but are driven to aggregate and form micelles as the temperature is raised. Further heating for concentrations above ~ 20 weight % leads to a polycrystalline gel-like phase which can be aligned to form a single crystal by imposing a weak shear field.

We have found in our SANS studies [3] of the commercially available triblock, $PEO_{25}PPO_{40}PEO_{25}$, known as P85, that shear can not only align polycrystalline domains, but can induce transformations to structures not previously observed which can be highly ordered and highly stable. For example, the application of large amplitude oscillatory shear (400% strain, 17 s^{-1} maximum shear rate) to a 30 weight % solution of P85 in D_2O at 30° C (in the gel-like phase), produces SANS patterns with several orders of

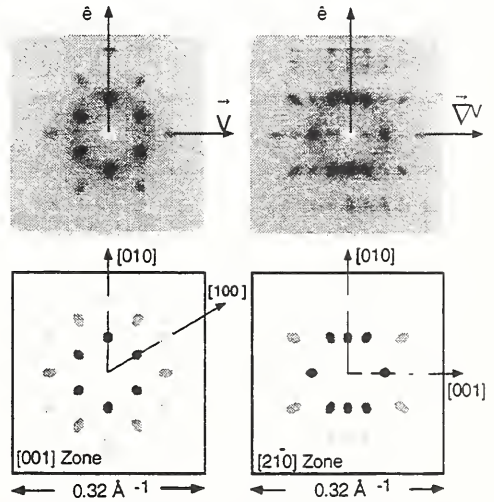

Fig. 4. Top: SANS patterns following the application of oscillatory shear to a 30 wt. % solution of spherical, triblock copolymer micelles at 30°C. The two patterns, measured with the beam perpendicular (upper left), and parallel (upper right) to the walls of the shear cell, are indicative of a hexagonal micellar crystal structure that is nearly HCP. The lower half of the figure shows the calculated diffraction peak positions, with approximate relative intensities in shades of gray, for this structure for the two measurement geometries.

sharply defined diffraction peaks as shown in Fig. 4. The peaks in these two patterns can be indexed on a simple hexagonal unit cell (space group P6/mmm), with cell dimensions a=b=13.3 nm and c=20.9 nm. The basal plane dimensions are in good agreement with the micellar "hard sphere" size of ≈ 6.0 nm determined in previous studies. The ratio c/a = 1.57 is close to that for an ideal hexagonal close-packed (HCP) structure (1.63). However, if the structure were HCP there would be no intensity at the (00*l*) reciprocal lattice points, for odd-*l*, whereas weak peaks are observed at (001) and (003) (see Fig. 4, top right). This is a surprising result since only cubic or cu-

batic structures have thus far been reported for this same triblock copolymer [4].

The hexagonal structure formed in P85 by large amplitude oscillatory shear showed no tendency to change over several hours and was disrupted only by imposing a steady continuous shear flow. The structure of the flowing system inferred from the SANS data (tangential views, in particular) appears to consist of highly oriented close-packed planes, parallel to the shear cell walls, that move relative to one another with a slip-stick type of motion among the interstitial sites in adjacent planes. This type of structure and motion is a common feature of concentrated charge-stabilized latex colloidal solutions. Most remarkably, when steady shear is stopped, the system transforms reversibly into still another structure that is presently not understood, but is neither simple hexagonal nor cubic (fcc or bcc).

Scaling Laws for Polymers in Marginal Solvents

The ability of scaling laws to predict fundamental physical parameters describing polymer chains in semidilute solution have produced a dramatic increase in theoretical and experimental interest in polymer solutions over the last two decades. As shown on a temperature-concentration (T-C) diagram for a particular polymer solvent system, scaling laws predicted the presence of three scaling regimes [5], the *dilute* regime where the polymer concentration ϕ is below the value where separate coils interact, the *good* solvent semidilute regime where the coils overlap (semidilute) and swell between contacts, and the *theta* semidilute solvent regime where coils overlap but do not swell. Each regime has physical parameters that scale by power-laws with respect to either the polymer volume fraction ϕ, or to the excluded volume parameter, υ which is proportional to the reduced temperature $\tau = (T-\theta)/\theta$, where T is the temperature and θ is the theta point (lower critical solution temperature) for the system.

Table 1. Scaling laws predicted for the screening length ξ.

Region	ξ
Good [5]	$\phi^{-3/4}\tau^{-1/4}$
Marginal [6]	$\phi^{-1/2}\tau^{-1/2}$
Theta [5]	ϕ^{-1}

Subsequent experimental investigations revealed some shortcomings of the scaling law predictions, particularly for shorter chains or poorer solvent quality. Schaefer [6] attributed much of the discrepancy to lack of incorporation of chain stiffness in the scaling theory. Using a perturbation approach and the blob model (where short lengths of the chain between contact points obey the ideal thermodynamic interactions, and the random walk of the individual blobs swell due to the excluded volume effect), and incorporating the effect of chain stiffness upon swelling at short length scales, a *marginal* semidilute solvent regime with its own scaling laws was predicted. Table 1 shows the predicted scaling exponents for the different semidilute regimes. To test the predictions for scaling behavior in marginal solvents over a wider region of T-C than ever before, the solvent Decalin (decahydronaphthalene) was used in place of the often used solvent cyclohexane. Like cyclohexane, this solvent has a strong dependence of υ upon reduced temperature τ, both having a small Flory's reduced residual partial-molar entropy of dilution for the system $\chi_S = 0.2$. has a larger range of accessible temperature t_{max} = 0.6 versus 0.1 for cyclohexane (due to its higher boiling point / theta temperature ratio). In addition most prior studies used polymer of insufficient molecular weight to clearly limit the effect of dilute solvent regime. In this study, very high molecular weight polystyrene M_w = 1.54 x 10^7 g/mole was used to keep the dilute solution regime as far as possible from the experimentally accessible T-C region as shown as shaded region

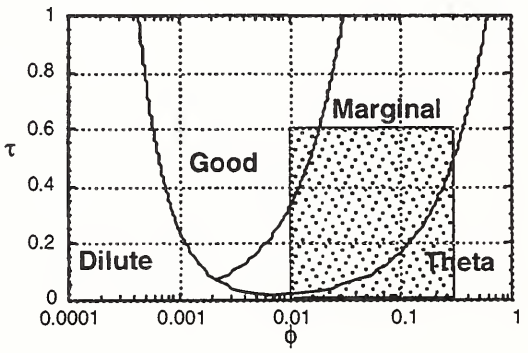

Fig. 5. Temperature-concentration diagram based on Schaefer et al model [6] for 1.54x10^7 g/mole molecular weight polystyrene in Decalin.

in Fig. 5. Using this system, both the concentration and solvent quality could be probed over a large range that is within the limits predicted for the marginal solvent regime. Figure 5 shows the

expected T-C diagram for the experimental system. Note that the transition between different scaling regimes is gradual, i.e., the scaling exponents are expected to have a gradual transition with respect to different parts of the diagram.

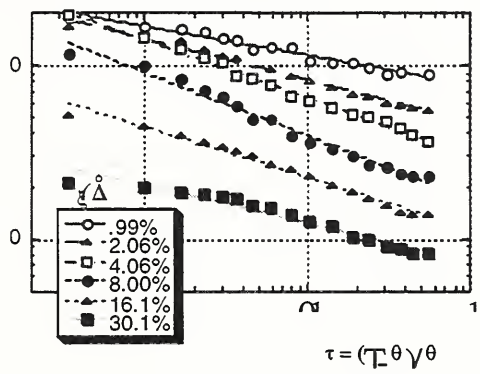

Fig. 6. Measured screening length versus reduced temperature τ. Legend indicates different sample polymer concentrations.

Figure 6 shows the measured screening lengths derived from the SANS measurement [7] as a function of τ and ϕ. All the trends in the data are as expected. The power-law fit exponents of the data as a function of τ are listed in Table 2.

Table 2. Measured exponents for the temperature dependence of the screening length: $\xi = A\tau^{-m}$.

ϕ	m	possible regime(s) fit.
.010	.17	dilute/good
.021	.24	good
.041	.33	good/marginal
.080	.37	good/marginal
.16	.29	good/marginal
.30	.22	marginal/theta

The measured scaling exponents agree qualitatively with T-C diagram. The theta regime is evident in the constancy of ξ for the low temperature data for the ϕ = 0.30 sample. The fit to the ϕ=0.021 sample data agrees with the good solvent regime. The rest of the higher concentration data lies within the marginal regime of the T-C diagram which should have an exponent of 0.5, while the observed value is ~ 0.35. These results indicate a transition to an exponent between the good and marginal solvent predictions, partly in agreement with Schaefer's prediction.

References

[1] S. R. Kline (to be published).
[2] R. Krishnamoorti, B. Hammouda, S. Rai, Bull. Amer. Phys. Soc. 43 (1998)
[3] T. M. Slawecki, C. J. Glinka and B. Hammouda (submitted to Phys. Rev. E, 1997).
[4] K. Mortensen, J. Phys.: Condens. Matter 8, A103-A124 (1996).
[5] M. Daoud and G. Jannink, J. Phys. (Les Ulis. Fr.) 37, 963 (1976).
[6] D. Schaefer, Polymer 25, 387 (1984).
[7] J. G. Barker, to be published.

Research Topics

POLYMERS

Polyolefin Blend Kinetics
N. Balsara[39], H. Wang[39] and B. Hammouda[31]

Homopolymer/Copolymer Blends under Pressure
N. Balsara[39], H. Lee[39] and B. Hammouda[31]

Pressure Effects on Blend Miscibility in PEB/PMB Polymer Mixtures
N. Balsara[39], A Lefebvre[39] and B. Hammouda[31]

Pressurized Crystalline/Amorphous Poly-(Ethylene-Butylene) Copolymers
R. Krishnamoorti[52] and B. Hammouda[31]

Polystyrene-Polyisoprene Copolymers under Poiseuille Shear
R. Krishnamoorti[52] and B. Hammouda[31]

Polystyrene-Polyisoprene Diblock Copolymer Phase Transitions
R. Krishnamoorti[52] and B. Hammouda[31]

Polymer Chain Conformation of Isotopic Polystyrene Blends in Controlled Pore Glass
R. Briber[53], D. Ho[53] and I. Teraoka[39]

Molecular Weight Dependence of the Conformation of Hypergraft Polymers in a Theta Solvent
R. Briber[54], S. Choi[54] M. Gauthier[64], B. Bauer[33] and A. Topp[33]

Polymer Chain Conformation in Thin Films: Deviations from Bulk Behavior in dPS/PS Films
S. Kumar[38], R. Jones[38] R. Briber[54], L. Ho[54] and T. Russell[55]

Effects of Surfactants on the Conformation of Grafted Polymer Brushes
T. Cosgrove[46] and R. Wesley[36]

Investigation into the Form and Intensity of the Fluctuation Term for Adsorbed Polyelectrolytes
T. Cosgrove[46], J. Hone[46] and T. Obey[46]

Effects of Pressure on the Lower Critical Ordering Temperature of Diblock Copolymers
A.-V. Ruzette[28] and A. Mayes[28]

Structure and Phase Separation of Ionomer Blends
R. Tucker[47] and R. Weiss[47]

Effects of Supercritical CO_2 on the Phase Behavior of Block Copolymer Melts
J. Watkins[55] T. Russell[55]

Structure of Anisotropically Swollen
F. Horkay[17] and E. Geissler[51]

Scattering Properties of Chemically Cross-linked Polyisoprene Gels
F. Horkay[17]and G. McKenna[33]

Electric Field-Induced Orientation of Diblock Copolymers in Thin Films
P. Mansky[55], J. DeRouchey[55] and T. Russell[55]

Morphology-Structure Relationships in Ionomer Blends
M. Moffitt[25], D. Nguyen[6], D. Schneider[6]

Structure of Polymers for Advanced Coatings
J. Higgins[1] and E. McConnell[1]

Morphology of Single Graft Block Copolymers
S. Trevino[3], N. Beck-Tan[3] S. Guido[55] and C. Lee[55]

COMPLEX FLUIDS AND GELS

Branched Gels
M. Diallo[7]and B. Hammouda[31]

Time Evolution Studies of Polymer and Silica Gel Structures
J. Samseth[20], M. B. Kirdedelen[20] and E. Sheu[45]

Aggregates in Heavy Oils
E. Sheu[45]

Electrostatic and Counterion-Specific Effects on Micelle Morphology
L. Magid[62], P. Butler[37] and Z. Han[62]

Kinetics of Poiseuille Flow-Induced Structures in Solutions of Threadlike Micelles
W. Hamilton[37], P. Butler[37], Z. Han[62] and L. Magid[62]

Morphology of Liquid-Crystalline Polymers in Blends under Shear
N. Wagner[50], W. Kernick[50], J. Amante[50] and B. Maranzano[50]

Microstructure of Shear Thickening and Shear Thinning Suspensions
N. Wagner[50], J. Bergenholtz[50] and R. Butera[14]

Flow-Induced Microstructural Transitions in Polyampholyte-Polymer Colloid Mixtures
N. Wagner[50], K. A. Vaynberg[50] and R. Sharma[50]

Shear-Induced Structural Transitions in Triblock Copolymer Micellar Solutions
T. Slawecki[31], C. Glinka[31] and B. Hammouda[31]

Shear-Induced Structure in Dilute Aqueous Solutions of Thread-like Surfactant Micelles
T. Slawecki[31] and C. Glinka[31]

Structure and Interactions in Dense Colloidal Mixtures
S. Kline[31] and E. Kaler[50]

Structure and Polymerization of CTAT/-Styrene/D_2O Microemulsions
S. Kline[31]

Polymerization of Rod-Like Micelles
S. Kline[31]

Structure of Middle-Phase Microemulsions
S. Kline[32] and N. Moll[13]

Structure of Sheared Dispersions of Colloidal Hard Plates
A. Rennie[8] and A. Brown[8]

Microstructure of Alkylpolyglucoside Micelles and Microemulsions
L. Ryan[50]and E. Kaler[50]

Effects of Shear on the Gelation of Dense Colloidal Silica: Combined Scattering and *in-situ* Rheology
H. J. M. Hanley[35], C. Munzy[33] B. Butler[33] and G. Straty[33]

Static and Flowing Microstructure of Drilling Muds
M. Paquette[13], N. Moll[13] and C. Glinka[31]

Pressure-Induced Swelling of Nonionic Micelles
M. McHugh[21], T. diNoia[21], J. van Zanten[21], C. Kirby[21] and M. Paulaitis[21]

Measurement of Interfacial Curvature in Microemulsions
S.-H. Chen[28] and S.-M. Choi[28]

Mixed Cationic/Anionic Vesicle Formation Kinetics Using Time-Resolved SANS
P. Huibers[28] and I. Goldmints[28]

CTAB Micellar Solutions under Shear
L. Walker[9], B. Thebaud[9] and B. Hammouda[31]

Effects of Pressure on Liquid Crystal Phases of Cesium Perfluoro-Octanoate
J. Mang[24], R. Hjelm[24], S. Kumar[22] and B. Hammouda[31]

Temperature Dependence of the Micellar Structure of Tri-Block Copolymers
I. Goldmints[28] and T. Alan Hatton[28]

SANS Study of the Pressure- and Temperature-Dependent Morphology of the Bile Salt/Lecithin System
R. Hjelm[24] and J. Mang[24]

SANS of Rod/Sphere Dispersions under Shear
R. Borsali[44] and R. Pecora[44]

Structure of Fourth Generation PMMA Dendrimers
S. Trevino[3] N. Beck-Tan[3] and L. Balogh[27]

Reversible Gel Formation in Organic Liquids
R. G. Weiss[18], O. Schurr[18] and C. J. Glinka[31]

Adsorption of Surfactants on a Trioctahedral Smectite Mineral
H. J. M. Hanley[35], B. Butler[35], C. Muzny[35], G. Straty[35] and L Aldridge[4]

Surface Enrichment in Ultrafine Aerosols
B. Wyslouzil[65], J. Cheung[65], G. Wilemski[22] and R. Strey[19]

BIOLOGY

Solution Structure of the Fibronectin Domain Associated with Integrin Cell Receptor
D. Torchia[30], Y. Tomita[30] and S. Krueger[31]

SANS Studies of Calmodulin/Target Enzyme Interactions
J. Krueger[24] J. Trewhella[24] and A. Wang[5]

SANS Study of the cAMP-Dependent Protein Kinase
J. Zhao[24], J. Trewhella[24], D. Walsh[49] and R. Bruschia[49]

Conformational Changes in SDS Micelles upon Binding of the 52-residue Bacteriophage fd Coat Protein
D. Tobias[59], G. Veglia[59] and S. Krueger[31]

Conformational Dynamics of Chaperonin Complexes Involved in Protein Refolding
E. Eisenstein[10], J. Zondlo[10] and S. Krueger[31]

Investigation of Cellulase Dimerization in Solution
S. Henderson[58]

SANS Studies of Pressure-Induced Interdigitated Phase in Lipid Bilayers
D. Worcester[57] and B. Hammouda[31]

Structural Changes in the Enzyme Endonuclease-1 (FEN-1) when Complexed with DNA
G. Olah[24] and M. Park[24]

Temperature Dependent Solution Structure of the Chaperonin Archaeosome
C.-Y. Ku[2] and P. Thiyagarajan[2]

Membrane Active Peptides: Phase Transitions and Supramolecular Assemblies of Peptides in Membranes
H. W. Huang[42], W. Heller[42], T. Harroun[42] and L. Yang[42]

Determination of the Molecular Size and Mass of a Murine Monoclonal Immunoglobulin G (IgG) Antibody
Z.-H. Li[26], M. Schenerman[26] and M. Lin[15]

SANS Studies of Actin Polymerization
R. Ivkov[53], S. C. Greer[53] and A. Drews[31]

Structural Configurations of Microtubules
R. Nossal[30], D. Sackett[30] and S. Krueger[31]

MATERIALS SCIENCE

Micro-Porosity in Amorphous Carbons and Li-Carbons
J. E. Fischer[59], P. Zhou[59], Y. Sorek[59], A. Claye[59] and W. Kamitakahara[31]

Hydrogen Induced Lattice Migration in Palladium/Nickel Alloys
T. Flanagan[63] and J. Barker[31]

Determination of the Size Distribution of Oxide Particles in an Internally Oxidized Platinum/Iron Alloy
T. Flanagan[63] and J. Barker[31]

Hydride Formation in Hydrogen Charged Aluminum Single Crystals
C. Buckley[53], H. Birnbaum[53] and J. Barker[31]

Hydrogen Trapping at Lattice Defects in Palladium
B. Heuser[53] and J. King[56]

Carbide Size Distribution Evolution with Ageing in an Experimental High Strength/-Toughness Steel
Y. Nagataki[36], G. Olson[36] and J. Barker[31]

Grain Size Dependence of the Magnetic Scattering from Nanocrystalline Nickel
C. Karmonik[31] and J. Barker[31]

Chemical Vapor Deposition of RuO_2 into SiO_2 Aerogels Investigated by SANS with Contrast Masking Solutions
C. Merzbacher[29] and J. Barker[31]

Magnetic Scattering from Nanocrystalline Cobalt
J. Weismüller[60], R. D. Shull[33], R. McMichael[33], U. Erb[40] and J. Barker[31]

Search for Templating Molecules in Zeolite Precursor Particles
P. Wagner[7] M. Davis[7] L. Beck[7] and C. Glinka[31]

Structural Properties of Silica-Aerogel Sensor Materials
R. Reidy[43] and A. Allen[32]

Pore Size Distribution Analysis of Activated Carbons
P. Pendleton[61] and C. Howard[4]

Morphological and Kinetic Study of Early Calcium-Silicate-Hydrate Gel Development during the Hydration of Cement and Tricalcium Silicate
H. M. Jennings[36], J. J. Thomas[36] and A. J. Allen[32]

Influence of Thermal Treatment on Void Morphology in Polyethylene-Carbon Black Composites
D. Marr[11], K. Schwartz[41] and M. Wartenberg[41]

Polymer Chain Conformation in Melt Intercalated Polymer-Silicate Nanocomposites

R. Krishnamoorti[52] and E. Giannelis[12]

SANS Studies of Irradiation Induced Microstructural Evolution in Pressure Vessel Steels

B. Wirth[48], D. Klingensmith[48] and G. R. Odette[48]

Effects of Silica Fume on Cement

R. Livingston[16] and A. Allen[32]

Porosity in Ceramic Plasma-Spray Coatings

J. Ilavsky[32] and A. Allen[32]

Affiliations

[1] Air Products Inc.
[2] Argonne National Laboratory
[3] Army Research Laboratory
[4] Australian Nuclear Science & Technology Organization
[5] Boston Biomedical Research Institute
[6] Brookhaven National Laboratory
[7] California Institute of Techology
[8] Cambridge University, United Kingdom
[9] Carnegie Mellon University
[10] Center for Advanced Research in Biotechnology
[11] Colorado School of Mines
[12] Cornell University
[13] Dow Chemical Company
[14] Dupont Marshall Laboratory
[15] Exxon Research and Engineering Company
[16] Federal Highway Administration
[17] General Electric Company
[18] Georgetown University
[19] Institut Füer Physikalische Chemie, Germany
[20] IFE, Norway
[21] Johns Hopkins University
[22] Kent State University
[23] Lawrence Livermore Laboratory
[24] Los Alamos National Laboratory
[25] McGill University
[26] MedImmune
[27] Michigan Molecular Institute
[28] Massachusetts Institute of Technology
[29] Naval Research Laboratory
[30] National Institutes of Health
[31] NIST Center for Neutron Research
[32] NIST, Ceramics Division
[33] NIST, Polymers Division
[34] NIST, Metallurgy
[35] NIST, Thermophysics
[36] Northwestern University
[37] Oak Ridge National Laboratory
[38] Pennsylvania State University
[39] Polytechnic University
[40] Queen's University, Canada
[41] Raychem Corporation
[42] Rice University
[43] Rothe Development, Inc.
[44] Stanford University
[45] Texaco Research and Development
[46] University of Bristol, United Kingdom
[47] University of Connecticut
[48] University of California at Santa Barbara
[49] University of California at Davis
[50] University of Delaware
[51] University of Grenoble, France
[52] University of Houston
[53] University of Illinois
[54] University of Maryland at College Park
[55] University of Massachusetts
[56] University of Michigan
[57] University of Missouri
[58] University of Oklahoma
[59] University of Pennsylvania
[60] Universität Saarlandes, Saarbrücken, Germany
[61] University of South Australia
[62] University of Tennessee
[63] University of Vermont
[64] University of Waterloo
[65] Worcester Polytechnic Institute

Neutron Beam Applications

Neutron Diffraction Measurement of Residual Stress

Considerable progress has been made in the last five years at NIST in a number of areas relating to the neutron diffraction measurement of residual stress. This includes the development of new methods of sample alignment ("ALIGN"), and the development of a comprehensive data reduction program ("STRESS"). The most significant accomplishment in FY97, however, is the essentially routine utilization of the new multipurpose double-axis diffractometer, "DARTS", with a number of state-of-the-art features specifically for improved residual stress measurement. The software with which data from this instrument is analyzed ("CONVERT") has been developed.

Titles of applications of the neutron diffraction technique using DARTS are listed in the Research Topics section. Selected projects are described in more detail below.

- **Instrumentation**

DARTS. A new multipurpose neutron diffraction instrument for residual stress, texture and single-crystal diffraction studies became operational in March of 1996. The principal features were summarized in the FY96 Annual Report and pictured on the WWW (at http: //rrdjazz /bt8.html) . Several features are unique to DARTS and have proved to be enormously important in facilitating sample handling, in maximizing the quality of data (e.g. signal/noise), and increasing thru-put relative to the instrument at BT-6 previously used for these measurements. In particular, the capability of accommodating large specimens is facilitated by the ability to withdraw the pre- and post-sample apertures, rotate and translate the sample, and then reposition the apertures *all under computer control, programmable in a command file.* This feature significantly reduces the number of times that a specimen must be removed from the sample table, which always requires a time-consuming re-alignment. Also, a number of safety features, unique to DARTS, have been incorporated, including carefully-integrated shielding which minimizes neutron background even up to the reactor face. Comparison of measurements at DARTS and the BT-6 instrument on comparable steel samples indicate that a target $\Delta d/d$ sensitivity (e.g. 5×10^{-5}) can be achieved $\approx 5\times$ faster on DARTS than on the old instrument.

Along with significantly improved measurement capabilities, CONVERT and STRESS, the data reduction/fitting and stress determination programs, have been re-coded to extend capabilities and to improve user friendliness. With relatively minor changes in data I/O to CONVERT (to accommodate local dataformats), it is expected that the programs could be generally useful to the entire neutron diffraction residual stress community.

Material Properties under Load Conditions. An important part on the field of residual stress analysis by neutron diffraction is the investigation of material behavior under applied load, that is, under a known stress state. Such experiments include the measurement of elastic compliance and the study of plastic deformation as well. Since stresses cannot be measured directly but only the strains, a residual stress analysis requires the knowledge of the elastic constants of the material. Although their measurement is possible by other methods as well, the phase and orientation selectivity of neutron diffraction offers new prospects for the determination of elastic properties for a particular group of materials. Such materials include multiphase materials in which the single phases cannot be synthesized, textured materials, and materials which can be synthesized as a powder only. While the phase selectivity enables the measurement of the strain state of one particular phase, the orientation selectivity leads to the diffraction elastic constants which are specific for every {hkl}.

The measurement of the elastic response of the material requires that the stress state of the sample can be varied in a wide range while the absolute stress has to be known with a high degree of accuracy. In addition to the stress, the macroscopic strain of the sample needs to be measured simultaneously for the investigation of the plastic deformation behaviour. These requirements are fulfilled by the stress rig which has recently been added to the BT8 sample environment. The mechanical design is shown in Fig.1.

This device was obtained from UKEA Harwell where it was specifically designed for neutron diffraction applications. It features a 10 kN load cell, a stepping motor with an attached ultrafine reduction mechanism and an adapter for measurements under compressive load. The maximum applied load depends on the sample diameter, but the standard specimen holder limits the diameter to 5 mm which leads to an upper limit of the applied stress of 510 MPa at this diameter. The high gear reduction together with the leadscrew

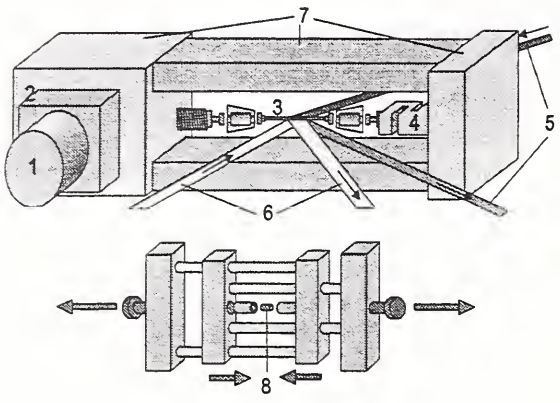

Fig. 1. Schematic of the stress rig.

1-stepping motor, resolution 1:360
2-gear, reduction 1:2500
3-tensile bar
4-kN load cell
5-beam orientation in transmission (Young's modulus)
6-beam orientation in reflection (Poisson's ratio)
7-stainless steel frame
8-compression sample in compression adapter

give a theoretical pathlength of 2.8×10^{-9} m per motor step. This way even very short and stiff samples can be measured, including ceramics which are preferably tested in compression mode.

The stress rig is fully integrated into the BT8 sample environment. All operations of the rig are now under full computer control with user access through command files. Even the operation in more sophisticated plastic deformation modes like strain rate control and fatigue can be easily achieved.The overall reliability of the rig has been tested by measurements in tensile and compression mode on a 2.25% Cr, 1% Mo steel. The result is shown in Fig. 2. The measurement of Poisson's ratio delivered 0.256. Therefore the diffraction elastic constants are: $s_1 = -1.131 \times 10^{-6} MPa^{-1}$ and $\frac{1}{2}s_2 = 5.550 \times 10^{-6} MPa^{-1}$.

It is also possible to calculate the diffraction elastic constants from the single crystal constants. Using C_{11}=228.09GPa, C_{12}=113.48 GPa and C_{44}=110.86 GPa as single crystal data, the corresponding calculated values are $s_{1calc} = -1.127 \times 10^{-6} MPa^{-1}$ and $\frac{1}{2}s_{2calc} = 5.579 \times 10^{-6} MPa^{-1}$. These results demonstrate that both in compression and tensile modes accuracies better than 2% can be achieved. The accuracy itself is limited mostly by the counting statistics and the determination of the peak position. The excellent agreement between measured and calculated values is very promising for the investigation of materials with unknown elastic constants by neutron diffraction.

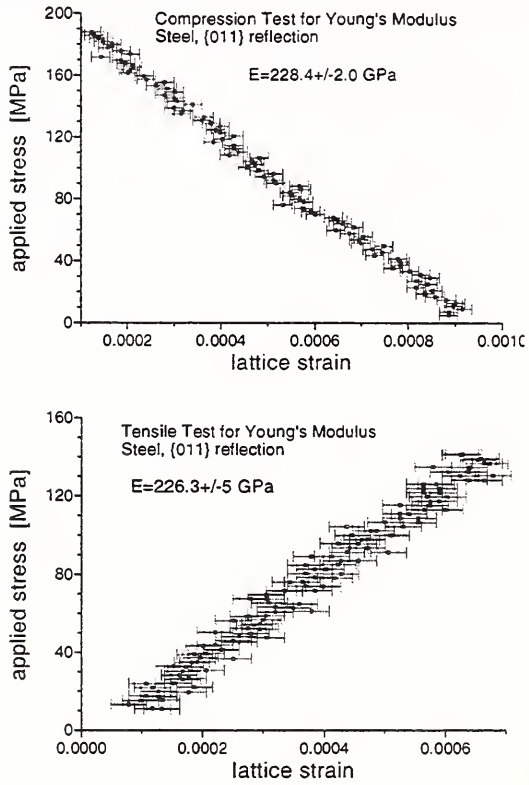

Fig. 2. Lattice strain vs. applied load for the {011} steel reflection in compression and tensile mode .

Experiments which have been scheduled for the near future will include the investigation of the elastic response of two phase single crystals and the plastic deformation of aluminum single crystals. An important example of two-phase single crystals are the γ/γ' hardened nickel based superalloys. Here the single phases cannot satisfactorily be synthesized so that elastic constants have to be measured on the two-phase composite. The purpose of the plastic deformation experiment will be the investigation of the formation of dislocation cell walls in the weakly anisotropic aluminum.

Future plans include the enhancement of the stress rig with a suitable heating device based on focusing intense light sources. In this mode the highly interesting temperature dependent properties of materials will become accessible.

- **Residual Stress Measurements**

Bent Pipes. A determination of residual stresses in two mild steel tubes (shown in Fig. 3)

which were subjected to four-point bends was completed in FY97. Tube I is seamless, tube II has a weld parallel to the cylindrical axis. After bending, the central 260 mm, together with end pieces, were cut out of the tubes for neutron diffraction measurements. Using a nominal 2x2x2 mm^3 gauge volume, strain components were measured as a function of depth beneath the surface at 22.5° intervals around the circumference of the tubes at the mid-plane, and with higher density around the bend/weld line on the bent tubes.

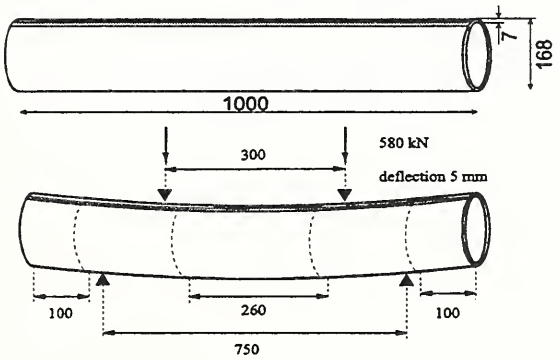

Fig. 3. Schematic of the bent tube before and after bending. The weld is parallel to the cylinder axis. The central 260 mm and the outer 100 mm portions were cut out and used for the neutron measurements.

At each measurement point, five Q-directions were examined in the r-θ plane, and one along the axial direction. The value of d_0 was obtained from the average of several position and orientation measurements on the tube end pieces. Diffraction elastic constants for the [110] reflection in steel were obtained from earlier measurements. All three normal residual stress components were determined along with the r-θ shear component. Results for the axial stress component is shown in Fig. 4.

It should be noted that the four point bending fixture was positioned along 0° and 180° on the tube and that the measured stresses are essentially mirror symmetric about the plane passing through these positions. It is also of interest that at ~90° away from the bend points a sharp compressive to tensile transition occurs in the stress profile. We expect to compare these results with an FE calculation and with results obtained with magnetic probes.

Residual Stress Standards. In January of 1996 a new, international collaboration was inititiated under the Versailles Project on Advanced Materials and Standards ("VAMAS"). The title of the technical work area (TWA) is "Measurement of Residual Stress" and the final objective is to collect the appropriate technical information required for the preparation of a draft standard for neutron residual stress measurements.

One of the first tasks agreed on within the TWA is to circulate reference samples among the participants in order to demonstrate the consistency of measurements even when performed at different types of neutron facilities. Two types of samples were prepared: a ceramic composite, and an aluminum shrink-fit ring/plug. For each type, two identical specimens were prepared -- one for circulation among European labs, one for circulation among North American labs. In addition, in the case of the shrink-fit specimens two "reference" plugs of the starting material were also provided. We have completed measurements on a ring/plug and the associated reference plug.

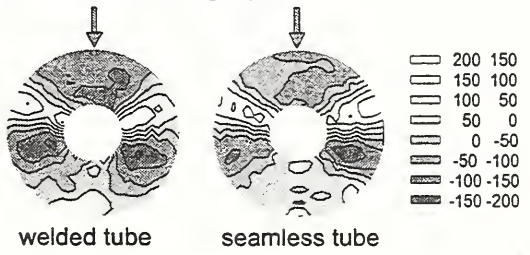

Fig. 4. Axial stress distribution for both bent tubes. The arrows correspond to the direction of applied force (0°).

Some of the relevant technical details are as follows: The "reference plug" is a cylinder 25 mm diameter and 50 mm long; the "ring/plug" sample is a cylinder 50 mm in diameter and 50 mm long. A scribed line with an arrow on each indicates a common direction. A very specific protocol was developed for the measurements so that all participating laboratories would have data sets which could be compared without interpolation or ambiguity. For example, measurements along the scribed diameter at mid-height for certain radii were specified. The reference d_0's would be obtained at the center of the reference plug. The reflection(s) examined would be chosen by the experimenters since not all instruments can access all Bragg reflections equally well. As of the third meeting for this TWA (June, 1997), about half of the participants -- including NIST -- had completed their measurements on the ring/plug samples. Although some variations occur among the reporting labs, the results are overall in quite good agreement. One negative aspect is the fact that grain-grain interaction microstresses are significant. The result is that d's determined from the center of the reference plug

are not representative of d_0's over the entire ring/plug sample. Because of this a comparison with the well-known analytical model for a shrink-fit ring/plugs fails.

Characterization of both reference specimens by all participants should be completed in FY98.

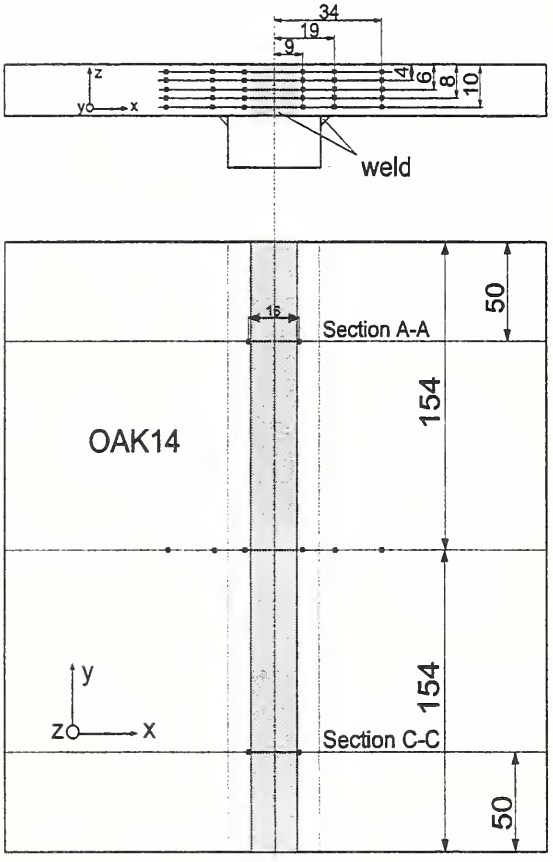

Fig. 5. Sketch of the welded plate in butt-weld geometry

Welded Steel Plates. Within the framework of cooperation with industry, weldments on steel plates in different geometries have been investigated. The first weldment in butt-weld geometry is shown in Fig. 5. The dimensions of that sample were 305 ×305 ×12.7 mm^3. The total number of measurement points was 30 for the middle section and 10 for each of the outer sections. The sampling volume dimensions were 2×2×2 mm^3. The d_0 measurement was performed for both geometries on one of the plate corners. The close proximity of three free surfaces and the distance to the source of the residual stresses approximates nearly unstressed material.

The strain measurements were performed in 3 directions of the scattering vector **Q**: normal to the weld in the plane, parallel to the weld and normal to the surface. The maximum thickness of this structure is 25.4 mm, so that neutron path lengths of no more than about 40 mm were achieved. One result of the residual stress analysis is shown for the parallel direction in Fig. 6. This contour plot demonstrates that the comparatively simple geometry leads to a smooth decay of the high tensile stresses close to the weld to rather weak compressive stresses at 25 mm distance. There is also no pronounced depth dependence. However, there is a slight asymmetry of the stress distribution normal to the surface which indicates some influence by the backing plate.

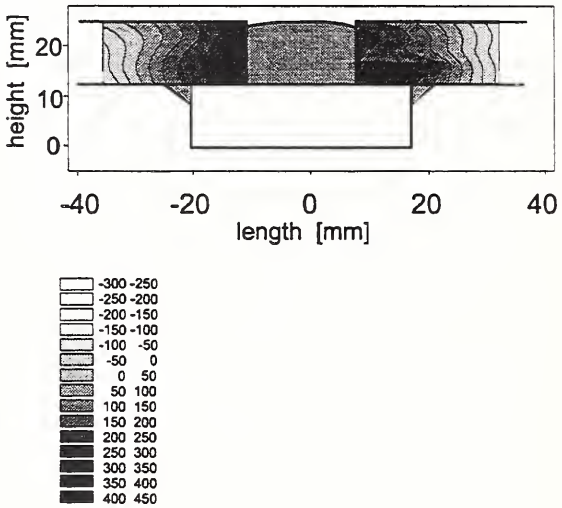

Fig. 6. Contour plot of the residual stresses parallel to the weld

The second weldment was in lap-joint geometry, with similar plate dimensions. Comparing results for the butt welded plates and the lap joint weldments shows quite different properties. For example, residual stress components determined along the mid-plane (i.e. at 6.35 mm depth in the 12.7 mm thick plates), parallel to the weld line differ with distance from the fusion zone interface as shown in the Table. These results are typical of the detail that can be obtained with the DARTS instrument, most probably the most versatile in the world for sub-surface residual stress determination. It is clear that the differences in the weldments are significant. Furthermore, the correctness of models should be clearly distinguishable when predictions are compared to the complete neutron results.

Distance (mm).....	4	8	10	25
Stress (Mpa)				
in				
Buttweld (left/rt avg.)	280±18		201±16	80±10
Lap Joint (top plate)	225±20	99±10		-7±9
Lap Joint (bottom plate)	104±18	141±12		-167±12

Thermally Sprayed Coatings. Among the most widely used applications of plasma spraying are th thermal barrier coatings (TBC) for combustion engines and aircraft turbines, where their thermal protection helps achieve higher efficiencies and longer engine life [1]. The coating properties – and threrefore the service life – are strongly affected by residual stress. Stresses result from the unique production process, involving high temperature differences, as well as from thermal cycles during service. High residual stress can lead to cracking and spallation of the coating, which shortens its service life. Therefore it is necessary to know the residual stress in order to optimize the production process.

Although the x-ray diffraction method of stress determination was developed long ago and is widely used for "classical" bulk materials, its application to thermally sprayed coatings is complicated by the coatings' inhomogeneous structure with cracks and pores. Therefore, interpretation of the results is sometimes problematic. Neutrons can overcome some of the drawbacks of x-rays, yet their application to plasma sprayed coatings has begun only recently [2]. In principle, the neutron diffraction method has several distinct advantages over other methods. 1) It is possible to perform triaxial stress analysis throughout the thickness of both the coating and the substrate without material removal. 2) The stress can be determined in all phases of a multi-phase coating. 3) Repeated measurements can be performed on mechanically or thermally fatigued specimens. 4) Stress concentrations and shape/edge effects in actual parts can be located.

In the initial experiments on the DARTS instrument at the NCNR, all coatings were plasma sprayed in air on steel substrates using a Plasma Technik PT-F4 system, except for one Ni coating produced by vacuum plasma spraying (VPS) using a PT-F4V torch. For the NiCrAlY coatings [Ni + 16.5Cr + 5.5AL + 0.5Y (wt%; UCAR Ni-346], two different deposition temperatures were selected by using air cooling or no cooling during spraying. These were 250 °C and 460 °C, respectively. Some of the specimens were annealed in a vacuum furnace (650 °C for 5 hours), to provide a stress-free reference. Some coatings were detached from the substrates. Details concerning samples and measurement conditions are available elsewhere [3]. Although the stress-free lattice spacing was measured, which normally allows this stress to be calculated, this procedure could not be employed because of lattice parameter changes associated with chemistry (a different amount of nickel and aluminum oxides was observed on bottom and surface side of the coatings). The stresses were measured along a line through the specimen thickness, assuming that the obtained profile is valid for the whole cross-section.

Application of this method to coatings poses certain challenges, as compared to application to bulk materials. For example, there is a relatively small volume of material available for diffraction. Depending on the specimen geometry, there are two solutions to this problem. For thin coatings (Ni), the largest apertures were used, defining a gauge volume (5x5x5 mm^3) that was larger than the diffracting material thickness. Then, data were taken for different positions of the coating in the gauge volume. The intensity vs. position profile was fitted by a theoretical curve whose maximum marked the position of specimen exactly centered in the gauge volume; only those data were then used for stress evaluation. For thicker specimens (NiCrAlY, YSZ, steel), where stress gradients were of interest, the gauge volume had to be relatively narrow but could be extended in the direction perpendicular to the plane of the beams (the dimensions were 1x1x7 or 0.5x0.5x7 mm^3).

In both cases, there were instances where more than one material was immersed in the gauge volume. Therefore, the diffraction conditions had to be selected so as to obtain sufficiently separated peaks, and contamination of the measured peaks by higher-order reflections of other peaks has to be avoided. A special computer program was developed to aid in optimization of diffraction conditions for a given combination of specimen materials and instrument characteristics.

In cases when the gauge volume is only partially filled with the diffracting material (near-surface measurement), there are certain artificial

effects on diffraction peak position, which override changes due to stress. These were quantified by a calibration measurement on annealed (stress-free) NiCrAlY and steel specimens; other experimental data were then corrected with this calibration. Stress measurements were complemented by calculations, which required knowledge of thermal and mechanical properties of the materials under study. Therefore, the coefficient of thermal expansion (CTE) and deformation characteristics (elastic constants) were experimentally determined. Some of the stress calculations were done using the Multitherm computer program [4].

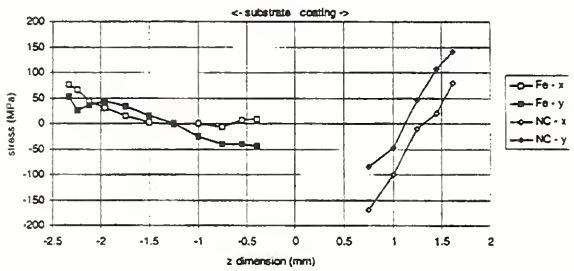

Fig. 7. Residual stress vs. depth (in mm) in the as-sprayed (T = 460 °C) NiCrAlY coating on a steel substrate. The abbreviations NC and Fe refer to the coating and substrate, respectively. The x and y axes are parallel with the specimen length and width direction in the coating plane, the z axis (thickness direction) is perpendicular to the plane. Position z = 0 marks the interface.

Figure 7 shows the through-thickness profile of in-plane residual stresses in the steel substrate and NiCrAlY coating deposited at 460 °C. The stress state is a complex result of quenching and thermal mismatch stress. Stresses of both signs can be observed in the coating as well as the substrate, with a slight difference in the x and y directions. A strong stress gradient is present in the coating, with tension near the surface and compression near the interface. A leveling of the substrate stress near the interface suggests that plastic deformation in compression has taken place there. Fig. 8 presents the stress profile in an identical specimen after annealing at 650 °C. Residual stress present in this specimen should be a result of thermal mismatch only. Here the residual stress in the coating is compressive and in the substrate mostly tensile. Also included in the figure are the results of the Multitherm calculation with experimentally determined properties:

NiCrAlY: E = 172 GPa

$CTE = (12.41 + 0.0056\ T)\times10^{-6}\ °C^{-1}$

Steel: E = 209 GPa

$CTE = (11.36 + 0.0117\ T)\times10^{-6}\ °C^{-1}$.

The stress values in the coating were rescaled by an E(bulk)/E(coating) factor to allow direct comparison with diffraction data (i.e., both are presented "as seen by neutrons" which probe the inside of the splats where bulk elastic constants apply, whereas the coating as a whole acts on the substrate with its stiffness reduced by pores and cracks). As can be seen, a satisfactory agreement is reached.

From these data, (and results for a coating detached from a substrate) an approximate qualitative "history" of the stress evolution during and after spraying can be constructed. As a new coating layer is being deposited, its contraction during rapid cooling (from the solidification temperature to the current substrate temperature) is restricted by adherence to the substrate. Therefore, a tensile stress develops in the deposit. Subsequent layers experience a similar process; this leads to a stress gradient with more tensile stress on the surface, whose magnitude is limited by the coating strength. This gradient creates a significant bending moment which can lead to coating delamination when the coating thickness reaches a critical point. Tensile stress in the coating is balanced by compression in the substrate and is partially accommodated by substrate contraction and bending. If the forces and moments acting on the substrate reach sufficient magnitude to cause yielding, plastic deformation occurs (most likely at the substrate/coating interface). When the deposition is finished the whole couple cools down to ambient temperature and the thermal mismatch (difference in their thermal expansivities) becomes a controlling factor. In this case, the substrate's CTE is slightly higher over most of the actual temperature range. Therefore, the stress in the substrate shifts towards tension and stress in the coating shifts towards compression, thus partially reverting previous stress distribution (Fig. 8). When the coating is detached, the net force imposed on it by the substrate (and vice versa) is removed; therefore, the average in-plane stress in any cross-section is zero, as the coating is free to expand or contract. The remaining moment, resulting from the stress gradient, also diminishes, as it is accommodated by free bending. If the stress distribution before detachment was linear and all dilation and bending took place elastically, the residual stress in the free coating would be zero. Thus, the residual stress observed in our detached specimen

can be a result of non-linear stress distribution and/or inelastic deformation.

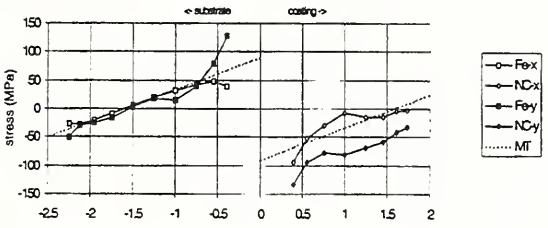

Fig. 8. Residual stress vs. depth (in mm) in the annealed (T = 650 °C) counterpart of the previous specimen. Solid lines refer to neutron diffraction data, dashed line (MT) represents the calculation 0 °C) counterpart of the previous specimen. Solid lines refer to neutron diffraction data, dashed line (MT) represents the calculation.

In order to compare the deformation measured in unbroken crystal grains to macroscopic deformation of the whole coating, an *in situ* three-point bending test was conducted. Initially, the measured slope follows the one of a bulk material, but deviates from it at a relatively small strain (about 2×10^{3}). This indicates that inelastic deformation has occurred; this phenomenon can be roughly compared to plastic yielding in bulk metals. Upon unloading, the experimental slope did not follow the "elastic" part. This can be explained as follows: When the specimen was loaded beyond the elastic limit and then unloaded, the strain distribution would be no longer linear but rather assume a "zigzag" pattern. The spatial resolution of neutron diffraction at these conditions was not sufficient to distinguish this change; averaging over a certain volume (0.5x0.5x7 mm^3) would then reduce the apparent strain gradient magnitude.

In summary, neutron diffraction was successfully applied for residual stress determination on various plasma sprayed coatings, as the only method capable of non-destructive in-depth stress profiling. Measurements were performed on as-sprayed, annealed and free-standing specimens and complemented with calculation based on experimentally determined material properties. This approach allows us to assess the individual role of quenching and thermal mismatch stresses in the final residual stress distribution and to discuss qualitatively the stress evolution during various processing stages. This research was supported by the MRSEC program of the National Science Foundation under award number DMR 9632570.

Texture Studies

Texture measurements were performed on the reference plug of the VAMAS ring/plug system described above. The sampling volume used was 5x5x5 mm^3 centered in the plug so no absorption correction was needed. The results for the (111), (002), (022) and (113) pole figures are summarized in Fig. 9. For convenience, the numbers accompanying each pole figure are multiples of average intensity (rather than "X random"). Nevertheless, the pole figures do show the degree of preferred orientation, which is directly relevant to the significance of the round robin results.

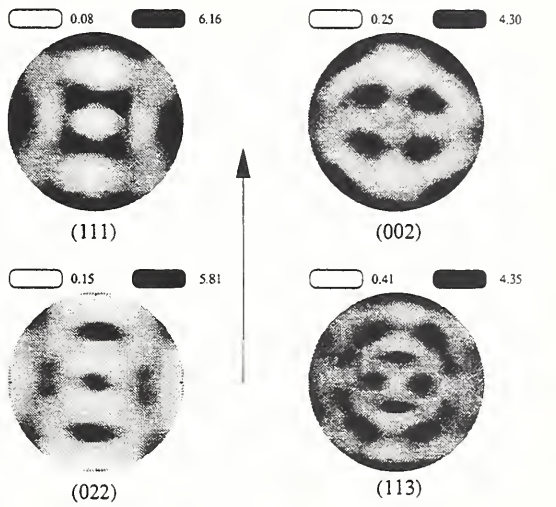

Fig. 9. Pole figures for the reference plug of the VAMAS round robin specimen.

References

[1] Miller, R. A.; Proc. Thermal Barrier Coating Workshop, Cleveland, OH, NASA Conf. Publ. 3312, 17-34 (1995).

[2] Ceretti, M., Michaud, H., Perrin, M., and Lodini, A.; Exp. Tech., **19(3)**, 17-21 (1995).

[3] Matejicek, J., Brand, P. C., Prask, H. J. and Herman, H., Proc. 10th Nat'l. Thermal Spray Conf. (Indianapolis, IN, Sept. 1997) in press.

[4] Finot, M., Suresh, S., Bull, C., and Sampath, S.; Mater. Sci. Eng., **A205**, 59-71 (1996).

Research Topics

Evaluation of New Neutron Area-Detectors

Y. T. Cheng[11,10]

"DARTS": A New Neutron Diffractometer for Residual Stress Measurement, Texture Determination, and Single Crystal Diffraction

P. C. Brand[12], H. J. Prask[12] and T. Gnäupel-Herold[1].

'CONV' and 'STRESS': New Codes for Data

Reduction in Neutron Diffraction Residual Stress Measurements
P. C. Brand[12].

Software Development for Texture Studies on "DARTS"
P. C. Brand[12]

A New Stress Rig for the Residual Stress Measurement Project
T. Gnäupel-Herold[20], P. C. Brand[12] and H. J. Prask[12]

Possible Correlation of FWHM and d_0 for Diffraction Peaks in Weldments
P. C. Brand[12] and H. J. Prask[12]

Characterization of a Standard Reference Specimen for Residual Stress Measurements as Part of VAMAS
P. C. Brand[12], H. J. Prask[12] and T. Gnäupel-Herold[20].

Measurement and Modeling of Residual Stresses in Multi-phase Weldments
P. C. Brand[12], T. Gnäupel-Herold[20], J. Blackburn[9], R. J. Fields[14], H. J. Prask[12] and T. Zacharia[15].

Residual Stresses around Weldments in Various Steel-Plate Configurations
T. Gnäupel-Herold[20], P. C. Brand[12], I. Varhol[15] and H. J. Prask[12]

Determination of Residual Stresses in an Al plate for Helicopter Applications
P. C. Brand[12], H. J. Prask[12] and D. Ludin[4]

Residual Stresses in a Stub Beam of a 737 Aircraft
P. C. Brand[12], T. Gnäupel-Herold[20], H. J. Prask[12] and R.Y Hom[3]

Residual Stresses in a Failed Steel Structural Member
P. C. Brand[12], H. J. Prask[12], E. Drescher-Krasicka[14] and C. Ostertag[20]

Residual Stresses around a Weld in Inconel-617
P.C. Brand[12], H.J. Prask[12], T. N. Crump[6] and E. Drescher-Krasicka[14]

Residual Stresses in Infrastructure Components
P. C. Brand[12], H. J. Prask[12], R. Livingston[7], D. Balzor[13], A. Clark[13] and D. McColskey[13]

Residual Stress Studies for Science Based Stockpile Stewardship
P.C. Brand[12], H.J. Prask[12] and M. Bourke[8]

Residual Stresses in Thermally-Sprayed Coatings
J. Matejicek[19], P. C. Brand[12], H. J. Prask[12], S. Sampath[19] and H. Herman[19]

Residual Stresses in a Shrink-Fit Fe/SiC Ring
P. C. Brand[12] and S. F. Trevino[2]

Residual Stresses in Functionally-Graded Coatings
H. Bruck[22], P. C. Brand[12] and H. J. Prask[12]

Residual Stress Measurements on Railroad Rails
P. C. Brand[12], J. Gordon[10], G. M. Hicho[14], and H. J. Prask[12]

Residual Stress Analysis of Bent Steel Pipes
P. C. Brand[12], J. Goff[17], M. T. Hutchings[1], D. J. Buttle[1], and H. J. Prask[12]

Neutron Diffraction Validation of Residual Stress Measurements by Scanning Acoustic Imaging
P.C. Brand[12], H.J. Prask[12], and E. Drescher-Krasicka[14]

Neutron Autoradiography of Paintings
Y.-T. Cheng[11,10] and J. Olin[18,16]

Affiliations
[1] AEA Technology, United Kingdom.
[2] Army Research Laboratory
[3] Boeing Corporation, Seattle
[4] Boeing Helicopter Group, Philadelphia
[5] Caterpillar Company
[6] Dupont
[7] Federal Highway Administration
[8] Los Alamos National Laboratory
[9] Naval Surface Warfare Center at Carderock
[10] Neutek Inc.
[11] NIST, Analytical Chemistry Division
[12] NIST Center for Neutron Research
[13] NIST, Materials Reliability Division, Boulder
[14] NIST, Metallurgy Division
[15] Oak Ridge National Laboratory
[16] Olin Conservation, Inc.
[17] Oxford University, United Kingdom
[18] Smithsonian Institution
[19] State University of New York at Stony Brook
[20] University of California at Berkeley
[21] University of Maryland at College Park
[22] University of South Carolina
[23] U.S. Department of Transportation

Instrumentation Development

The Disk Chopper Spectrometer

The Disk Chopper Spectrometer (DCS), located at the NG-4 neutron guide, will be used for a variety of experiments such as studies of magnetic and vibrational excitations, tunneling spectroscopy, and quasielastic neutron scattering investigations of local and translational diffusion [1]. One of the challenges in designing this instrument was to provide a high energy resolution option, albeit at the expense of intensity, without having to resort to neutron wavelengths which severely limit the range of available wave vector transfers. The instrument promises to be versatile, popular, and fully competitive with comparable instruments in Europe.

The DCS uses a set of seven chopper disks and a partitioned (channeled) guide to produce monochromatic pulses of neutrons at the sample position. The first and last chopper pairs determine the incident wavelength and the three intermediate choppers remove contaminant wavelengths and unwanted pulses [1]. There are three slots, with different angular widths, in each of the disks belonging to the first and last counter-rotating chopper pairs. By appropriately phasing these disks the instrument can be operated in one of three distinct "resolution modes", without having to change the incident wavelength or the speed of the choppers. Other design features of the DCS include the optical filter [2], a general purpose sample chamber, a gas-filled flight chamber, a support structure for the flight chamber and its shielding, and a set of racks which hold three banks of detectors (see Fig. 2 in ref. [3]).

The chopper pedestals and lower housings have been installed and aligned, and the channeled neutron guide has been installed and aligned within the housings and a series of steel guide casings mounted between the housings (Fig. 1). A pneumatically operated local beam shutter has been installed at the upstream end of the chopper system. Gold foil measurements at this location gave an estimated thermal neutron capture flux of 2.7×10^{9} $n\cdot cm^{-2}\cdot s^{-1}$, in excellent agreement with the results of Monte Carlo calculations. The measured average capture flux at the end of the guide (at the downstream end of the chopper system) is 1.0×10^{9} $n\cdot cm^{-2}\cdot s^{-1}$. This result is consistent with calculation if certain deleterious effects, such as possible waviness of the internal glass plates in the channeled guides, are included in the simulations. The capture flux distribution in the beam at the end of the chopper system is shown in Fig. 2. Individual channels within the guide are clearly seen. At the time of writing we do not fully understand the ratios of intensities in the different channels.

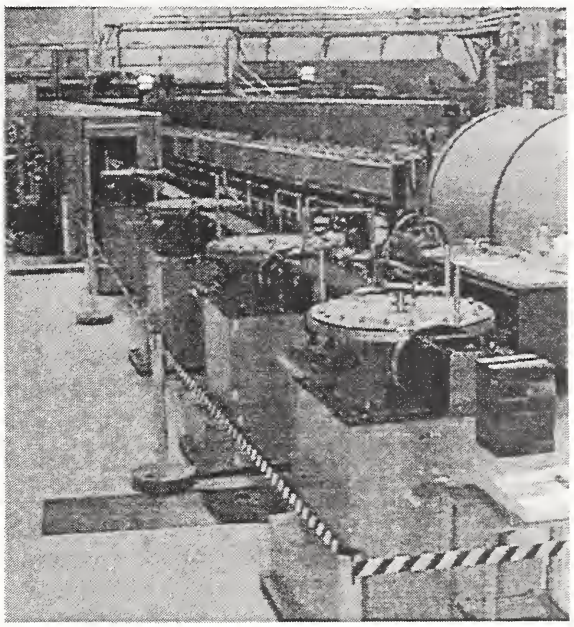

Fig. 1. A photograph of the NG-4 beam line, looking towards the cold source, taken in September 1997. Standard shields surround the first ≈23.5m of guide within the neutron guide hall. Roughly 1.8m thereafter, there is a beam shutter (not visible), followed by ≈10.5m of guide enclosed in rectangular cross section metal casings. Each of the four chopper pedestals supports a lower housing penetrated by the guide. The upper surfaces of the lower vacuum housings are sealed with plates to permit vacuum tests of the system. They will later be replaced with upper housings that carry the choppers themselves.

Measurements at the end of the chopper system indicate that the combined fast neutron and gamma ray dose rate in the beam amounts to less than (possibly much less than) 2 mrem/h with the local beam shutter closed. This finding is consistent with detailed calculations of anticipated dose rates by N. Rosov (private communication). Important (and very welcome) conclusions are that the optical filter performs very well [2], and

that there will be no need to install an additional crystal filter.

We have continued to test the chopper system, in close collaboration with our colleagues Stephan Polachowski and Juergen Raebiger of the Forschungszentrum (FZ) Jülich (Germany). In order to improve the mechanical stability of the choppers with respect to axial disturbances it was decided to replace the original magnetic bearing control modules, which had linear power stages. Initially, they were replaced with newly designed modules equipped with pulse width modulated (PWM) power stages previously tested at FZ Jülich. These tests were performed using a chopper essentially identical to the choppers in the time-of-flight instrument "NEAT" at the Hahn Meitner Institute (HMI), Berlin. However, extensive tests at NIST forced all concerned to conclude that the new magnetic bearing control modules, as then designed, could not be field-modified to permit high-speed operation of our choppers due to mechanical differences between the two chopper designs. The development of an acceptable electronic design for the control modules proved to be more challenging than expected. An acceptable design was finally achieved in mid-August as demonstrated by full speed tests of one of the NIST choppers to 20,000 rpm. Following fabrication of these new modules, our colleagues from FZ Jülich will come to NIST to install them on the choppers. They will also perform extensive tests to convince all concerned that the complete chopper system is working properly and according to expectations.

The sample chamber, and its interface to the guide, has been designed and fabrication should begin soon. An important feature is a removable guide section which will be mounted within the chamber; its purpose is to bring the beam close to the sample in order to minimize intensity losses due to beam divergence. The chamber is designed to enable access to the sample from the side and from above. It has multiple gas-tight feedthroughs. There is also provision to form a flexible gas-tight seal, above the beam height but within the chamber, in order to be able to backfill with a gas such as argon. The seal will normally take the form of an annulus, stretching from the outer surface of the sample environmental equipment (e.g. a cryostat) to the inner surface of the sample chamber. The design of the seal permits limited translational and orientational adjustments in order to align the sample.

The flight chamber (see Fig. 2 in ref. [3]) is complete and will be ready for installation upon completion of the sample chamber assembly. The fifteen detector racks, which accurately locate 913 ^{3}He proportional detectors relative to the sample, have been fabricated and assembled. (The final machining of the rails which support the detector brackets (see Fig. 2 in ref. [4]) was performed

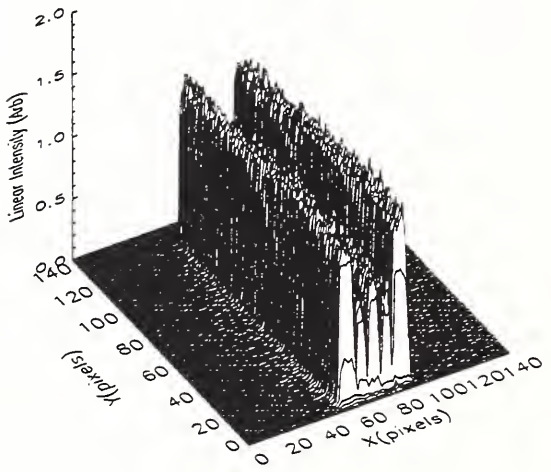

Fig. 2. A surface plot of the thermal neutron capture flux at the end of the NG-4 guide (measured at the window visible in the foreground of Fig. 1). The ratios of neutron intensities in the different channels are not presently understood.

using the Octahedral Hexapod machine in the Shops [5].) All of the shielding material required for the spectrometer assembly has been purchased and received. We are developing a detailed plan for the assembly, installation and alignment of the sample chamber, flight chamber, support structure and detector racks.

Considerable progress has been made in the design and initial testing of the data acquisition system. The heart of the system is a set of 20 MHz 32-input time-to-digital converter (TDC) boards, each of which encodes neutron events into 30-bit data words containing 10 bits of detector information and 20 bits of time information (with 100 ns resolution). Virtually all of the board logic is handled within a single field programmable gate array (FPGA) chip. Up to 29 TDC boards, needed in order to process events from as many as 913 individual detectors, will reside in two VME crates. A bus controller (also an FPGA device) will serialize events received from the TDC boards and feed them to a VME digital I/O module. A VME-based Pentium CPU will read event words from the digital I/O module and map them into 20-bit words using table lookup procedures. The 20-bit words will then be treated as addresses

to be incremented in a data histogram stored in 4 Mbyte reflective memories residing in the VME computer and in the host computer (see below). The TDC boards have been designed and tested, the TDC bus controller is nearing the final stages of its design, and the software to read, perform table look up, and histogram events has been written.

Data acquisition and instrument control will be accomplished with a 166 MHz Pentium host computer running the Linux operating system. An autonomous "core" program responsible for all interactions with the instrument hardware (i.e., chopper control, data acquisition control, etc) will communicate with user programs via TCP/IP protocols. The core program is written in the Tcl scripting language, and low-level communications with devices are achieved through C extensions to Tcl. Our intent is to store experimental data in the self-describing hierarchical data format (HDF) adhering to the NeXus standard for neutron/x-ray data exchange[6].

The High Flux Backscattering Spectrometer

The NCNR High-Flux Backscattering Spectrometer (HFBS) is nearing completion and testing is already underway on the primary spectrometer which is located at the end of guide NG-2. This new instrument will enable scientists to perform high energy resolution studies ($\lesssim$ 1μeV) of the low-frequency dynamics of a large variety of systems over a wide dynamic range. The applications of backscattering spectroscopy are numerous and include studies of rotational tunneling, molecular reorientations, diffusion, dynamics of liquids and glasses, and critical scattering near phase transitions.

A backscattering spectrometer can be viewed most simply as a limiting case of a triple-axis spectrometer where the scattering angles 2θ of both the monochromator and analyzer are 180°. In this limit the backscattered neutrons will have a wavelength $\lambda = 2d$ that is set by the spacing d between Bragg planes. The HFBS uses the (111) reflection from silicon to monochromate and analyze the neutron energies so that $\lambda = 6.27$ Å.

In keeping with the triple-axis analogy, the HFBS will operate in a fixed final-energy mode with $E_f = 2.08$ meV. The incident neutron energy E_i cannot be varied in the traditional way, i.e. by changing the scattering angle of the monochromator, as this would cause the crystal to move out of the backscattering condition. Instead, E_i is varied using a Si(111) monochromator attached to a Doppler drive which, when running at full speed, will give users access to a maximum neutron energy transfer of $\Delta E = \pm 60$ μeV. The target energy resolution for the HFBS is 0.75 μeV FWHM with a Q-range of 0.15 to 1.8 Å^{-1}.

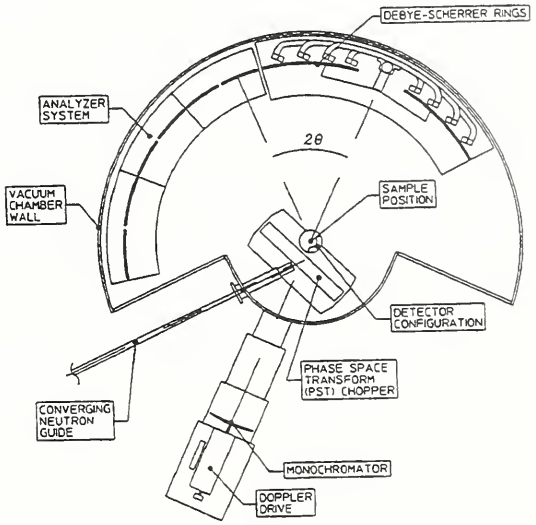

Fig. 3. Schematic diagram of the HFBS located on NG-2.

The principle limitation of backscattering spectroscopy lies in the low neutron flux that results from having such a sharp energy resolution. This can be compensated for in part by using large analyzer crystals that integrate the scattered signal over a large solid angle, thereby increasing the intensity on the detectors while reducing the overall Q-resolution. However, this geometry creates a severe mismatch between the neutron beam divergences of the primary and secondary spectrometers because the primary beam divergence is limited by the critical angle for total reflection of the guide. This has been a long-standing problem with backscattering spectrometers throughout the world.

The primary design goal of the HFBS is to minimize this mismatch as much as possible using state-of-the-art neutron optics while still meeting the target energy resolution. To this end, the instrument design incorporates a 4 meter long converging guide, a large spherically-focussing monochromator and analyzer, and a novel device known as a phase-space transformation (PST) chopper. It is hoped that these elements, in conjunction with the new liquid hydrogen cold source, will provide a significant increase in flux beyond what is presently available at other backscattering facilities.

This fiscal year has seen the completion of the beam delivery system for the HFBS. This includes the installation and testing of the liquid nitrogen cooled Be/Bi crystal filters, the neutron velocity selector, the thermal shutter, and the converging guide. In addition, all of the guide shielding has been installed. The converging guide has $2\theta_c^{Ni}$-equivalent supermirror coatings on all interior surfaces and focuses the 15 cm by 6 cm neutron beam cross section down to 2.8 cm by 2.8 cm. Gold foil activation measurements of the thermal neutron flux both before and after the converging guide indicate a flux gain of 3.9. While this value is higher than the ideal gain factor of 3.1, it is consistent with calculations that include small deviations in the reflectivity profiles of both the NG-2 and converging guides. The effective flux at 6.27 Å after the converging guide is 2.4 x 10^8 n/cm^2/sec. Autoradiographs of the beam profile from Dy foils indicate a uniform neutron intensity pattern at the exit of the converging guide that does not vary by more than 8% over the guide area.

The PST chopper, which follows the converging guide, exploits the physics of Bragg diffraction from moving mosaic crystals to convert the incident spread in neutron energies into angular divergence. The chopper consists of a 1 meter diameter disk that is divided into six sectors. The periphery of alternate sectors is covered with highly-oriented pyrolytic graphite (HOPG) crystals 3.5 cm high, 2.8 cm wide, and 0.15 cm thick which are mounted inside magnesium cassettes. The HOPG (002) lattice planes are aligned perpendicular to the axis of rotation of the chopper disk so that when spinning, the crystals move perpendicular to the scattering vector.

Neutrons that are Bragg diffracted from the rotating PST chopper are Doppler-shifted up or down in energy depending on whether their energiers are less than or greater than 2.08 meV, respectively. This corresponds to a tilting of the outgoing Bragg-diffracted phase space element with respect to the nominal final neutron wavevector $\boldsymbol{kf}$. Monte Carlo simulations suggest that the phase-space transformation process could enhance the incident neutron by up to a factor of 4 or 5 relative to that diffracted from a stationary chopper. The total diffracted flux, however, will depend directly on the reflectivity of the HOPG crystals. The PST chopper system is now complete. The chopper disk has been dynamically balanced, mounted inside its housing, and a new motor drive system has been installed. Tests of the PST gain factor and chopper performance are underway.

An additional flux increase is obtained by spherically bending the silicon crystals used to monochromate and analyze the incident and scattered neutrons. The bending introduces a small lattice gradient along the [111] direction, thereby increasing the bandwidth of neutron energies that satisfy the backscattered Bragg condition. In the case of the analyzer, this bending is achieved by gluing thin Si(111) wafers onto spherically cut aluminum backing plates. The flux increase that results from this bending scales with the FWHM of the energy resolution, assuming a constant reflectivity. The finished analyzer will stand 2 meters tall, span $-39° < 2\theta < 126°$ in scattering angle, and cover 20% of 4π steradians, nearly 70% more than that on IN16.

The monochromator has been completed, and most of the analyzer assembly is finished. Delivery of the entire analyzer is expected by the end of 1997. Several other major items have been completed in this fiscal year, and they include the Doppler drive system, a laser Doppler vibrometer (which will be used to measure the instantaneous velocity of the monochromator), and a VME-based data acquisition system.

The Neutron Spin Echo Spectrometer

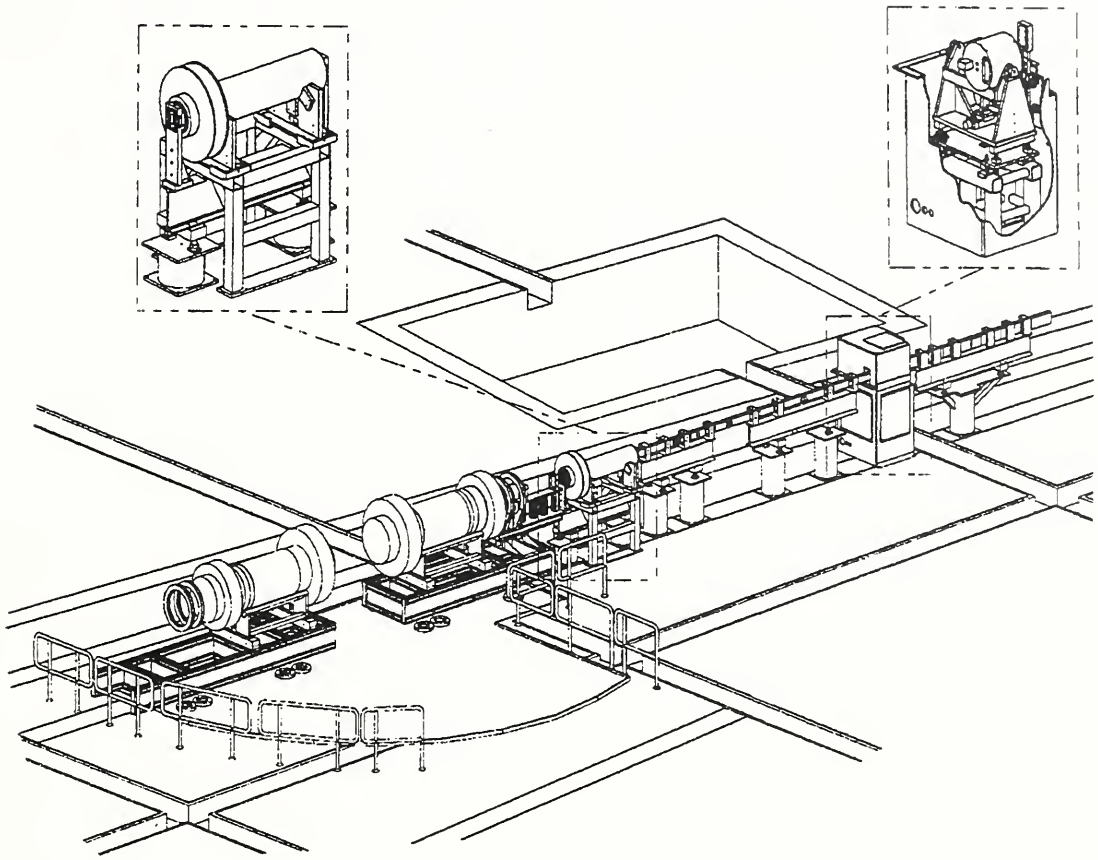

Fig. 4. NG-5 Spin Echo Spectrometer. Right and left inserts show expanded views of the neutron velocity selector and neutron polarizer, respectively.

The Neutron Spin Echo (NSE) spectrometer is being built and will be operated as a PRT facility involving NIST, Forschungszentrum (FZ) Jülich, and Exxon Research and Engineering Co. The FZ-Jülich has been operating a similar spectrometer that has been fully operational since the beginning of 1997. The NSE spectrometer (Fig. 4) is being installed at the end position of guide NG-5. The instrument is optimized to maximize the neutron flux on the sample by keeping the length as short as possible, while achieving as high a resolution as practicable. The practical maximum Fourier time is roughly $6x10^{19}\ \lambda^3$ s m^{-3} (i.e. 30 ns for 8 Å neutrons). The design has reduced the magnetic field coupling between the two main coils in order to allow access to large momentum transfers (up to 2 $Å^{-1}$). The incident beam will be monochromatized typically to 10% by a mechanical velocity selector, although a backup $\Delta\lambda\backslash\lambda$ = 20% selector that is shared with the backscattering spectrometer is also available. The beam will be polarized by a transmission cavity similar to that developed for SANS; delivery of the cavity is expected at the end of September 1997. An optical filter, similar to that designed for the NG-4 Disk Chopper Spectrometer, has been constructed and will be installed in October 1997. This optical filter will eliminate the requirement for a Bi/Be filter, and so increase the flux on the sample by 40%. The flux transmission through the optical filter is estimated to be 75% at 6 Å and 100% above 8 Å.

Correction elements have been constructed (at the FZ-Jülich) that will allow not only off-axis neutrons to satisfy the echo condition but also divergent neutrons. Tests performed at Jülich have shown that the echo condition at 30 ns can be satisfied over the entire area of a 30x30 cm^2 detector. This allows experiments to be per-

formed more quickly. A recent test at Jülich showed that a complete data set of 15 Fourier times at each of 12 Q-values could be collected in 12 hours on a dilute polymer solution (2.5% polyisoprene in dmethylcyclohexane).

Unlike SANS, where the polarization analysis can be performed anywhere along the scattered flight path, the polarization analysis for NSE can only be performed just before the detector. In order to satisfy the demand on mechanical stability for good polarization efficiency, a monolithic array of polarizing supermirror elements has been designed that will allow all neutrons from a sample of up to 5 cm in diameter to be analyzed and detected. Delivery of the supermirror elements for a 5x7 cm^2 prototype array is expected in October 1997.

The epoxy tanzboden is almost completed. The initial layers of gravel and epoxy (necessary to provide a level subsurface) were laid down very successfully. There have been some difficulties with the epoxy-only pour to provide the final surface: The pot life of the epoxy is not long enough to allow mixing and pouring, in a single container, the 55 gallons required to cover 35 m^2 so that the entire floor self-levels. The final pour will be done with ten or eleven 5 gallon batches performed in parallel.

Thermal Neutron Instrument Monernization Program

We are presently in a multi-year modernization to develop a suite of modernized instruments that would have the highest scientific and technological impact in the long term. This upgrade will eventually include two new double-focussing thermal neutron triple-axis spectrometers, one dedicated filter analyzer spectrometer (FANS), and a horizontally focussed sub-thermal (2-20meV) triple axis. In addition to these inelastic instruments, a Perfect Crystal SANS instrument will be located at the BT-5 position. These new instruments will complement the existing High Resolution Powder Diffractometer at BT-1 and the Residual Stress/Single Crystal Diffractometer recently installed at BT-8. Detailed descriptions of the status of individual spectrometers are included below in separate sections. Here we describe progress on the early design effort which has focussed on components common to all of the new inelastic spectrometers.

We have developed a new standard beam-shutter system that will allow full utilization of the beam tube diameter available at NCNR. This required abandoning the existing design where the shutter and beam collimators are combined in a single unit. The new design featuures a beam tube liner and rotating shutter section that will operate inside the biological shield of the reactor and will allow for a beam as large as 16 cm tall and 7.5 cm wide. The beam collimators will be placed within a rotating drum external to the reactor biological shielding. A complete shutter system has been constructed and will be installed and tested at BT-7 in the coming year.

Detailed design has also been completed on a new monochromator drum that will allow use of the larger beams available with the new shutters. We have optimized the design for a monochromator height of 20 cm. Our design was based on a preliminary design for a monochromator drum originally developed for the Advanced Neutron Source. Three units have been ordered and are now under construction.

The Filter Analyzer Neutron Spectrometer (FANS)

The increasing complexity of new materials and processes is an important factor driving the development of new characterization tools. The traditional vibrational spectroscopies, infrared absorption and Raman scattering, have long played a central role. In principle, neutrons are a more versatile dynamical probe than photons because the fundamental nature of the neutron-nucleus interaction permits the observation of all the vibrations, not just those which satisfy appropriate symmetry-based selection rules. Furthermore the output of an inelastic neutron spectrum can be directly related to the vibrational density of states, providing a powerful testing ground for theoretical modeling of materials as well as a means to design materials with specific thermal properties.

However inelastic neutron scattering spectra have long suffered from the rather low intensity. To address this, a new, high intensity filter-analyzer neutron spectrometer (FANS) is being designed and constructed for installation in the reactor hall by a consortium of scientists from the University of Pennsylvania, the University of California at Santa Barbara, NIST, Hughes Aircraft, and DuPont. The throughput and sensitivity of FANS will exceed by a factor of at least 50 that of the filter-analyzer currently in use on the BT4 spectrometer over an energy range of 10 to 150 meV (80 cm^{-1} to 1200 cm^{-1}). This will provide opportunities for new users and new kinds of ex-

periments with much smaller samples. For instance, FANS will be used to study intra- and intermolecular vibrations in molecular crystals and liquids, polymers, guest-host systems (hydrogen in metals, hydrocarbons in zeolite catalysts, sorbed gases on surfaces etc.), to characterize novel forms of carbon (fullerenes, tubules, foams and aerogels, amorphous carbons, fibers, etc.), novel candidate molecules for environmentally acceptable refrigerants, gas separation materials, aging of cements etc.

The operation of FANS is conceptually simple [7]. Monochromatic neutrons of variable energy E_i are inelastically scattered from the sample. Then, using a low-pass Bragg cutoff filter, only those neutrons with a final energy less than the filter cutoff energy are detected. The low-pass filter consists of a cooled polycrystalline material (lattice constant *d*) which transmits only those neutrons with wavelengths longer than 2*d*. The cutoff wavelength cooresponds to an energy cutoff of about 3 meV for beryllium or about 1.1 meV if powdered graphite is placed in series with the beryllium. Inelastic spectra are recorded by scanning the incident energy and detecting all scattered neutrons with $E_f < E_{cutoff}$. The accessible energy transfer range of this instrument is limited on the high end to 200 meV (1600 cm^{-1}) by the anticipated beam divergence which places a lower limit on the monochromator angle, and on the low end to 10 meV (80 cm^{-1}) by leakage of short-wavelength neutrons from higher-order monochromator diffraction.

Most of the gain of FANS compared to the current filter analyzer option on BT4 arises from the much larger solid angle covered by the secondary spectrometer (0.2% of 4π sr compared to 9%). Thus, most of the work to date has been directed toward the design of this much larger, cryogenically cooled, filter system. In fact, the development of the FANS spectrometer has been divided into two phases. In the first phase a subsection of the full filter-analyzer assembly will be used with the existing BT-4 drum and monochromators. This will allow us to realize a significant portion of the intensity gain rather quickly. Later, in the second phase, the existing BT-4 drum will be removed and a new thermal shutter system and monochromator drum (discussed above) will be installed. A second "wedge" will be added to complete the filter analyzer assembly and attached to the new drum. Detailed design is nearly complete for the first phase of the filter assembly and fabrication of these parts will begin shortly.

The design effort has included calculations of the neutronics in the filter material. These results demonstrated that the entire filter assembly will operate successfully at liquid nitrogen temperatures, forgoing the need for more a complicated closed-cycle He refrigeration system. We have calculated the heat load on the filter material to determine the amount of thermal shielding required and performed a finite element analysis to ensure the mechanical integrity of the vacuum chamber including the neutron windows. In addition, extensive neutron background tests have been made at BT-4 to optimize the amount and type of neutron shielding required for the analyzer assembly.

Furthermore, we have accepted delivery of all of the detectors, detector electronics, and all of the machined beryllium filter components. Procurement of the graphite portion of the filter and of the shielding pieces that separate the filter elements is in progress. Barring unforeseen problems, the phase I portion of the spectrometer should be ready for installation sometime in 1998. Engineering design is well underway for the phase II portion of the analyzer. We have also developed a procedure for fabricating appropriate Ge(311) monochromators which will be used to cover the low energy range of the spectrometer. Recently, a monochromator of this type was installed on the BT-1 powder diffractometer and is performing well.

Monochromator Development

The intensity-limited science of neutron scattering constantly calls for instrumental developments that provide an increase of flux on the sample. In most situations an improved monochromator offers a relatively inexpensive intensity gain, or better instrument resolution, with little or no change to other existing instrumentation. Monochromator crystals should have a large coherent structure factor, small absorption and incoherent scattering cross sections, and a high Debye temperature to minimize thermal diffuse scattering. Ideally the monochromator crystal should possess an anisotropic mosaic distribution that is matched to the angular acceptance of the instrument collimation system in the horizontal direction, and comparatively small in the vertical direction to maximize the flux on the sample when used in a focusing condition. Finally, the diamond structure is preferred as it eliminates second order contamination for some reflections. Both silicon and germanium satisfy many of these

requirements, and are commercially available as large single crystals.

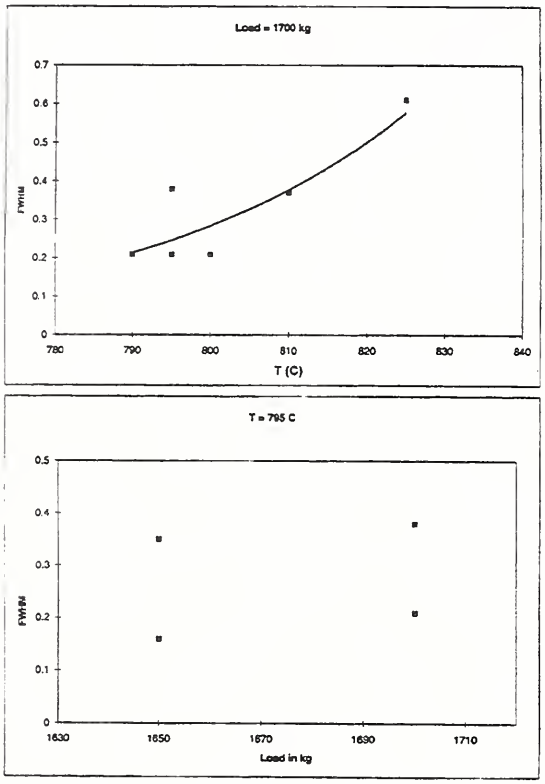

Fig. 5. Plots of Ge(311) pressing data: Crystal mosaic vs. temperature at a constant load of 1700 kg (3750 psi), and crystal mosaic vs. pressure at a constant temperature of 795 degrees C.

With these criteria in mind, we chose to upgrade the NIST BT-1 high resolution powder diffractometer by replacing the vertically focusing Cu(220) monochromator with a vertically focusing Ge(311) monochromator at $2\theta=75°$, where 2θ is the scattering angle from the monochromator. The new monochromator would have the same angular resolution as the Cu (220) monochromator it was designed to replace, but the larger d-spacing, and therefore longer wavelength of 2.0775 Å, would provide better resolution in Q-space, where Q is the magnitude of the wave vector transfer. Furthermore, the minimum in the resolution for this configuration occurs at $Q \approx 3.5$ $Å^{-1}$, which compliments the characteristics of the other two monochromators, Cu(311) $2\theta=90°$ and Si(531) $2\theta=120°$, which have minima in the resolution at Q values of 5.8 Å and 7.2 Å respectively. In addition, because of the diamond structure of Ge, the use of the Ge(311) reflection results in the elimination of second order ($\lambda/2$) beam contamination and so dismisses the need for intensity reducing filters.

The Ge(311) crystals, of dimension 50 x 20 x 10 mm, were plastically deformed in a vacuum hot press at temperatures between 780 and 825°C, and pressures between 1600 - 1700 kg (3527 - 3748 psi.). The crystals were placed on their (311) face between stainless steel pressrams (ground flat and parallel to within 0.005 inches) in a nitrogen environment, and brought up to the pressing temperature over a period of approximately an hour. The load was applied for three minutes and released, and the crystal was allowed to cool to room temperature over a minimum of five hours.

The induced crystal mosaic as a function of pressure and temperature was slightly unstable and seems to behave differently depending on the sample. This somewhat scattered response can be seen in Fig. 5 where we plot the crystal mosaic vs. temperature at a constant pressure, and the mosaic vs. pressure at a constant temperature. Although some samples had to be pressed twice to attain the desired mosaic, other samples, at the same pressure and temerature settings, overshot the ideal mosaic in only one cycle.

The assembled monochromator is comprised of five Ge(311) crystals clipped into aluminum support fingers that are fixed to a vertical focusing device. Each crystal has a Gaussian peak profile with a FWHM in the range 0.20° to 0.37°, and a peak neutron reflectivity (that varies with position on the crystal) of approximately 15-20% at 2.08 Å.

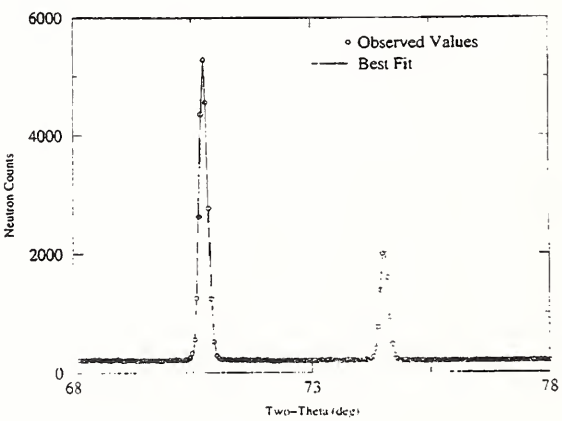

Fig. 6. Sample curves produced by Ge(311) monochromator. Al_2O_3 at $\lambda=2.077$ Å, peaks are fit with Gaussians.

The Ge(311) monochromator installed in the NIST BT-1 powder diffractometer yields the

highest neutron flux (7 x 10^5 n/cm^2 sec with 15' in-pile collimation), and best resolution at low values of the scattering vector Q, of the three available monochromators. Diffraction patterns obtained using the Ge(311) monochromator display nearly perfect Gaussian lineshapes (Fig. 6). The Ge(311) monochromator has been used successfully for measurements on zeolite materials, magnetic ordering and phase change studies, and in cases where high-angle diffraction data are not needed.

Perfect Crystal SANS Diffractometer

In order to extend the measurement range of the NCNR's two, 30 m, pinhole geometry SANS instruments to larger length scales (up to ~10^4 nm), a perfect crystal diffractometer (PCD) with large triple-bounce, channel-cut crystals (Bonse-Hart geometry) is being constructed at a dedicated thermal neutron beam port (BT-5). The multiple reflections suppress the "wings" of the beam profile in order to improve the signal-to-noise at the lowest scattering angles. By using three reflections before and after the sample, the wings decay as Q^{-6}. The PCD will cover a Q-range from 0.001 to 0.1 nm^{-1}, thus extending the low-Q limit of the present SANS instruments by more than an order of magnitude.

Due to space limitations and the desire to maximize the intensity on this generally flux-limited type of instrument, the PCD was originally planned to operate close to the reactor face in a vertical scattering plane. During the past year, however, a way has been found to build the instrument in a horizontal scattering geometry without compromising the estimated beam intensity [8]. The redesigned layout of the instrument is shown in Fig. 7. A key element of this design is the premonochromator which ideally should produce a diffracted beam with the nearly perfect correlation between wavelength and angle needed to satisfy the Bragg condition at the first channel-cut crystal. The required λ-θ_m correlation at the channel-cut monochromator implies that $d\theta_m/d\lambda = d(2\theta_{pm})/d\lambda$ where θ_{pm} is the Bragg angle at the premonochromator. This equation leads to the relation $d_{pm}^2 = 4d_m^2 - 3\lambda^2/4$ for the optimum premonochromator d-spacing d_{pm} (d_m is the d-spacing of the channel-cut crystal monochromator). The premonochromator must also have a mosaic spread, η_{pm}, such that $2\eta_{pm} \approx \Delta\theta$ where $\Delta\theta$ is the divergence required to give the desired $\Delta\lambda/\lambda$. For Si(220) channel-cut crystals and a wavelength of 2.4 Å, either 30' mosaic Ge(111) or pyrolytic graphite (002) as the premonochromator would closely satisfy these conditions. With this approach, the premonochromator can be located some distance from the beam port with minimal loss of useful flux since the required (horizontal) beam divergence before the premonochromator is small. The premonochromator will also be vertically curved to focus on the sample and tall enough (~ 10 cm) to accept the full vertical divergence of the beam port.

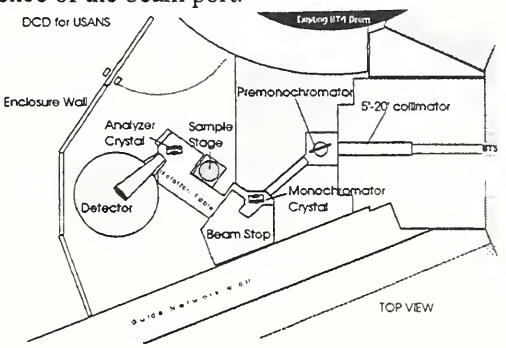

Fig. 7. The planned layout of the Perfect Crystal SANS Diffractometer. The premonochromator will be a vertically focusing mosaic crystal (~30') of either pyrolytic graphite (002) or Ge(111). The triple-bounce monochromator and analyzer crystals are Si(220) and the operating wavelength is 2.4 Å.

Two triple-bounce, channel-cut Si(220) crystals have been acquired which preliminary tests have shown to have the required degree of perfection. The beam port liner, beam shutter and front end shielding for the instrument have been constructed and will be installed in early 1998. Detailed design of the remainder of the instrument will be completed in the spring of 1998.

The construction of the PCD is partially supported by the National Science Foundation through Agreement No. 94-23101.

References

[1] J.R.D. Copley and T.J. Udovic, J. Res. NIST 98, 71 (1993).
[2] J.R.D. Copley, J. Neut. Research 2, 95 (1994).
[3] "NIST Reactor: Summary of Activities, October 1995 through September 1996", ed. L.K. Clutter, NISTIR 6000 (1997), p. 111.
[4] "NIST Reactor: Summary of Activities, October 1994 through September 1995", ed. L.K. Clutter, NISTIR 5829 (1996), p. 98.
[5]http://www.nist.gov/publicaffairs/gallery/hexpod.html
[6] The Nexus web site is at http://www/neutron.anl.gov/NEXUS
[7] J.R.D. Copley, D.A. Neumann, W.A. Kamitakahara, Can. J. Phys. **73** 763 (1995).

[8] A. R. Drews, J. G. Barker, C. J. Glinka and M. Agamalian, Physica B (in press, 1997).

Research Topics

The Disk Chopper Time-of-Flight Spectromter
J. R. D. Copley[7], F. B. Altorfer[1], N. C. Maliszewskyj[7], C. W. Brocker[9], H. P. Layer[7], and J. C. Cook[7]

Performance Tests of the Choppers for the Disk Chopper Time-of-Flight Spectrometer
F. B. Altorfer[9], and J. R. D. Copley[7]

Acceptance Tests of Detectors and Amplifiers for the Disk Chopper Time-of-Flight Spectrometer
P. C. Tobin[7]

Mechanical Design of the Disk Chopper Time-of-Flight Spectrometer
C. W. Brocker[9]

Design of the Data Acquisition System for the Disk Chopper Time-of-Flight Spectrometer
H. P. Layer[7]

Software Development for the Disk Chopper Time-of-Flight Spectrometer
G. C. Greene[7], N. C. Maliszewskyj[7], and P. Klosowski[7]

Ray-Tracing Calculations of Neutron Focusing Properties of Toroidal Mirrors
J. R. D. Copley[7] and C. Hayes[5]

Calculations of Fast Neutron and Gamma-ray Dose Rates Exiting a Neutron Optical Filter
N. S. Rosov[7] and J. M. Rowe[7]

Backscattering Tests of Variable Thickness Si(111) Analyzer Plates
P. M. Gehring[7], D. A. Neumann[7], B. F. Frick[4], C. H. Appel[10], M. D. Shaw[4]

Mosaic Measurements of ZYH Grade Highly-Oriented Pyrolytic Graphite
P. M. Gehring[7], K. T. Forstner[7], D. A. Neumann[7], A. W. Moore[10]

Core Gamma Transmission Through the NG^4 and NG^5 Optical Filters
J. M. Rowe[7] and J. R. D. Copley[7]

Construction of an Epoxy Tanzboden
R. Williams[7] and W. Clow[7]

Field Dependence of Diffuse Scattering from Polarizing Supermirrors
J. Barker[7]

Construction of New Sample Furnance
A. Clarkson[7]

Development of Perfect Crystal SANS Diffractometer
A. Drews[7], J. G. Barker[7], J. Moyer[7], M. Agamalian[8], and C. Glinka[7]

SANS Polarized Beam Development
J. G. Barker[7], D. B. Fulford[7], B. Hammouda[7], and C. G. Glinka[7]

Pressed Cu for Neutron Monochromators
K. T. Forstner[7] and S. F. Trevino[2,7]

Pressed Ge for Neutron Monochromators
K. T. Forstner[7], S. F. Trevino[2], D. A. Neumann[7], J. Blendell[7] and B. Chakomakos[9]

Synthetic Mica for Neutron Monochromators
K. T. Forstner[7], C. F. Majkrzak[7], L. Passell[3], D. A. Neumann[7]

Design of the New Filter Analyzer Neutron Spectrometer (FANS)
P. Papanek[11], D. A. Neumann[7], R. Christman[7], D. Pierce[7], J. E. Fischer[11], J. J. Rush[7], M. L. Klein[11] and A. K. Cheetham[12]

Hydrogen Cold Source Development
R. E. Williams[7], P. A. Kopetka[7], and J. M. Rowe[7]

Monte Carlo Methods for Nuclear Applications
R. E. Williams[7]

Affiliations

[1] Advanced Ceramics Corporation
[2] Army Armament Research Development and Engineering Center
[3] Brookhaven National Laboratory
[4] Eagle-Picher Research Laboratory
[5] Institute Laue-Langevin, France
[6] Johns Hopkins University
[7] NIST Center for Neutron Research
[8] Oak Ridge National Laboratory
[9] University of Maryland at College Park
[10] SFA Inc.
[11] University of Pennsylvania
[12] University of California at Santa Barbara

Reactor Operations and Engineering

For the second year in a row, the reactor has operated well, with no major problems. On-line time was at 70% of real time, in spite of a one-month shutdown for maintenance of the neutron guides, and an additional one week shutdown for shipment of spent reactor fuel. There were very few unplanned reactor shutdowns, and almost all of those which occurred were the result of commercial power interruptions. As a result of the unique fuel management program, fuel utilization remains the highest of any reactor of comparable power in the world.

We have moved to a seven-week operating cycle, 38 days at power and 11 days shut down for refueling, maintenance and surveillance testing. This has allowed us to predict availability substantially in advance, and provide a better planning basis for experimental activities. In addition to this basic cycle, there is one longer shutdown each year to allow for special requirements, such as operator training.

During the year, NIST has signed interagency agreements and awarded contracts that will assure a long term supply of fuel, heavy water and control rods. With this accomplished, we have all of the necessary supplies and arrangements required for the next decade of reactor operation. A revised Safety Analysis Report has been drafted, and chapter by chapter review and approval by all concerned is underway. In anticipation of the upcoming retirement of senior personnel, three operator trainees, one electronics engineer and two guest researchers have been added to the Reactor Operations and Engineering staffs. A new, full scale refueling mockup stand allows staff to be trained in the complex procedures in an off-line mode, without requiring reactor shutdown.

Numerous reactor upgrades and improvements are planned and/or underway. These include a new digital fuel transfer panel, an actual size fuel transfer training station, modernization of the cooling tower and the ventilation system, complete redesign and upgrade of the pneumatic irradiation system and associated radiochemistry laboratories. In addition a new public address system is being installed and major improvements in nuclear, process and radiation monitoring systems are planned. All of these activities are an integral part of our plan to apply for a new license the reactor extending 20 years beyond the current expiration date in 2004.

During the past year, the group was awarded a group Gold Medal, the highest award of the Department of Commerce, for their "...small, excellent staff...with an unrivaled record of safe operation and high availability." A key element in the award was the high cost effectiveness of the NIST facility compared to any comparable neutron source in the world.

Polymers Division
Materials Science and Engineering Laboratory

Blends

- **Polystyrene/Polybutadiene/Poly (styrene-*b*-butadiene) Blends Under Shear**

The effects of shear on the behavior of a blend of polystyrene (PS), polybutadiene (PB), and poly(styrene-*b*-butadiene) (PS-PB) diblock copolymer have been examined by SANS as a function of copolymer concentration, shear rate, and temperature for a fixed ratio of PS to PB. The quiescent behavior has been previously examined, and for a range of copolymer concentrations (<12 wt %), the phase separation temperature is lower than for the pure two-component blend of PS and PB.

In experiments on samples where all polystyrene is deuterium labeled (PSD), shear induced a suppression of concentration fluctuations in the low block copolymer concentration samples (3 and 5 wt %), as was observed in the blend without copolymer present. However, a sample containing 8.6 wt % copolymer demonstrated shear enhancement of concentration fluctuations. Hence, at higher concentrations, the copolymer appeared to destabilize the phase behavior of the mixture during shear. The data were fit to the Ornstein-Zernike equation to obtain the correlation length of the labeled species, ξ and the susceptibility, S(q=0). From these two quantities, the interfacial contribution to the Ginzburg-Landau free energy, κ, was obtained. The magnitude of κ decreased with increasing copolymer content and was independent of shear rate. The decrease in κ with increasing copolymer content indicates the energy cost for formation of interfaces decreased at higher copolymer concentrations.

Another set of experiments was conducted on samples with the polystyrene in the block copolymer being the only deuterium labeled component in the mixture. Due to the low concentration of the labeled component, data was only obtained on a sample containing 8.6 wt % copolymer. A peak in the scattering was observed, which increased in intensity and shifted to lower angle as the critical temperature was approached from the one-phase region. No shear rate dependence in the scattering was observed. Data was also obtained on a 8.6 wt % solution of the labeled copolymer in dioctyl phthalate. Over the same range of temperatures and shear rates used on the three component mixture, no shear rate or temperature dependence was observed in the scattering from the copolymer solution. The scattering from the copolymer solution was assumed to represent the copolymer form factor, so that the structure factor for the copolymer-only-labeled sample could be obtained. The resulting structure factor was fit to the Ornstein-Zernike relation to obtain a correlation length for the copolymer in the mixture. The magnitude of the copolymer correlation length is consistent with the picture of the copolymer location being primarily where $|\nabla \psi|$ is a maximum.

- **Stilbene Labeled PS/PVME Blends**

Deuterated polystyrene (PS) labeled with a stilbene derivative dye (3 mol %) was blended with poly(vinyl methyl ether) (PVME) to examine the effect of photoisomerization of the dye on the phase behavior of the blend as a function of temperature and dye irradiation time by SANS. The non-irradiated samples are presumed to contain only dye in the *trans* isomeric state. With increasing exposure time, the dye is converted to the *cis* isomeric state. The isomeric state of the dye is presumed to influence the PS chain conformation as well as the interaction with the PVME. The phase behavior has been previously examined by light scattering [1].

The random phase approximation (RPA) for two component mixtures was used to fit the data and extract the average segment length in the mixture and the interaction parameter, χ. Plots of χ versus inverse temperature for various irradiation times are linear, with the slope increasing with increasing irradiation time. Further data analysis is in progress.

- **Polyolefin Blends Under Shear**

This work is part of a CRADA with Exxon to study the phase behavior of their metallocene catalyzed polyolefin materials. As part of this work the influence of shear on the phase behavior of these blends was examined by SANS using the in-situ SANS shear cell of the Polymers Division. Two model blends of the polyolefins were examined. One of the blends displayed lower critical solution temperature (LCST) behavior while the other blend exhibited upper critical solution tem-

perature (UCST) behavior. Qualitatively both systems appear to demonstrate shear induced suppression of concentration fluctuations, however, quantitative evaluation of the data is still in progress.

Filled Polymers

- **SANS Characterization of Silicone Polymer Filler Blends**

The goal of this work is to measure the chain dimensions of poly(dimethyl siloxane) (PDMS) polymers in solution, bulk, and in the presence of a variety of fillers at various filler concentrations by SANS. Preliminary measurements have concentrated on the solution characterization of the individual fillers and polymers. Radius of gyration values for the polymers in solution have been obtained and are in good agreement with values derived from gel permeation chromatography. Data analysis on the filler materials is still in progress.

Isotopic blends of deuterated and protonated PDMS were prepared, and the scattering as a function of deuterated polymer concentration was obtained. The low concentration data were analyzed using the traditional Zimm plot formalism. The random phase approximation (RPA) formalism was also utilized for fitting higher deuterated polymer concentrations. The zero concentration limit for the radius of gyration (R_g) with the Zimm and RPA formalisms were identical. From the RPA fits, there is apparently a strong dependence of R_g with the ratio of deuterated to protonated polymer, which will be explored in more detail. Measurements to obtain R_g in the presence of filler materials are in progress.

- **SANS as a Method for Characterization of Filled Polymers**

In this study, the utility of SANS will be assessed as a characterization method for filled polymers. A number of other techniques exist for characterization of these materials, hence parameters uniquely obtainable by SANS are desired which may be correlated to bulk properties of the filled materials. Test samples have been evaluated from two sources. The first set of samples was received from the Building and Fire Research Laboratory (BFRL) of NIST. The samples were polypropylenes filled with silica gel particles. The samples were examined as a function of primary particle size (5 and 20 μm), mechanical history (once or twice extruded), pore volume, and surface treatment. Preliminary results indicate that SANS could distinguish differences in the samples based on pore volume and surface treatment, but not on primary particle size and mechanical history. Evaluation of various schemes for quantitative fitting of the scattering and determination of mechanical properties of the materials is in progress.

A second set of samples was obtained from Goodyear Tire and Rubber Company. The samples were polybutadiene and styrene-butadiene rubber (SBR) filled with fumed silica or carbon black. Three different types of carbon black and three different types of fumed silica, with different surface areas, were examined in each matrix as a function of filler concentration. No differences among the fumed silicas could be observed and only one of the carbon blacks showed any significant differences in the scattering. Measurements on samples with other variations are planned.

Interfaces and Thin Films

- **Wetting Transition in Polymer Thin Films**

In this project Neutron Reflectivity measurements are used to study the composition profile of a binary polymer blend near a surface. Monitoring the adsorption profile of one component affords the possibility to observe a wetting transition close to the blend's critical point. A wetting transition is defined as the change from an incomplete to a complete wetting state of a substrate by a second phase. This wetting transition is well established in binary mixtures of small molecules in the vicinity of the critical point of the phase diagram [2]. However, little experimental work has been done on polymer mixtures concerning the wetting transition [3-5].

Neutron reflectivity experiments are in progress in order to measure the surface enrichment in blends of deuterated polystyrene (dPS) and polybutadiene (PB). This blend exhibits an upper critical solution temperature type phase behavior. In several experiments the adsorption behavior of a blend with a near critical composition on different surfaces was studied as a function of temperature approaching the binodal curve. The results show that PB preferentially adsorbs on hydrogenated silicon surfaces. Further experiments showed that it is possible to change from preferential adsorption of PB to a preferential dPS adsorption by modifying the surface with a grafted polystyrene monolayer. Due to this surface modification, a thick dPS-rich adsorption layer now forms at the polymer brush/polymer blend interface as the binodal curve is approached. The in-

fluence of such a brush layer on the wetting properties of a small molecule binary system has recently been studied [6].

Currently, we are studying the composition dependence of the adsorption. More reflectivity experiments will be done with polymer films of different bulk composition.

- **Copolymer Composition Effects on Homopolymer / Random Copolymer Interface**

Many important practical applications utilize blends of homopolymers with random copolymers, where the copolymers act as reinforcing agents at the interfaces. The interfacial toughness in these systems depends primarily on the number of effective entanglements across the immiscible interface and how far one phase penetrates into the other. A knowledge of the interface width between a homopolymer and a copolymer [7] is therefore vital for predicting properties of such materials. In this project we investigate one such system, deuterated polyphenylene oxide (dPXE) and a random copolymer styrene acrylonitrile (SAN), in which there is no chemical or grafting reaction [8], but only a favorable interaction. Here we have used neutron reflection to investigate the interface width between dPXE and SAN for varying AN composition.

Neutron reflection measurements were performed for a series of Si/dPXE/SAN floated bilayer samples, with SAN having $\phi_{AN} = 0.^{15}$, 0.20, 0.25, 0.31 and 0.40. Films as-cast and after annealing at 140 °C for 1.5 hours, 9 hours and 180 °C for 3 hours were measured. All as-cast samples exhibited sharp interface widths on the order of typically 1 nm, indicative of good sample quality. These interfaces broadened upon annealing at 140 °C for 1.5 hours in inverse relationship to ϕ_{AN}. Through swap experiments, deuterium labeling effects were found to be unimportant for this system which is dominated by strong interactions. Such a trend is qualitatively expected from calculations estimating the ternary interaction parameters, $\chi_{dPPO/PS}$, $\chi_{dPPO/AN}$ and $\chi_{PS/AN}$ for this system. Quantitative fits to the data indicate that the interface widths are in acceptable range of calculated values from theory. Annealing longer for 9 hours at 140 °C, or at the higher temperature of 180 °C did not significantly alter the reflectivity profiles. Additional broadening may arise from capillary waves in thin film geometry. This idea was tested in bilayer films with very thin layer thicknesses. The interface widths were confirmed to be substantially broader in these samples. For sufficiently low ϕ_{AN}, the homopolymer and random copolymer should become miscible. Neutron reflection measurements on a reference dPXE/PS ($\phi_{AN} = 0$) system confirmed that the system is miscible in this limit.

Investigation of the Regimes in Dendrimer Solution

This study is the first to focus on the behavior of dendrimers in solution over the whole range of concentration (range of mass fraction x, $0.01 \leq x \leq 0.80$) [9]. The two poly(propylene imine) dendrimers $DAB(PA)_{32}$ and $DAB(PA)_{64}$ were used. Based on the result of this study we give the first definition of solution regimes for dendrimers [10].

We define the 'dilute solution regime' for dendrimers to reach to a dendrimer volume fraction, $\phi^+ < \phi^*_{RCP} = 0.64$, the value ϕ^+ being calculated from the radius of the dendrimer at infinite dilution. In this regime, the radius of the dendrimer does not depend on the concentration.

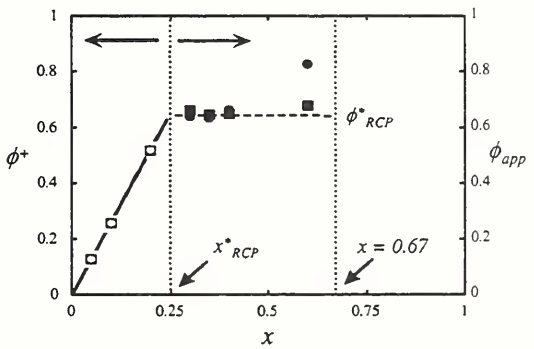

Fig. 1. Values of the volume fraction of poly(propylene imine) dendrimers, plotted versus the dendrimer mass fraction x (○and ●: $DAB(PA)_{32}$; □ and ■: $DAB(PA)_{64}$).

At the threshold value $\phi^+ = \phi^*_{RCP} = 0.64$, the dendrimers take a random close packing arrangement. In concentrated solution, i.e. $\phi^+ \geq \phi^*_{RCP}$, the dendrimers collapse by an amount that the value of the dendrimer volume fraction, ϕ, equals the value of random close packing spheres ($\phi = \phi_{RCP} = 0.64$). The validity of the model is limited to high concentrations by the point where the dendrimers have a segment density close to the value of the bulk dendrimer. We refer to this model as the 'random close packing of collapsing dendrimers'.

The collapse of the dendrimers is observed experimentally by measuring the SANS at various dendrimer mass fractions up to $x = 0.80$ in the solvent CD_3OH, and calculating the structure factor $S(q)$ on the basis of the decoupling approximation by using an extrapolated form factor $P(q)$. $S(q)$ is analyzed in terms of a mean dendrimer-dendrimer distance. The figure shows the data for the dendrimer volume fraction, ϕ, as a function of the dendrimer mass fraction x (ϕ^+), calculated from the radius of the dendrimer dilute solution; ϕ_{app}, calculated from the dendrimer-dendrimer distance).

Effect of Solvent Quality on Starburst Dendrimers

Dendrimers are unique molecules in respect to their regular and highly branched structure. Extensive characterization studies of dendrimers by the polymer blends group have shown that dendrimers are spherical and very uniform. This makes them excellent candidates for calibration materials with a well defined diameter in the range 3 nm $\leq d \leq$ 15 nm, depending on the family and generation of the particular dendrimer. Crucial for the introduction of dendrimers as calibration standards is to know the sensitivity of the dendrimer to parameters such as solvent quality and temperature.

- **Dendrimer in Pure Solvents of Different Solvent Quality**

The radius of gyration of a generation 8 poly(amidoamine) (PAMAM) dendrimer was measured by SANS in dilute solution using water, methyl- , ethyl-, and *n*-butyl alcohol as solvents. The solvent quality for PAMAM dendrimers decreases from water to *n*-butyl alcohol. The radius of gyration was calculated from the SANS data by applying a Guinier fit. A weak dependence of the dendrimer size on the solvent quality is found (Fig. 2). The radius of gyration varies by 4 Å when changing the solvent from water to *n*-butyl alcohol.

- **Dendrimer in Solvent Mixtures**

The quality of the solvent for PAMAM dendrimers can also be varied by adding a non-solvent to a dendrimer solution. This procedure allows a study of the effect of solvent quality close to the solubility limit. The shape and size of generation 5 and generation 8 PAMAM dendrimer was investigated by using methyl alcohol/acetone mixtures of different composition as solvent. The PAMAM dendrimers were found to be soluble in these solvent mixtures in the range of composition $0 \leq x_{solvent} \leq 0.5$, with an interesting narrow miscibility gap around $x_{solvent} \approx 0.3$ ($x_{solvent}$, mass fraction of acetone d_6). A variation of the temperature in the range - 10 °C ≤ T ≤ 50 °C had virtually no effect on the size and shape of the dendrimers for all the solvent compositions studied. Scattering patterns of the solutions close to the solubility limit, i.e. $x_{solvent} \approx 0.5$, are dominated by the miscibility gap.

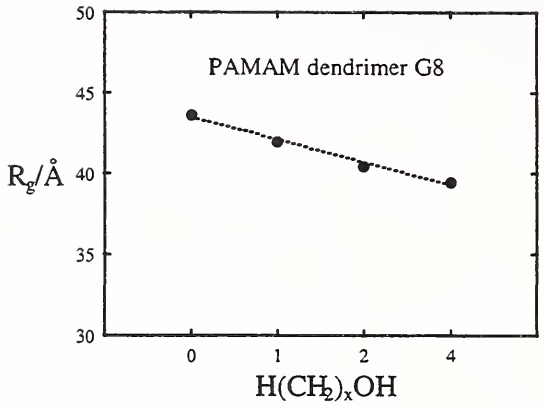

Fig. 2. Dependence of the radius of gyration of a generation 8 PAMAM dendrimer on the solvent quality(solvents: water, methyl-, ethyl- and *n*-butyl alcohol).

Domain Structure in Polyelectrolyte Solutions

Polyelectrolyte solutions are well known for their complex scattering behavior and remain among the least understood systems in macromolecular science. There are several experimental observations which are now considered universal to charged macromolecular systems at low ionic strength. In SANS these include an upturn at low wavevector and a maximum at finite wavevector. Although these phenomena have been observed and studied for decades, there is no clear molecular interpretation.

In this study, we use small angle neutron scattering to probe the structure of aqueous and non-aqueous polyelectrolyte solutions. Data from two configurations of the 30 m SANS facility were combined, yielding a scattering profile covering nearly two decades in q values. This extended q range, which is a factor of six lower than previous SANS measurements, allows overlap of the SANS data with the results of light scattering

from the same solutions (Fig. 3). The results confirm the presence of structures much larger than single chains, which we interpret in terms of multi-chain domains.

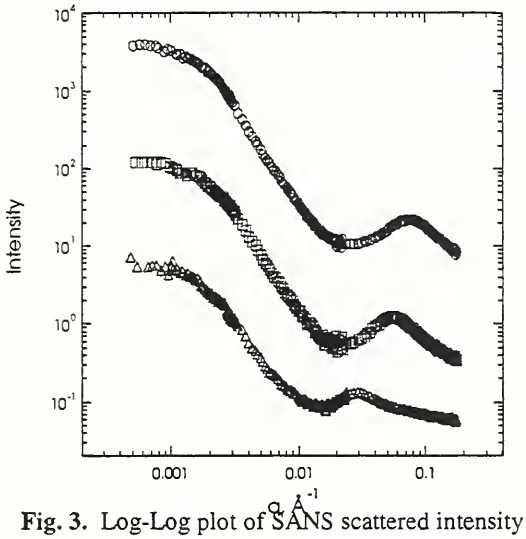

Fig. 3. Log-Log plot of SANS scattered intensity for the two instrument configurations (no arbitrary adjustments to the data) and SLS scattered intensity (data arbitrarily shifted to match the SANS data) plotted versus the scattering vector q for three different polymer.

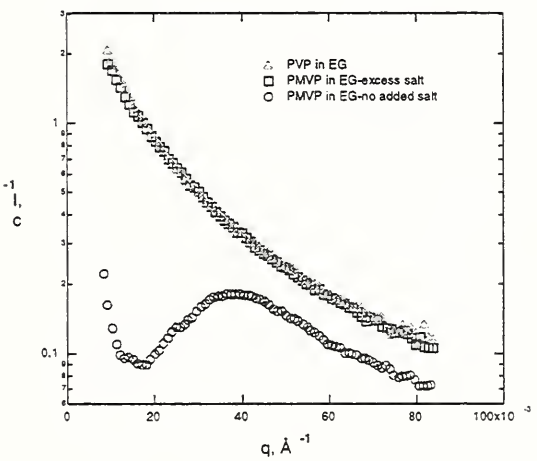

Fig. 4. SANS scattered intensity, I(q), plotted versus the scattering vector q for (○)PMVP in ethylene glycol-d_6 with zero added salt, for (□)PMVP in ethylene glycol-d_6 with excess NaCl, and for (△)PVP in ethylene glycol-d_6.

One complication for aqueous solutions is the influence of poor backbone-solvent interactions, which may contribute to the unusual scattering [13]. We have shown that small angle neutron scattering on a polyelectrolyte dissolved in a solvent where the hydrophobic effect is not present shows the same features as typical polyelectrolytes, a peak at finite wavevector and a steep upturn at low wavevector[14]. The scattering of the polyelectrolytes after the addition of excess salt suppresses the unusual peak and steep upturn yielding scattering nearly identical to that from neutral chains in the same solvent (Fig. 4). These results indicate that strong correlations promoted by electrostatic interactions dominate the physics of polyelectrolyte solutions and that the influences of poor backbone solvation are unessential for explaining the primary characteristics of polyelectrolyte scattering.

SANS Study of a Labeled PAMAM Dendrimer

Many of the potential technological applications of dendrimers depend on their segment density distribution. Previous scattering studies have shown that dendrimers have uniform interiors and are quite spherelike in their shape [13]. The location of the terminal groups is also of importance, since they are usually chemically different from the rest of the dendrimer.

Two samples of generation 7 PAMAM-Dendrimers with tetrafunctional cores based on ethylene diamine were used. One was a fully protonated dendrimer and the other had the first half of generation 7 labeled with deuterium by use of deuterated methyl acrylate-d_3 in the second last reaction step. SANS experiments with the unlabeled dendrimer were carried out under high contrast conditions (solvent: CD_3OH). The labeled dendrimer was dissolved in a CD_3OH/CH_3OH mixture that has the same average contrast as an unlabeled PAMAM dendrimer. The contrast

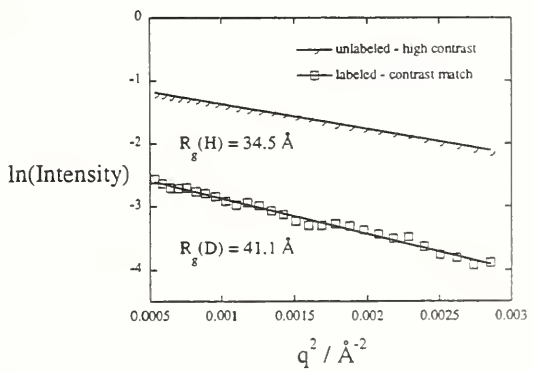

Fig. 5. Guinier plots of matched and unmatched G^7 dendrimers.

match conditions were found by preparing solutions of unlabeled dendrimer with different CD_3OH/CH_3OH mixtures.

A Guinier fit is applied to calculate the radius of gyration R_g for both samples. The fits are shown in Fig. 5. For the deuterated sample a larger value for R_g is obtained ($R_g(D)$ = (41.1 ± 1.2) Å) than for the unlabeled one ($R_g(H)$ = (34.5 ± 0.4) Å). Using the value $R_g(H)$ to calculate the equivalent hardsphere radius of the dendrimer, a value of R_h = 44.5 ± 0.5 Å is obtained. When the deuterated segments of the last generation are assumed to lie within a thin shell surrounding the dendrimer, the experimental radius of gyration $R_g(D)$ = 41.1 Å is equal to the radius of the thin shell. This value corresponds well to the calculated hydrodynamic radius R_h = 44.5 Å for the whole dendrimer. The units of the first half of the last generation of a seventh generation dendrimer have a radius of gyration that is larger than that of the whole dendrimer by a factor of 1.19 ± 0.06. This suggests that the terminal units are predominately towards the outside of the dendrimer [14].

- **Ternary Blends of Dendrimers and Linear Polymers.**

Blends of deuterated polystyrene (PSD)and poly(vinylmethyl ether) (PVME) have been extensively studies at NIST [1], and have a phase transition between 130 and 160 °C depending on composition and molecular weight. Blends made of PSD and PVME have been modified by the addition of hydrophobically modified dendrimers. SANS has been used to estimate the change in the spinodal temperature as a function of dendrimer content.

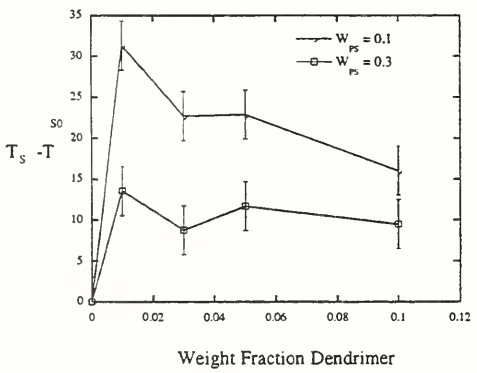

Fig. 6. Increase of spinodal temperatures with addition of hydrophobically modified dendrimer.

Hydrophobically modified dendrimers were synthesized by reacting 1,2 - epoxy octane with amino terminated poly(propylene imine) dendrimers. Blends were made with 10, 30, 50, and 70 weight % PSD with the remainder PVME. To these blends, 0, 1, 3, 5, and 10 weight % hydrophobically modified dendrimer was added. Ornstein-Zernike fits were made of the scattering and the spinodal was calculated from the divergence of the correlation length and the zero angle scattering.

Figure 6 is a plot of the increase of the spinodal temperatures as a function of dendrimer content. For samples with 10 weight % PSD, addition of 1% dendrimer increased the spinodal over 30 °C. Blends with 30 weight % PSD had an increase of around 15 °C. In all cases with low PSD weight fractions, miscibility was increased by a condiderable amount. In blends with higher PSD content, immiscible blends resulted.

References

[1] Q. Tran-Cong, T. Ohta, and O. Urakawa, "Soft-mode Suppression in the Phase Separation of Binary Polymer Mixtures Driven by a Reversible Chemical Reaction", Phys. Rev. E, **56**, 1, (1997).

[2] D. Beysens, in Iquid at Interfaces, Les Houches Lectures 1988, edited by J. Charvolin, J. Joanny, and J. Zinn-Justin (North Holland, Amsterdam, Oxford, New York, Tokyo 1990), p 502.

[3] L. J. Norton, E. J. Kramer, F. S. Bates, M. D. Gehlsen, R.A.L. Jones, A. Karim, G.P. Felcher and R. Kleb, Macromol. **28**, 8621 (1995).

[4] A. Budkowski, F. Scheffold, L. J. Fetters, and J. Klein, J. Chem. Phys. **106**, 719 (1997).

[5] J. Genzer and R.J. Composto, Europhys. Lett. **38**, 171 (1997).

[6] A. Karim, J. F. Douglas, F. Horkay, L. J. Fetters, and S. K. Satija, Physika B **221**, 331 (1996).

[7] "Neutron Reflection Studies on Segment Distribution of Bloick Chains in Lamellar Microphase-Separated Structures," N. Torikai, I. Noda, A. Karim, S. K. Satija, C. C. Han, Y. Matsushita, T. Kawakatsu, Macromol. **30**, 2907 (1997).

[8] "Phase Separation In Chemically Reactive olymer Blend Films, A. Karim, J.F. Douglas," S.K. Satija, A.P.Y. Wong, C.C. Han, Macromol., revised - submitted.

[9] A. Topp, B. J. Bauer, E. J. Amis, R. Scherrenberg, "Small Angle Neutron Scattering from Dilute and Concentrated $DAB(PA)_x$ Dendrimer Solutions", *ACS PMSE Proc*, *7* (1997)p. 82..

[10] A. Topp, B. J. Bauer, E. J. Amis, R. Scherrenberg, "Random Close Packing of Collapsing Dendrimers in Concentrated Solution", in review.

[11] B. D. Ermi and E. J. Amis, Macromol. **29**, 2703 (1996).

[12] B. D. Ermi and E. J. Amis, Macromol., 1997, in press.

[13] "A SAXS Study of the Internal Structure of Dendritic Polymer Systems", Ty J. Prosa, Barry J.

Bauer, Eric J. Amis, Donald A. Tomalia, Rolf Scherrenberg, J. Polymer Science, Polymer Physics **35** ,17 (1997).

[14] "SANS Study of Labeled PAMAM Dendrimer", E.J. Amis, A. Topp, B.J. Bauer, D.A. Tomalia, ACS PMSE Proceedings **77,** 183 (1997).

[15] "Temperature, Composition, and Molecular Weight Dependence of the Binary Interaction Parameter of Polystyrene/Poly(vinyl methyl/ether) Blends," C. C. Han, B. J. Bauer, J. C. Clark, Y. Muroga, Y. Matsushita, M. Okada, Q. Tran-cong, T. Chang and I. C. Sanchez, Polymer **29**, 2002 (1988).

Research Topics

Polystyrene/Polybutadiene/Poly(styrene-b-butadiene) Blends Under Shear
A. I. Nakatani[16], L. Sung[15], E. K. Hobbie[16], and C. C. Han[16]

Stilbene Labeled PS/PVME Blends
A. I. Nakatani[16], C. C. Han[16], O. Urakawa[9], and Q. Tran-Cong[9]

Polyolefin Blends Under Shear
A. I. Nakatani[16], K. Migler[16], M. Rabeony[6], R. Garner[6], and D. Lohse[6]

SANS Characterization of Silicone Polymer Filler Blends
A. I. Nakatani[16], W. Chen[5], R. Schmidt[5], and G. Gordon[5]

SANS as a Method for Characterization of Filled Polymers
A. I. Nakatani[16], C. C. Han[16], J. Gilman[14], Y. Feng[8], and A. Halassa[8]

Wetting Transition in Polymer Thin Films
H. Gruell[16], and C. C. Han[16]

Copolymer Composition Effects on Homo-Polymer / Random Copolymer Interface
A. Karim[16], L. Sung[16], N. Balsara[13], and C. C. Han[16]

Mobility near interfaces in thin glassy films
A. Karim[16], G. P. Felcher[1], S. K. Satija[15], and J. Koberstein[19]

Phase separation in hydrogen-bonded blend films
C. Zhou[16], A. Karim[16], C. Han[16]

Investigation of the Regimes in Dendrimer Solution
A. Topp[16], B. J. Bauer[16], and E. J. Amis[16]

Effect of Solvent Quality on Starburst Dendrimers
A. Topp[16], B. J. Bauer[16], and E. J. Amis[16]

Domain Structure in Polyelectrolyte Solutions
E. J. Amis[16], B. D. Ermi[16] and D. E. Valachovic[22]

Model Polyelectrolytes in Aqueous and Non-aqueous Solutions
E. J. Amis[16], B. D. Ermi[16], Y. Zhang[16]

Polyelectrolytes with Variation in Counterion and Co-ion Valency
E. J. Amis[16], Y. Zhang[16], R. Ivkov[16], B. D. Ermi[16], and A. Topp[16]

Location of Counterions in Polyelectrolyte Solutions
E. J. Amis[16], Y. Zhang[16], A. Topp[16], and B. D. Ermi[16]

Polymer-Colloid Interactions
E. J. Amis[16] and R. Ivkov[16]

SANS Study of a Labeled PAMAM Dendrimer
A. Topp[16], B. J. Bauer[16], E. J. Amis[16], and D. A. Tomalia[11]

Ternary Blends of Dendrimers and Linear Polymers.
A. Topp[16], B. J. Bauer[16], and E. J. Amis[16]

Affiliations

[1] Argonne National Laboratory
[2] Army Research Laboratory
[3] CNRS, France
[4] Cornell University
[5] Dow Corning Corporation
[6] Exxon Research and Engineering Company
[7] General Electric Corporation
[8] Goodyear Tire and Rubber Company
[9] Kyoto Institute of Technology, Japan
[10] Michigan Technological University
[11] Midland Macromolecular Institute
[12] Nagoya University, Japan
[13] New York State University
[14] NIST, Building and Fire Research Laboratory
[15] NIST Center for Neutron Research
[16] NIST, Polymers Division
[17] Polytechnic University
[18] University of Alabama
[19] University of Connecticut
[20] University of Delaware
[21] University of Maryland at College Park
[22] University of Southern California
[23] University of Texas
[24] University of Tennessee
[25] Tokyo University, Japan

Other MSEL Programs with NCNR Participation

Ceramic Coatings

The Ceramic Coatings Program is a measurement and characterization effort which addresses the processing reproducibility and performance prediction issues that are primarily associated with thermal-spray deposited ceramic coatings. The program focuses on plasma-spray-deposited ceramic thermal barrier coatings used in aircraft gas turbines and expected to be used in land-based turbines and diesel engines. Sales in the thermal-spray industry are currently valued at more than one billion dollars annually, a significant portion of which is ceramic thermal-barrier coatings. Collaborations have been established with industrial organizations including Pratt and Whitney, General Electric, Caterpillar, METCO, MetTech and Zircoa as well as the Thermal Spray Laboratory at the State University of New York at Stoney Brook and the Thermal Spray Laboratory at Sandia National Laboratory. The program includes collaboration with the National Aerospace Laboratory and the National Mechanical Engineering Laboratory, both in Japan, to examine functionally gradient materials. Collaboration is also underway with BAM (Germany) for the development of characterization techniques for thin, hard films. Research is conducted on the processing and properties of Physical Vapor Deposited (PVD) ceramic coatings in collaboration with Praxair, an Advanced Technology Program (ATP) awardee.

Participants in the NIST program are located in the NIST Center for Neutron Research, the Ceramics and Materials Reliability Divisions of the Materials Science and Engineering Laboratory, and the Chemical Science and Technology Laboratory.

The approach taken in the plasma-spray (PS) research has been to build on the analytical capabilities at NIST and the material processing capabilities of collaborators. The program has the following elements:

- development of techniques for characterization of physical and chemical properties of stabilized zirconia and tungsten carbide feedstock to provide data for increased processing reproducibility as well as data required for production of a Standard Reference Material suitable for calibration of light-scattering size distribution instruments used in industry for analysis of PS powder;
- development of scattering techniques to determine the quantity, size and orientation of porosity and microcracks in PS ceramic coatings suitable for use in modeling the thermomechanical behavior of these materials;
- development of methods to measure chemical, elastic modulus, and thermal properties on a scale suitable for use in microstructural models of behavior;
- development of techniques to model thermomechanical behavior of thermal-barrier coatings to enable more reliable performance prediction; and
- development of techniques for accurate measurement of the thermal conductivity of PS coatings, by use of the guarded hot-plate technique suitable for incorporation in ASTM standards and by the pulsed laser heating technique, to provide a method for comparison with routine industrial techniques.
- development and refinement of more sensitive methods for accurate analysis of oxide phases and residual stresses which affect performance and durability of coatings.

Research on chemical mapping of powders and microstructures is conducted in the Microanalysis Division of the Chemical Science and Technology Laboratory, while thermal property research is conducted in the Materials Reliability and Metallurgy divisions. The NIST Center for Neutron Research participates in both the powder analysis and scattering projects. A strong attribute of the PS coatings research is the use of common materials for which complementary data can provide a more complete understanding of processing micro-structure property relationships.

Evaluated Materials Data

The objective of the Evaluated Materials Data Program is to develop and facilitate the use of evaluated databases for the materials science and engineering communities. Both research- and application-directed organizations require readily available evaluated data to take advantage of the large volume of materials information developed on public and private sponsored programs. This information, particularly numeric data, is available in an ever increasing number of publications published worldwide. The necessity to consolidate and allow rapid comparison of properties for product design and process development underlies the database projects.

Evaluated databases are developed in cooperation with the NIST Standard Reference Data Program Office and, often, coordinated with the activities of other laboratories and scientific/ technical societies. Research consists of the compilation and evaluation of numeric data as well as recently initiated efforts directed at more effective distribution and use of data. Database activities reflect laboratory programs with scientific capabilities required for appropriate data evaluation.

Database projects in MSEL include:

- Phase Equilibria Diagrams (PED), conducted in cooperation with the American Ceramic Society;
- the Structural Ceramics Database (SCD), a compilation of evaluated mechanical and thermal data for nitrides, carbides, and oxides of interest to engineers and designers;
- a ceramic machinability database, developed by the Ceramic Machining Consortium (see Ceramic Machining Program);
- a high T_c superconductivity database developed in cooperation with the Japanese Agency for Industrial Science and Technology (see High Temperature Superconductivity Program);
- development and implementation of the STEP protocol for the exchange of materials data, under the auspices of the ISO 10313 activity;
- the NACE/NIST Corrosion Performance Database developed by NACE and the Metallurgy Division to provide a means to select structural alloys for corrosive applications; and
- the Crystal Data Center, developed by the NIST Center for Neutron Research, which provides fundamental crystallographic data on inorganic materials.

High Temperature Superconductivity

A significant program in high T_c superconductivity is being conducted in MSEL and other Laboratories at NIST. The primary focus of the MSEL program is on bulk superconducting materials for wire and magnet applications. In carrying out this program, researchers in MSEL work closely with their counterparts in other NIST Laboratories, and collaborators in U.S. industry, universities, and other National Laboratories.

The primary thrusts of the program are as follows:

- Phase equilibria - Work is being performed in close collaboration with the U.S. Department of Energy (DOE) and its national laboratories to provide the phase diagrams necessary for processing these unique ceramic materials. A prime objective is the development of the portions of the phase diagram for the Pb-Bi-Sr-Ca-Cu-O system relevant to production of the high T_c materials.
- Flux pinning - Use is made of a unique magneto-optical imaging facility to examine flux pinning in a variety of materials, with much of this work being conducted in collaboration with American Superconductor Corporation. In addition techniques for better interpretation of magnetic measurements are being developed. Structure and dynamics of flux lattices and melting phenomena, critical to applications, are investigated with small-angle neutron scattering techniques.
- Damage mechanisms - Work is being carried out under a joint CRADA (cooperative research and development agreement) with American Superconductor Corporation as part of the "Wire Development Group" which involves a number of DOE National Laboratories and

the University of Wisconsin to elucidate the effects of strain on the loss of current in superconducting wires. The primary tool being employed is the use of microfocus radiography available at the NIST beamline at the Brookhaven National Laboratory.

- Database - A high temperature superconductor database has been developed in collaboration with the National Research Institute for Metals (NRIM) in Japan. The High Temperature Superconductor Database (HTSD) includes evaluated open-literature data on numerous physical, mechanical, and electrical properties of a variety of chemical systems. The first version of the database is now for sale by the Office of Standard Reference Data.

- Crystal structure - Thermal neutron scattering techniques and profile refinement analyses are being utilized to investigate crystal and magnetic structures, composition, dynamics and crystal chemical properties. This research is being carried out in collaboration with a number of industrial and university experts and researchers at National Laboratories.

EXXON Research at the NCNR

Exxon Research and Engineering Company is a member of the Participation Research Team (PRT) that operates, maintains and conducts neutron-related research activities on NCNR's NG7-30 m SANS instrument. Most experiments are in the fields of polymers, complex fluids, and petroleum mixtures, using SANS as a tool to study their structure-property relations. We also partic-ipate in other type of activities at NCNR, for example, neutron imaging, neutron reflectivity. The following short reports briefly describe some of the programs, while a more complete list of the programs and their participants can be found at the end of this Section in Research Topics.

Effect of Pressure on the Thermodynamics of Polyolefin Blends

For the last several years we have been engaged in a study of the basic thermodynamics of mixtures of polyolefins which has relied heavily on SANS experiments at NIST. Polyolefins are saturated hydrocarbon polymers which are among the most common plastics (polyethylene, poly-propylene) and elastomers (ethylene-propylene copolymer, polyisobutylene). These are often used as blends, and their phase behavior has an important effect on the properties and so utility of such materials. It is difficult to obtain data on polyolefin blend thermodynamics in the liquid state by conventional due to the lack of density and refractive index differences. Deuterium labeling and SANS has allowed the direct determination of the interactions in these blends. This technique has now been used on over 100 blends involving some 40 different polyolefins.

A wide variety of phase behavior has been seen in these polyolefin blends - UCST (that is, phase separation upon cooling), LCST (that is, phase separation upon heating), and combinations of both. For the great majority of these blends, we have found that a Hildebrand regular solution scheme can be used to describe the Flory interaction parameter, χ that is measured. That is, we can assign a solubility parameter to each polymer, based either on SANS measured interactions or independently by PVT measurements, and from these predict quite well how the polyolefin mix. For a small fraction of the blends, these regular solution ideas do not work, and most of these irregular blends have a much lower interaction energy density than such a model would predict. In fact some of them even have negative χ values. Since there are no strong, specific interactions between these saturated hydrocarbon components, it is hard to understand the origins of such irregularity. In an attempt to find the reasons for this, as well as to understand the behavior of such blends in applications like extrusion and molding, we have studied the effect of pressure on interactions in several of these blends over the last year.

Some general trends have been seen. For those blends which display UCST phase behavior it is always found that the critical temperature increases with pressure. We have now seen this in several polyolefin blends: in particular, blends of various ethylene copolymers with each other and in isotopic blends of the hydrogenous and deuterons versions of the same polymer. In a similar fashion, in a mixture that displays LCST behavior the critical temperature also increases with pressure. This was seen in a blend of polyisobutylene (PIB) with a head-to-head polypropylene (hhPP), and it has also been observed in blends of polyvinyl methyl ether) and polystyrene (S. Janssen et al., Macromolecules 1994, 27, 5587). So increasing pressure reduces the degree of miscibility in UCST blends (pressure raises the UCST) while it increases the degree of miscibility in LCST blends (by raising the LCST).

There is a certain consistency in these results. In UCST systems, the mixed state is destabilized by an increase in density, either by cooling or by pressurization. On the contrary, in an LCST system densification increases the stability of the one-phase state. This led us to consider how the interaction parameters of these blends depend on density, rather than pressure or temperature alone. For the UCST blends the data for all of the temperatures collapse together when plotted versus density, showing that the interaction energy density is a simple function of blend density for these cases. For the PIB/hhPP blend the data clearly come closer together, but do not overlap for the UCST blends. So it appears that a simple equation of state may apply for these polyolefin blends. We are now in the process of further quantifying these results and will be examining other systems as well.

Micelles and Microemulsions of Polyelectrolytes Copolymers

Diblock polyelectrolyte copolymers styrene-b-sodium acrylate (PS-PANa) with PANa molecular weight (Mw) ~ 34K and PS 3.5K, 9K and 12.3K were studied in aqueous solution using SANS. Spherical micellar aggregates were found to self-assemble with polydispersity around 10%. The aggregation number for the 3.5K PS was 60 and 9K PS 160, which remain roughly constant for different concentrations. Due to the intra-micellar charge repulsion, polyelectrolyte micelle hairs were found to be extremely stretched into rod-star configuration. The interaction between the charged micelles is prominent even at 0.1% diblock concentration. The inter-micellar structure factors as a function of polymer can be best fit using a hard sphere/square well potential with a Sharma-Sharma mean spherical approximation. We propose that the hard sphere interaction is due to an induced dipole dispersion interaction. Introducing a third phase, toluene, into the micelle dispersion, monodisperse micro-emulsion were found to form by core-swelling with no reorganization of the micellar aggregates. Increasing toluene to a content higher than that of copolymer, polydispersed spherical emulsions of 1 to 100 microns size were observed.

Polymer Aggregates with Crystalline Cores: The System Polyethylene-poly (ethylenepropylene)

We have studied the aggregation behavior of polyethelyene-poly(ethylenepropylene) (PE-PEP) diblock copolymers dissolved in decane. For this purpose PE-PEP diblock copolymers of various molecular weights, compositions, and degrees of deuteration were synthesized via an anionic route. The structure and morphology of the aggregates was studied by SANS varying both the contrast as well as the polymer labeling. We found a hierarchy of structures: The PE component crystallizes in lamellar sheets (thickness 40-80 Å) surrounded on both sides by a PER brush which exhibits a close to parabolic density profile. Different aggregates form macroaggregates of needle like shape with the PER lamellar planes in the long direction. This macroaggregation is well described by a paracrystalline structure factor. The structural parameters depending on composition and molecular weight can be well understood in terms of a free energy of formation based on a scaling model. A quantitative evaluation of the different contributions to the free energy reveals an important role of defect structures resulting from the ethylene side branches in the polyethylene component. Finally, we show in a semiquantitative approach that the van der Waals energy between the brushes is large enough to facilitate macroaggregation.

Melt Chain Dimensions of Poly-(ethylene-1-butene) Copolymers

The radii of gyration for a series of poly(ethylene-1-butene) copolymers of varying ethyl branch content were measured as a function of temperature in the melt via SANS, and their temperature coefficients, d(lnC)/dT, changed from negative to positive. The characteristic ratio C decreased with increasing ethyl branch frequency. When possible, these results were compared with those obtained from Theta solvents and from rotational isomeric state (RIS) theory. The SANS-based chain dimensions were slightly larger than those obtained from Theta solvents. The values of d(lnC)/dT differed significantly from those extracted from theta-solvent measurements. Serious discrepancies with RIS-based calculations were observed.

Characterization of Soot in Diesel Engine Oils

Diesel engines produce a significant amount of soot during combustion cycles which causes the viscosity of the lubricant oil to increase nonlinearly. Various research over the years has concentrated on characterizing the soot in an effort to understand the mechanism of induced viscosity. However, until recently, there has been a lack of in situ techniques not requiring stripping the soot from its original oil environment such as dilution for light scattering and freeze fracture for microscopy studies. We have demonstrated that neutron scattering techniques are an ideal tool to fulfill this need. Like most hydrocarbons, the absorption of neutrons by the oil is relatively low, while contrast between the soot particles (mostly carbon) and the oil is very high so that no deuteration is needed. In addition, most sooty oil's soot contents are below 1% by volume, ideal as dilute solution, so that no more dilution is necessary. Most importantly, the information that SANS can provide, such as particle size, fractal

dimension, other morphological parameters, as well as particle mass, is very crucial in understanding the physical behavior of the oil, including its viscosity. We have been studying oils samples "as is" from various engine tests with varying temperatures and under shear. The results are well correlated with viscosity measurements.

Neutron Imaging for In-situ Measurements of Water Transport Gradients in Polymer Electrolyte Fuel Cells

Water transport is an important consideration in the optimization of polymer electrolyte fuel cell (PEFC) performance, affecting both internal resistance and cathode polarization losses. Preliminary experiments are performed using neutron radiography to measure water gradient profiles within Nafion in an operating PEFC. The resulting neutron intensity gradients show qualitative agreement with expected response of membrane water content to changes in feed gas humidification and fuel cell current. Previous experimental measurements of similar water gradients have generally relied on "integral" measurements such as AC impedance spectroscopy which cannot probe details of the gradient within the membrane. This is one of the first "differential" measurements of water gradients within Nafion.

Research Topics

Effect of Pressure on the Thermodynamics of Polyolefin Blends
D. J. Lohse[1], M. Rabeony[1], R. T. Garner[1], and K. Migler[4]

Chain Dimensions of Polypropylene in the Theta Condition
D.J. Lohse[1], M.Y. Lin[4], and R.T. Garner[1]

Polymer-Polyelectrolytes Micelles and Microemulsions
J. S. Huang[1], J.Z. Li[1] and M.Y. Lin[4]

Diblock Copolymer Aggregates
D. Richter[6], D. Schneiders[6], L. Willner[6], L. J. Fetters[1], J. S. Huang[1], and M.Y. Lin[4]

Polymer Adsorption on Hydrate Surfaces
H. E. King[1], J. Hutter[1] and M.Y. Lin[4]

Wax Crystallization
E. B. Sirota[1] and M.Y. Lin[4]

Aggregation in Living Polymer Solutions
L. J. Fetters[1], J. Z. Li[1], and M.Y. Lin[4]

Miscibility in Lube Oils
H. S. Aldrich[1] and M.Y. Lin[4]

Clay Surfactant Interactions
D. G. Peiffer[1] and M.Y. Lin[4]

Soot Characterization in Lubricants
M. A. Francisco[1], W. Green[1], J. Z. Gao[3], and M.Y Lin[4]

Hydrogel Structure for Contact Lenses
P. J. Valint[5], J. S. Huang[1], J. Z. Li[1], and M. Y. Lin[4]

Crosslinking Structure in Polyelastomers
A. J. Dias[2], D. G. Peiffer[1], and M. Y. Lin[4]

Mixing in Blends of Saturated Hydrocarbon Polymers
M. Rabeony[1], R. T. Garner[1] and D. J. Lohse[1]

Temperature and Shear Dependence of Crude Oils
M. Y. Lin[4], G. Hu[1] and E. B. Sirota[1]

Fuel Cell Radiography
R. J. Bellows[1], M. Y. Lin[4], M. Arif[4], A.K.Thompson[4], and D. Jacobson[4]

Affiliations

[1] Exxon Research and Engineering Company
[2] Exxon Chemical Company
[3] Imperial Oil Ltd., Canada
[4] NIST
[5] Bausch and Lomb
[6] IFF, KFA Jülich, Germany

University of Minnesota Programs

The University of Minnesota through its Center for Interfacial Engineering, is a member of NCNR's participating research teams (PRT) in small-angle neutron scattering (SANS) (with NIST, Exxon Research and Engineering Company, and Texaco R & D) and reflectometry (with NIST and IBM). During the past year the research emphasis was on polymeric materials with participation by eleven graduate students, two post-docs, three faculty members, six staff scientists located at two National Laboratories, and two academic collaborators. Work performed at NIST plays an integral part in a comprehensive research program at the University of Minnesota that addresses fundamental and applied aspects of soft materials science and engineering.

Research Projects

- **Polyolefin Blends**

Saturated hydrocarbon polymers such as polyethylene and polypropylene constitute the largest sector of the synthetic polymer market. Improvements in the ultimate properties of these inexpensive commodity plastics generally relies on blending thermodynamically incompatible polyolefins. Based on our recent discovery of miscibility between isotactic polypropylene (iPP) and certain poly(ethylene/ethylethylene) random copolymers in the melt state, we have developed a variety of polyolefin block copolymers that can be dispersed in iPP. SANS experiments at NIST have provided crucial evidence linking the high temperature phase behavior with the morphologies that result upon crystallization of the iPP component. This work plays a key role in our program to develop new strategies for toughening this important class of thermoplastics.

- **Polymeric Bicontinuous Microemulsions**

Block copolymers are capable of emulsifying immiscible homopolymer blends in much the same way that surfactants disperse water in oil, or vice versa. We have explored several three-component systems composed of equal molecular weight homopolymers and a symmetric diblock copolymer. SANS and TEM measurements have revealed that fluctuation effects destroy the isotropic Lifshitz point anticipated by mean-field theory, leading to the formation of a bicontinuous microemulsion. This phase behavior has been demonstrated over a wide range of molecular weights. Using the couette shear cell available on the SANS instruments we have examined how flow influences PDMS-PEE/PDMS/PEE bicontinuous microemulsions, as a function of temperature and shear rate. These experiments have shown that sufficiently high rates of shear destroy the microemulsion state, as evidenced by the loss of the SANS peak and the concomitant development of visible turbidity. Rheological and light scattering measurements (both static and dynamic) complement the SANS experiments. This project addresses a fascinating area of critical phenomena that is relevant to polymer blending, surfactancy and other areas of soft materials.

- **Block Copolymer Thin Films**

A powerful method for controlling the internal microstructure and defect density in block copolymer thin films was recently developed. Confinement, imposed by capping a spin cast film with a polymer layer having a high glass transition temperature, permits annealing under conditions that prohibit the formation of surface defects known as islands and holes. The efficacy of this method was confirmed in lamellar forming PS-PVP diblock copolymers and diblock copolymer blends. After solvent stripping, the capping layer, the resulting "strained" films nucleate and grow surface defects upon heating. We have discovered that homogeneous nucleation can be entirely suppressed in the very thin film limit, and that heterogeneous nucleation leads to fractal hole patterns with classical two-dimensional transport limited power law growth. This process is closely related to Hele-Shaw fluid flow and dendritic crystal growth.

- **Block Copolymers in the Strong Segregation Limit**

As the degree of incompatibility between blocks increases (i.e., the χ parameter increases) diblock copolymers become more strongly segregated at fixed degree of polymerization. Scaling theory indicates that the microdomain dimensions should increase as $d \sim N^{2/3}$. However, achieving equilibrium under these conditions is difficult, if not impossible. High molecular weight PS-PDMS diblocks were synthesized to test the strong segregation limit (SSL) prediction. d spacings in excess of 1000Å were achieved; these measurements were made possible by the combination of long wavelengths and the aximum sample to detector distance available at NIST.

- **Solvent Distribution in Block Copolymers**

Many industrial applications of block co-polymers involve addition of low molecular weight modifiers. For example, pressure sensitive adhesives (PSA), a multibillion dollar industry, are typically 30% to 50% tackifier, a complicated mixture of oligomers. In order to better understand the properties of such mixtures the Polymer Group has been investigating how solvent quality and concentration affect the partitioning of low molecular weight diluents in block copolymers. By taking advantage of the contrast matching technique the (weak) localization of solvent at the interface between styrene and isoprene microdomains has been documented using SANS. These experiments rely on subtle variations in local scattering length density, that produce a weak signal on a substantial incoherent background intensity. Our recent success in documenting this effect was facilitated by the enhanced flux made available by the cold source upgrade. We have recently added detailed self-consistent calculations of the solvent distribution to both interpret the data and guide the experimental design.

- **Correlation Length in Polymer Solutions**

Modern theories for the dynamics of polymers such as viscosity, elasticity, and diffusion, make explicit predictions connecting the structure of the liquid with its dynamics. The latter, of course, are central to understanding the processing of polymeric fluids. We are using SANS to measure the correlation length, ξ, in polymer solutions over the entire composition range. These data then support our measurements of dynamics on the same systems, to provide a definitive test of theoretical concepts.

- **Thermo-reversible Gelation in Methyl-Cellulose Solutions**

Methyl cellulose is a commercial water-soluble polymer that gels near 50°C at low concentrations (~ 1%). It is useful as a thickening agent in, *e.g.*, food and cosmetics. We have used SANS to follow S(q) as a function of temperature and concentration, to obtain a detailed picture of the structure of these gels.

Research Topics

Polyolefin Blends
K. Chaffin[4], T. Jones[4], P. Weimann[4], C. Macosko[4] and F. S. Bates[4]

Polymeric Bicontinuous Microemulsions
F. S. Bates[4], T. P. Lodge[4], W. W. Maurer[4], B. Chapman[4], M. Hillmyer[4], G. H. Fredrickson[1], D. Pine[1], K. Almdal[2], K. Mortensen[2], C. Glinka[3] and T. Slaweeki[3]

Block Copolymer Thin Films
N. Koneripalli[4], R. Levicky[4], F. S. Bates[4], S. K. Satija[3] and G. H. Fredrickson[1]

Block Copolymers in the Strong Segregation Limit
K. Almdal[2], M. Vigild[2] and F. S. Bates[4]

Solvent Distribution in Block Copolymer Solutions
C. Huang[4], M. Hamersky[4], K. Hanley[4],T. Lodge[4] and B. Chapman[4]

Correlation Length in Polymer Solutions
H. Tao[4], C. Huang[4], and T. Lodge[4]

Thermo-reversible Gelation in Methyl-cellulose Solutions
K. Kobayashi[4,5] , C. Huang[4], and T. Lodge[4]

Affiliations

[1] University of California at Santa Barbara
[2] Risø National Laboratory, Denmark
[3] NIST
[4] University of Minnesota
[5] Shinetsu Chemical Company, Japan

Neutron Interactions and Dosimetry Physics Laboratory

This group provides measurement services, standards, and fundamental research in support of NIST's mission as it relates to neutron technologyand neutron physics. The industrial sectors served include materials development, scientific instrument calibration, electric power production, radiation protection, national defense, and radiation therapy.

This project maintains, develops, and applies well-characterized neutron fields for detector development, methods evaluation, and standardization as needed for materials dosimetry in nuclear reactor applications and for personnel dosimetry in radiation protection. These neutron fields include thermal neutron beams, ``white" and monochromatic cold neutron beams, a thermal-neutron-induced ^{235}U fission neutron field, and ^{252}Cf fission neutron fields, both moderated and unmoderated. The calibration of these neutron fields is derived from related artifacts, facilities, and capabilities maintained by the project: the national standard neutron source NBS-I, a manganous sulfate bath for neutron source comparisons, a collection of fissionable isotope mass standards (FIMS), a collection of boron and lithium isotopic standards, spectroscopy facilities for both gamma rays and alpha particles, and a capability to perform radiation transport calculations. The group also performs experimental tests of critical neutron transport data and computation methods.

The group carries out forefront research at the NIST Center for Neutron Research in neutron physics and tests of fundamental symmetry principles, develops advanced measurement techniques in neutron interferometry, and is developing neutron spin filters based on laser polarization of ^{3}He.

Highlights of activities are given below.

Fundamental Neutron Physics

- **Neutron Interferometry and Optics Facility (NIOF)**

In this year we have begun to get very significant results from several years of developmental efforts at the NIOF.

A measurement of the scattering length for silicon has been completed, achieving an accuracy level ± 0.005% (68% confidence level) which is a factor of five better than the previous best measurement. This accuracy was possible because of the superior performance of the NIST interferometer and environmental control systems, and because of an innovative wavelength-independent measurement technique perfected by A. Ioffe and a Czech collaborator M. Vrana. A report of this work has been accepted for publication.

High quality phase contrast images have been obtained of two test specimens. Images of an aluminum step wedge and an aluminum/copper test piece were made to verify the performance of our new setup for phase contrast imaging.

An initial measurement of the ^{208}Pb scattering length has been completed, and additional work is in progress to evaluate the uncertainties in the sample density and homogeneity. This particular isotope is "doubly magic"; i.e., it has closed shells for both protons and neutrons. Thus the strong nuclear interactions of ^{208}Pb are suppressed like the chemical reactions of an inert gas with closed electron shells. The result is that the electric field of the ^{208}Pb nucleus reacts in an less complicated way with the internal electric charge distribution of the neutron, and the scattering length measurement can give definitive information about that charge distribution.

A major accomplishment of another kind was the successful imaging of water distribution in an operating polymer electrolyte fuel cell (PEFC), by means of high-resolution neutron radiography. Extremely tight collimation (0.9 milliradians) was required to image the cell's membrane edge-on. This PEFC experiment was performed in collaboration with Dr. Richard Bellows of Exxon Research and Engineering. A report of these results has been accepted for publication in *Electrochimica Acta*.

- **Asymmetries of the Weak Interaction and the Neutron Lifetime**

During 1997, one major experiment was completed and a second one has gotten under way at the NIST cold neutron user facility for fundamental neutron physics.

The time-reversal asymmetry experiment ran for five reactor cycles during 1997, accumulating more than 15 million electron-proton coincidence events on a polarized neutron beam at the end station of the NG6 cold neutron guide. This large collaboration called *emiT* involves physicists from the U. Washington, U. California-Berkeley, U. Michigan, U. Notre Dame, Los Alamos, and

NIST. Despite serious problems with proton energy loss in the ion-implanted silicon proton detectors, it is anticipated that the results of these runs will permit an improvement of about a factor of two in the current best limit on the time-reversal asymmetry (triple product correlation) coefficient in neutron beta decay. Detailed data analysis is still going on at Berkeley, Washington, and Michigan. A proposal has been submitted to DoE that would support replacement of the ion-implanted detectors with surface barrier detectors in future runs planned for FY99.

The Harvard-NIST experiment to measure the neutron lifetime by creating and trapping ultra cold neutrons in a very cold liquid helium cell (0.1 K) has just begun operating at the NG6 station. All systems seem to be working as expected, and various sources of background counts are being evaluated. Various methods of observing scintillations from neutron decay in the superfluid helium cell are being tested, and several alternative methods for reducing background are being tried.

A new monochromatic beam line has been set up near the end of the NG6 guide, with the new beam going into the laser-polarization hut. In this hut at NG6 much less space is now required for the laser setup, because of conversion to compact laser diode arrays; and the remaining room in the hut will accommodate other experiments on the monochromatic beam line. The laser polarization work will coexist with the cryogenic neutron calorimeter or the alpha-gamma black detector or the boron total cross section experiment in the hut during the coming year.

Two NIST physicists joined Russians from the Petersburg Nuclear Physics Institute (PNPI) at the Institut Laue-Langevin in Grenoble to work on a measurement of the antineutrino asymmetry coefficient for neutron beta decay. This provided a good opportunity for the NIST staff to learn the subtleties of operation of the 2A2F (two analyzer, two flipper) neutron polarimeter, which NIST purchased from the PNPI. A preliminary report of this experiment has been accepted for publication in a Russian journal (in Russian). A more complete report (in English) is nearly ready for submission to *Phys. Rev. C.*

- **Laser Polarization of ^{3}He for Neutron Spin Filters and MRI Applications**

The five-year competence program in Laser Polarization of ^{3}He for Neutron Spin Filters has grown into a fully integrated part of our research and services in neutron interactions and dosimetry. This work is receiving both continued internal support and DoE funding through a collaboration with Indiana University.

A closed-loop ^{3}He recirculation system has been built and tested for preparing polarized ^{3}He at atmospheric pressure by the metastable optical pumping method. The system consists of an optical pumping cell, cold traps, a modified (now non-magnetic) commercial diaphragm pump, storage cell, getter, and capillary return line. In non-recirculation mode, polarization in the storage cell of up to 20% was obtained at a pressure of about one atmosphere. Pressures up to 2.5 atmospheres have been obtained in the storage cell by collecting the polarized gas at liquid nitrogen temperature and then letting it warm up. This current level of polarization is already high enough for medical imaging applications, and the low cost of the present system may be important in these applications. Much higher levels are required for most neutron spin polarization experiments, and several modifications of the present system are in progress to see what may be achievable. In addition, our collaborators at Indiana University (IU) are constructing a much more sophisticated (and expensive) compressor system, similar to a very high performance system developed at the University of Mainz.

Several flat-windowed, ^{10}B-free cells were produced for use on NIST cold neutron beams. For two of these cells, the initial polarization lifetime was more than 130 hours, although these slowly degraded to less than 50 hours. As part of our DoE supported collaboration with IU, we made high pressure cells for epithermal neutron experiments at Los Alamos National Laboratory (LANL), as well as both polarizer and analyzer cells for a LANL experiment on neutron spin rotation in ^{129}La.

We have assisted researchers at the U. Pennsylvania in making high quality lung images and a sinus cavity image by magnetic resonance imaging (MRI) with polarized ^{3}He inhalation. Additional collaborations in MRI applications are being explored with researchers at Johns Hopkins University, the University of Nottingham, and the company Intermagnetics General.

- **Neutron Dosimetry for Reactor Safety Assessment**

Through a cooperative agreement with the Office of Nuclear Regulatory Research, NIST provides measurement assurance services and consultation related to neutron dosimetry and nuclear reactor safety.

Round-robin tests of ^{237}Np and ^{238}U fissionable dosimeters involving four U.S. participants and one international participant are currently under way. These fissionable dosimeters were irradiated to NIST-certified fluences in the Materials Dosimetry Reference Facility at the Phoenix Laboratory of the University of Michigan. The fission product of interest in these tests is ^{137}Cs, which has a very suitable half-life but a rather low-energy gamma-ray, requiring careful handling of interferences from higher-energy fission product gamma-rays.

Progress continues on assistance to the Nuclear Regulatory Commission in preparation of Draft Guide 1053, *Calculational and Dosimetry Methods for Determining Pressure Vessel Neutron Fluence*. A resolution-of-comments document is currently being prepared in response to formal comments from power reactor operators and suppliers, regarding the first public release of the draft guide.

NIST has organized a ^{93}Nb activation round-robin and is expecting four participants. This dosimeter is of particular interest because the energy dependence of its cross section closely matches the energy dependence of the iron damage function. Several major technical difficulties are encountered in x-ray spectrometry for ^{93}Nb, and inaccurate results are often obtained unless there is careful standardization of the sample purity and spectrometry technique.

- **Calibrations, Irradiation Services, and Special Tests**

The numbers of calibrations of radiation protection survey instruments increased somewhat this year despite our encouragement of many potential customers to use secondary calibration laboratories. Continuing efforts to achieve better consistency between calibrations made at NIST and calibrations at the Pacific Northwest Laboratories have resulted in good agreement for measurements made with unmoderated californium fission neutrons, but some difficulty remains in resolving discrepancies in measurements with the moderated californium fission neutron source. In all, 18 radiation protection instrument calibrations were performed this year for 15 different customers. The NIST system for performing these calibrations is increasingly automated, reducing the staff hours required per calibration.

A large number of neutron source calibrations were also completed this year. In all, 20 source calibrations were reported for 9 different customers.

Special tests of industrial neutron detectors were carried out at the reactor thermal column for two industrial customers, Westinghouse Science and Technology Center and the Imaging and Sensing Technology Corporation. Two irradiations were also made at the Californium Neutron Irradiation Facility to test a fast neutron imaging system being developed by Industrial Quality, Inc. and the University of Virginia.

- **Neutron Cross Section Standards**

The NIST role in the advancement of neutron cross section standards is now performed primarily through evaluation, compilation, and dissemination of standards in collaboration with the U.S. Cross Section Evaluation Working Group and two international committees, the International Nuclear Data Committee (INDC) and the Nuclear Energy Agency Nuclear Science Committee (NEANSC). The NEANSC has planned a new measurement of the $^{10}B(n, \alpha)$ branching ratio, to be carried out at the Institute for Reference Materials and Measurements in Geel, Belgium. The INDC has published a new report "Update to Nuclear Data Standards for Nuclear Measurements."

In addition, a limited NIST experimental role continues, with plans for a new measurement of the ^{10}B total cross section at the new NG6 monochromatic neutron beam facility and with NIST participation in a collaborative remeasurement of the H(n,n) angular distribution measurement at Ohio University (OU) at 10 MeV. This work at OU is particularly timely, because European standards groups have recently expressed considerable scepticism about the latest U.S. evaluation of the H(n,n) angular distribution and because the H(n,n) cross section is one of the most widely used cross section standards.

Research Topics

Neutron Interferometry and Optics

M. Arif[11], D. Jacobson[11], R. Clothier[3], A. Thompson[11], S. Werner[16], A. Ioffe[4], A. Zeilinger[14], K. Raum[17], B. Schillinger[17], C. Rausch[17], and W. Richards[10]

Determination of the Neutron Lifetime

M.S. Dewey[11], G.L. Greene[9], D. Gilliam[11], W.M. Snow[6], and X. Fei[6]

Accurate Determination of Neutron Capture Flux

M. S. Dewey[11], M. Arif[11], D. Gilliam[11], G. L. Greene[9], W.M. Snow[6], J. Pauwels[7], C. Inglebrecht[7], and R. Scott[10]

Study of Time Reversal Invariance in Neutron Beta Decay
J. Wilkerson[20], E. Wasserman[8], J. Nico[11], R. G. H. Robertson[9], S. Freedman[8], A. Garcia[18], T. Chupp[15], K. Coulter[15], M. S. Dewey[11], G. L. Greene[9], A. Thompson[11], B. Fujikawa[8], G. L. Jones[11], J. Adams[11], F. Wietfeldt[11], L. Lising[8], S. Hwang[15], and T. Steiger[20]

Parity Non-Conserving Neutron Spin Rotation
B. Heckel[20], D. Markoff[20], E. Adelberger[20], S. Penn[20], and F. Wietfeldt[11]

Highly Accurate Neutron Wavelength Measurements
M. S. Dewey[11], K. Coakley[12], W. M. Snow[6], and M. Arif[11]

LASER Polarization of ^{3}He for Neutron Spin Filters and Medical MRI
A. Thompson[11], T. Gentile[11], M. S. Dewey[11], G. L. Jones[11], F. Wietfeldt[11], W. M. Snow[6], and R. Rizi[19]

Trapping of Ultra Cold Neutrons
J. Doyle[5], S. Lamoreaux[9], R. Golub[4], G. L. Greene[9], M. S. Dewey[11], P. Huffman[5], C. Brome[5], C. Mattoni[5], J. Butterworth[5], and D. McKinsey[5]

Utilization of the Materials Dosimetry Reference Facility-Tests of New IRMM ^{237}Np and ^{238}U Fast Neutron Dosimeters
E. D. McGarry[11], J. Grundl[11], C. Eisenhauer[11], D. Gilliam[11], J. Adams[11], and P. Simpson[15]

Benchmark Measurements and Calculations of Neutron Transport
D. Gilliam[11], M. S. Dewey[11], J. Nico[11], C. Eisenhauer[11], J. Grundl[11], and H. Gerstenberg[1]

Neutron Fluence Rate Measurements
D. Gilliam[11], J. Nico[11], and J. Adams[11]

Defined-Geometry Alpha Counting
D. Gilliam[11], and J. Nico[11]

Certified Neutron Fluence Standards from the Cavity Fission Source
J. Grundl[11] and J. Adams[11]

Quality Assurance Checks on Masses and Impurities in Neutron Dosimeters for NRC Reator Pressure Vessel Embrittlement Surveillance
J. Adams[11], D.Gilliam[11], and J. Grundl[11]

Intercomparison of NIST and PNL Calibration Facilities
R. Schwartz[11], J. McDonald[2], M. Murphy[2], and A. Thompson[11]

Response of Albedo Dosimeters Versus Distance from a Neutron Source
R. Schwartz[11] and A. Thompson[11]

Response of Albedo Neutron Dosimeters as a Function of Angle
R. Schwartz[11]

Neutron Calorimetry
W. M. Snow[6], Z. Chowdhuri[6], X. Fei[6] and M. S. Dewey[11]

Neutron Radiography/Tomography
T. Gentile[11], M. Arif[11], D. Jacobson[11], and F. Wietfeldt[11]

Affiliations

[1] Armed Forces Radiobiology Research Institute
[2] Battelle Pacific Northwest Laboratory (PNL)
[3] Bethany College
[4] Hahn-Meitner Institute, Germany
[5] Harvard University
[6] Indiana University
[7] Institute for Reference Materials & Measurements (IRMM), Belgium
[8] Lawrence Berkeley Laboratory, University of California at Berkeley
[9] Los Alamos National Laboratory
[10] McClellan Nuclear Radiation Center
[11] NIST, Ionizing Radiation Division
[12] NIST, Statistical Engineering Division
[13] Scottish Universities Research and Reactor Centre, United Kingdom
[14] University of Innsbruck, Austria
[15] University of Michigan
[16] University of Missouri at Columbia
[17] University of Munich, Germany
[18] University of Notre Dame
[19] University of Pennsylvania
[20] University of Washington

Analytical Chemistry
Chemical Science and Technology Laboratory

Nuclear Methods Group

The development and application of nuclear analytical techniques for the determination of elemental compositions with greater accuracy, higher sensitivity and better selectivity are the principal goals of the Nuclear Methods Group (NMG). A high level of competence has been developed in both instrumental and radiochemical neutron activation analysis (INAA and RNAA). In addition, the group has pioneered the use of cold neutron beams as analytical probes with both prompt gamma activation analysis (PGAA) and neutron depth profiling (NDP). PGAA measures the total amount of a particular analyte present throughout a sample by the analysis of the prompt gamma-rays emitted during neutron capture. NDP, on the other hand, determines concentrations of several important elements (isotopes) as a function of depth within the first few micrometers of a surface by energy analysis of the prompt charged-particles emitted during neutron bombardment. These techniques (INAA, RNAA, PGAA, and NDP) provide a powerful combination of complementary tools to address a wide variety of analytical problems of great importance in science and technology. During the past several years, a large part of the Group's efforts has been directed towards the exploitation of the analytical applications of the cold-neutron beams available at the NIST Center for Neutron Research. The Group's involvement has been to design and construct state-of-the-art cold neutron instruments for both PGAA and NDP and provide facilities and measurements for outside users, while retaining and utilizing our existing expertise in INAA and RNAA.

- **SRM Analysis and Certification**

The nuclear analytical methods have continued to contribute to the Standard Reference Material (SRM) certification effort. This year's efforts involve measurements performed on a number of SRMs including: NY - NJ Harbor Sediment, Buffalo River Sediment, Coal, Oyster Tissue, two Steels, two Petroleum Cokes, three Zeolites, Arsenic Implanted in Silicon, two Mussel Tissues and a High Temperature Alloy. Group members are serving as Technical Project Leaders for several of these new SRMs, and as such are responsible for scientific decisions made throughout the production and certification processes of these materials. In addition, this year has seen an increase in cooperative efforts internationally with other standards organizations. Once again we have provided certification values for the NRC-Canada due to their lack of INAA capabilities. A marine sediment CRM was analyzed for 24 elements by INAA. Cooperative work was also initiated with the German Bundesanstalt für Materialforschung und -prüfung (BAM), looking at two trace elements in a copper metal material.

- **Neutron Activation Analysis Method Development**

Although NAA has been in use for many years, new developments continue to provide improvements in detection sensitivities, elemental specificity, precision, and overall accuracy. The procedures are extensively used in the certification of elemental composition in the SRM program; one important reason is that NAA has unique quality assurance characteristics that provide accurate analyses and often allow the analytical values obtained to be internally evaluated and cross-checked. In addition, the capability of INAA for nondestructive analyses eliminates dissolution errors and minimizes analytical blanks. Consequently, NAA has become one of the primary analytical techniques for the certification of elemental concentrations in biological SRMs. The use of INAA for homogeneity determinations at the ng/g level for common sample sizes (i.e., 100 - 500 mg), as well as for small samples (1 mg) has made this technique an integral component of trace element analyses at NIST. Furthermore, the relative matrix independence of NAA has resulted in applications to a wide variety of materials including high temperature superconductors, soils, fly ash, rocks and ores, foods, and many types of biological materials.

Optimizing the gamma-ray counting conditions for the various forms of NAA can generally improve precision, increase sample throughput, or both. This is especially important when counting the very small amount of radioactivity produced by ultratrace quantities of impurities, for example, in semiconductor silicon or (after radiochemical separations) noble metals in human tissue. Sensi-

tivity can be gained by using high-efficiency, low-background detectors; a subsidiary benefit is that less radioactive material needs to be generated, handled, and discarded. The sources of background in gamma-ray detectors have been reexamined at NIST and elsewhere in recent years, resulting in improved understanding. It is now clear that with care in the selection of the materials from which the detector and the shielding are constructed, the only important source of gamma-ray background is the interaction of cosmic ray particles with the shield and the detector itself. Experiments are underway to reduce this component by active, anti-cosmic ray shielding.

The new RT-2 rapid pneumatic tube irradiation and analysis system described last year was evaluated for timing and for neutron fluence rate. The time required to send the sample from the reactor to the detector was determined to be 473 ± 8 ms (1s, n = 27). The thermal neutron fluence rate has been determined to be 5.0×10^{13} neutrons • cm^{-2} s^{-1}, using both copper and cobalt foils. In addition, sensitivities have been determined for the elements Se, F, and Ag in real samples. These measured analytical detection limits are 0.05 μg for Se, 0.2 μg for Ag, and 5 Fg for F. These results confirm the analytical usefulness of this new facility for our program.

A number of reactor modifications and pneumatic tube changes have been made since the last complete characterization of the NAA irradiation facilities about ten years ago. Therefore, recharacterization measurements have been undertaken to determine whether there are any significant changes to the neutron fluences experienced by the samples we irradiate. It was found that the thermal neutron fluence rate in the RT-1 and RT-4 pneumatic tubes had increased by 26 % over the previous measurements. This is apparently due to changes in the uranium distribution in fuel elements close to these facilities. It should be noted that these changes do not affect the accuracy of the analytical measurements made using these facilities, since all NAA measurements are made using pure element standards that are irradiated together with the samples, or very shortly before or after the sample irradiations. Fast neutron measurements have also been made in these facilities using nickel foils, which show that the thermal/fast neutron ratio has not changed as a result of the different fuel loadings.

Many analytical techniques used in industry and academia rely on the analysis of very small samples (i.e., 1 mg), typically in the solid (undissolved) form. Unfortunately most SRMs are certified with minimum sample sizes of 100-500 mg, and are therefore unsuitable for use as control materials for these techniques unless additional information is made available. We have therefore been studying the homogeneity of existing SRMs at small sample sizes to help meet this need. The use of INAA for homogeneity studies of small sample sizes (currently 1 mg) has been evaluated and implemented for the determination of sampling characteristics of a number of biological SRMs (and research materials) and air particulate matter. The minimal analytical uncertainty associated with the INAA measurements allows extraction of the variability due to material inhomogeneity from the observed total variability in a set of measurements. This year we have demonstrated that uncertainties for a number of elements due to inhomogeneity are in the 1% (relative) range or lower when 1 mg samples of SRMs Peach Leaves or Urban Particulate Matter are analyzed. Certification of selected elements at sample sizes in the milligram range will permit the use of natural matrix SRMs for the different solid sampling techniques that are used in industry and research.

A new radiochemical separations project has been initiated to develop methods to measure additional elements which do not decay with the emission of characteristic gamma rays, such as phosphorus and sulfur. Quantitation is accomplished by beta counting the isolated activation products of interest. A radiochemical procedure has been developed for the measurement of P in steels. Preliminary analyses of P are in agreement with certified values in several existing Steel SRMs, while the detection limit for the method is < 10 ng/g. Efforts are currently underway to critically evaluate the method to determine its suitability for SRM certification.

Many years ago an RNAA method was developed for the determination of low levels of Cd in biological materials. This method involves a single element separation for Cd and has an interference free detection limit of approximately 20 pg/g. Although this method has been used to detect tens of pg/g of Cd in serum, greater difficulty would be expected in the analysis of whole blood due to the much higher amounts of Zn present in whole blood as compared with serum. To optimize the original RNAA procedure for the determination of Cd in whole blood, additional steps were included to exchange the radioactive Zn of blood samples with nonradioactive Zn carrier added after irradiation. Results show that the yield is high and reproducible with a 97.6% ± 0.3% (1s) average recovery from eight blood samples with Cd tracer added. This

method will be used for the determination of ng/g levels of Cd in whole blood.

- **Development of Methods for Speciation Measurements**

The accurate determination of speciated forms of trace elements is an ongoing and difficult problem. When NIST had need of a second method to certify several potential SRMs for organic mercury content, a study was made to determine whether an NAA procedure was able to fill this need. A new chemical separation method has been developed for the measurement of organically bound Hg (primarily methylmercury) in mussel tissues. The procedure involves distillation of the organomercury from a mixture of powdered sample, sulfuric acid and cupric sulfate, and this distillate is then bound chemically to a cysteine-doped filter paper. The mercury bound to the papers is then determined using NAA. The accuracy of the method has been confirmed using several different CRMs certified for methylmercury. This technique has been used for analysis of two mussel tissues SRMs, SRM 2976 and SRM 2974, and the results used for the certification of these materials for methylmercury content.

- **Specimen Bank Research**

The NMG continues to support the National Biomonitoring Specimen Bank (NBSB) research programs through analyses of selected portions of the banked materials and by providing quality assurance (QA) for the laboratories of other agencies that analyze banked materials. A study on the long-term stability of the banked tissues was completed this past year to evaluate the stability and integrity of the specimens stored under NBSB standard conditions and to demonstrate that there is adequate analytical quality assurance throughout and beyond the lifetime of the various projects for which specimens have been included in the NBSB. Evaluation was achieved through analyses of specimens which were previously analyzed and then stored at -80 °C or -150 °C for up to 17 years. Results of INAA of these tissues for 17 elements show no changes in specimen composition as a function of storage temperature or time. Other work completed during the past year include multi-element NAA of marine mammal tissues performed as part of the QA program for the NOAA's NMFS laboratories. Analyses of total arsenic in marine mammal liver tissues were completed as part of a collaboration with group from the University of Graz, Austria, for the determination of the chemical species of arsenic in the same tissues.

- **Superconductivity Research**

In cooperation with materials scientists at NIST and elsewhere, we are measuring impurities in superconductor starting materials and final products, as well as determining the stoichiometry of major constituents. The needs of the superconductivity program have stimulated the development of methods for accurate, rapid analysis of these materials by both NAA and PGAA. In particular, an effort is underway to establish monitor-activation analysis techniques at NIST. Conventional NAA requires the irradiation and counting of a standard for each element to be determined in a given sample. Preparing numerous standards requires much labor, and the accurate quantitation of unanticipated activities in the gamma spectrum is not possible. An elegant solution uses a dimensionless compound nuclear constant called k_0, which can be measured far more accurately than the cross sections and other constants that comprise it. We find this to be the case in cold-neutron PGAA, which is especially subject to systematic errors from neutron scattering effects, and have found that the k_0 approach for determining element ratios offers all the advantages that internal standards offer other methods. We are applying the k_0 formalism to traditional NAA as well. Initial trials with a commercial software package show good agreement with many-monitor NAA. In addition to measurements to support the superconductivity program, the k_0 approach will be used in parallel with the traditional method for SRM analyses, as a quality check on both.

- **Neutron Depth Profiling**

NDP is a nondestructive analytical technique which measures the concentrations, and determines the near surface distributions, of selected elements. Increasingly, manufacturers of semiconductor components are finding NDP to be an important tool for calibration, quality control and basic research. The NDP instrument is located at the end of the new NG-0 cold neutron curved guide which has a coating of nickel-titanium supermirror. This gives an increase of about a factor of 3 in neutron current density relative to a ^{58}Ni guide. The two-meter long curved section has a radius of curvature of 57 m, which is sufficient to remove line-of-sight fast neutrons and gamma rays from the cold neutron beam. The beam area at the guide exit is 3 cm x 5 cm and the neutron fluence rate is $2.45 \pm 0.05 \times 10^9$ $cm^{-2}s^{-1}$.

Current experiments of interest at the NDP instrument include the measurement of nitrogen profiles in thin TiN films in conjunction with Intel Corp., and the measurement of lithium migration in

electrochromic films in cooperation with SAGE Electrochromics. Depth profiling of nitrogen is based on the measurements of the proton from the $^{14}N(n,p)^{14}C$ reaction. These nitrogen measurements are the first quantitative evaluation of nitrogen concentrations since the instrument was reconfigured and placed on the curved neutron guide. The advantages of this new arrangement are apparent in the higher signal rate and the lower background compared with nitrogen measurements made at the previous instrument location.

Lithium depth profiles are based on the measurement of the energy of alpha particles from the $^{6}Li(n,\alpha)^{3}H$ reaction. The energy of the detected particle provides a direct measurement of the depth of the originating lithium nucleus. In this case, in situ measurements were taken with different bias voltages on the film layers. The bias causes the lithium to migrate between different layers and changes the optical transparency of the film, which is quantitatively reflected in the NDP spectrum.

- **Prompt-Gamma Activation Analysis**

Prompt-Gamma Activation Analysis allows accurate, nondestructive measurements of a number of elements, including H, B, C, N, S and Cd. Recent improvements to the cold neutron prompt gamma activation analysis (CNPGAA) instrument, constructed as part of the CNRF, have greatly improved its measurement capabilities. Furthermore, both the CNPGAA and University of Maryland-NIST thermal-neutron PGAA instruments have found research applications in many diverse areas within chemistry, physics, and materials sciences.

During the reactor shutdown considerable effort was directed toward an upgrade of the CNPGAA instrument in the Cold Neutron Research Facility. Installation of the new liquid hydrogen cold source and the increase in reactor power have resulted in a factor of 6 improvement in neutron capture rate at the PGAA station, while PGAA sensitivities (counts·mg^{-1} s^{-1}) for most elements are a factor of 3 - 4 better than measured before the shutdown, which were already the best in the world. As a result of these improvements in sensitivities and backgrounds, elemental detection limits have improved by up to a factor of 2.

The CNPGAA facility continued to provide measurements and assistance to outside users during this past year. Hydrogen has been measured in lithium carbons, in obsidian, in hydrided aluminum, in lanthanum copper oxides, in deuterated copper oxide, and in samples of Nd, Sc, and Ho-doped $SrCeO_3$ which act as protonic conductors. Other analyses include the determination of B and H in mineral separates and in diamond powders, Cl in basalts, H, B, and Si in zeolites, and Ca, Mg, and major elements in substituted compounds of Y_2NiBaO_5. Additional measurements have been made which include the measurement of N in reference materials, and the determination of k_0- factors for PGAA.

A procedure has been demonstrated for doping titanium alloy specimens with a known amount of hydrogen. In the reversible reaction $Ti+H_2 \rightleftharpoons TiH_2$, the equilibrium pressure is less than 10^{-13} atmospheres at room temperature, and 150 atmospheres at 900°. Reaction is rapid at 300°C. This gettering reaction with hot titanium is in common use in geochemistry for separating hydrogen from oxygen and nitrogen (which react irreversibly) and from noble gases. Massive hydrides are prepared industrially by the same direct reaction process for hydrogen-based energy storage and nuclear applications. Batches of a few grams of titanium alloy specimens have been doped with hydrogen using a simple closed gas handling system. Means are provided for pumping away air and hydrogen from samples at high temperature and for admitting a known pressure of hydrogen in a calibrated volume at room temperature, then raising the temperature of the system to carry out the reaction. The accuracy of the doping is limited by that of the pressure measurement, better than 0.5%. The amount of H in the metal samples was measured in 100-mg specimens by CNPGAA. The quantity measured agreed with the quantity added. The method should be scalable to produce 1-kg quantities of metal SRMs. This study indicates that certification of Hydrogen in Titanium SRMs can be made following the approach used for the trace gases, many solution SRMs and the recent As in Si implant: considering the quantitative preparation and the subsequent chemical analysis as two independent methods.

- **Focused Neutron Beams**

A long-range program to explore and develop the analytical applications of focused beams of cold neutrons continues within the Group. The goal of this research is to produce beams of neutrons which have intensities several orders of magnitude greater than previously available. The new hydrogen cold source has given the neutron beams an increase of up to six times in the current densities delivered by neutron guides at longer wavelengths. This enables neutron absorption measurements on samples with fine (submillimeter) spatial resolution by increasing the current densities even further using focusing techniques. Such beams will greatly enhance the

capabilities of both PGAA and NDP and increase their elemental sensitivities, and may ultimately lead to a neutron probe for microanalysis.

The best method of transporting and focusing a white beam of long wavelength neutrons is based on specular reflection from smooth surfaces. Neutrons from the macroguide enter the narrow channels of polycapillary glass fibers, curved such that the neutron trajectories are directed towards a common focus. Narrow (.10 μm) channels enable the neutron beam to be bent more sharply than wide (0.5 mm) guides. The high intensity beam is placed on a small sample area for improvement of both the spatial resolution and the detection limits for individual elements using neutron absorption measurements in analytical research.

Our original focusing lens for the NG-7 ^{58}Ni neutron guide compresses a neutron beam of cross section 50 x 45 mm^2 and a current density of $6.5x10^8$ $cm^{-2}s^{-1}$ onto a spot of diameter 0.53 mm (FWHM) at a distance of 52 mm from the exit of the lens, with an average gain of 80 in neutron current density. PGAA measurements have shown a gain in gamma count rate of 60, a gain in signal-to-noise of 7, a spatial resolution at the focus of better than 0.5 mm, and an improvement in detection limits of 20.

The instrumental background may be also reduced by a polycapillary bender-focuser lens that not only focuses but also bends the beam downward out of the shadow of the incident beam in order to improve the signal-to-noise ratio. Such a lens has been constructed. The glass fibers point towards a common focus 95 mm away from the exit and a distance 42.5 mm below the incident beam centerline, 20 mm below the bottom edge of the beam. The lens can be moved out of the beam by computer control when not needed. The spatial intensity distribution at the focal plane has a FWHM of 0.65 mm, and the current density gain over the area for this diameter is a factor of 20. Though the complex curvature of the fibers allows only a gain of about 20, this lesser gain is compensated for by a lower background to achieve a better detection limit. Measurements indicate that the background with a small sample in position may be reduced by a factor as great as 6 relative to the previous lens. It therefore provides better contrast for elemental mapping and an improved signal-to-noise response for PGAA determinations. Moreover, the displacement of the focal spot away from the adjacent neutron guide allows samples of larger dimensions to be analyzed, and reduces the background originating from the material in the upper guide. This type of optic is therefore effective for examining small areas within large inhomogeneous samples.

A monolithic lens consisting of a fused tapered bundle of polycapillaries has been shown to provide a smaller focus of about 0.16 mm (FWHM at the focal spot), with a focal length of 20 mm, and gains in neutron current density gain of ~60, comparable with the polycapillary lenses. Each optic contains many thousands of 10 μm channels occupying 50% of the entrance area, and are proportionately tapered towards the exit. The smaller physical dimensions of these devices is useful for the NDP instrument with its constrained space. The goal is to perform three-dimensional compositional mapping of thin-film semiconductor materials using NDP with the monolithic tapered lens to achieve greater lateral resolution and higher sensitivity.

The transmission characteristics of neutrons through a tapered channel can be described using the same analytic expressions derived for the straight channel but with an effective lower critical angle. The cold neutron transmission through a monolithic polycapillary lens has been studied by scanning a pinhole beam across the entrance cross section of the lens to obtain the relative transmission as a function of bending radius. The results may be explained using a calculation for a uniformly bent cylindrical channel with a reduced critical angle for total reflection.

Attempts have been made to translate neutron focusing studies made with glass focusing elements to other materials which may have improved reflection properties. Transmission measurements have been performed on nickel capillaries, both straight and bent, using both a white and a monochromatic neutron beam. The results have been compared with those produced by computer simulation. The experimental transmission is usually less than that calculated, probably on account of large reflection losses caused by surface roughness and waviness. However these results are more promising than previous ones for stainless steel capillaries.

- **Group Interactions**

The strong interaction with industrial scientists using NDP, PGAA, and NAA has continued during the year with a growing number of guest workers, research associates, and joint publications. For example, working this year with researchers from SEMATECH, we have used NDP to study various aspects of quality control using CVD (chemical vapor deposition) reactors. These measurements will be useful in optimizing process yield and reliability as well as establishing confidence for the industrial in-house analytical techniques. In addition, cooperative research with the University of

Virginia Nuclear Engineering Department helped them to resolve problems with the determination of nitrogen in biological materials using the nuclear track technique.

Food and Drug Administration

The Food and Drug Administration (FDA) maintains a neutron activation analysis (NAA) facility at the National Institute of Standards and Technology (NIST) 20 megawatt research reactor. This facility is directed by FDA's Center for Food Safety and Applied Nutrition and provides agency-wide analytical support for special investigations and applications research. NAA complements other analytical techniques used at FDA and serves as a reference technique and confirmatory quality assurance (QA) tool. Instrumental, neutron-capture prompt-γ, and radiochemical NAA procedures (INAA, PGAA, and RNAA, respectively) continue to be the prime nuclear analytical approaches. Radioisotope X-ray fluorescence spectrometry (RXRFS) provides support for FDA programs that monitor potentially toxic elements (e.g. Pb, Cd and Ba) in housewares. A low-level γ-ray counting facility developed by the Nuclear Methods Group of the NIST Inorganic Analytical Research Division is used to determine radioactivity concentrations of naturally occurring ^{40}K and and other γ-ray emitters (e.g., fission products such as ^{137}Cs, ^{134}Cs, ^{131}I, ^{103}Ru, and ^{106}Ru) in foods. This combination of analytical techniques enables diverse multielement and radiological information to be obtained for foods and related materials.

Annually, FDA's facility at NIST performs multielement analysis with INAA (60 foods) and radionuclide analyses (15 foods) for quality assurance (QA) in conjunction with the Agency's Total Diet Study (TDS) Program. In another important QA exercise, soy-based infant powder and cocoa powder in-house reference materials were developed for use in FDA programs. Production of a seafood reference material is planned. As a third part of FDA's QA effort, four 17- to 20-year old NIST food Standard Reference Materials (SRMs) were analyzed by INAA and PGAA: SRM 1566 (Oyster Tissue), SRM 1567 (Wheat Flour), SRM 1568 (Rice Flour), and SRM 1570 (Trace Elements In Spinach). The results show that, over the long-term, element concentrations of these materials are stable in a variety of storage conditions. A total of 26 element concentrations were determined for SRM 1566, 23 for SRM 1567, and 22 for both SRM 1568 and SRM 1570. Original certificates values for Na, Al, K, Ca, V, Mn, Cu, Cd, Cr, Co, Fe, Rb, Se, Zn, and As still represent accurate concentrations. In addition, concentrations determined for H, B, C, N, Mg, S, Cl, Br, Cs, Sb, Sc, Mo agree well with available literature values. As a result of the revalidation study, FDA plans to use its supply of these materials as analytical controls even though the original certificates have expired.

Over several years, a formalized INAA method for sodium analysis was developed by FDA and tested at NIST and 4 other laboratories. The method, recently published (*J. AOAC Int.* **80**, 871-882, 1997), is suitable for use at most research reactor facilities and can be used as a model for multielement INAA. By specifying detailed procedures, uncertainties are controlled at critical stages of analysis. Therefore highly accurate and precise quantitation is assured.

RXRFS analyses of ceramic glazes were conducted to screen commercial products for Pb and Cd prior to official leach-testing or the use of other potentially more efficient methods by other FDA personnel. RXRFS was also used to detect Pb in soldered food cans (use of Pb solders in food cans has recently been banned). Methods are being developed to quickly screen cans (and other metalware) for the presence of Pb and to determine Pb and Sn concentrations in solders on food containers.

In another reference material-related study, PGAA was used to determine H, B, C, N, Cl, S, K, Ca, and Cd concentrations in algae, a candidate reference material being developed by the International Atomic Energy Agency. Boron determinations by PGAA were performed as part of an interlaboratory round-robin exercise in which leaf, fish, and animal tissues, human and animal diet composites, and human serum were analyzed by a variety of techniques.

INAA performed at the NIST Reactor supported investigations of the use of potassium bromate in the manufacture of baked bread products. Potassium bromate is a commonly used dough conditioner that is regulated by FDA. The safety of using potassium bromate to manufacture bread products has been debated because bromate residues have been commonly found in these products. Bromate has been considered a carcinogen and some organizations are striving to have potassium bromate banned in the baking industry. INAA was used to determine the bromine content of various doughs and bread products to help demonstrate that this type of analysis can be used to screen for products most likely to contain bromate residues. A paper entitled "Total Br Concentration as an Indication of Pre-baking Bromation of Bread Products"

is being written. This paper will be submitted for publication in *Food Additives and Contaminants*.

FDA's NAA laboratory provided technical assistance to FDA's Center for Devices and Radiological Health which completed a document entitled "Accidental Radioactive Contamination of Human Food and Animal Feeds: Recommendations for State and Local Agencies". The document has been published for comment in the *Federal Register*.

Smithsonian Institution

The Conservation Analytical Laboratory of the Smithsonian Institution maintains an INAA research facility within the Nuclear Methods Group at NIST. This facility, which consists of two automated sample changers and four gamma detectors with associated electronics, provides high precision multi-element chemical data for use in a wide range of Smithsonian and Nuclear Methods Group research projects. In the past year 1550 archaeological samples have been analyzed in support of 7 Smithsonian research projects. The projects include studies of Classic Maya pottery, prehistoric Ramos polychrome pottery from Casas Grande in Mexico, Ceramics from the Valley of Mexico, Bronze age ceramics from ancient Gordian and Hacinebi in Turkey and Raqui in Syria, and obsidian artifacts and geological source samples from the Red Sea coast of Yemen.

University of Maryland

The University of Maryland (at College Park, UMCP) aerosol chemistry group has used the NBSR reactor for instrumental neutron activation analysis to characterize atmospheric aerosol particles and gases for more than 20 years. Detailed and accurate multielement analyses are routinely achieved, nondestructively, for up to 40 elements in samples collected for periods of several hours to a few days on various types of filters and in cascade impactors which size fractionate the aerosol into as many as 10 size domains. Some of the elements measured, e.g., As, Se, and Hg, are highly toxic and are, therefore, of epidemiological interest, especially in the Chesapeake Bay and Coastal Marine environments. Equally important is that information on elemental constituents remains a powerful, fundamental tool with which atmospheric sources, transport, and processes may be elucidated. Current projects are discussed below.

- **Characterization of Submicrometer Aerosol Particles**

Detailed investigations of the size-distribution and composition of urban aerosols are important to the scientific community because they contain information about the formation, sources, transport, and atmospheric behavior of particles containing toxic and nutrient substances, and respiratory irritants. This work extends measurement to very small (often <100 μg) samples of submicrometer aerosol particles size-fractionated with low-pressure-drop Micro-Orifice Impactors (MOI). We have developed more than 1500 size spectra for important atmospheric source marker elements in aerosol particles for a variety of environments including, urban nonindustrial, urban industrial, rural, rural over-water, and urban/industrial over water sites. These spectra have been used to determine important information on the sources and atmospheric behavior of primary particles from anthropogenic high-temperature combustion sources, i.e., the particles that carry the bulk of the atmospheric particulate toxins. The studies show that urban fine particulate aerosol in the Northeastern US is comprised of a complex collection of physically discrete primary particles from the myriad of HTCSs. These remain physically discrete during transport over the urban scale, therefore, highly-significant increases in morbidity and mortality now associated with urban fine particles may be linked with emissions from specific types of sources. Furthermore, combined with theoretical studies, our work shows that urban fine particle size is determined more by hygroscopic growth accompanied by heterogeneous sulfur oxidation on wet particles and in cloud droplets, than by homogeneous nucleation and coagulational growth, as originally proposed by Whitby in the now 20-year-old trimodal model of aerosol mass and its major constituent, sulfate. We recently submitted a paper discussing an extended aerosol paradigm, largely based on observations made from our enormous data base.

- **Environmental Justice Project**

An important component of urban aerosol, diesel soot is a known respiratory irritant and contains mutagenic and carcinogenic organic compounds. To estimate student exposures to soot emitted from public diesel buses during commutes to city high schools, a portion of the Baltimore municipal fuel supply was tagged with an iridium tracer and exposure was monitored during commutes with personal aerosol monitors as a part of the Baltimore Environmental Justice Project. A total of 68.2 g of Ir as iridium (III) 2,4 pentanedion-

ate was used to induce a concentration of 48.5 μg Ir L^{-1} of fuel. Samples were collected over 10 days while 4 students commuted on regularly-scheduled buses and a fifth student commuted by private car. Individual samples integrated from 1 to 4 round trips. Iridium analyses were performed instrumentally after neutron activation with a detection limit (DL) of about 500 fg using the NIST reactor. For students commuting by bus and following protocols, Ir tracer concentrations ranged from 53±38 to >1980±49 fg m^{-3}. Concentrations up to 3,530±200 fg m^{-3} were observed for student #5 who sampled only when boarding and disembarking. Exposures were greatest for students commuting through the heavily-trafficked central business district. Corresponding estimates of exposures to soot emitted from municipal buses ranged from ≤3 to 82 ng soot m^{-3} (≤145 ng m^{-3} for student #5), i.e., well below the exposure level of 2 to 10 μg m^{-3} total C from all sources, including the more than 30,000 diesel trucks which pass through the city's major toll facilities each day. Ir was undetectable in samples collected by the student commuting by car when its windows were closed, but comparable to those of the other students when commutes were made with windows open. The Ir tracer DL corresponds to about 21 ng soot, about half of which is carbon. This is far below the 230 ng reported for analysis by a highly-sensitive thermal-optical technique. This work was sponsored by the National Institute of Environmental Health Sciences under grant number IR25ES07734-01.

EPA Great Waters Studies - Atmospheric deposition by wet and dry processes is known to be an important source of several anthropogenic, particulate-bound metals in critically important waters such as the north atlantic Ocean, the coastal mid-Atlantic waters, and the Great Lakes. The Chesapeake Bay, perhaps the world's most productive bay, is especially subject to deposition of anthropogenic air pollutants as it lies in close proximity to heavily polluted urban areas, e.g., Baltimore, MD, Washington, DC, Norfolk, VA, and receives polluted air masses from the heavily industrialized Ohio Valley.

We are now in the fourth year of a project to characterize the spatial and temporal variations in the concentrations of various elements in aerosol particles depositing on the Chesapeake Bay and on Lake Michigan as a part of EPA's Great Waters' project, Atmospheric Exchange Over Lakes and Oceans (AEOLOS).

- **Lake Michigan Studies**

Dry deposition flux and aerosol size distribution measurements were made concurrently aboard the R.V. *Lake Guardian* 19 km east of the Chicago shore line during Summer, 1994, to assess atmospheric inputs of minor and trace elements to Southern Lake Michigan. Size-segregated aerosol measurements were made over consecutive 12-h periods with Micro-Orifice and Noll Rotary Impactors (MOI and NRI), and depositing-particulate collections to aerodynamically-smooth airfoils made over were made over periods of 3-4 days. The combination of the MOI and NRI provided size-segregated particulate samples in 12 discrete intervals between 0.059 and, nominally, 100 μm. The samples were analyzed for As, Ca, Mg, Se, Sb, V, and Zn by instrumental neutron activation analysis and for S by X-ray fluorescence. Aerosol and deposition data for individual elemental constituents were fit with a chemical mass balance deposition model (CMBDM), in which a set of particle-size-specific deposition velocities (V_d), best reconciling the data, were determined by iterative (constrained) solution of a series of 6 linear equations using the Levenberg-Marquardt method. Under stable conditions and mean wind speed of 4.0 m s^{-1}, minimum V_ds for particles with physical diameters between 0.09 and 0.53 Fm averaged 0.006 ± 0.005 cm s^{-1}, wherein uncertainties were determined by Monte Carlo Analysis. This agrees favorably with values determined by microscopy for which uncertainties were much larger, and is nearly 3-fold greater than those predicted by the Williams Model for the same period.

- **Chesapeake Bay Studies**

In our most recent work, aerosol particles have been sampled with micro-orifice impactors at sites in the Baltimore Inner Harbor, on the eastern shore (Still Pond Cost Guard Station), and aboard the EPA Research Vessel Anderson on the Chesapeake Bay.

Analyses have been completed for more than 300 samples, field blanks, and laboratory blanks. In addition to INAA, inductively-coupled plasma-atomic emission spectrometry (ICP-AES), and graphite furnace atomic absorption spectrometry with Zeeman background correction (GFAAS) are also used to analyze some of the samples.

An important part of our Baltimore area studies is to determine the influence of the area's mobile sources on deposition of soot and associated toxic polynuclear aromatic hydrocarbons. To this end, a unique tracer release was conducted, in part, to determine the size distributions and fate of soot

particles emitted from a specific source. In this study, size-segregated ambient outdoor aerosol was collected with University of Maryland fine-particle samplers (UMFPS) and 9-stage micro-orifice impactors (MOI) during two 30-day periods when 800 diesel sanitation trucks operated by the City of Baltimore burned fuel tagged with iridium (III) 2,4 pentanedionate to determine the size distributions of soot from a fleet of heavy-duty diesels. Additionally, several emission samples were collected with 8-stage MOIs mounted down stream of a radial diluter installed aboard a diesel sanitation truck burning tagged fuel while in normal operation. Background samples were collected between release periods and afterwards. Ambient, emission, and background samples were analyzed gravimetrically for particulate mass, for iridium by instrumental neutron activation analysis and for organic and elemental carbon (OC and EC) by combustion. Size distributions of freshly-emitted Ir-containing particles contained a major accumulation aerosol peak at a modal aerodynamic diameter of 0.12 μm, however, 43±1% of the Ir mass was contained in particles with diameters between 0.22 and 1.8 μm. The fractions of particulate mass, OC and EC contained in this interval were similar. Tagged soot aerosol collected in Baltimore city contained modes at 0.4 and, sometimes, 2.4 μm, in addition to the primary particle mode at 0.12 μm. Submicrometer modes are attributed to fresh SV emissions, whereas the 2.5-μm mode is attributed to resuspension. The results suggest that inferences on the evolution of urban soot aerosol made from size distribution data may be invalid unless a unique tracers are employed.

Research Topics

Certification of Standard Reference Materials by Neutron Activation Analysis
D. A. Becker[9], R. Demiralp[9], R. R. Greenberg[9], R. M. Lindstrom[9], E. A. Mackey[9], B. R. Norman[9], and R. Zeisler[9]

Improvements to INAA Methodology
D. A. Becker[9], R. Demiralp[9], R. R. Greenberg[9], R. M. Lindstrom[9], E. A. Mackey[9], and R. Zeisler[9]

Quality Assurance Improvements for NAA
D. A. Becker[9], R. Demiralp[9], R. R. Greenberg[9], R. M. Lindstrom[9], E. A. Mackey[9], and R. Zeisler[9]

Development of Radiochemical Separation for NAA
D. A. Becker[9], R. R. Greenberg[9], E. A. Mackey[9], and B. R. Norman[9]

Reactor Characterization for NAA
D. A. Becker[9]

Evaluation of Errors and Interferences in NAA
D. A. Becker[9], M. J. Blackman[18], R. R. Greenberg[9], R. M. Lindstrom[9], and R. Zeisler[9]

Determination of Phosphorus via RNAA with Beta Counting
R. L. Paul[9]

Trace Elemental Characterization of Silicon Semiconductor Materials
D. A. Becker[9]and R. M. Lindstrom[9]

Improvements to PGAA Methodology
D. L. Anderson[2], R. M. Lindstrom[9], E. A. Mackey[9], and R. L. Paul[9]

Evaluation of Accuracy and Precision in INAA of Botanical Materials
D. A. Becker[9]

Neutron Scattering Effects on PGAA
R. M. Lindstrom[9], E. A. Mackey[9], and R. L. Paul[9]

New Developments in Monitor Activation Analysis
G. P. Lamaze[9], R. M. Lindstrom[9], E. A. Mackey[9], and R. L. Paul[9]

Bio-analytical and Specimen Bank Research
K. A. Fitzpatrick[9], R. R. Greenberg[9], G. V. Iyengar[11], J. K. Langland[9], E. A. Mackey[9], B. J. Porter[10], and R. Zeisler[9]

Studies in Elemental Speciation
D. A. Becker[9], E. A. Mackey[9], and R. Zeisler[9]

Multielement Analysis of Foods and Related Materials by NAA
D. L. Anderson[2], and W. C. Cunningham[2]

High Sensitivity Gamma-Ray Spectrometry
R. M. Lindstrom[9]

Application of Radioisotope-Induced X-Ray Emission to the Identification of Lead and Other Elements in Ceramic Glazes and Housewares
D. L. Anderson[2] and W. C. Cunningham[2]

Elemental Characterization of High Temperature Superconductors
D. A. Becker[9], R. R. Greenberg[9], R. M. Lindstrom[9], and R. L. Paul[9]

New Developments in NDP
H. H. Chen-Mayer[9], G. P. Lamaze[9], and J. K. Langland[9]

Neutron Depth Profiling of AlN Thin Films
H. H. Chen-Mayer[9], G. P. Lamaze[9], and S. McGuire[1]

Neutron Depth Profiling of c-BN
H. H. Chen-Mayer[9], G. P. Lamaze[9], and L. Pilione[14]

Comparison of Nuclear Reactors for Analytical Chemistry
D. A. Becker[9]

Determination of Hydrogen by PGAA
R. R. Greenberg[9], R. M. Lindstrom[9], E. A. Mackey[9], and R. L. Paul[9]

Analytical Applications of Cold Neutrons
H. H. Chen-Mayer[9], R. Demiralp[9], R. R. Greenberg[9], G. P. Lamaze[9], J. K. Langland[9], R. M. Lindstrom[9], E. A. Mackey[9], D. F. R. Mildner[9], R. L. Paul[9], and V. A. Sharov[24]

Nitrogen Profiling of Thin Titanium Nitride Films
G.P. Lamaze[9], H. H. Chen-Mayer[9], and N. Cox[4]

Lithium Migration in Electrochromic Thin Films
G.P. Lamaze[9], H. H. Chen-Mayer[9], M. Badding[17], and A. Gerouli[19]

Test of a Novel High Sensitivity Neutron Detector
B. Feller[7], H. H. Chen-Mayer[9], and G.P. Lamaze[9]

Neutron Focusing for Analytical Chemistry
H. Chen-Mayer[9], G. P. Lamaze[9], J. K. Langland[9], Rm. M. Lindstrom[9], D. F. R. Mildner[9], V. A. Sharov[24], and J. R. Swider[20]

Metal Capillaries for Neutron Lenses
H. H. Chen-Mayer[9], V.S. Fokin[4], D.F.R. Mildner[9], P.L. Reeder[13], and V.A. Sharov[24]

Neutron Dosimetry for Instrument Development
R. M. Lindstrom[9]

Neutron Distribution Measurements by Neutron Induced Autoradiography
Z. En[22], J. S. Brenizer[22], and D. A. Becker[9]

Neutron Transmission through Curved Capillaries
H. H. Chen-Mayer[9], V. S. Fokin[4], D. F. R. Mildner[9], and V. A. Sharov[24]

Neutron Imaging with Scintillating Fiber Faceplates
H. H. Chen-Mayer[9], V. S. Fokin[4], D. F. R. Mildner[9], P. L. Reeder[13], and V. A. Sharov[24]

Neutron Transmission through Tapered Capillaries
H. H. Chen-Mayer[9], D. F. R. Mildner[9], and V. A. Sharov[24]

Applications of Neutron Laue Diffraction Focusing Methods
H. H. Chen-Mayer[9], V. V. Kvardakov[16], J. W. Lynn[8], D. F. R. Mildner[9], and V. A. Sharov[24]

Focusing Methods for Radiography and Topography
H. H. Chen-Mayer[9], D. F. R. Mildner[9], K. M. Podurets[16], and V. A. Sharov[24]

Neutron Beam Spatial Distributions Using Imaging Plate Technology
H. J. Bahre[3], H. H. Chen-Mayer[9], Y. T. Cheng[6], D. F. R. Mildner[9], and V. A. Sharov[24]

Hydrogen Detection in Industrial Materials by Incoherent Neutron Scattering
H. H. Chen-Mayer[9], V. V. Kvardakov[16], and D. F. R. Mildner[9]

A Bender-Focuser for Prompt Gamma Activation Analysis
H. H. Chen-Mayer[9], R. M. Lindstrom[9], D. F. R. Mildner[9], R. L. Paul[9], Q.-F. Xiao[23], and V. A. Sharov[24]

Low-Angle Neutron Diffraction from Polycapillary Fibers
M. Agamalian[13] and D.F.R. Mildner[9]

Development of a Position-Sensitive Video Radiation Detector
H. H. Chen-Mayer[9] and C. J. Zeissler[12]

Homogeneity and Composition of Small Solid Samples
R. Zeisler[9]

Characterization of Submicrometer Aerosol Particles
J. M. Ondov[20], S. F. Heller-Zeisler[20], and R. Zeisler[9]

Characterization of Sources and Fluxes of Particulate Pollutants Depositing to Great Waters
P. F. Caffrey[20], A. E. Suarez[20], and J. M. Ondov[20]

Archeological Applications of NAA
R. Bishop[18], M. J. Blackman[18], and J. E. Myers[18]

Radionuclides in Foods
D. L. Anderson[2] and W. C. Cunningham[2]

Quality Assurance Programs
D. L. Anderson[2] and W. C. Cunningham[2]

Revalidation of Food SRMs
D. L. Anderson[2] and W. C. Cunningham[2]

Bromation in Breadmaking
W. C. Cunningham[2] and C. R. Warner[2]

Affiliations

[1] Cornell University
[2] Food and Drug Administration
[3] Fuji Medical Systems USA, Inc
[4] Institute of Physics and Technology, Russian Academy of Sciences, Russia
[5] Intel, Inc.
[6] Neutek, Inc.
[7] Nova Scientific
[8] NIST Center for Neutron Research
[9] NIST, Nuclear Methods Group
[10] NIST, Organic Analytical Methods Group
[11] NIST, Standard Reference Materials Program
[12] NIST, Surface and Microanalysis Division
[13] Oak Ridge National Laboratory
[14] Pacific Northwest National Laboratory
[15] Pennsylvania State University

[16] Russian Scientific Center, Kurchatov Institute, Russia
[17] SAGE Electrochromics
[18] Smithsonian Institution
[19] Tufts University
[20] University of Maryland at College Park
[21] University of Michigan
[22] University of Virginia
[23] X-Ray Optical Systems, Inc
[24] X-Ray Optical Systems, Inc. and ETOM Tech. Corporation

NCNR Guest Researchers and Collaborations: 1997

The NCNR provides some of the nation's most advanced capabilities in the area of neutron beam related research. A major role of the division is to make these capabilities available to all qualified U.S. researchers - from universities, industry, and government laboratories. As shown in Fig. 1, this role has steadily expanded since the advent of the CNRF around the turn of the decade.

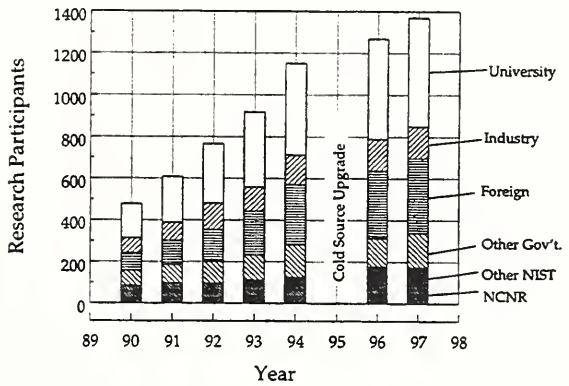

Fig. 1. Research participations at the NBSR

Along with strong, steady growth this figure also shows the predominance of outside user participation in experiments performed at the NBSR. The rightmost column represents participants from 54 U.S. industrial laboratories, 92 universities, 33 other government institutions, and over 100 foreign institutions. Participants include those who were at the facility at least once for an experiment or by collaborating in other ways (e.g. sample preparation, co-authors on publications).

The development over the years of new instrumentation at the NCNR is certainly the most important factor contributing to the increasing number of facility users as represented in Fig. 1. However the inauguration of new instruments has paused during this last fiscal year, as development on the neutron guide system has advanced to the point where only the sophisticated high-resolution instruments remain to be completed. Thus, the most recent program expansion is in research communities using already established instruments. In general, refinement and expansion of existing instrumentation and techniques have aided this. The number of different research participants must at some point saturate, and will to some degree be determined by policies regarding the granting of beam time. Current policy allows for considerable extension of already approved projects, which show merit based on reports and publications. This necessarily takes away beam time which could be used for new projects.

Facility users obtain access to NCNR instrumentation in several ways. The first and most straightforward route is through a formal research proposal system, as described in the following paragraph. A second avenue lies in direct collaborations between external facility users and NIST scientists, involving experiments of limited duration on specific research topics. A third, also very important mode of access involves more formal collaborations of longer duration with larger groups, i.e., research consortia, rather than with individual scientists. The third mode has been used to build and operate several of the new instruments.

The formal research proposal system is based on a submission deadline and subsequent review at six- or seven-month intervals. During FY97 there were two such proposal cycles with assignments of beam time occurring in March and November. The total number of proposals on peer reviewed instruments is up to 130 for the November call, compared to 100 proposals for the FY96 call, and the total number of instrument days requested has increased to more than 800 compared to 400 a year ago. The Program Advisory Committee (PAC), which is a group of seven prominent scientists makes final decisions about the allocation of beam time by NIST management. The PAC membership represents a wide range of expertise in neutron beam research, and advises NIST on many aspects of the research activities and instrumentation at the reactor, especially those concerning user interaction. At a meeting once every proposal cycle the PAC considers the peer reviews of proposals by expert referees, technical reviews made by NIST scientists, reviews for safety, and the proposals themselves, in order to approve or reject proposals, and to allocate specific amounts of instrument time.

The instruments in greatest demand continue to be the two small-angle neutron scattering (SANS) diffractometers, and the two neutron reflectometers, which accounted for 65 proposals and 290 instrument days requested, and 40 proposals for 290 days respectively. SANS is oversubscribed by a factor of greater than two in days requested compared with available days to allocate (125), and the approval rate for new SANS proposals continues a trend in declining from 66% in March to 47% in November. The reflec-

tometers show the greatest increases in demand, and is now oversubscribed by almost a factor of 3 for the 110 available instrument days. The approval rate for new reflectometry proposals has thus been forced to decline from about 90% last year to only 53% this last cycle.

The demand for high resolution instruments for inelastic neutron scattering has already begun to increase, as over-subscription for the SPINS spectrometer has reached about a factor of two for the 82 instrument days available per scheduling cycle. Many of the SPINS experiments are among the most challenging in terms of the counting rates and signal-to-noise. This has led to a number of requests for blocks of time exceeding one week. While review has often justified such amounts of instrument time, the pressures for approval have typically favored truncation of the allotments over rejection. The three new high-resolution inelastic scattering instruments (back-scattering, time-of-flight and spin-echo) are nearing completion, and increased demand for these types of experiments is anticipated. A workshop on high-resolution neutron spectroscopy was held in August of FY97 in order to help identify and educate possible new users of these instruments.

Direct collaborations remain a common way to access the instruments at the NCNR, accounting for approximately 60% of the total number of instrument days. The thermal-neutron instruments, i.e., triple-axis spectrometers and high-resolution powder diffractometer were mainly scheduled in this way. An on-line proposal system for use of the powder diffractometer resulted in 120 accepted proposals for measurements and a wide variety of samples (altogether, over 1000 data sets were collected from 320 samples).

The third method of obtaining access to NCNR instruments is through research consortia. For example, the 30-meter SANS diffractometer on neutron guide NG-7 was built and is operated by a group consisting of NIST, Exxon Research and Engineering Co., the University of Minnesota, and Texaco R & D. Three-quarters of the beam time on the instrument is reserved for the consortium, and the remaining time is allocated to general user proposals. Similar arrangements involving other consortia apply for the horizontal-sample reflectometer and the high-resolution powder diffractometer.

Personnel from other organizational units of NIST wholly or partially operate several of the experimental stations at the NCNR. A group from the Analytical Chemistry Division carries out chemical analysis by nuclear methods. There are several experimental stations operated by this group. For example, cold-neutron prompt-gamma neutron activation analysis (PGAA), an in-beam method, is offered directly to users through proposals, while activation analysis after removal from a neutron beam is an in-house activity offered to users through collaborations.

Services such as irradiation, radiography, and materials characterization are provided to other government agencies using the facilities at the NCNR. The FDA and Smithsonian have maintained long-term, continuing associations, while other institutions receive services at the NCNR on a short-term, case-by-case basis. Such services are provided to non-government agencies as well. These techniques prove to be complementary to many of the scientific research projects at the NCNR where materials characterization is crucial.

In some cases, industrial R & D of a proprietary nature is carried out at the NCNR, provided that appropriate beam-time charges are paid on a full-cost-recovery basis to the U.S. government.

Feedback from facility users concerning operation and policies at the NCNR is gathered in several ways. Firstly, the NCNR local contact persons interact directly with each research group using the facility. This informal method typically identifies concerns about a specific instrument, and the responsibility for action then resides with NCNR staff responsible for the instrument. Feedback of a more general nature needs to be transmitted to NCNR administration and the PAC, and a more formal process involving on site forms and/or electronic mail is currently taking shape.

This past year a complete set of detailed information on investigators, proposals, referees and experiments, has been gathered into a comprehensive database. This is extremely useful in the increasingly complicated task of assigning and scheduling beam-time and equipment, and in making administrative decisions concerning NCNR operations. This was largely made possible by using the Internet to efficiently collect beam-time proposals and other information from users. On the World Wide Web at http://rrdjazz.nist.gov further information on the NCNR, its instrumentation, staff and the guest researcher program can be found.

National Institute of Standards and Technology

Organizational Chart

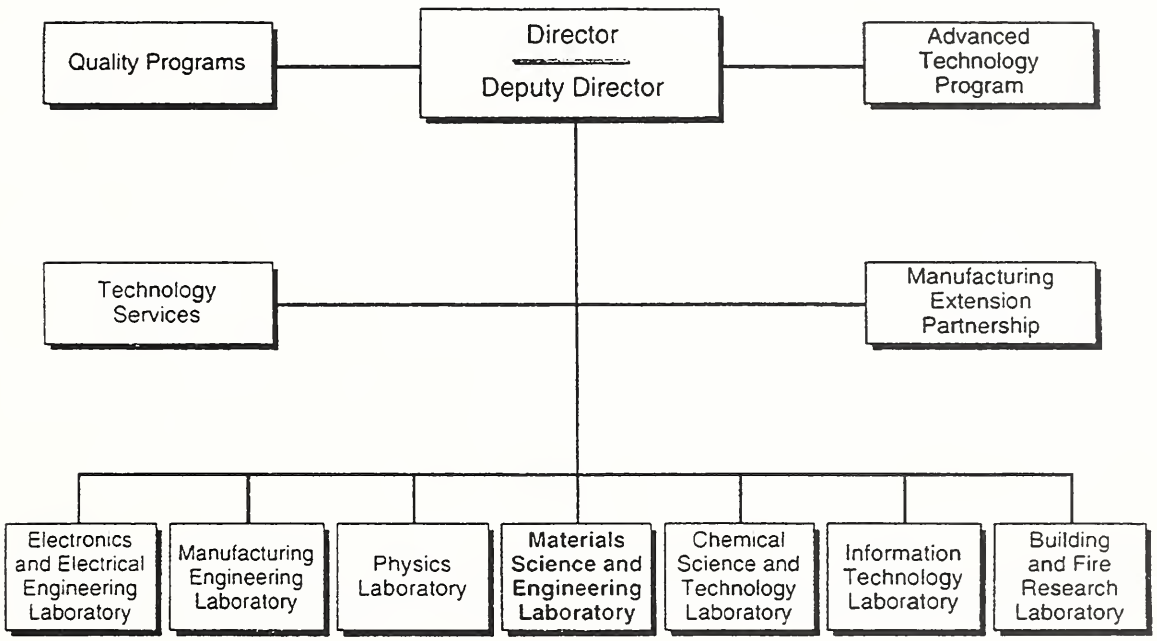

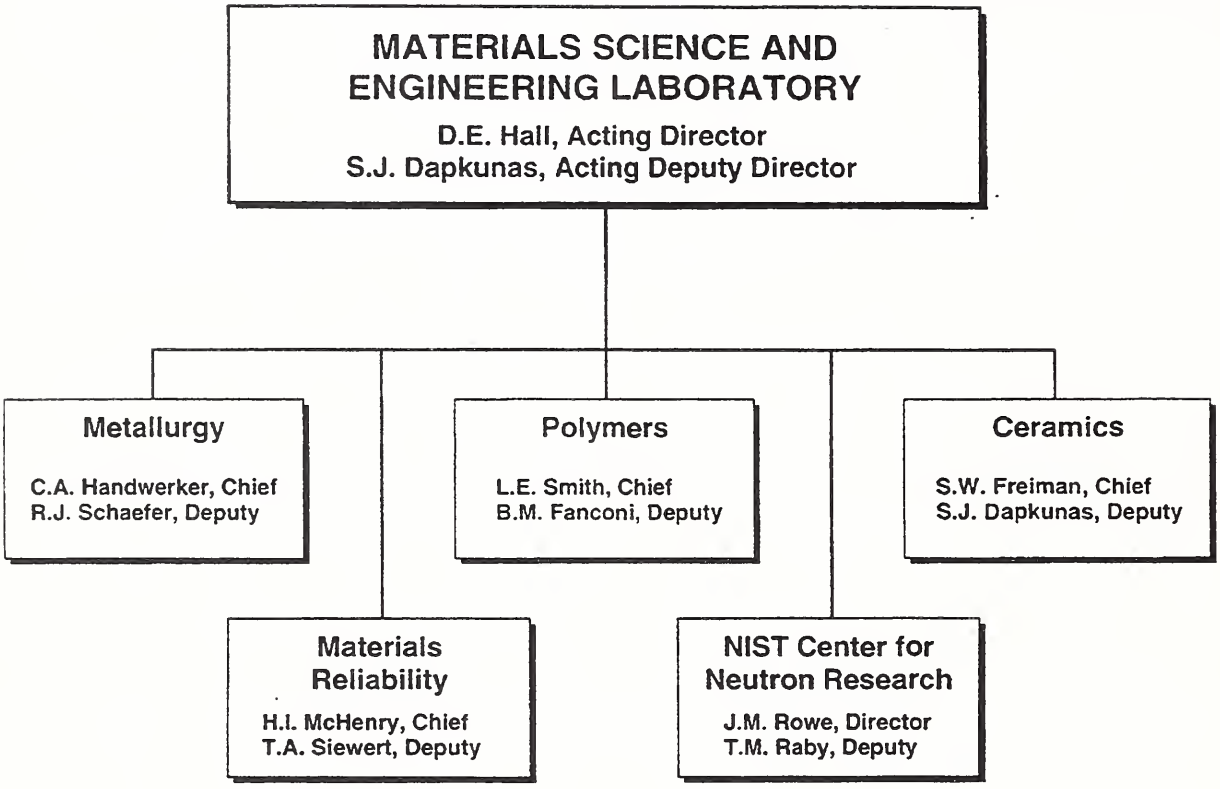
MATERIALS SCIENCE AND ENGINEERING LABORATORY
D.E. Hall, Acting Director
S.J. Dapkunas, Acting Deputy Director
Metallurgy
C.A. Handwerker, Chief
R.J. Schaefer, Deputy
Polymers
L.E. Smith, Chief
B.M. Fanconi, Deputy
Ceramics
S.W. Freiman, Chief
S.J. Dapkunas, Deputy
Materials Reliability
H.I. McHenry, Chief
T.A. Siewert, Deputy
NIST Center for Neutron Research
J.M. Rowe, Director
T.M. Raby, Deputy

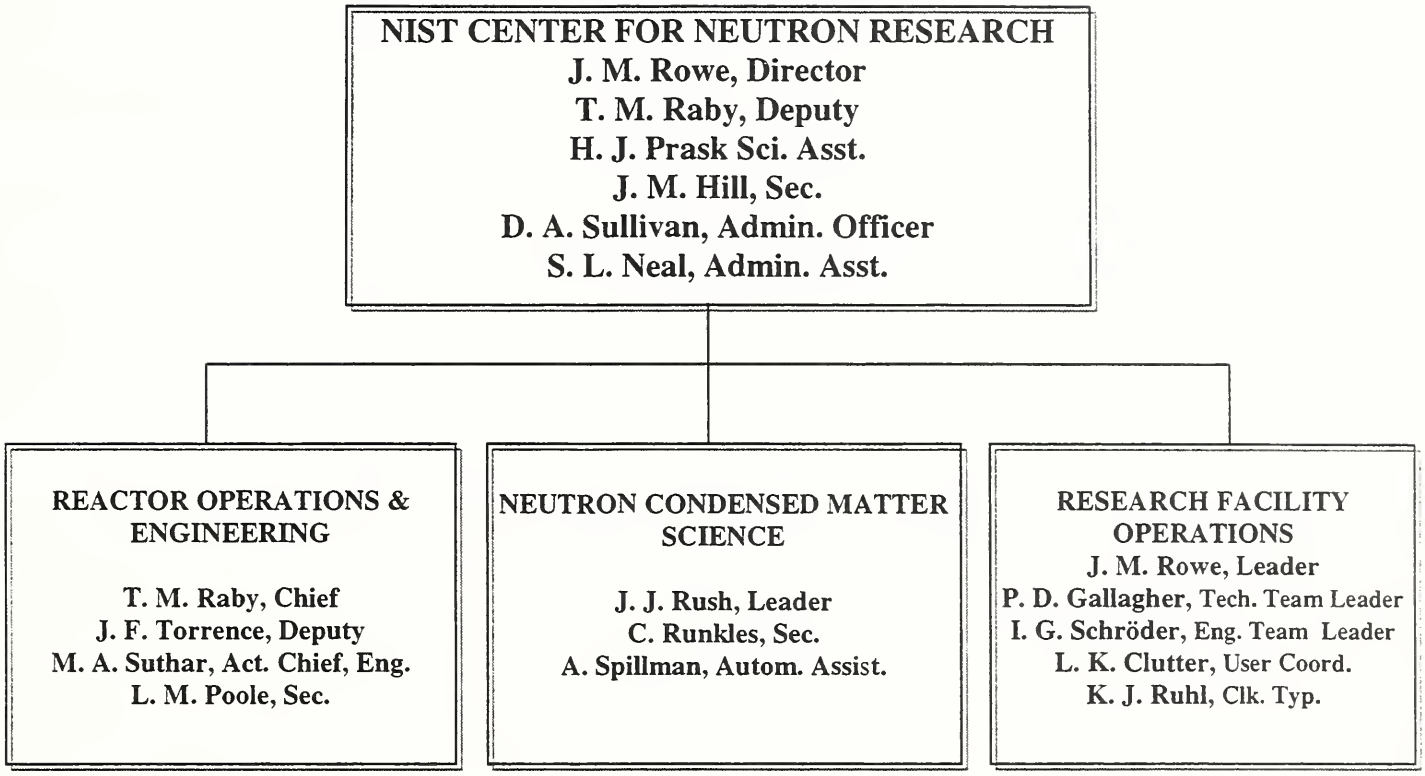

The Division staff is organized formally into three groups, as shown in the chart above; however, staff are utilized where necessary, irrespective of group. Below the group level of organization, personnel are grouped into research teams according to their predominant interest. Once again, these groupings are not hard and fast; there are many overlapping interests. These teams, including long-term guest researchers, are shown in Table 1. A great number of "non-resident" Ph.D. students and continuing collaborators from universities and industry are not listed. It should be noted that scientific contributions of the Research Facility Operations Group are included in the teams by scientific interest, even though in most cases, their predominant responsibility is for cold neutron instrument building and/or operation. In fact, they have only 30% of their time given to the conduct of research, while 70% is dedicated to the facility. Likewise, many members of the Neutron Condensed Matter Science Group have sizable Research Facility responsibilities, which may amount to as much as ½ time when needed.

NCNR/NIST Resident Staff and Visiting Scientists

(as of September 30, 1997)

CENTER OFFICE - (856)

Rowe, J. M., Director
Sullivan, D. A., Admin. Off.
Neal, S. L., Admin. Asst.
Hill, J. M., Secretary
Prask, H. J., Sci. Asst.
Barker, J. G., Matls. Sci.
Klosowski, P., Physicist

REACTOR OPERATIONS & ENGINEERING

Raby, T. M., Chief
Torrence, J. F., Deputy
Poole, L. M., Secretary

Operations

Beasley, R.D.
Bickford, N. A.
Bobik, P. A.
Cassells, M. G.
Clark, F. C.
Dilks, H. W.
Flynn, D. J.
Guarin, E. L.
Lindstrom, L. T.
McDonald, M. J.
Mueller, W. W.
Myers, T. J.
Pierce, S. C.
Ring, J. H.
Sprow, R. P.
Slaughter, S. S.
Stiber, R. F.
Toth, A. L.
Wilkison, D. P.
Wright, K. D.

Engineering

Suthar, M. A., Chief
Poole, L. M., Secretary
Beatty, J. A.
Brady, D. E., Inst. Supv.
Boyd, J. M.
Hall, K. D.
Liposky, P. J.
Reilly, G. D.
Shuman, L.A.
Thompson, R. G.

Research Associates

Anderson, D. A. (FDA)
Billos, J. (Montg. College)
Cunningham, W. C. (FDA)
Kornfeld, C.
Heine, C. J.
Olin, J.
Yee, K.

NEUTRON CONDENSED MATTER SCIENCE GROUP

Rush, J. J., Leader
Runkles, C. L., Secretary
Spillman, A.. R., Autom. Assist.
Berk, N. F.
Brand, P.

Chemical Physics of Materials

Copley, J. R. D.
Forstner, K. T.
FitzGerald, S. A.
Gehring, P. M.
Maliszewskyj, N. C.
Neumann, D. A., Team Leader
Udovic, T. J.

Crystallography

Karen, V. L.
Santoro, A.
Stalick, J. K.
Toby B. H., Team Leader

Magnetism and Superconductivity

Borchers, J. A.
Erwin, R. W.
Ijiri, Y., NRC Post-Doc.
Lynn, J. W., Team Leader
Santodonato, L.

Macromolecular and Microstructure

Butler, P. D.
Glinka, C. J., Team Leader
Hammouda, B.
Kline, S. R.
Readon, J. P.
Slawecki, T. M.

Surfaces and Interfaces

Dura, J. A.
Krueger, S. T.
Majkrzak, C. F., Team Leader
Satija, S. K.

Guest Scientists

Altorfer, F. B.
Broholm, C.
Cook, J.
Dender, D.
Doloc, L.
Feigin, L. A.
Gnaupel-Herold, T.
Huang, Q. Z.
Kepa, H.
Karmonik, C.
Khosrovani, N.
Lee, S.-H.
Lin, M. Y.
Mighell, A.. D.
Mrose, M.
Meyer, A.
Papanek, P.
Prince, E.
Sung, L.
Tarek, M.
Trevino, S. F.
Tobias, D.
Yildirim, T.
Zaliznyak, I.

RESEARCH FACILITY OPERATIONS

Rowe, J. M., Leader
Clutter, L. K., User Coord.
Hill, J. M., Secretary
Ruhl, K. J., Clerk Typist
Baltic, G. M., Tech. Suprv.
Bostian, C. D.
Clarkson, A.
Clem, D. L.
Clow, W. R.
Dickerson, W. E.
Fravel, D. H.
Fulford, D.
Gallagher, P. D.
Green, T. A.
Greene, G. C.
Heald, A. E.
Kamitakahara, W. A.
Knill, W. C.
Kopetka, P. H.
Kulp, D. L.
LaRock, J. G.
Layer, H. P.
Pierce, D. J.
Rinehart, M. J.
Rosov, N. S.
Schroder, I. G.
Thai, T. T.
Tobin, P. J.
Williams, R. E.

Guest Engineers

Brocker, C. W.
Christman, R.
Moyer, J. J.
Williams, R. H.
Wrenn, C. W.

OTHER NIST GROUPS

NEUTRON INTERACTIONS & DOSIMETRY GROUP– (846)

Gilliam, D. M., Leader
Rhodes, S. E., Secretary
Adams, J. M.
Arif, M.
Carlson, A. D.
Dewey, M. S.
Eisenhauer, C. M.
Gentile, T. R.
Jacobson, D. L.
Jones, G. L.
Nico, J. S.
Thompson, A. K.
Weitfeld, F. E.

Guest Scientists

Brome, C. R.
Butterwoth, J. S.
Chowdhuri, S. Z.
Eisenhauer, C. M.
Fei, X.
Grundl, J. A.
Huffman, P. R.
Hwang, S-R.
Mattoni, C. E. H.
Ioffe, A.
Schwartz, R. B.
Steiger, T.

NUCLEAR METHODS GROUP-(839)

Greenberg, R. R., Leader
Wilson, J. M., Secretary
Becker, D. A.
Chen-Mayer, H. H.
Demiralp, R.
Fitzpatrick, K. A.
Lamaze, G. P.
Langland, J. K.
Lindstrom, R. M.
Mackey, E. A.
Mildner, D.F.R.
Paul, R. L.
Porter, B. J.
Zeisler, R. L.

Guest Scientists

Bishop, R. L.
Blackman, M. J.

HEALTH PHYSICS - Div. 354

Slaback, L. A., Leader
Thomas, C. L., Secretary
Brown, D. R.
Campbell, C. D.
Cassells, L. H.
Clark, J. S.
Deardorff, G. E.
Fink, L. E.
Mengers, T. F.
Shubiak, J. J.

Research and Engineering Staff (September 30, 1997)

J. G. Barker	SANS instrumentation and research Microstructure of materials
N. F. Berk	Condensed matter theory Scattering theory for microstructure analysis Computer software for graphics and data analysis
N. A. Bickford	Reactor operations Reactor irradiations Reactor utilization
J. A. Borchers	Thin-film analysis Artificially modulated materials Magnetism
D. E. Brady	Electrical/electronic engineering Nuclear reactor instrumentation NDE diffraction methods
P. C. Brand	Materials engineering Neutron residual stress measurements Engineering physics
J. M. Boyd	Electrical/electronic engineering Nuclear reactor instrumentation
J. R. D. Copley	Time-of-flight spectrometer development Neutron instrumentation conceptual design Condensed matter physics
W. E. Dickerson	Neutron scattering instrumentation Microcomputer interfacing Nuclear and engineering physics

J. A. Dura	Combined molecular beam epitaxy and neutron reflectivity Instrumentation Surface, interfacial, and epitaxial physics
R. W. Erwin	Magnetic materials Phase transformations Cryogenics
S. A. FitzGerald	Neutron and optical spectroscopy Condensed matter physics Fullerenes and cements
K. T. Forstner	Instrumentation Monochromator development
D. B. Fulford	SANS equipment development and maintenance Mechanical engineering
P. D. Gallagher	Neutron reflectometry instrumentation Interfacial phenomena in polymer systems and complex fluids Phase transitions and critical phenomena
P. M. Gehring	Neutron backscattering instrumentation Magnetic and structural phase transitions in disordered systems Dynamics of high Tc materials
C. J. Glinka	SANS microstructure of metals and porous media CHRNS\ project director Cold neutron instrument development
G. C. Greene	System and user software for cold neutron instrumentation Spectrometer and data acquisition systems interfaces
B. Hammouda	SANS from polymers, liquid crystals, and colloids Dynamics of polymers in solution Scattering from sheared fluids
A. E. Heald	Design engineering Neutron instrumentation Shielding
W. A. Kamitakahara	The CNRF guest researcher program Dynamics of disordered solids Condensed matter physics
V. L. Karen	Crystallographic database development Theory of lattices and symmetry Neutron and x-ray diffraction
S. R. Kline	Microstructure of colloids and microemulsions Novel surfactant systems SANS instrumentation

P. Klosowski	Scientific data visualization Numerical computer modeling Data acquisition software and hardware
P. A. Kopetka	Mechanical engineering Cold source design Electro-mechanical systems
S. T. Krueger	SANS instrumentation Structure of biological materials Software development for biological problems
Y. Ijiri	Condensed matter physics Thin films and multilayers Magnetism
J. G. LaRock	Mechanical engineering Neutron instrumentation design
H. P. Layer	Electronics and data processing Advanced instrumentation Fundamental physics
P. J. Liposky	Design engineering Nuclear systems and components
J. W. Lynn	Condensed matter physics Magnetic and superconducting materials Neutron scattering methods
C. F. Majkrzak	Condensed matter physics Polarized neutron scattering and instrumentation development Neutron reflectivity measurements
N. C. Maliszewskyj	Time-of-flight instrumentation Condensed matter physics Computer software development
T. J. Myers	Reactor operations Safety analysis
D. A. Neumann	Molecular and layered materials Condensed matter physics Neutron and x-ray scattering instrumentation
D. J. Pierce	Mechanical engineering Neutron instrumentation design
H. J. Prask	Residual stress measurement methodology Neutron NDE applications Neutron NDE instrumentation

T. M. Raby	Reactor operations and standards Nuclear engineering Nuclear systems and components
G. D. Reilly	Design engineering Nuclear systems and components
N. Rosov	Spin echo techniques Phase transformations Magnetic materials
J. M. Rowe	Orientationally disordered solids Cold source development Cold neutron research and instrumentation
J. J. Rush	Catalysts and molecular materials Hydrogen in metals Inelastic scattering methods
L. Santodonato	Condensed matter physics Cryogenics
A. Santoro	Structure of electronic and structured ceramics Theory of crystal lattices Powder diffraction methods
S. K. Satija	Low-dimensional molecular systems Fractal aspects of microporous media Neutron reflectometry
I. G. Schröder	Cold neutron instrumentation development Nuclear and engineering physics Optical devices for neutron transport
T. M. Slawecki	SANS and reflectometry from polymers Complex fluid microstructure SANS instrumentation
J. K. Stalick	Neutron and x-ray diffraction Inorganic chemistry Crystal database development
M. A. Suthar	Design engineering Nuclear systems and components
B. H. Toby	Neutron and synchrotron diffraction Zeolite crystallography Structure determination methods
J. F. Torrence	Reactor supervision Reactor maintenance Nuclear engineering

T. J. Udovic	Neutron time-of-flight instrumentation Properties of catalysts and adsorbates Hydrogen in metals
R. E. Williams	Cold neutron source development Nuclear engineering

TECHNICAL AND PROFESSIONAL COMMITTEE PARTICIPATION AND LEADERSHIP

American Crystallographic Association
- B. Toby, Organizer and Session Co-Chair, Technological Materials Session

American Nuclear Society/American National Standards Institute
- T. M. Raby, Standards Steering Committee, Member
  - -National Chairman, N-17
  - -Working Groups, Chairman ANS-15.1, ANS-15.4, ANS-15.11
  - -National Standards Service Award Recipient (Nov. 1996)
- J. F. Torrence, Working Group, ANS-15.1
  - -N-17 National Committee Member

American Physical Society
- J. W. Lynn, Symposium Organizer, March Meeting (1997)
  - -Organizer and Interim Member-at-large, Topical Group on Magnetism and Its Applications
  - -Chair, Fellowship Committee, Topical Group on Magnetism and Its Applications

American Society for Testing and Materials
- H. J. Prask, Member, Subcommittee E28.13 on Residual Stress Measurement

Australian Nuclear Science and Technology Organization
- J. M. Rowe, Member, Advisor Committee on Research Reactors

Brookhaven National Laboratory
- C. G. Glinka, Member, HFBR Proposal Review Sub-Committee in Materials Science
- C. F. Majkrzak, Chairman, HFBR Program Advisory Committee
- J. M. Rowe, Co-Chairman, Physics Visiting Committee
- J. J. Rush, Member, Neutron Crystallography Facility Scheduling Committee
- T. M. Raby, High Flux Beam Reactor Review Board

Canadian Journal of Physics
- J. M. Rowe, Member, International Advisory Council

Department of Energy
- D. A. Neumann, Member, SNS Conceptual Design Review Committee
- H. J. Prask, Invited Participant, Neutron Residual Stress Analysis Discussion Meeting, October 1996
- T. M. Raby, Member, Basic Energy Sciences Special Committee on High Flux Beam Reactors
- J. J. Rush, Member, BESAC Panel on Future of DOE Synchrotron Facilities
  - -Scientific Advisor, DOE Recommendation Board for New BNL Contractor

Gordon Research Conference on Disorder in Materials
- D. A. Neumann, Vice-Chairman

Graduate Texts in Contemporary Physics (Springer-Verlag)
- J. W. Lynn, Series Editor

Institute for Nuclear Energy Research, Tawain
- J. M. Rowe, Member, Advisory Committee on TRR-II

International Advisory Committee for Fifth Conference on Application of Nuclear Techniques
- H. Prask, Organizer

International Centre for Diffraction Data - JCPDS
- J. K. Stalick, Chairman, Neutron Powder Diffraction Subcommittee
- B. H. Toby, Chairman, PDF Database Subcommittee

International Conference on Composites Engineering (Kona, Hawaii – July, 1997)
- H. J. Prask, Session Chairman

International Conference on Neutron Scattering (Toronto, Canada – August, 1997)
- C. J. Glinka, Member, Program Committee
- J. W. Lynn, Member, Organizing Committee
  -Treasurer
- C. J. Majkrzak, Session Chairman, Reflectometry
  -Member, Publication Committee
- D. A. Neumann, Member, Program Committee

International Conferences on Hydrogen in Metals
- J. J. Rush, Member, Advisory Committee

International Union of Crystallography
- C. F. Majkrzak, Session Chairman
- B. H. Toby, Commission on the Crystallographic Information File

International Workshop on Itinerant Electron Magnetism (Moscow, Russia – September, 1997)
- J. W. Lynn, Member, Program Committee

International Zeolite Association
- B. H. Toby, Member, Local Organizing Committee for 1998 International Meeting

Journal of Neutron Research (Gordon & Breach)
- C. F. Majkrzak, Member, Editorial Board

Los Alamos National Laboratory
- C. Broholm, Vice Chairman, Executive Committee of Los Alamos Neutron Science Center Users Group
- P. D. Gallagher, Member, LANSCE Proposal Evaluation Committee for Spectrometer Enhancement Project (Dec. 1996 –present)
- J. W. Lynn, Member, External Advisory Committee, 30T Pulsed Neutron Magnet Development Program
- C. F. Majkrzak, LANSCE SPSS Enhancement Project (March, 1997)
- J .M. Rowe, Member, Advisory Board on LANSCE

Magnetism and Magnetic Materials Conference
- J. L. Borchers, Member, Program Committee
- J. W. Lynn, Symposium Chairman
  -Member, Advisory Committee

Massachusetts Institute of Technology
- J. M. Rowe, Member, Visiting Committee, Nuclear Engineering Department

National Academy of Science/National Research Council
- J. J. Rush, Member, Solid State Sciences Committee

National Organization of Test, Research, and Training Reactors
- T. M. Raby, Past Chairman and Member of Executive Committee

National Science Foundation
J. W. Lynn, Member, Evaluation Panel on International Programs

National Science Foundation Materials Research Science and Engineering Center (through Univ. Maryland)
J. W. Lynn, Member, Board of Directors

National Science and Technology Council
J. J. Rush, Member, Subcommittee on Research Infrastructure

National Spallation Neutron Source
J. W. Lynn, Member, National Steering Committee

Neutron Scattering Satellite Meeting to the XVII IUCr Congress
S. Krueger, Local Chairman
E. Prince, Member, Program Committee

Neutron Scattering Society of America
C. F. Majkrzak, Secretary

NIST Center for Neutron Research Workshop on High Resolution Cold Neutron Spectroscopy
J. R. D. Copley, Organizer
C. J. Glinka, Organizer
D. A. Neumann, Organizer

NIST/NSF Center for High Resolution Neutron Scattering (CHRNS)
C. J. Glinka, Project Director

Oak Ridge National Laboratory
J. M. Rowe, Review Committee for Cold Neutron Source

Rare Earth Research Conference
J. W. Lynn, Session Chairman and Member of the Board of Directors

Southeastern Universities Research Association
J. W. Lynn, NIST Representative, Council on Materials Science and Engineering

Strongly Correlated Electron Systems Conference (SCES'98)
J. W. Lynn, Member, International Advisory Committee

Surface X-Ray and Neutron Scattering Conference (Oxford, UK – July, 1997)
C. F. Majkrzak, Member, International Advisory Committee

University of Michigan Reactor Review
J. M. Rowe, Member

University of Minnesota, Center for Interfacial Engineering
C. J. Glinka, Member, Surfactancy and Self-Assembly Technical Advisory Committee
S. K. Satija, Member, Polymer Microstructure Technical Advisory Committee

Publications

Aeppli, G., Broholm, C., DiTusa, J. F., Hayden, S. M., Ito, T., Lee, S. H., Mason, T. E., Mook, H. A., Oka, K., Perring, T. G., Schroder, A., Takagi, H., Xu, G., "Magnetic Coherence in the Transition Metal Oxides", Physica B **237**, 30 (1997).

Agamalian, M., Christen, D. K., Drews, A. R., Glinka, C. J., Matsouka, H., Wignall, G. D., "Surface-Induced Parasitic Scattering in Bonse-Hart Double Crystal Crystal Diffractometers", J. Appl. Crystallogr., in press.

Altorfer, F., Essmann, R., "NH_3 Dynamics in $Zn(NH_3)_4I_2$ and $Zn(NH_3)_4Br_2$ Investigated by Incoherent Quasielastic Neutron Scattering", Physica B **234-236**, 61 (1997).

Balmer, M. L., Huang, Q., Wong-Ng, W., Roth, R. S., Santoro, A., "Neutron and X-Ray Diffraction Study of the Crystal Structure of $CsTiSi_2O_6$", J. Solid State Chem. **130**, 97 (1997).

Balsara, N. P., Lin, C., Hammouda, B., "Early Stages of Nucleation and Growth in a Polymer Blend", Phys. Rev. Lett. **77**, 3847 (1996).

Bao, W., Broholm, C., Aeppli, G., Carter, S. A., Dai, P., Frost, C. D., Rosenbaum, T. F., Honig, J. M., Metcalf, P., "Magnetic Correlations in a Classic Mott System: Pure and Doped V_2O_3", Proceedings of the International Conference on Magnetism, 1997, in press.

Bao, W., Broholm, C., Aeppli, G., Dai, P., Honig, J. M., Metcalf, P., "Dramatic Switching of Magnetic Exchange in a Classical Transition Metal Oxide: Evidence for Orbital Ordering", Phys. Rev. Lett. **78**, 507 (1997).

Bao, W., Broholm, C., Honig, J. M., Metcalf, P., Treviño, S. F., "Itinerant Antiferromagnetism in the Mott Compound $V_{1.973}O_3$", Phys. Rev. B: Cond. Matt. **54**, R3762 (1996).

Bauer, B., Briber, R., Hammouda, B., Tomalia, D., Barnes, J., "Scattering Studies of the Internal Structure of Large Dendrimer Molecules", Macromol., in press.

Benmouna, M., Briber, R., Hammouda, B., "Polymer Blends, Copolymers and Networks. Scattering Properties and Phase Behavior", Macromol. Theory Simul. **6**, 197 (1997).

Benmouna, M., Hammouda, B., "The Zero Average Contrast Completion", Prog. Polym. Sci. **22**, 49 (1997).

Berk, N. F., Majkrzak, C. F., "Inverting Specular Neutron Reflectivity from Symmetric, Compactly Supported Potentials", J. Phys. Soc. Jpn. **65**, Suppl. A, 107 (1996).

Bindra, C., Nalimova, V. A., Sklovsky, D. E., Kamitakahara, W. A., Fischer, J. E., "Statics and Dynamics of Interlayer Interactions in the 'Superdense' High Pressure Graphite Compound LiC_2", Phys. Rev. B, in press.

Birch, W. R., Knewtson, M. A., Garoff, S., Suter, R. M., Satija, S., "The Structure of Precursing Thin Films of an Anionic Surfactant on a Silicon Oxide/Silicon Surface", Langmuir **11**, 48 (1995).

Bödeker, P., Sonntag, P., Schreyer, A., Zabel, H., Borchers, J. A., Hamacher, K., Kaiser, H., "Effects of Fe Cap Layers on the Spin Density Wave in Epitaxial Cr(001) Films", J. Appl. Phys. **81**, 5247 (1997).

Borchers, J. A., Gehring, P. M., Erwin, R. W., Ankner, J. F., Majkrzak, C. F., Hylton, T. L., Coffey, K. R., Parker, M. A., Howard, J. K., "Antiferromagnetic Interlayer Correlations in $Ni_{80}Fe_{20}$/Ag Multilayers", Phys. Rev. B **54**, 9870 (1996).

Borchers, J. A., Gehring, P. M., Majkrzak, C. F., Zeltser, A. M., Smith, N., Ankner, J. F., "Dependence of the Interlayer Coupling on Anneal Temperature in Ni-Fe/Cu Evaporated Multilayers", J. Appl. Phys. **81**, 3771 (1997).

Borchers, J. A., Ijiri, Y., Lee, S.-H., Majkrzak, C. F., Felcher, G. P., Takano, K., Kodama, R. H., Berkowitz, A. E., "Spin-Flop Tendencies in Exchange-Biased Co/CoO Thin Films", J. Appl. Phys., in press.

Brand, P. C., Prask, H. J., Gnaeupel-Herold, T., "Residual Stress Measurements at the NIST Reactor", Physica B, in press.

Brand, P. C., Prask, H. J., Hutchings, M. T., Buttle, D. J., Goff, J. P., "Residual Stresses in Bent Steel Tubes Measured by Means of Neutron Diffraction and Magnetic Methods", Proceedings of the ICRS-5 (Linkoping, Sweden, June 16-18, 1997), in press.

Broholm, C., "Proposal for a Doubly Focusing Cold Neutron Spectrometer at NIST", Nucl. Instr. Meth. Phys. Res. **A369**, 169 (1996).

Broholm, C., Reich, D. H., Aeppli, G., Lee, S.-H., Dender, D. C., Hammar, P, Xu, G., Ditusa, J. F. Ramirez, A. P., "Neutron Scattering Studies of Non-Metallic Low-Dimensional Quantum Antiferromagnets", Proceedings of the Geilo Winter School on Dynamical Properties of Unconventional Magnetic Systems, 1997, in press.

Buchenau, U., Wischnewski, A., Dianoux, A. J., Kamitakahara, W. A., Zarestky, J. L., "Neutron Scattering Analysis of Low Frequency Modes in Silica", Phys. Rev. Lett., in press.

Burton, B. P., McCormack, R. P., Toby, B. H., Goo, E. K., "Cation Ordering in Some ABO_3 Perovskites", Ferroelectrics **194**, 187 (1997).

Butler, P. D., Hamilton, W. A., Magid, L. J., Slawecki, T. M., Han, Z., Hayter, J. B., "Effect of a Solid/Liquid Interface on Bulk Solution Structures Under Flow", Physica B, in press.

Butler, P. D., Hamilton, W. A., Magid, L. J., Hayter, J. B., Slawecki, T. M., Hammouda, B., "Use of Complementary Neutron Techniques in Studying the Effect of a solid/Liquid on Bulk Solution Structures", Faraday Discuss. **104**, 65 (1996).

Clutter, L. K., editor, *NIST Reactor: Summary of Activities, October 1995 through September 1996*, NISTIR 6000 (1997).

Clutter, L. K., editor, *Reactor Radiation Technical Activities - 1996*, NISTIR 5966 (1997).

Copley, J. R. D., "The Conceptual Design of a Disk Chopper Spectrometer", Proceedings of the Workshop on Methods for Neutron Scattering Instrument Design (Lawrence Berkeley National Laboratory, September 23-25, 1996); LBNL Report, in press.

Copley, J. R. D., Michel, K. H., "Multiple Orientational Order Parameters in Solid C_{60}", Physica B, in press.

Dender, D. C., Hammar, P. R., Reich, D. H., Broholm, C., Aeppli, G., "Direct Observation of Field-Induced Incommensurate Fluctuations in a One-Dimensional S = ½ Antiferromagnet", Phys. Rev. Lett. **79**, 1750 (1997).

Drews, A. R., Barker, J. G., Glinka, C. G., Agamalian, M., "Development of a Thermal-Neutron Double-Crystal Diffractometer for USANS at NIST", Physica B, in press.

Drews, A. R., Cline, J. P., Vanderah, T. A., Salazar, K., "High-Temperature X-Ray Diffraction Studies of a Precursor Mixture for Pb-substituted Bi-2223 Superconducting Wires", J. Mater. Res., in press.

Drews, A. R., Wong-Ng, W., Vanderah, T. A., Roth, R. S., "Preparation and Crystal Structure of $Sr_6TiNb_4O_{18}$", J. Alloy. Compd. **255**, 243 (1997).

Edler, K. J., Reynolds, P. A., Brown, A. S., Slawecki, T. M., White, J. W., "Shear and Salt Effects on the Structure of MCM-41 Synthesis Gels", Faraday Commun., in press.

Ermi, B. D., Karim, A., Douglas, J. F., Sung, L., "Atomic Force Microscopy Investigation of Phase Separation in Ultrathin Polymer Blend Films", PSME preprint **77**, 602 (1997).

Everitt, B. A., Salamon, M. B., Borchers, J. A., Erwin, R. W., Rhyne, J. J., Park, B. J., Donovan, K. V., McMorrow, D. F., Flynn, C. P., "Helimagnetic Structures in Epitaxial

Nd/Y Superlattices and Alloys", Phys. Rev. B **56**, 5452 (1997).

Gehring, P. M., Neumann, D. A., "Backscattering Spectroscopy at the NIST Center for Neutron Research", Physica B, in press.

Glinka, C. J., Barker, J. G., Hammouda, B., Krueger, S., Moyer, J. J., Orts, W. J., "The 30-Meter Small Angle Neutron Scattering Instruments at the National Institute of Standards and Technology", J. Appl. Crystl., in press.

Godart, C., Alleno, E., Tominez, E., Gupta, L. C., Nagarajan, R., Hossain, Z., Lynn, J., Sanchez, J. P., "Some Chemical and Physical Properties of Quaternary Borocarbides", J. Solid State Chem., in press.

Goldman, K. I., Giebultowicz, T. M., Kepa, H., Sinha, S. K., "Numerical Simulation of Neutron Diffraction from Correlated/Uncorrelated Magnetic Multilayers", Physica B, in press.

Goldman, K. I., Springholz, G., Kepa, H., Giebultowicz, T. M., Majkrzak, C. F., Bauer, G., "Interlayer Correlations in Antiferromagnetic Semiconductor Superlattices EuTe/PbTe", Physica B, in press.

Goodwin, T. J., Radousky, H. B., Shelton, R. N., Rosov, N., Lynn, J., "Pr and Cu Magnetism in $(Pr_{1.5}Ce_{0.5})Sr_2Cu_2MO_{10-\delta}$ (M = Nb, Ta): Correlations with a Suppression of Superconductivity", Phys. Rev. B **55**, 3297 (1997).

Green, M. A., Dalton, M., Prassides, K., Day, P., Neumann, D. A., "Lattice Vibrations of the Superconducting Oxide Spinels $(Li, Mg)_{1+x}Ti_{2-x}O_4$", J. Phys. Cond. Matt., in press.

Green, M. A., Prassides, K., Stalick, J. K., Day, P., "The Crystal Structure of $SrSnO_3$", Inorg. Chem., in press.

Gygax, F. N., Amato, A., Pinkpank, M., Schenck, A., Anderson, I. S., Solt, G., Udovic, T. J., "Electric Field Gradients Probed by μ^+SR in Sc and α-ScH_x Solid Solutions", Hyperfine Interact. **106**, 91 (1997).

Hammouda, B., Balsara, N. P., Lefebvre, A., "SANS from Pressurized Polyethylbutylene/ Polymethylbutylene Polymer Blends", Macromol. **30**, 5572 (1997).

Hauer, B., Hempelmann, R., Udovic, T. J., Rush, J. J., Jansen, E., Kockelmann, W., Schäfer, W., Richter, D., "Neutron Scattering Studies of the Vibrational Excitations and the Structures of Ordered Niobium Hydrides: I. The ϵ Phase", J. Chem. Phys., in press.

Hauer, B., Hempelmann, R., Udovic, T. J., Rush, J. J., Kockelmann, W., Jansen, E., Schäfer, W., Richter, D., "Structure and Microdomain Structure of Ordered Niobium Hydrides and Deuterides by Means of Neutron Scattering", J. Alloy. Compd. **253**, 258 (1997).

Hayes, C., Alefeld, B., Copley, J. R. D., Lartigue, C., Mezei, F., "On the Use of a Toroidal Mirror to Focus Neutrons at the ILL Neutron Spin Echo Spectrometer IN15", Proceedings of the Workshop on Methods for Neutron Scattering Instrument Design (Lawrence Berkeley National Laboratory, September 23-25, 1996); LBNL Report, in press.

Hayes, C., Lartigue, C., Kollmar, A., Copley, J. R. D., Alefeld, B., Mezei, F., Richter, D., Springer, T., "The Focusing Mirror at the ILL Spin-Echo Spectrometer IN15: Experimental Results", J. Phys. Soc. Jpn. **65**, Suppl. A, 312 (1996).

Henderson, P., Beyer, D., Jonas, U., Karthaus, O., Ringsdorf, H., Heiney, P. A., Maliszewskyj, N. C., Ghosh, S. S., Mindyuk, O. Y., Josefowicz, J. Y., "Complex Ordering in Thin Films of Di and Tri-Functionalized Hexaalkoxy-Triphenylene Derivatives", J. Am. Chem. Soc. **119**, 4740 (1997).

Hjörvarsson, B., Dura, J. A., Isberg, P., Watanabe, T., Udovic, T. J., Anderson, G., Majkrzak, C. F., "Reversible Tuning of the Magnetic Exchange Coupling in Fe/V (001) Superlattices Using Hydrogen", Phys. Rev. Lett. **79**, 901 (1997).

Huang, Q., Lynn, J. W., Santoro, A., Chakoumakos, B. C., Cava, R. J., Krajewski, J. J., Peck Jr., W. F., "Neutron Powder Diffraction Study of the Nuclear and Magnetic Struc-

tures of $HoNi_{1.985}Co_{0.015}B_2C$ and HoNiBC", Physica C **271**, 311 (1996).

Huang, Q., Santoro, A., Lynn, J. W., Erwin, R. W., Borchers, J. A., Peng, J. L., Ghosh, K., Greene, R. L., "Structure and Magnetic Order in Undoped Lanthanum Manganite", Phys. Rev. B **55**, 14987 (1997).

Huang, Q., Santoro, A., Lynn, J. W., Erwin, R. W., Borchers, J. A., Peng, J. L., Greene, R. L., "Neutron Powder Diffraction Study of the Nuclear Structures of $La_{1-x}M_xMnO_3$ (M=Ca, Sr)", Phys. Rev. B, in press.

Ijiri, Y., Borchers, J. A., Erwin, R. W., Lee, S.-H., van der Zaag, P. J., Wolf, R. M., "Perpendicular Coupling in Exchange-biased Fe_3O_4/CoO Superlattices", Phys. Rev. Lett., in press.

Ijiri, Y., Borchers, J. A., Erwin, R. W., Lee, S.-H., van der Zaag, P. J., Wolf, R. M., "Role of the Antiferromagnet in Exchange-Biased Fe_3O_4/CoO Superlattices", J. Appl. Phys., in press.

Ilavsky, J., Allen, A. A., Long, G. G., Krueger, S., Berndt, C. C., Herman, H., "Influence of Spray Angle on the Pore and Crack Microstructure of Plasma-Sprayed Deposits", J. Am. Ceram. Soc. **80**, 733 (1997).

Ilavsky, J., Stalick, J. K., "Phase Composition of Plasma-Sprayed YSZ", Proceedings of the 1st United Thermal Spray Conference (Indianapolis, IN, Sept. 15-18, 1997), in press.

Irvine, D. J., Mayes, A. M., Satija, S. K., Barker, J. G., Sofia-Allgor, S. J., Griffith, L. G., "Comparison of Tethered Star and Linear Poly(Ethylene Oxide) for Control of Biomaterials Surface Properties", J. Biomedical Mater. Res., in press.

Isaacs, E. D., Zschack, P., Broholm, C., Burnes, C., Aeppli, G., Ramirez, A. P., Oglesby, C. S., Bucher, E., Erwin, R. W., "Suppression of the Antiferromagnetic Moment in the Superconducting Phase of UPt_3", Phys. Rev. Lett. **75**, 1178 (1995).

Jackson, C. L., Sung, L., Han, C. C., "Evolution of Phase Morphology in Compatibilized Polymer Blends at Constant Quench Depths: Complementary Studies by Light Scattering and Transmission Electron Microscopy", Polym. Eng. Sci. **37**, 1449 (1997).

Jackson, C. L., Sung, L., Han, C. C., "Morphology and Phase Separation Kinetics of a Compatibilized Blend", ANTEC Proceedings **1**, 1559 (1996).

Kaduk, J. A., Toby, B., Wong-Ng, W., Greenwood, W., "Crystal Structure and Standard X-Ray Pattern of $Ba_4Ti_{10}Al_2O_{27}$", Powder Diffraction, in press.

Karen, P., Kjekshus, A., Huang, Q., Lynn, J. W., Rosov, N., Natali-Sora, I., Karen, V. L., Mighell, A. D., Santoro A., "Neutron and X-ray Powder Diffraction Study of $YBa_2Fe_3O_{\delta+w}$ Phases", J. Solid State Chem., in press.

Karim, A., Douglas, J. F., Satija, S. K., Wong, A. P. Y., Han, C. C., "Phase Separation in Chemically Reactive Polymer Films", Macromol., in press.

Karim, A., Douglas, J. F., Sung, L., Ermi, B., "Demixing of Polymer Blends in Ultrathin Films", Physics News in 1996 AIP, 70 (1997).

Karim, A., Slawecki, T. M., Kumar, S. K., Douglas, J. F., Han, C. C., Russell, T. P., Rafailovich, M., "Phase Separation in Symmetrically Segregating Thin Polymer Blend Films", Macromol., in press.

Karmonik, C., Udovic, T. J., Huang, Q., Rush, J. J., Andersson, Y., Flanagan, T. B., "Neutron Scattering Study of the Dynamics of Hydrogen and Deuterium Solved in Crystalline Pd_9Si_2", Physica B, in press.

Karmonik, C., Udovic, T. J., Paul, R. L., Rush, J. J., Lind, K., Hempelmann, R., "Observation of Dopant Effects on Hydrogen Modes in $SrCe_{0.95}M_{0.05}H_xO_{3-\delta}$ by Neutron Vibrational Spectroscopy", Solid State Ionics, in press.

Kellogg, G. J., Mayes, A. M., Stockton, W. M., Ferreira, M., Rubner, M. F., Satija, S. K., "Neutron Reflectivity Investigations of Self-Assembled Conjugated Polyion Multilayers", Langmuir **12**, 5109 (1996).

Kellogg, G. J., Walton, D. G., Mayes, A. M., Lambooy, P., Russell, T. P., Gallagher, P. D., Satija, S. K., "Observed Surface Energy Effects in Confined Diblock Copolymers", Phys. Rev. Lett. **76**, 2503 (1997).

Kent, M. S., Factor, B. J., Satija, S. K., Gallagher, P. D., Smith, G. S., "Structure of Bimodal Polymer Brushes in a Good Solvent by Neutron Reflectivity", Macromol. **29**, 2843 (1996).

Kent, M. S., Smith, G. S., Majewski, J., Lee, L. T., Satija, S. K., "Tethered Chains in Theta Solvent Conditions: An Experimental Study Involving Langmuir Diblock Copolymer Monolayers", J. Chem. Phys., in press.

Kepa, H., Goldman, K. I., Giebultowicz, T. M., Majkrzak, C. F., Springholz, G., Krenn, G., Holl, S., Schinagl, F., Bauer, G., "Antiferromagnetic Phase Transition and Interlayer Spin Coherence in Short-period EuTe/PbTe Superlattices", Superlattices and Microstructures, in press.

Kepa, H., Kleinwaks, L. J., Berk, N. F., Majkrzak, C. F., Berzina, T. S., Troitsky, V. I., Antolini, R., Feigin, L. A., "Neutron and X-Ray Reflectometry Studies of Rough Interfaces in a Langmuir-Blodgett Film", Physica B, in press.

Khasanova, N. R., Izumi, F., Hiroi, Z., Takano, M., Huang, Q., Santoro, A., "Redetermination of the Structure of $La_2Cu_2O_5$ by Neutron Powder Diffraction", Acta Crystallogr. C **52**, 2381 (1996).

Kline, S. R., Kaler, E. W., "Interactions in Colloidal Mixtures: Partial Structure Factors in Mixtures of Colloidal Silica and an Anionic Oil-in-Water Microemulsion", J. Colloids Interface Sci., in press.

Kline, S. R., Kaler, E. W., "An Optimization Regularization Method for Determination of Partial Structure Factors from Small-Angle Scattering Experiments", J. Appl. Cryst. **29**, 427 (1996).

Klosowski, P., Tischler, J., Könnecke, M., "NeXus—HDF-Based Data Exchange Standard: A Proposal for the Neutron Scattering Community", Physica B, in press.

Koneripalli, N., Levicky, R., Bates, F. S., Ankner, J. F., Kaiser, H., Satija, S. K., "Confined-Induced Morphological Changes in Diblock Copolymer Films", Langmuir **12**, 6681 (1996).

Koneripalli, N., Levicky, R., Matsen, M., Bates, F. S., Satija, S. K., Ankner, J. F., Kaiser, H., "Ordering in Blends of Diblock Copolymers", Macromol., in press.

Krueger, S., "SANS Provides Unique Information on the Structure and Function of Biological Macromolecules in Solution", Physica B, in press.

Krueger, S., Koenig, B. W., Orts, W. J., Berk, N. F., Majkrzak, C. F., Gawrisch, K. "Neutron Reflectivity Studies of Single Lipid Bilayers Supported on Planar Substrates", in *Neutrons in Biology*, ed. B. Schoenborn & R. Knott (Plenum Publishing Corp., New York, 1996), p. 205.

Kvardakov, V. V., Somenkov, V. A., Shilstein, S. Sh., Lynn, J. W., Mildner, D. R. R., Chen-Meyer, H., "Laue Focusing Effect and Its Applications", Physica B, in press.

Lartigue, C., Copley, J. R. D., Mezei, F., Springer, T., "Focusing of Neutron Beams Using Curved Mirrors for Small Angle Scattering", J. Neutron Research **5**, 71 (1996).

Lee, C., Guido, S. P., Pitskialis, M., Mays, J. W., Tan, N. B., Treviño, S. F., Hadjichristidis, N., "Asymmetric Single Graft Block Copolymers: Effect of Molecular Architecture on Morphology", Macromol. **30**, 3732 (1997).

Lee, C., Guido, S. P., Poulos, Y., Hadjichristidis, N., Tan, N. B., Treviño, S. F., Mays, J. W., "H-Shaped Double Graft Copolymers: Effect of Molecular Architecture on Morphology", J. Chem. Phys., in press.

Lee, S.-H., Broholm, C., Collins, M. F., Heller, L., Ramirez, A. P., Kloc, C., Bucher, E., Erwin, R. W., Lacevic, N., "Less than 50% Sublattice Polarization in an Insulating S=3/2 Kagomé Antiferromagnet at T≈0", Phys. Rev. B **56**, 8091 (1997).

Lee, S.-H., Cheong, S. W., "Melting of Quasi-Two-Dimensional Charge Stripes in $La_{1⅔}Sr_{⅓}NiO_4$", Phys. Rev. Lett **79**, 2514 (1997).

Levicky, R., Koneripalli, N., Tirrell, M., Satija, S. K., "Stratification in Bidisperse Polymer Brushes from Neutron Reflectivity", Phys. Rev. Lett., in press.

Li, W.-H, Chuang, W. Y., Wu, S. Y., Lee, K. C., Lynn, J. W., Tsay, H. L., Yang, H. D., "Superconductivity, Magnetic Fluctuations, and Magnetic Order in $TbSr_2Cu_{2.69}Mo_{0.31}O_7$", Phys. Rev. B **56**, 5631 (1997).

Lin, E. K., Wu, W.-L., Satija, S. K. Satija, "Measuring Polymer Dynamics near the Polymer-Solid Interface Using Neutron Reflectometry", Proc. ACS Div. Poly. Mat.: Sci. and Eng. **77**, 626 (1997).

Lin, E. K., Wu, W.-L, Satija, S. K., "Polymer Interdiffusion Near an Attractive Solid Substrate", Macromol., in press.

Lin, H., Steyerl, A., Satija, S. K., Karim, A., Russell, T. P., "Solvent Penetration into Ordered Thin Films of Diblock Copolymers", Macromol. **28**, 1470 (1995).

Lin, Y.-C., Chuang, W. Y., Li, W.-H., Lee, K. C., Lynn, J. W., Yang, C. L., Ku, H. C., "Crystal Structure and Magnetic Ordering of Pr in $(Pb_{0.5}Cu_{0.5})_2(Ba_{0.5})_2PrCu_2O_8$", J. Appl. Phys. **81**, 4940 (1997).

Lin, Y.-C., Wu, S. Y., Li, W.-H., Lee, K. C., Lynn, J. W., Lin, C. W., Lin, J.-Y., Yang, H. D., "Neutron Diffraction Studies of Pr Ordering in $PrBa_2Cu_4O_8$", Physica B, in press.

Livingston, R. A., Neumann, D. A., FitzGerald, S., Rush, J. J., "Quasi-elastic Neutron Scattering Study of the Hydration of Tricalcium Silicate", in *Neutrons in Research and Industry*, ed. G. Vourvopoulos (SPIE Proc. **2867**, 1997), p. 148.

Loezos, J. M., Vanderah, T. A., Drews, A. R., Roth, R. S., "A Series of 'Chemically Twinned Rutile' Oxides, $SrM_{2n+1}O_{4n+5}$ (M=Ti, Nb; $3 \geq n \geq 9$)", Powder Diffr. **12**, 117 (1997).

Lynn, J. W., "Rare Earth Magnetic Ordering in Exchange-Coupled Superconductors", J. Alloy. Compd. **250**, 552 (1997).

Lynn, J. W., Erwin, R. W., Borchers, J. A., Santoro, A.., Huang, Q., Peng, J.-L., Greene, R. L., "Magnetic, Structural and Spin Dynamical Properties of $La_{1-x}Ca_xMnO_3$", J. Appl. Phys. **81**, 5488 (1997).

Lynn, J. W., Skanthakumar, S., Huang, Q., Sinha, S. K., Hossain, Z., Gupta, L. C., Nagaragjan, R., Godart, C., "Magnetic Order and Crystal Structure in the Superconducting RNi_2B_2C Materials", Phys. Rev. B **55**, 6584 (1997).

Majkrzak, C. F., "Applications of Specular Neutron Reflectrometry in Materials Science", Workshop Proceedings, Gordon & Breach Publications, in press.

Majkrzak, C. F., Berk, N. F., Dura, J., Satija, S. K., Karim, A., Pedulla, J., Deslattes, R. D., "Direct Inversion of Specular Reflectivity", Physica B, in press.

Majkrzak, C. F., Berk, N. F., Dura, J., Satija, S. K., Karim, A., Pedulla, J., Deslattes, R. D., "Phase Determination and Inversion in Specular Neutron Reflectometry", Physica B, in press.

Mang, J. T., Kumar, S., Hammouda, B., "Lyotropic Liquid Crystals Under Simple Couette and Oscillatory Shear", Macromol., Proceedings of the 16th Conference on Liquid Crystals (1996).

Mansky, P., Russell, T. P., Hawker, C. J., Mays, J., Cook, D. C., Satija, S. K., "Interfacial Segregation in Disordered Block Copolymers: Effect of Tunable Surface Potentials", Phys. Rev. Lett. **79**, 237 (1997).

Markley, T. J., Toby, B. H., Pearlstein, R. M., Ramprasad, D., "New Synthesis Routes to Lithium and Cesium Cyanide Salts", Inorg. Chem. **36**, 3376 (1997).

Merzbacher, C. I., Barker, J. G., Swider, K. E., Rolison, D. R., "Structure of Ru-TI Oxide Aerogels: A SANS Study", J. Colloids Interface Science, in press.

Meuse, C. W., Krueger, S., Majkrzak, C. F., Dura, J. A., Fu, J., Conner, J. T., Plant, A. L., "Hybrid Bilayer Membranes in Air and Water: Infrared Spectroscopy and Neutron Reflectivity Studies", Biophys. J., in press.

Michel, K. H., Copley, J. R. D., "Orientational Fluctuations, Diffuse Scattering, and Orientational Order in Solid C_{60}", in *Fullerenes and Fullerene Nanostructures*, ed. H. Kuzmany, J. Fink, M. Mehring, S. Roth (World Scientific, Singapore, 1996), p. 318.

Michel, K. H., Copley, J. R. D., "Orientational Mode Coupling, Diffuse Scattering, and the Order-Disorder Phase Transition in Solid C_{60}", Z. Phys. B Cond. Matt. **103**, 369 (1997).

Moss, S. C., Robertson, J. L., Neumann, D. A., Reinhard, L., "Anomalous Static Displacements and Their Relation to Lattice Dynamics in $Fe_{0.53}Cr_{0.47}$", Comp. Mater. Science **8**, 33 (1997).

Moudden, A. H., Pinsard, L., Vasiliu-Doloc, L., Revcolevschi, A., "Spin Dynamics of $La_{2/3}Sr_{1/3}MnO_3$", Czech. J. Phys. **46**, S4 2163 (1996).

Moudden, A. H., Vasiliu-Doloc, L., Goukassov, A., de Leon-Guevara, A. M., Pinsard, L., Revcolevschi, A., "Spin Waves of Lightly Doped $La_{1-x}Sr_xMnO_3$", Physica B **234-236**, 859 (1997).

Nakatani, A. I., Sung, L., Hobbie, E. K., Han, C. C., "Shear-Induced Ordering in a Homopolymer Blend with Block-Copolymer 'Surfactant'", Phys. Rev. Lett., in press.

Noh, H., Flanagan, T. B., Sakamoto, Y., Barker, J. G., "Hydrogen-Induced Lattice Migration in Pd-Pt Alloys", Acta Mater., in press.

Okui, H., Omura, Y., Wada, N., Kamitakahara, W. A., Fujiwara, A., Suematsu, H., Murakami, Y., "Structural, Lattice-Dynamical and Magnetic Properties of Alkali-Metal Intercalated Vermiculite", Mol. Cryst. Liquid Cryst., in press.

Orts, W. J., VanderHart, D. L., Bluhm, T. L., Marchessault, R. H., "Cocrystallization in Random Copolymers of Poly[β-Hydroxybutyrate-Co-β-Hydroxyvalerate] and Its Effect on Crystalline Morphology", Can. J. Chem. **73**, 2094 (1995).

Papanek, P., Fischer, J. E., Murthy, N. S., "Molecular Vibrations in Nylon 6 Studied by Inelastic Neutron Scattering", Macromol. **29**, 2253 (1996).

Pellegrini, N. N., Sikka, M., Satija, S. K., Winey, K. I., "Interfacial Widths Between Poly(styrene-co-methyl methacrylate) Copolymers and Homopolymers", Macromol., in press.

Pellegrini, N. N., Sikka, M., Satija, S. K., Winey, K. I., "Segregation of a Random Copolymer from Miscible Blends", Macromol., in press.

Petrash, S., Liebmann-Vinson, A., Foster, M. D., Lander, L. M., Brittain, W. J., Majkrzak, C. F., "Neutron and X-Ray Reflectivity Studies of Human Serum Albumin Adsorption onto Functionalized Surfaces of Self-Assembled Monolayers", Biotechnol. Progr. **13**, 635 (1997).

Prask, H. J., "Nondestructive Characterization of Materials at the NIST Research Reactor", Proceedings of the Eighth International Conference on Nondestructive Characterization of Materials (Denver, CO, June 1997), in press.

Prask, H. J., Brand, P. C., "Determination of Residual Stress by Means of Neutron Diffraction", Proceedings of Energy Week Conference and Exhibition, in Book IV, *Energy Engineering* (1997), p. 189.

Prask, H. J., Brand, P. C., "The Determination of Residual Stress by Means of Neutron Diffraction," Proceedings of the Spring Conference of the Society for Experimental Mechanics (1997), p. 140.

Prask, H. J., Brand, P. C., "The Determination of Residual Stresses in Composites by Means of Neutron Diffraction," Proceedings of the Fourth International Conference on Composites Engineering, ed. D. Hui (1997), p. 807.

Prask, H. J., Brand, P. C., "Residual Stress Determination by Means of Neutron Diffraction", in *Neutrons in Research and Industry* (SPIE Proc. **2867**, 1997), p. 106.

Prince, E., "Neutron Instrumentation", *American Chemical Society Encyclopedia of Scientific Instrumentation*, ed. Thomas Bruno, in press.

Prince, E., Wilkinson, C., McIntyre, G. J. "Comparison of the σ[I]/I and Least Squares Methods for Integration of Bragg Relflections", J. Appl. Crystallogr. **30**, 133 (1997).

Richter, D., Schneiders, D., Monkenbusch, M., Willner, L., Fetters, L. J., Huang, J. S., Lin, M., Mortensen, K., Farago, B., "Polymer Aggregates with Crystalline Cores: The System Polyethylene-Poly(ethylenepropylene)", Macromol. **30**, 1053 (1997).

Rowe, J. M., Williams, R. E., Prask, H. J., "Utilization of the NIST Research Reactor", Proceedings of the Asian Symposium on Research Reactors (Taejon, Korea), 1996.

Sachidanandam, R., Yildirim, T., Harris, A. B., Aharony, A., Entin-Wohoman, O., "Single Ion Anisotropy, Crystal Field Effects, Spin Reorientation Transitions, and Spin Waves in R_2CuO_4", Phys. Rev. B **56**, 260 (1997).

Samuelson, S., Tobias, D. J., Mortyna, G. J., "Modern Computational Methodology Applied to the Simulation of Blocked Trialanine Peptide in Vacuo, Water Clusters, and Bulk Water", J. Phys. Chem. B **101**, 7592 (1997).

Sanders, P. G., Weertman, J. R., Barker, J. G., "Structure of Nanocrystalline Palladium and Copper Studied by Small Angle Neutron Scattering", J. Mater. Res. **11**, 3110 (1997).

Santodonato, L. J., Neumann, D. A., Erwin, R. W., "Template Mediated Growth of Rare Earth Carbides", J. Am. Chem. Soc. **118**, 12860 (1996).

Satija, S. K., Gallagher, P. D., "Neutron Reflectivity Study of a Chemically End-Grafted Polystyrene Brush in a Binary Solvent Mixture", Proceedings of the 5th International Conference on Surface X-Ray and Neutron Scattering, in press.

Satija, S. K., Gallagher, P. D., Karim, A., Fetters, L. J., "Density Profile of a Polystyrene Brush in a Critical Binary Solvent Mixture", Physica B, in press.

Sauvajol, J. L., Papanek, P., Fischer, J. E., Dianoux, A. J., McNeillis, P. M., Mathis, C., Francois, B., "Dynamics of Pristine and Doped Conjugated Polymers: A Combined Inelastic Neutron Scattering and Computer Simulation Analysis", Synthetic Metals **84**, 941 (1997).

Savin, S., Harris, A. B., Yildirim, T., "Towards a Microscopic Approach to the Intermolecular Interaction in Solid C_{60}", Phys. Rev. B **55**, 14182 (1997).

Schreyer, A., Majkrzak, C. F., Zeidler, Th., Schmitte, T., Bödeker, P., Theis-Brohl, K., Abromeit, A., Dura, J. A., Watanabe, T., "The Magnetic Structure of Cr in Exchange Coupled Fe/Cr(001) Superlattices", Phys. Rev. Lett., in press.

Sichla, T., Altorfer, F., Hohlwein, D., Reimann, K., Steube, M., Wrzesinski, J., Jacobs, H., "Crystal Structure Determination of a Strontium Hydride Imide Nitride – $Sr_2(H)N/SrNH$ resp. $Sr_2(D)N/SrND$ – by X-Ray, Neutron, and Synchrotron Radiation", Z. Anorg. Chem. **623**, 414 (1997).

Sinha, S. K., Feng, Y. P., Melendres, C. A., Lee, D. D., Russell, T. P., Satija, S. K., Sirota, E. B., Sanyal, M. K., "Off-Specular X-Ray Scattering Studies of the Morphology of Thin Films", Physica A **231**, 99 (1996).

Skanthakumar, S., Lynn, J. W., Dogan, F., "Spin Dynamics of Er^{3+} in $ErBa_2Cu_3O_{7-\delta}$", J. Appl. Phys. **81**, 4934 (1997).

Skanthakumar, S., Lynn, J. W., Mazumdar, C., Nagarajan, R., Gupta, L. C., "Magnetic Phase Transitions in $R_2Ni_3Si_5$", Physica B, in press.

Skanthakumar, S., Lynn, J. W., Rosov, N., Cao, G., Crow, J. E., "Observation of Pr Magnetic Order in $PrBa_2Cu_3O_7$", Phys. Rev. B **55**, R3406 (1997).

Skripov, A. V., Cook, J. C., Karmonik, C., Hempelmann, R., "Localized Motion of Hydrogen in C15-type TaV_2: A Quasielastic Neutron Scattering Study", J. Phys. Cond. Matt. **8**, L319 (1996).

Skripov, A. V., Cook, J. C., Karmonik, C., Hempelmann, R., "Localized Motion of Hydrogen in C15-type TaV_2: Nuclear Magnetic Resonance and Neutron Scattering Study", J. Alloy. Compd. **253**, 432 (1997).

Skripov, A. V., Cook, J. C., Sibirtsev, D. S., Karmonik, C., Hempelmann, R., "Quasielastic Neutron Scattering Study of Hydrogen Motion in C15-type TaV_2H_x", J. Phys. Cond. Matt., in press.

Slade, R. C. T., Hall, G. P., Ramanan, A., Prince, E., "Structure and Proton Conduction in Pyrochlore-type Antimonic Acid: A Neutron Diffraction Study", Solid State Ionics **92**, 171 (1996).

Springholz, G., Chen, J. J., Frank, N., Ueta, Y., Marschner, G., Pichler, C., Bauer, G., Dresselhaus, M. S., Dresselhaus, G., Giebultowicz, T. M., Nunez, V., Salamanaca-Riba, L., "Monolayer Short Period Superlattices of Narrow Gap PbTe and Antiferromagnetic Wide Band Gap EuTe", Inst. Phys. Conf. Ser. **144**, 167 (1995).

Stalick, J. K., Santoro, A., "Crystal Chemistry of the Substitution Compounds of $Ba_2YCu_3O_7$", in *Current Status and Future Directions in Condensed Matter Physics*, ed. S.K. Malik (Plenum, New York), in press.

Stoffel, N. C., Dai, C-A., Kramer, E. J., Russell, T. P., Deline, V., Volksen, W., Wu, W.-L., Satija, S. K., "High Resolution Profiling of the Polyimide-Polyimide Interface", Macromol. **29**, 2880 (1996).

Straty, G. C., Munzy, C. D., Butler, B. D., Lin, M. Y., Slawecki, T., Glinka, C. J., Hanley, H. J. M., "A Rheometric Shearing Apparatus at the NIST Center for Neutron Research (NCNR)", Nucl. Instr. Meth., in press.

Straty, G. C., Munzy, C. D., Butler, B. D., Lin, M. Y., Slawecki, T., Glinka, C. J., Hanley, H. J. M., "An In-Situ Rheometric Shearing Apparatus for SANS", Physica B, in press.

Subramanian, M. A., Toby, B. H., Ramirez, A. P., Marshall, W. J., Sleight, A. W., Kwei, G. H., "Colossal Magnetoresistance without $Mn^{3+}Mn^{4-}$ Double Exchange in the Stoichiometric Pyrochlore $Tl_2Mn_2O_7$", Science **273**, 81 (1996).

Sung, L., Hess, D. B., Jackson, C. L., Han, C. C., "Phase Separation Kinetics and Morphology in a Polymer Blend with Diblock Copolymer Additive", J. Polym. Res. (Taiwan) **3**, 139 (1996).

Sung, L., Nakatani, A. I., Han, C. C., Karim, A., Douglas, J. F., Satija, S. K., "The Role of the Copolymer Additives on Phase Behavior of a Polymer Blend", Physica B, in press.

Thirtle, P. N., Li, Z. X., Thomas, R. K., Rennie, A. R., Satija, S. K., Sung, L. P., "Structure of Non-Ionic Surfactant Layers Adsorbed at the Solid/Liquid Interface on Self-Assembled Monolayers with Different Surface Functionally: A Neutron Reflection Study", Langmuir, in press.

Tobias, D. J., Mar, W., Blasie, V. K., Klein, M. L., "Molecular Dynamics Simulations of a Protein on Hydrophobic and Hydrophilic Surfaces", Biophys. J. **71**, 2933 (1996).

Tobias, D. J., Tu, K., Klein, M. L., "Assessment of All-Atom Potentials for Modeling Membranes: Molecular Dynamics Simulations of Solid and Liquid Alkanes and Crystals of Phospholipid Frangments", J. Chim. Phys. **94**, 1482 (1997).

Tobias, D. J., Tu, K., Klein, M. L., "Atomic-Scale Molecular Dynamics Simulations of Lipid Membanes", Curr. Opin. Colloid In. **2**, 15 (1997).

Torikai, N., Noda, I., Karim, A., Satija, S. K., Han, C. C., Matsushita, Y., Kawakatsu, T., "Neutron Reflection Studies on Segment Distribution of Block Chains in Lamellar Microphase-Separated Structures", Macromol. **30**, 2907 (1997).

Udovic, T. J., Huang, Q., Rush, J. J., "Comment on 'Theoretical Prediction of the Structure of Insulating YH_3'", Phys. Rev. Lett., in press.

Udovic, T. J., Rush, J. J., Flanagan, T. B., Noh, H., Andersson, Y., "Vibrational Dynamics of Hydrogen and Deuterium in Crystalline Pd_9Si_2", J. Alloy. Compd. **253-254**, 255 (1997).

Udovic, T. J., Rush, J. J., Huang, Q., Anderson, I. S., "Neutron Scattering Studies of the Structure and Dynamics of Rare-Earth Hydrides and Deuterides", J. Alloy. Compd. **253-254**, 241 (1997).

Uma, S., Schnelle, W., Gmelin, E., Rangarajan, G., Skanthakumar, S., Lynn, J. W., Walter, R., Lorenz, T., Buchner, B., Walker, E., Erb, A., "Magnetic Ordering in Single Crystals of $PrBa_2Cu_3O_{7-\delta}$", J. Phys. Lett., in press.

Vasiliu-Doloc, L., Lynn, J. W., Moudden, A. H., de Leon-Guevara, A. M., Revcolevschi, A., J. "Neutron Scattering Investigation of the Structure and Spin dynamics of $La_{0.85}Sr_{0.15}MnO_3$", J. Appl. Phys. **81**, 5491 (1997).

Vasiliu-Doloc, L., Lynn, J. W., Mukovskii, Y. M., Arsenov, A. A., Shulyatev, D. A., "Spin Dynamics of Strongly-Doped $La_{1-x}Sr_xMnO_3$", J. Appl. Phys., in press.

Vierheller, T. R., Foster, M. D., Schmidt, A., Mathauer, K., Knoll, W., Wegner, G., Satija, S. K., Majkrzak, C. F., "Structure and Stability of Two-Component Langmuir-Blodgett Multilayers Containing Cadmium Arachidate and Polyglutamate Determined by Reflectivity", Langmuir **13**, 1712 (1997).

Vierheller, T. R., Foster, M. D., Wu, H., Schmidt, A., Knoll, W., Satija, S., Majkrzak, C. F., "Stability of Cadmium Arachidate Langmuir-Blodgett Multilayers as Determined by Neutron and X-Ray Reflectivity", Langmuir **12**, 5156 (1996).

Walton, D. G., Soo, P. P., Mayes, A. M., Algor, S. J. S., Fujii, J. T., Griffith, L. G., Ankner, J. F., Kaiser, H., Johansson, J., Smith, G. D., Barker, J. G., Satija, S. K., "Creation of Stable Hydrophilic Surfaces with Branched Copolymers", Nature, in press.

Walton, D. G., Soo, P. P., Mayes, A. M., Algor, S. J. S., Fujii, J. T., Griffith, L. G., Ankner, J. F., Kaiser, H., Johansson, J., Smith, G. D., Barker, J. G., Satija, S. K., "Creation of Stable Poly(Ethylene Oxide) Surfaces on Poly(Methyl Methacrylate) Using Blends of Branched and Linear Polymers", Macromol., in press.

Wang, H., Kesani, P. K., Balsara, N. P., Hammouda, B., "Undulations and Disorder in Block Copolymer Lamellae under Shear Flow", Macromol. **30**, 982 (1997).

Wiesler, D. G., Majkrzak, C. F., "Growth and Dissolution of Protective Oxide Films on Titanium: An In-Situ Neutron Reflectivity Study", Proceedings of the Symposium BB 1994 Fall Meeting of the MRS, ed. D. A. Neumann, T. P. Russell, and B. J. Wuensch (Pittsburgh, PA, 1995).

Wiesler, D. G., Suzuki, M., Suzuki, I. S., Rosov, N., "Magnetic Neutron Scattering Study of $MnCl_2$ Graphite Intercalation Compound", Phys. Rev. B **55**, 6382 (1997).

Weissmüller, J., McMichael, R. D., Barker, J. G., Brown, H. J., Erb, U., Shull, R. D., "Magnetic Microstructure of a Nanocrystalline Ferromagnet-Miromagnetic Model and Small Angle Neutron Scattering", MRS Symp. Proc. **457**, 231 (1997).

Williams, R. E., Rowe, J. M., Blau, M., "Benchmark of the Nuclear Heat Deposition in the NIST Liquid Hydrogen Cold Source", Proceedings of the 9th International Symposium on Reactor Dosimetry (Prague, Sept. 2-6, 1996), in press.

Wilson, A. J. C., Karen, V. L., Mighell, A., "The Space-group Distribution of Molecular Organic Structures", Int. Tables for Crystallography, Vol. C, in press.

Wischnewski, A., Buchenau, U., Dianoux, A. J., Kamitakahara, W. A., Zarestky C., "Sound Wave Scattering in Silica", Philosophical Magazine, in press.

Wong-Ng, W., Toby, B. H., Greenwood, W., "Crystallographic Studies of BaR_2ZnO_5 (R = La, Nd, Dy, Ho, Er and Y)", Powder Diffraction, in press.

Worcester, D., Hammouda, B., "Interdigitated Hydrocarbon Chains in C20 and C22 Phos-

phatidylcholines Induced by Hydrostatic Pressure", Physica B, in press.

Wu, W.-H., Li, K. C., Lynn, J. W., Meen, T. H., Yang, H. D., "Two- and Three-dimensional Magnetic Correlations of Tb in $Pb_2Sr_2TbCu_3O_8$", Phys. Rev. B **54**, 10019 (1996).

Wu, Y.-C., Wu, S. Y., Li, W.-H., Lee, K. C., Lynn, J. W., Lin, C. W., Lin, J.-Y., Yang, H. D., "Neutron Diffraction Studies of Pr Ordering in $PrBa_2Cu_4O_8$", Physica B, in press.

Ye, X., Narayanan, T., Tong, P., Huang, J. S., Lin, M. Y., Carvalho, B. L., Fetter, L. J., "Depletion Interactions in Colloid-Polymer Mixtures", Phys. Rev. E, in press.

Yildirim, T., "Ordering Due to Disorder in Frustrated Quantum Magnetic Systems", Turkish J. Phys., in press.

Yildirim, T., Barbedette, L., Fischer, J. E., Bendele, G. M., Stephens, P. W., Lin, C. L., Goze, C., Rachdi, F., Robert, J., Petit, P., Palstra, T. T. M., "Synthesis and Properties of Mixed Alkali-Metal-Alkaline-Earth Fullerides", Phys. Rev. B **54**, 11981 (1996).

Yildirim, T., Gehring, P. M., Neumann, D. A., Eaton, P. E., Emrick, T., "Solid Cubane: A Brief Summary", Carbon, in press.

Yildirim, T., Gehring, P. M., Neumann, D. A., Eaton, P. E., Emrick, T., "Unusual Structure, Phase Transition, and Dynamics of Solid Cubane", Phys. Rev. Lett. **78**, 4938 (1997).

Yildirim, T., Harris, A. B., Shender, E. F., "Frustrations and Quantum Fluctuations in Heisenberg FCC Antiferromagnets", Phys. Rev. B, in press.

Yildirim, T., Sachidanandam, R., Harris, A. B., Aharony, A., and Entin Wohlman, O., "Single Ion Anisotropy, Crystal Field Effects, and Spin Waves in R_2CuO_4", Phys. Rev. B, in press.

Zaliznyak, I. A., Dender, D. C., Broholm, C., Reich, D. H., "Tuning the Spin Hamiltonian of NENP by External Pressure: A Neutron Scattering Study", Phys. Rev. B, in press.

Zhou, C. L., Hobbie, E. K., Bauer, B. J., Sung, L., Jiang, M., Han, C. C., "Control of Interaction Strength in Hydrogen-Bonded Polymer Blends via the Density of Hydroxyl Group", Macromol., in press.

Zhou, P., Papanek, P., Lee, R., Fischer, J. E., Kamitakahara, W. A., "Local Structure and Vibrational Spectroscopy of Disordered Carbons for Li Batteries: Neutron Scattering Studies", J. Electrochem. Soc. **144**, 1744 (1997).

Zielinski, R. G., Kline, S. R., Kaler, E. W., Rosov, N., "A Small-Angle Neutron Scattering Study of Water in Carbon Dioxide Microemulsions", Langmuir **13**, 3934 (1997).

Independent Publications

Abdurashitov, J.N., Nico, J.S., et al., "The Russian-American Gallium Experiment (SAGE) Cr-neutrino Source Measurement", Phys. Rev. Lett. **77**, 4708 (1996).

Abe, K., Akagi, T., Anderson, B. D., Thompson, A. K., et al., "Next-to-leading Order QCD Analysis of Polarized Deep Inelastic Scattering Data", Phys. Lett. B **405**, 180 (1997).

Abe, K., Thompson, A.K., et al., "Measurement of the Neutron Spin Structure Function g^n_2 and Asymmetry A^n_2", Phys. Lett. B **404**, 377 (1997).

Abe, K., Thompson, A.K., et al., "Precision Determination of the Neutron Spin Structure Function g^n_1", Phys. Rev. Lett. **79**, 26 (1997).

Adams, J.M., McGarry, E.D., Hawari, A.I., and Venkataraman, R., "The Materials Dosimetry Reference Facility Round Robin Tests of ^{237}Np and ^{238}U Fissionable Dosimeters", Reactor Dosimetry, World Scientific Publishing, July, 1997, in press.

Alamo, R. G., Graessley, W. W., Krishnamoorti, R., Lohse, D. J., Londono, J. D., Mandelkern, L., Stehling, F. C., Wignall, G. D., "SANS Investigations of Melt Miscibility and Phase Segregation in Blends of Linear and Branched Polyethylenes as a Function of Branch Content", Macromol. **30**, 561 (1997).

Amis, E. J., Topp, A., Bauer, B. J., Tomalia, D. A., "SANS Study of Labeled PAMAM Dendrimer", ACS PMSE Proceedings **77**, 183 (1997).

Anderson, D. L., Cunningham, W. C., "Nondestructive Determination of Lead, Cadmium, Tin, Antimony, and Barium in Ceramic Glazes by Radioisotope X-Ray Fluorescence Spectometry", J. AOAC Int. **79**, 1141 (1996).

Andonie Zaror, O., Soria Juarez, R., Zeiller, E., Zeisler, R.L., "A Separation Method to Overcome the Interference of Calcium on the Uranium Determination by ICP-ES", Fresen. J. Anal. Chem. **355**, 696 (1996).

Baker, J. E., Poster, D. L., Church, T. M., Scudlark, J. R., Ondov, J. M., Dickhut, R. M., Cutter, G., "Loadings of Atmospheric Trace Elements and Organic Contaminants to the Chesapeake Bay", in *Atmospheric Deposition of Contaminants to the Great Lakes and Coastal Waters*, ed. J. E. Baker (Setac Publication Series), 1996.

Bardayan, D.W., daCruz, M.T.F., Hindi, M.M., Barghouty, A.F., Chan, Y.D., Garcia, A., Larimer, R.M., Lesko, K.T., Norman, E.B., Rossi, D.F., Wietfeldt, F.E., and Zlimen, I., "Radioisotope Yields from 1.85-GeV Protons on Mo and 1.85- and 5.0-GeV Protons on Te", Phys. Rev. C **55**, 820 (1996).

Bauer, B. J., Topp, A., Prosa, T. J., Amis, E. J., Yin, R., Qin, Q., Tomalia, D. A., "SANS and SAXS Investigations of the Internal Structure of Dendritic Molecules", ACS PSME Proceedings **77**, 82 (1997).

Beaucage, G., Rane, S., Sukumaran, S., Satkowski, M. M., Schechtman, L. A., Doi, Y., "Persistence Length of Isotactic Poly(hydroxy butyrate)", Macromol. **30**, 4158 (1997).

Beaucage, G., Sukumaran, S., Clarson, S. J., Kent, M. S., Schaefer, D. W., "Symmetric, Isotopic Blends of Poly(dimethylsiloxane)", Macromol. **29**, 8349 (1996).

Becker, D.A., "Characterization and Use of the New NIST Rapid Pneumatic Tube Irradiation Facility", J. Radioanal. Nucl. Chem., in press.

Becker, D.A., "Nuclear Analytical Methods: Past, Present, and Future", Trans. Am. Nucl. Soc. **75**, 11 (1996).

Becker, D.A., Brinkman, D.W., "Recycled Oil", (1996 Revision) *Kirk-Othmer Encyclopedia of Chemical Technology, Fourth Edition*, ed.

J. Kroschewitz (John Wiley & Sons, New York, 1997), p. 1.

Becker, P., Mackey, E.A., Demiralp, R., Schantz, M., Koster, B.J., Wise, S.A., "Concentrations of Chlorinated Hydrocarbons and Trace Elements in Marine Mammal Tissues Archived in the U.S. National Biomonitoring Specimen Bank", Proceedings of the Chemosphere BESB-2 Symposium, Chemosphere **34**, 2067 (1997).

Becker, P.R., Mackey, E.A., Demiralp, R., Koster, B.J., Wise, S.A., "Establishing Baseline Levels of Elements in Marine Mammals through Analysis of Banked Liver Tissues", Chapter 23 ACS Symposium Series 654, *Environmental Biomonitoring: Exposure Assessment and Specimen Banking*, ed. K.S. Subranian and G.V. Iyengar, American Chemical Society, Washington, DC (1997).

Bellows, R.J., Lin, M.Y., Arif, M., Thompson, A.K., Jacobson, D., "Neutron Imaging Technique for In-Situ Measurement of Water Transport Gradients Within Nafion in Polymer Electrolyte Fuel Cells", Electrochimica Acta, in press.

Benenson, R. E., Chen-Mayer, H. H., Sharov, V., "A Portable Time-of-Flight System for Thermal and Cold Neutron Applications", Rev. Sci. Instru. **67**, 2770 (1996).

Bindra, C., Nalimova, V. A., Fischer, J. E., "In-plane Structure and Thermal Instability of $LiC_{2.18}$ Based on Boron-doped Graphite", Mol. Cryst. Liquid Cryst., in press.

Bindra, C., Nalimova, V. A., Sklovsky, D. E., Benes, Z., Fischer, J. E., "Super-dense LiC_2 as a High Capacity Li Intercalation Anode", J. Electrochem. Soc., in press.

Bishop, R. L., van Zelst, L., "Chemical Charaterization of Archaeological Ceramics at the Conservation Analytical Laboratory", Techne **5**, 46 (1997).

Brasher, L. L., Kaler, E. W., "A Small-Angle Neutron Scattering (SANS) Contrast Variation Investigation of Aggregate Composition in Catanionic Surfactant Mixtures", Langmuir **12**, 6270 (1996).

Briber, R. M., Fodor, J. S., Russell, T. P., Miller, R. D., Carter, K. R., Hedrick, J. L., "Characterization of Thin Polymeric Nanofoam Films by Transmission Electron Microscopy and Small Angle Neutron Scattering", in *Morphological Control of Multiphase Polymer Mixtures*, ed. R. M. Briber, C. C. Han, D. G. Peiffer, MRS Symposium Proceedings Series **461**, 108 (1997).

Butler, B. D., Muzny, C. D., Hanley, H. J. M., "Dynamic Structure Factor Scaling in Dense Gelling Silica Suspensions", J. Phys. Cond. Matt. **8**, 9457 (1996).

Butler, B. D., Muzny, C. D., Hanley, H. J. M., "Scaling of Small-Angle Neutron Scattering Intensities from Gelling Colloidal Silica", Int. J. Thermophys., in press.

Caffrey, P. F., Ondov, J. M., "Determination of Particle Dry Deposition Velocities Over Southern Lake Michigan Using Elemental Compositions Determined by Instrumental Neutron Activation Analysis", Trans. Amer. Nuc. Soc., in press.

Caffrey, P. F., Ondov, J. M., Zufall, M. J., Davidson, C. I., "Determination of Size-Dependent Dry-Particle Deposition Velocities with Multiple Intrinsic Elemental Tracers", Environ. Sci. Technol., in press.

Caffrey, P. F., Suarez, A. E., Ondov, J. M., Han, M., "Importance of Fine Particle Loading to Fluxes of Trace Elements Dry Depositing onto Lake Michigan", J. Aerosol Sci. **27**, S31 (1996).

Carlson, A.D., "Status of the NEANSC Subgroup Working on Improving the $^{10}B(n, \alpha)$ Standard Cross Sections", Proceedings of the 9th International Symposium on Reactor Dosimetry (Prague, Sept. 2-6, 1996), in press.

Carlson, A.D., Chiba, S., Hambsch, F.-J., Olsson, N., Smirnov, A.N., "Summary of the Update to Nuclear Data Standards for Nuclear Measurements", Proceedings of the International Conference on Nuclear Data for Science and Technology (Trieste, Italy, May 19-24, 1997), in press.

Carlson, A.D., Chiba, S., Hambsch, F.-J., Olsson, N., Smirnov, A.N., "Update to Nuclear Data

Standards for Nuclear Measurements," Summary Report of an International Atomic Energy Agency Consultants' Meeting on Nuclear Data Standards (Vienna, Austria, Dec. 2-6, 1996), INDC(NDS)-368 (1997).

Chen, S.-H., Choi, S.-M., "The Gaussian Curvature of the Oil-Water Interface in an Isometric Bicontinuous Microemulsion", Physica A **236**, 38 (1997).

Chen, S. H., Lee, D. D., Kimishima, K., Jinnai, H., Hashimoto, T., "Measurement of the Gaussian Curvature of the Surfactant Film in an Isometric Bicontinuous One-Phase Microemulsion", Phys. Rev. E **54**, 6526 (1996).

Chen-Mayer, H.H., Lamaze, G.P., "Depth Distribution of Boron Determined by Slow Neutron Induced Lithium Emission", Nucl. Instrum. Meth. B, in press.

Chen-Mayer, H.H., Lamaze, G.P., Mildner, D.F.R., Downing, R.G., "Neutron Depth Profiling of Elemental Concentration Using a Focused Neutron Beam", Neutrons in Research and Industry (SPIE Proc. **2867**, 1997), p. 140.

Chen-Mayer, H.H., Mildner, D.F.R., Sharov, V.A., Ullrich, J.B., Ponomarev, I.Yu., Downing, R.G., "Monolithic Polycapillary Neutron Focusing Lenses: Experimental Characterizations", J. Phy. Soc. Japan, **65**, Suppl. A, 319 (1996).

Chen-Mayer, H.H., Mildner, D.F.R., Sharov, V.A., Xiao, Q.F., Cheng, Y.T., Lindstrom, R.M., Paul, R.L., "A Polycapillary Bending and Focusing Lens for Neutrons", Rev. Sci. Instrum., in press.

Chen-Mayer, H.H., Sharov, V.A., Mildner, D.F.R., Downing, R.G., Paul, R.L., Lindstrom, R.M., Zeissler, C.J., Xiao, Q.F., "Capillary Neutron Optics for Prompt Gamma Activation Analysis", J. Radioanal. Nucl. Chem. **215**, 141 (1997).

Cunningham, W. C., Anderson, D. L., Capar, S. G., "Determination of Sodium in Biological Materials by Instrumental Neutron Activation Analysis", J. AOAC Int. **80**, 871 (1997).

Dender, D. C., Lefmann, K., Reich, D., Broholm, C., Aeppli, G., "Magnetic Properties of a Quasi-One-Dimensional S=1/2 Antiferromagnet: Copper Benzoate", Phys. Rev. B **53**, 2583 (1996).

Divita, F., Ondov, J. M., "Size Spectra and Growth of V-Containing Aerosol in Washington, D. C.", Aerosol Sci. Tech. **25**, 256 (1996).

Donais, M.K., Saraswati, R., Mackey, E.A., Demiralp, R., Porter B.J., Vangel, M., Levenson, M., Mandic, V., Azemard, S., Horvat, M., May, K., Emons, H., Wise, S.A., "Certification of Three Mussel Tissue Standard Reference Materials (SRM) for Methylmercury and Total Mèrcury Content", Fresen. J. Anal. Chem. **358**, 424 (1997).

Downing, R.G., Iyengar, G.V., "Methodological Issues in the Analytical Determination of Boron", Environ. Health Perspect., in press.

Downing, R.G., Lamaze, G.P., "Nondestructive Characterization of Semiconductor Materials Using Neutron Depth Profiling", Proceedings International Workshop on Semiconductor Characterization: Present Status and Future Needs, in press.

Downing, R.G., Xiao, Q.F., Sharov, V.A., Ponomarev, I.Yu., Ullrich, J.B., Gibson, D.M., Chen-Mayer, H.H., Mildner, D.F.R., Lamaze, G.P., "Improvements in Neutron Beam Applications by Using Capillary Optics", Neutrons in Research and Industry (SPIE Proc. **2867**, 1997), p. 566.

Ejnisman, R., Goldman, I.D., Pascholati, P.R., da Cruz, M.T.F., Olivera, R.M., Norman, E.B., Zlimen, I., Wietfeldt, F.E., Larimer, R.M., Chan, Y.D., Lesko, K.T., and Garcia, A., "Cross-Sections for $^{45}Sc(p,2n)^{44}Ti$ and Related Reactions", Phys. Rev. C **54**, 2047 (1996).

En, Z., Brenizer, J.S., Hostica, B., Gao, J., Becker, D.A., "Nitrogen Distribution Measurements by Neutron Induced Autoradiography", J. Radioanal. Nucl. Chem., in press.

Ermi, B. D., Amis, E. J., "Influence of Backbone Solvation on Small Angle Neutron Scattering from Polyelectrolyte Solutions", Macromol., in press.

Ermi, B. D., Amis, E. J., "Model Solutions for Studies of Salt-Free Polyelectrolytes", Macromol. **29**, 2701 (1996).

Factor, B. J., Mopsik, F. I., Han, C. C., "Dielectric Behavior of a Polycarbonate/Polyester Mixtures Upon Transesterification", Macromol. **29**, 2318 (1996).

Fajgelj, A., Zeisler, R., "Particle Size Determination of Some IAEA and NIST Environmental and Biological Reference Materials", Fresen. J. Anal. Chem., in press.

Fetters, L. J., Graessley, W. W., Krishnamoorti, R., Lohse, D. J., "Melt Chain Dimensions of Poly(Ethylene-1-Butene) Copolymers via Small Angle Neutron Scattering", Macromol. **30**, 4973 (1997).

Fetters, L. J., Huang, J. S., Stellbrink, J., Willner, L., Richter, D., "Association Behavior of Living Anionic Lipophobic Head-Groups in Hydrocarbon Mileau", Macromol. Symp. **121**, 1 (1997).

Flynn, C. P., Salamon, M. B., "Synthesis and Properties of Single Crystal Nanostrucutres", *Handbook on the Physics and Chemistry of Rare-Earths, Vol. 22*, ed. K. A. Gschnieder and R. Eyring (Elsevier Science, Amersterdam, 1996), Ch. 147.

Fokin, V.S., Chen-Mayer, H. H., Sharov, V.A., Mildner, D.F.R., "Neutron Transmission Through Curved Nickel Capillaries", Nucl. Instrum. Meth. A, in press.

Glatter, O., Strey, R., Schubert, K.-V., Kaler, E. W., "Small Angle Scattering Applied to Microemulsions", Ber. Bunsenges. Phys. Chem. **100**, 323 (1996).

Goldmints, I., von Gottberg, F. K., Smith, K. A., Hatton, T. A., "Small-Angle Neutron Scattering Study of PEO-PPO-PEO Micelle Structure in the Unimer-to-Micelle Transition Region", Langmuir **13**, 3659 (1997).

Greenberg, R.R., "Unique Quality Assurance Aspects of Neutron Activation Analysis", Proceedings of the 9th International Symposium on Trace Elements in Man and Animals, in press.

Greenberg, R.R., "The Role of Neutron Activation Analysis in the Development and Certification of NIST Environmental Standard Reference Materials", Proceedings of the International Symposium on Harmonization of Health Related Environmental Measurements Using Nuclear and Isotopic Techniques, in press.

Haight, R.C., Bateman, F.B., Grimes, S.M., Brient, C.E., Massey, T.N., Wasson, O.A., Carlson, A.D., and Zhou, H., "Measurement of the Angular Distribution of Neutron-Proton Scattering at 10 MeV", Fusion Eng. Design **37**, 49 (1997).

Hanley, H. J. M., Muzny, C. D., Butler, B. D., "Dynamic Scaling in a Dense Silica Gel", J. Phys. Cond. Matt. **8**, 9457 (1996).

Hanley, H. J. M., Muzny, C. D., Butler, B. D., "Surface Adsorption in a Surfactant/Clay Mineral Solution", Int. J. Thermophys., in press.

Hanley, H. J. M., Muzny, C. D., Butler, B. D., "Surfactant Adsorption on a Clay Mineral: Application of Radiation Scattering", Langmuir **13**, 5276 (1997).

Henderson, S. J., "The Second Virial Coefficient of C_{60} in CS_2 Measured by Small-Angle Neutron Scattering", Langmuir, in press.

Hillmyer, M. A., Bates, F. S., "Influence of Crystallinity on the Morphology of Poly(ethylene oxide) Containing Diblock Copolymers", Macromol. **117**, 121 (1997).

Hines, J. D., Fragneto, G., Thomas, R. K., Garrett, P. R., Rennie, G. K., Rennie, A. R., "Neutron Reflection from Mixtures of Sodium Dodecyl Sulfate and Dodecyl Betaine Adsorbed at the Hydrophobic Solid/Aqueous Interface", J. Colloid Interf. Sci. **189**, 259 (1997).

Hjelm, R. P., Schteingart, C., Hofmann, A. F., Sivia, D. S., "Form and Structure of Self-Assembling Particles in Monoolein-Bile Salt Mixtures", J. Phys. Chem **99**, 16395 (1995).

Hobbie, E. K., Merkle, G., Bauer, B. J., Han, C. C., "Spinodal Decomposition in Hydrogen-

Bonded Polymer Blends", Modern Phys. Lett. B **10**, 1219 (1996).

Hoff, J., Borgoul, P., Ondov, J. M., Kelly, W. R., Chen, L. T., "Feasibility of Applying a New Tracer for Direct Determination of Dry Particulate Deposition", J. Air Waste Management, in press.

Hofsaess, H.C., Biegel, J., Ronning, C., Downing, R.G., Lamaze, G.P., "Characterization of Doped Diamond-like Carbon Films and Multilayers", MRS Proceedings, in press.

Ikkai, F., Shibayama, M., Nomura, S., Han, C. C., "Effect of Degree of Cross-linking on Spatial Inhomogeneity in Charged Gels: 2. Small Angle Neutron Scattering Study", Macromol., in press.

Ilavsky, J., Allen, A. J., Long, G. G., Herman, H., Berndt, C. C., "Characterization of the Closed Porosity in Plasma-Sprayed Alumina", J. Mater. Sci. **32**, 3407 (1997).

Ioffe, A., Jacobson, D., Arif, M., Vrana, M., Werner, S.A., Fischer, P., Greene, G., Mezei, F., "A New Neutron Interferometric Method Used to Measure the Scattering Length of Silicon", Physica B, in press.

Ioffe, A., Jacobson, D., Arif, M., Vrana, M., Werner, S.A., Fischer, P., Greene G., Mezei, F., " The Precision Neutron Interferometric Measurement of the Coherent Neutron-Nuclear Scattering Length in Silicon", Phys. Rev. Lett., in press

Ivkov, R., Forbes, J. G., Greer, S. C., "The Polymerization of Rabbit Muscle Actin: Study by Small Angle Neutron Scattering", J. Chem. Phys., in press.

Jach, T., Steel, E., Chen-Mayer, H. H., Ullrich, J., Downing, R. G., Thurgate, S., "The Characterization of X-Ray Polycapillary Optics with a High-Resolution X-Ray Optical Bench", in *Neutrons in Research and Industry*, Proceedings of the 5th International Conference on Applications of Nuclear Techniqes, SPIE **2805**, 192 (1996).

Jacobson, D. L., Allman, B. E., Zawisky, M., Werner, S. A., Rauch, H., "Neutron Interferometric Measurement of Neutron Pair Correlations for Multiple Detectors", J. Phys. Soc. Jpn. **65**, Suppl. A, 94 (1996).

Jinnai, H., Hashimoto, T., Lee, D., Chen, S.-H., "Morphological Characterization of Bicontinuous Phase-Separated Polymer Blends and One-Phase Microemulsions", Macromol. **30**, 130 (1997).

Keith, C.D., Black, T.C., Fei, X., Flamini, M., Gentile, T.R., Jones, G.L., Rich, D.R., Snow, W.M., Thompson, A.K., and Wietfeldt, F.E., "Neutron Polarizers Based on Polarized ^{3}He", Nucl. Inst. Meth., in press.

Kidwell, C., Divita, Jr., F., Ondov, J. M., "Identification of an Incinerator Plume from Ground Level Sampling with a Micro-Orifice Impactor", J. Aerosol Sci. **27**, S29 (1996).

Kitade, S., Ochiai, N., Takahashi, Y., Noda, I., Matsushita, Y., Karim, A., Nakatani, A. I., Han, C. C., "Lamellar Orientation of Diblock Copolymer Solutions Under Steady Shear Flow", Macromol., in press.

Krone, C.A., Robisch, P.A., Tilbury, K.L., Stein, J.E., Mackey, E.A., Becker, P.R., O'Hara, P.R., Philo, L.M., "Heavy Metals and Other Elements in Liver Tissues of Bowhead [Balaena mysticetus] Whales", Mar. Mammal Sci., in press.

Krueger, J. K., Olah, G. A., Rokop, S. E., Zhi, G., Stull, J. T., Trewhella, J., "Structures of Calmodulin and a Functional Myosin Light Chain Kinase in the Activated Complex: A Neutron Scattering Study", Biochem. **36**, 6017 (1997).

Krueger, J. K., Olah, G. A., Trewhella, J., Zhi, G., Stull, J. T., "The Structures of Calmodulin and a Functional Myosin Light Chain Kinase in Their Complex: A Study Using Small-Angle Neutron Scattering with Contrast Variation", Biophys. J. **72**, A 129 (1997).

Lamaze, G.P., "A High Efficiency Device for the Detection of Radioactive Xenon Isotopes", Nucl. Instrum. Meth. A **385**, 285 (1997).

Lamaze, G.P., Chen-Mayer, H.H., Langland, J.K., Downing, R.G., "Neutron Depth Profiling

with the New NIST Cold Neutron Source", Surf. Interface Anal. **25**, 217 (1997).

Lamaze, G.P., Downing, R.G., "Boron Analysis in Synthetic Diamond Films Using Cold Neutron Depth Profiling", Proceedings of the International Workshop on Semiconductor Characterization: Present and Future Needs (1996), p. 351.

Lindstrom, R.M., "Neutron Beam Methods in the Analysis of Reference Materials", Proceedings of the IAEA International Symposium on Harmonization of Health Related Environmental Measurements Using Nuclear and Isotopic Techniques, in press.

Lindstrom, R.M., "Reference Material Certification by Prompt-Gamma Activation Analysis", Fresen. J. Anal. Chem., in press.

Lindstrom, R. M., Anderson, D. L., Paul, R. L., "Analytical Applications of Neutron Capture Gamma Rays", Proceedings of the 9th International Symposium on Neutron-Capture Gamma-Ray Spectroscopy and Related Topics (Budapest, Hungary, October 1996), Springer, in press.

Lindstrom, R.M., Asvavijnijkulchai, C., "Ensuring Accuracy in Spreadsheet Calculations", Fresen. J. Anal. Chem., in press.

Lindstrom, R.M., Becker, D.A., Langland J.K., Greenberg, R.R., "The NIST Rapid Irradiation and Counting System", J. Radioanal. Nucl. Chem. **215**, 47 (1997).

Lindstrom, R.M., Chen-Mayer, H.H., Sharov, V.A., Langland, J.K., Cheng, Y.-T., Mildner, D.F.R., "Installation of a Neutron Bender-Lens for Spatially Resolved Prompt-Gamma Activation Analysis", Trans. Am. Nucl. Soc. **75**, 16 (1996).

Lindstrom, R.M., Greenberg, R.R., Mildner, D.F.R., Mackey, E.A., Paul, R.L., "Neutron Scattering and Neutron Reaction Rates", Proceedings of the 2nd International k_0 Users Workshop (1997), p. 50.

Liu, Z., Bauer, B. J., Briber, R. M., "Conformation of Free Linear Polymer Chains in a Polymer Network", Macromol. **30**, 4704 (1997).

Lodge, T. P., Hamersky, M. W., Hanley, K. J., Huang, C.-I., "Sovent Distribution in Weakly-Ordered Block Copolymer Solutions", Macromol. **30**, 6139 (1997).

Mackey, E.A., Becker, D.A., "Determination of Methylmercury in Two Mussel Tissue Standard Reference Materials by Pre-Irradiation Separation and Neutron Activation Analysis", The Analyst, in press.

Mackey, E. A., Demiralp, R., Becker, P. R., Greenberg, R. R., Koster, B. J., Wise, S. A., "Trace Element Concentrations in Cetaccean Liver Tissues Archived in the National Marine Mammal Tissue Bank", Sci. Total Environ. **175**, 25 (1995).

Mayer, R.R., Welsh, J., Chen-Mayer, H.H., "Focused Neutron Beam Dose Deposition Profiles in Tissue Equivalent Materials: A Pilot Study for BNCT", Neutrons in Research and Industry (SPIE Proc. **2867**, 1997).

Migler, K. B., Han, C. C., "Pressure Effects on a Diblock Copolymer: Optical Birefringence and Neutron Scattering", Macromol., in press.

Mildner, D.F.R., "Polycapillary Neutron Lenses", IAEA Technical Document: Trends and Techniques on Neutron Beam Research for Medium and Low Flux Research Reactors, in press.

Mildner, D.F.R., Chen-Mayer, H.H., Downing, R.G., "Characteristics and Applications of a Polycapillary Neutron Focusing Lens", J. Phys. Soc. Jpn. **65**, Suppl. A, 308 (1996).

Mildner, D.F.R., Chen-Mayer, H.H., Lamaze, G.P., Sharov, V.A., "Characterization of a Cold Neutron Beam from a Curved Guide", Nucl. Instrum. Meth. A, in press.

Mildner, D.F.R., Chen-Mayer, H.H., Sharov, V.A., "Neutron Focusing Lens Using Capillary Optics", Proceedings of the 9th International Symposium on Capture Gamma Spectroscopy and Related Topics, in press.

Mildner, D.F.R., Chen-Mayer, H.H., Sharov, V.A., Fokin, V.S., Reeder, P.L., "The Number of Reflections for Neutron Trans-

mission through Cylindrical Channels", J. Appl. Crystallogr. **30**, 324 (1997).

Mildner, D.F.R., Sharov, V.A., Chen-Mayer, H.H., "Neutron Transmission Through Tapered Channels", J. Appl. Cryst., in press.

Molnar, G.L., Lindstrom, R.M., "Nuclear Reaction Prompt Gamma-Ray Analysis", Chapter XI in *Nuclear Techniques in Mineral Analysis*, ed. A. Vertes, S. Nagy, K. Suvegh, in press.

Murthy, N. S., "Fibrillar Structure and Its Revelance to Diffusion, Shrinkage, and Relaxation Processes in Nylon Fibers", Textile Res. J. **67**, 511 (1997).

Murthy, N. S., Zero, K., Grubb, D. T., "Full-Pattern Analysis of Two-Dimensional Small-Angle Scattering Data from Oriented Polymers Using Elliptical Coordinates", Polymer **38**, 1021 (1997).

Muzny, C. D., Butler, B. D., Hanley, H. J. M., Tsvetkov, F., Peiffer, D. G., "Silicate Clay Platelet Dispersion in a Polymer Matrix", MRS Proc. **435**, 85 (1996).

Muzny, C. D., Hansen, D., Straty, G. C., Evans, D. J., Hanley, H. J. M., "Simulation and SANS Studies of Gelation under Shear", Int. J. Thermophys. **16**, 337 (1995).

Nakatani, A. I., Han, C. C., "Shear Dependence of the Equilibrium and Kinetic Behavior of Multicomponent Systems", in *Structure and Properties of Multi-Phase Polymeric Materials*, ed. T. Araki, M. Shibayama, Q. Tran-Cong (Marcel Dekker Inc., New York, 1997).

Nakatani, A. I., Morrison, F. A., Douglas, J. F., Mays, J. W., Jackson, C. L., Muthukumar, M., "The Influence of Shear on the Ordering Temperature of a Triblock Copolymer Melt", J. Chem. Phys. **104**, 1589 (1996).

Nakatani, A. I., Morrison, F. A., Jackson, C. L., Douglas, J. F., Mays, J. W., Muthukumar, M., Han, C. C., "Shear-induced Changes in the Order-Disorder Transition Temperature and the Morphology of a Triblock Copolymer", J. Macromol. Sci. Phys. **B35**, 489 (1996).

Nico, J.S., Adams, J.M., Eisenhauer, C., Gilliam, D.M., Grundl, J.A., "^{252}Cf Fission Neutron Transport Through an Iron Sphere", Reactor Dosimetry, World Scientific Publishing, July 1997, in press.

Norman, E.B., Browne, E., Chan, Y.D., Goldman, I.D., Larimer, R M., Lesko, K.T., Nelson, M., Wietfeldt, F.E., and Zlimen, I., "On the Half-Life of ^{44}Ti", Nucl. Phys. **A261**, 92c (1997).

Norman, B.R., Mackey, E.A., "Concentrations of Iodine Determined by Pre-Irradiation Combustion and Neutron Activation Analysis in Powdered Grass as a Function of Particle Size", Fresen. J. Anal. Chem., in press.

Olah, G. A., Trewhella, J., "The Structure of the Muscle Protein Complex 4Ca^{2+} Troponin C Troponin I: A Monte Carlo Modeling Analysis of Small-Angle Neutron Scattering Data", in *Neutrons in Biology, Basic Life Sciences Vol. 64*, ed. P. Schoenborn, R. B. Knott, (Plenum Press, New York, 1996).

Ondov, J. M., "Particulate Tracers for Source Attribution: Potential for Application to California's San Joaquin Valley", J. Aerosol Sci. **27**, S687 (1996).

Ondov, J. M., "Size-Spectra, Growth, and Deposition of Urban Aerosol Particles Bearing Minor Trace Elecments from Generic Sources", in NATO ASI Series, Partnership Sub-Series: 2. Environment **8**, Urban Air Pollution, ed. I. Allegrini, F. DeSantis, (Springer-Verlag, Berlin, 1996).

Ondov, J. M., Divita, Jr. F., Suarez, A. E., Quinn, T. L., "Size Spectra and Atmospheric Behavior of Respirable Urban Aerosol Particles Bearing Minor and Trace Elements: An Improved Paradigm for the Structure and Dynamics of the Urban Atmospheric Aerosol in the Mid-Atlantic Region", J. Air Waste Management, in press.

Ondov, J. M., Quinn, T. L., "Influence of Humidity on Aerosol Size and Dry Deposition Fluxes of Trace Elements", in *Atmospheric Deposition of Contaminants to the Great*

Lakes and Coastal Waters, SETAC Special Publications Series, ed. J. E. Baker, 1996.

Ondov, J. M., Wu, C., Lin, Z.-B., Kidwell, C. B., "Neutron Activation Analysis of an Ir Tracer to Determine Soot Exposure to Students Commuting on Baltimore Public Buses", Trans. Amer. Nuc. Soc., in press.

Ondov, J. M., Wu, C., Lin, Z.-B., Suarez, A. E., Kidwell, C. B., Borgoul, P. V., Sattler, B., "Application of an Ir Tracer to Determine Soot Exposure to Students Commuting to School on Baltimore Public Buses", J. Air Waste Management, in press.

Parr, R.M., Stone, S.F., Bel-Amakeletch, T., Zeisler, R., "Survey of Reference Materials for Trace Elements, Nuclides, and Organic Microcontaminants", Fresen. J. Anal. Chem., in press.

Paul, R.L., "Determination of Phosphorus in Steels by Radiochemical Neutron Activation Analysis", J. Radioanal. Nucl. Chem., in press.

Paul, R.L., "Hydrogen Measurement by Prompt Gamma-Ray Activation Analysis at NIST", The Analyst **122**, 35R (1997).

Paul, R.L., Lindstrom, R.M., "Applications of Cold Neutron Prompt Gamma Activation Analysis to Characterization of Semiconductors", Proceedings of the International Workshop on Semiconductor Characterization: Present Status and Future Needs, in press.

Paul, R.L., Lindstrom, R.M., "Measurement of k_0-factors for Prompt Gamma-Ray Activation Analysis", Proceedings of the 2nd International k_0 Users Workshop (1997), p. 54.

Paul, R.L., Lindstrom, R.M., Heald, A.E., "Cold Neutron Prompt Gamma-ray Activation Analysis at NIST - Recent Developments", J. Radioanal. Nucl. Chem. **215**, 63 (1997).

Paul, R.L., Privett, H.M., Lindstrom, R.M., Richards, W.J., Greenberg, R.R., "Determination of Hydrogen in Titanium Alloys by Cold Neutron Prompt Gamma Activation Analysis", Metall. Mater. Trans. A **27A**, 3682 (1996).

Podurets, K.M., Sharov, V.A., Mildner, D.F.R., "Spatial Distribution of Neutrons Guided Through a Monolithic Tapered Lens", Appl. Phys. Lett., in press.

Polkowska-Motrenko, H., Dubczynski, R., Danko, B., Becker, D.A., "Very Accurate Simultaneous Determination of Trace Amounts of Co and Ni in Biological Materials by Radiochemical Neutron Activation Analysis", J. Radioanal. Nucl. Chem. Art., **207**, 401 (1996).

Quinn, T. L., Ondov, J. M., "Influence of Temporal Changes in Relative Humidity on Dry Deposition Velocities and Fluxes of Aerosol Particles Bearing Trace Elements", Atmos. Environ., in press.

Redford, S., Blackman, M. J., "Luster and Fritware Production and Distribution in Medieval Syria", J. Field Archaeology **24**, 233 (1997).

Reeder, P.L., Peurrung, A.J., Richey, W.C., Chen-Mayer, H..H., Sharov, V.A., Fokin, V.S., Mildner, D.F.R., "Imaging Neutron Beams with Scintillating Fiber Faceplates", Nucl. Instrum. Meth. A, in press.

Reeder, P.L., Peurrung, A.J., Sunberg, D.S., Stoffel(s), J.J., Chen-Mayer, H..H., Mildner, D.F.R., Sharov, V.A., Fokin, V.S., "Metal Capillaries for Neutron Lenses", Nucl. Instrum. Meth. A, in press.

Regev, O., Ezrahi, S., Aserin, A., Garti, N., Wachtel, E., Kaler, E. W., Khan, A., Talmon, Y., "A Study of the Microstructure of a Four-Component Nonionic Microemulsion by Cryo-TEM, NMR, SAXS, and SANS", Langmuir **12**, 668 (1996).

Reichart, G. C., Graessley, W. W., Register, R. A., Krishnamoorti, R., Lohse, D. J., "Anomalous Attractive Interactions in Polypropylene Blends", Macromol. **30**, 3036 (1997).

Reichart, G. C., Graessley, W. W., Register, R. A., Krishnamoorti, R., Lohse, D. J., "Measurement of Thermodynamic Interaction in Ternary Polymer Blends by Small Angle Neutron Scattering", Macromol. **30**, 3363 (1997).

Rizi, R.R., Dimitov, I.E., Thompson, A.K., Jones, G.L., Gentile, T.R., Ishii, M., Reddy, R., Schnall, M.D., Leigh, J.S., "MR Imaging of Hyperpolarized ^{3}He Gas in Human Paranasal Sinuses", Magnetic Resonance in Medicine, in press.

Sanders, P. G., Eastman, J. A., Weertman, J. R., "Elastic and Tensile Behavior of Nanocrystalline Copper and Palladium", Acta Mater. **45**, 4019 (1997).

Sanders, P. G., Youngdahl, C. J., Weertman, J. R., "The Strength of Nanocrystalline Metals With and Without Flaws", Mater. Sci. Eng. **A234**, 77 (1997).

Schantz, M. M., Demiralp, R., Greenberg, R.R., Hays, M.J., Parris, R.M., Porter, B.J., Poster, D.L., Sander, L.C., Sharpless, K.S., Wise, S.A., Schiller, S.B., "Certification of a Frozen Mussel Tissue Standard Reference Material (SRM 1974a) for Trace Organic Constituents", Fresen. J. Anal. Chem. **358**, 431 (1997).

Serebrov, A.P., Dewey, M.S., Wietfeldt, F.E., et al., "Measurements of the Asymmetry of Antineutrino Escape with Respect to Spin Direction of Decaying Neutron", Phys. Rev. C, in press.

Sharpless, K.E., Welch, M.J., Greenberg, R.R., Iyengar, G.V., Colbert, J.C., "Recent SRMs for Organic and Inorganic Nutrients in Food Matrices", Fresen. J. Anal. Chem., in press.

Shibayama, M., Ikkai, F., Inamoto, S., Nomura, S., Han, C. C., "pH and Salt Concentration Dependence of the Microstructure of Poly(N-isopropylacrylamide-co-acrylic acid) Gels", J. Chem. Phys. **105**, 4358 (1996).

Sorek, Y., Zhou, P., Fischer, J. E., Ishihara, T., "Effect of Oxidation Treatment on Li Capacity in Disordered Carbons: The Surfing Cards Model", Carbon, in press.

Sottman, T., Strey, R., Chen, S.-H., "A Small-Angle Neutron Scattering Study of Nonionic Surfactant Molecules at the Water-Oil Interface: Area per Molecule, Microemulsion Domain Size, and Rigidity", J. Chem. Phys. **106**, 6483 (1997).

Stone, S.F., Donais, M.K., Zeisler, R., "Instrumental Neutron Activation Analysis for Quality Assurance of a Hair Reference Material for Mercury Speciation", J. Radioanal. Nucl. Chem., in press.

Stone, S.F., Fajgelj, A., Bernasconi, G., Tajani, A., Zeisler, R., "Examination of a Procedure for the Production of a Filter-Based Air Particulate Matter Reference Material", Fresen. J. Anal. Chem., in press.

Suarez, A. E., Caffrey, P. F., Ondov, J. M., Divita, Jr. F., "Use of an Ir Tracer to Determine the Size Distribution of Aerosol from Diesel Sanitation Trucks", Environ. Sci. Technology, in press.

Suarez, A. E., Caffrey, P. F., Ondov, J. M., Thaung, K. C., "Size Distribution of Ir-tagged Soot from Diesel Sanitation Trucks", J. Aerosol Sci. **27**, S697 (1996).

Takahashi, Y., Kitade, S., Ochiai, N., Noda, I., Matsushita, Y., Imai, M., Nakatani, A. I., Kim, H., Han, C. C., "Order-Disorder Transition of Symmetric Styrene-2-Vinylpyridine Diblock Copolymers in Melts and Solutions", Polymer Journal (Japan), in press.

Then, S.S., Geurink, F.D.P., Bode, P., Lindstrom, R.M., "A Pulse Generator Simulating Ge-detector Signals for Dead-time and Pile-up Correction in Gamma-ray Spectrometry in INAA without Distortion of the Detector Spectrum", J. Radioanal. Nucl. Chem. **215**, 249 (1997).

Thompson, A.K., Gentile, T.R., "Status of the NIST Spin Filter Project," J. Neutron Res. **5**, 25 (1996).

Topp, A., Bauer, B. J., Amis, E. J., "Small Angle Neutron Scattering from Dilute and Concentrated DAB(PA)$_x$ Dendrimer Solutions", ACS PMSE Proceedings **77**, 82 (1997).

Trewhella, J., "Conformational Flexibility in the Regulation of Target Proteins by Calmodulin and Troponin C", Biophys. J., in press.

Trewhella, J., "Insights into Biomolecular Function from Small-Angle Neutron Scattering", Current Opinion in Structural Biology **7**, 702 (1997).

Valachovic, D. E., Bauer, B. J., Amis, E. J., Tomalia, D. A., "Dendrimer End Group Localization Determined by Counterion Mirroring", ACS PMSE Proceedings **77**, 230 (1997).

Wagh, A. G., Rakhecha, V. C., Summhammer, J., Badurek, G., Weinfurter, H., Allman, B. E., Kaiser, H., Hamacher, K., Jacobson, D. L., Werner, S. A., "Experimental Separation of Geometric and Dynamical Phases Using Neutron Interferometry", Phys. Rev. Lett. **78**, 755 (1997).

Wu, C. C., Suarez, A. E., Lin, Z.-B., Kidwell, C. B., Borgoul, P. V., Caffrey, P. F., Ondov, J. M., Sattler, B., "Application of an Ir Tracer to Determine Soot Exposure to Students Commuting to School on Baltimore Public Buses", Atmos. Environ., in press.

Wyslouzil, B. E., Cheung, J. L., Wilemski, G., Strey, R., "Small Angle Neutron Scattering from Nanodroplet Aerosols", Phys. Rev. Lett. **79**, 431 (1997).

Xiao, Q.F., Sharov, V.A., Downing, R.G., Chen-Mayer, H.H., Mildner, D.F.R., "Neutron Beam Control Using Polycapillary Optics", J. Phys. Soc. Jpn. **65**, Suppl. A, 316 (1996).

Xiao, Q.F., Sharov, V.A., Gibson, D.M., Chen, H., Mildner, D.F.R., Downing, R.G., "Capillary Neutron Optics for Boron Neutron Capture Therapy", Proceedings of the 6th International Symposium on Neutron Capture Therapy for Cancer, *Cancer Neutron Capture Therapy*, ed. Y. Mishima (Plenum Press, New York, 1996), p. 399.

Xu, G., DiTusa, J. F., Ito, T., Oka, K., Takagi, H., Broholm, C., Aeppli, G., "Y_2BaNiO_5: A Nearly Ideal Realization of the S=1 Heisenberg Chain with Antiferromagetic Interactions", Phys. Rev. B **54**, R6827 (1996).

Zeisler, R., "Environmental Specimen Banking: Contributions to Quality Management of Environmental Measurements", Special Publication of the American Chemical Society, Environmental Monitoring and Specimen Banking, ACS Symposium Series, **654**, 246 (1997).

Zeisler, R., Dekner, R., Zeiller, E., Doucha, J., Mader, P., Kucera, J., "Single Cell Green Aglae Reference Materials with Managed Levels of Heavy Metals", Fresen. J. Anal. Chem., in press.

Zeisler, R., Haselberger, N., Makarewicz, M., Ogris, R., Parr, R.M., Stone, S.F., Valkovic, O., Valkovic, V., Wehrstein, E., "Nuclear Techniques Applied To Air Particulate Matter Studies", J. Radioanal. Nucl. Chem. **217**, 5 (1997).

Zeissler, C.J., Wight, S.A., Lindstrom, R.M., "Detection and Characterization of Radioactive Particles", Appl. Rad. Isotop., in press.

Zhao, J., Hoyer, E., Boylan, S., Walsh, D., Trewhella, J., "Quaternary Structure of the CAMP-Dependent Protein Kinase by Neutron Scattering", Biophys. J., in press.

Zhou, P., Lee, R. S., Claye, A., Fischer, J. E., "Layer Disorder in Carbon Anodes", Carbon, in press.

Zielinski, R. G., Paulaitis, M. E., Kaler, E. W., "A Sapphire Cell for Neutron Scattering at Elevated Pressure", Rev. Sci. Instrum. **67**, 2612 (1996).

Zufall, M. J., Davidson, C. I., Caffrey, P. F., Ondov, J. M., "Airborne Concentrations and Dry Deposition Fluxes of Particulate Chemical Species to Southern Lake Michigan", Environ. Sci. Technol., in press.